University of Plymouth

PEARL **https://pearl.plymouth.ac.uk**

04 University of Plymouth Research Theses 01 Research Theses Main Collection

2017

Holocene sea-level changes in the Falkland Islands: new insights into accelerated sea-level rise in the 20th Century

Newton, Thomas Lee

http://hdl.handle.net/10026.1/9650

http://dx.doi.org/10.24382/1181
University of Plymouth

All content in PEARL is protected by copyright law. Author manuscripts are made available in accordance with publisher policies. Please cite only the published version using the details provided on the item record or document. In the absence of an open licence (e.g. Creative Commons), permissions for further reuse of content should be sought from the publisher or author.

Holocene sea-level changes in the Falkland Islands: new insights into accelerated sea-level rise in the 20th Century

Thomas L. Newton

A thesis submitted to Plymouth University in partial fulfilment for the degree of

DOCTOR OF PHILOSOPHY

School of Geography, Earth and Environmental Sciences

Faculty of Science and Technology

Plymouth University

April 2017

Copyright

This copy of the thesis has been supplied on condition that anyone who consults it is understood to recognise that its copyright rests with its author and that no quotation from the thesis and no information derived from it may be published with the author's prior consent.

Author Declaration

At no time during the registration for the degree of Doctor of Philosophy has the author been registered for any other university award without prior agreement of the Graduate Committee.

This study was financed with the aid of a studentship from the School of Geography, Earth and Environmental Sciences, Plymouth University.

During the course of study relevant scientific seminars, conferences and workshops were attended, at which work was often presented. External institutions were visited for training purposes.

Word count: 67,416

Author: Thomas L. Newton

Signature:  Date: 11/04/2017

Additional funding awards:

Natural Environment Research Council (NERC). Radiocarbon Facility Allocation Number 1694.0413 (£20,804)

International Union for Quaternary Research (INQUA) Financial support to attend XIX INQUA 2015 (£995)

Conferences and presentations:

Newton, T.,(2013) 'Testate amoebae as precise sea-level indicators' February 2013, Phunch Seminar, University of Plymouth.

Newton, T., Gehrels, W. R., Daley, T.J**,** Bentley, M.J., Long, A.J. and Milne G.A. (2014) 'Holocene sea-level changes in the Falkland Islands' April 2014, Poster presentation: European Geophysical Union General Assembly, Vienna.

Newton, T. Gehrels, W.R., Daley, T.J. (2014) 'Reconstructing sea-level change using testate amoebae: A case study from the Falkland Islands' Oral presentation: Postgraduate Research Conference, University of Plymouth. May 2014

Newton, T., Gehrels, W. R., Daley, T.J**.,** Bentley, M.J. , Long, A.J. and Milne G.A. (2014) 'Holocene sea-level changes in the Falkland Islands' (July 2014) Poster presentation: UK Sea Level IGCP / INQUA CMP Working Group Field Meeting, SW Ireland.

Newton, T. (2014) 'Reconstructing sea-level changes from low energy intertidal sediments' (August 2014) Invited seminar and workshop: Instituto Nacional de Ecologia y Cambio Climatico (INECC) Mexico City, Mexico.

Newton, T., Gehrels, W.R., Daley, T.J. (2014) 'Reconstructing Holocene sea-level changes in the Falkland Islands' (August, 2014) Invited Seminar: El departamento de geomagnetismo y exploracion geofisica, Universidad Nacional Autónoma de México (UNAM).

Newton, T. Gehrels, W.R., Daley, T.J. (2015) 'Holocene and recent sea-level changes in the Falkland Islands: testing the Greenland melt hypothesis.'(June 2015) Oral presentation: Workshop on Global Sea-Level Variability and Change, Palma de Mallorca, Spain.

Newton, T. Gehrels, W.R., Daley, T.J. (2015) 'Holocene and recent sea-level changes in the Falkland Islands: testing the Greenland melt hypothesis.'(August 2015) Oral presentation: XIX INQUA congress 2015, Nagoya Japan.

Newton, T., Gehrels, W.R., Daley, T.J. (2015) 'Seasonal distributions of salt-marsh testate amoebae: implications for sea-level studies' (August 2015) Poster presentation: XIX INQUA congress 2015, Nagoya Japan.

ABSTRACT

Holocene sea-level changes in the Falkland Islands: new insights into accelerated sea-level rise in the 20th Century

Thomas L. Newton

This thesis investigates sea-level changes in order to test the hypothesis that the main contribution to early 20th century sea-level rise was Northern Hemisphere land-based ice melt. Multiproxy sea-level reconstructions were established for the Falkland Islands, a location where models suggest sea-level rise from Northern Hemisphere ice melt produces the largest signal. The Falklands reconstruction indicated sea levels in the early 20th century accelerated compared to the long-term rate, synchronous with accelerations observed globally. The magnitude of the acceleration in the Falklands reconstruction was greater than Northern Hemisphere rates, consistent with the spatial pattern from a Northern Hemisphere melt source, but likely less than in New Zealand and Australia. It is therefore not possible rule out other contributions to the observed sea-level acceleration. The Falklands reconstruction indicated a rapid sea-level jump around 8.4 ka BP, synchronous with a jump observed in the Northern Hemisphere, which has been attributed to the sudden drainage of Laurentide proglacial lake Agassiz-Ojibway associated with the 8.2 ka BP climatic downturn. A maximum estimate of 0.89 ± 0.22 m for this jump in the Falklands is considerably less than estimates from Northern Hemisphere records. This difference could indicate additional contributions from the Southern Hemisphere are being recorded in the Northern Hemisphere signal.

This thesis also focused on developing testate amoebae as sea-level indicators. In the Falklands, testate amoebae transfer functions were able to reconstruct sea level with precision (±0.08 m) comparable to diatoms (±0.07 m). However, preservation issues were indicated in the fossil testate amoebae assemblages which limits their use as tools for sea-level reconstruction. In addition, contemporary distributions of salt-marsh testate amoebae were investigated over one annual cycle. Seasonal variations in the live assemblages were observed to be asynchronous between taxa. Variations in the death assemblages were also observed which were correlated with variations in the live assemblages. This observation suggests the commonly applied assumption in palaeoenvironmental studies that analysing the death population negates temporal bias is invalid. Further research is required to investigate the impact these observed variations have on reconstructive performance.

ACKNOWLEDGEMENTS

First and foremost I'd like to thank my supervisory team, Prof. Roland Gehrels and Dr. Tim Daley for having belief in me to begin with, and for their continued support over the duration of my PhD studies. Roland, it was, after all, you who first piqued my interest in sea-level studies. On a similar note, I wish to thank my secondary school and A-level geography and geology teacher John Payne who first inspired me to pursue my interests in these fields. More broadly, I'd like to thank the staff, and the Department of Geography as a whole, at Plymouth University without whom this PhD would not have been possible. I am grateful for the assistance of the South Atlantic Environmental Research Institute for providing lab space in the Falkland Islands, Margarita Caballero and Paola Massyel for hosting me in Mexico, INQUA for providing financial support to attend the Japan congress, and Tom Hill hosting me at the Natural History Museum, London. This work was supported by the NERC Radiocarbon Facility NRCF010001 (allocation number 1694.0413).

I would personally like to thank, in no particular order, Katie Head, Rich Hartley, Will Blake, Dan Charman, Tom Hill, Paola Massyel, Margarita Caballero, Rob Barnett, Ralph Fyfe, James Smith, Geoff Millward, Emma Edwards, Emma Rice, Francis Rowney, Glenn Milne, Kurt Lambeck, Andrew Parnell, Antony Long, Mike Bentley, Margot Saher, Jamie Quinn and Arthur Guinness for their generous assistance, contribution of data and/or insightful discussions at various stages of my PhD studies. Finally I wish to give my sincere, indiscriminate thanks to my friends, new and old, and family who have supported me with their company, kept me sane, and in good spirits throughout what has been a challenge of a lifetime – you know who you are. Cheers! ☺

Contents

Index of Tables

Index of Figures

Chapter 1 – Introduction

1.1 Research context

The climatic, economic and environmental consequences of humankind's continued extraction and burning of fossil fuels are well documented, albeit not fully understood (Church *et al.*, 2013; Höök and Tang, 2013). Current assessments agree that the global impact of sea-level rise is one of the greatest challenges posed as a consequence of present, and future, climate change (e.g. Church *et al.*, 2013; Melillo *et al.*, 2014). The direct risk is to low-lying (<10m above sea level) coastal populations which account for ~9% of the global population and generate ~10% of global GDP (McGranahan *et al*. 2007). Hence the issue of rising sea levels features prominently in the Intergovernmental Panel on Climate Change (IPCC) 5th Assessment Report (AR5). Chapter 13 of the IPCC's AR5 report (Church *et al*. 2013) is dedicated to the subject of sea level; extensively evaluating the components, contributions, observations, historical reconstructions and future projections of global mean sea level (GMSL) rise. The IPCC's key findings are: GMSL is rising; there has been a post-industrial (late 19th to early 20th century) acceleration in sea-level rise; and sea levels are projected to continue accelerating along a positive trajectory (**Figure 1.1**) – largely as a response to increases in global mean temperatures. However, there still remains much uncertainty surrounding the future estimations of projected sea-level rise. This uncertainty is captured in the IPCC's AR5 future projections (based on process-based models) of GMSL rise which range from 28 to 98 cm by AD2100. Recent studies which use semi-empirical models (calibrated with proxy sea-level data; Rahmstorf, 2007) result in a projected sea-level rise of 28-131 cm by AD2100 (Kopp *et al,.* 2016, Mengel *et al.,* 2016) which extend the maximum rise projected by the process-based models

favoured by the IPCC. Much of the projected range reflects the possible future climates (regional climate projections) based on a range of emissions scenarios. However, there still remains uncertainty regarding the climate-related responses of the main contributors to sea-level rise e.g. the polar ice sheets. With this uncertainty in mind and the practically immeasurable socio-economic costs that would be incurred by a loss of, or severe reduction in, functionality in urbanised coastal areas, it is of critical importance to improve our understanding of the threat of future sea-level rise. To this end, understanding past sea-level changes are a key requisite to improving our understanding of the future threat of sea-level rise.

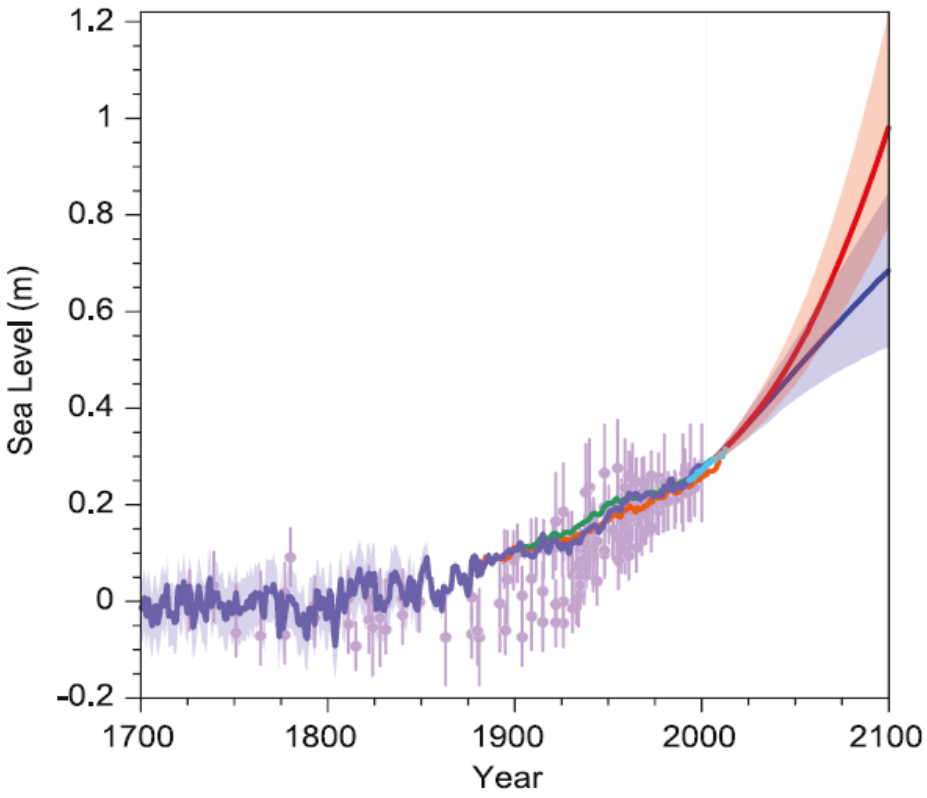

Figure 1.1*: Past and future sea-level rise. For the past, salt marsh proxy reconstructions are shown by the light purple symbols , tide gauge records are shown by the dark purple (with shaded uncertainties), orange and green timeseries and satellite altimetry in blue. For the future, the IPCC model projections for very high emissions (red, RCP8.5 scenario) and very low emissions (blue, RCP2.6 scenario) are shown, all relative to pre-industrial values. Source: IPCC AR5 Fig. 13.27 (Church et al. 2013).*

Reduction of the uncertainty in sea-level projections can be facilitated by improved understanding of the magnitude and timing of past sea-level changes. This is critical for determining the contributions to past changes in the height of the sea surface (e.g. Dutton *et al.* 2015), constraining and calibrating semi-empirical sea-level models (e.g. Kemp *et al.,* 2011; Vermeer and Rahmstorf, 2009; Mengel *et al.,* 2016) and presenting a plausible context for considering future scenarios and assessing mitigation options (e.g. Rahmstorf, 2007; Grinsted *et al*., 2009; Mengel *et al.,* 2016). Whilst instrumental observations provide directly measured and accurate records of sea-level variability, they are of insufficient temporal and/or spatial resolution necessary for the detection of subtle deviations from the long-term trend (e.g. Jevrejeva *et al*., 2008; Woodworth *et al.,* 2009).

Geological methods (Shennan *et al*., 2015) extend sea-level histories beyond the limit of the instrumental record, yet lack the resolution necessary for identifying the onset of the accelerated rate of sea-level rise. Proxy information from temporally high-resolution sequences bridges the gap between instrumental observations and geological reconstructions. Such valuable proxy information for sea-level reconstructions derives from a number of sources (Shennan *et al.,* 2015). The most developed and widely utilised proxy sea-level data are sourced from intertidal microfauna which inhabit salt-marsh sediments. The virtue of these microfauna is that they exhibit a specific vertical zonation along the salt marsh surface which is intrinsically linked with tidal inundation, and they are readily preserved in the fossil record. The exploitation of this relationship has proven to be a valuable tool, facilitating quantitative determinations of the timing of sea-level accelerations and of the magnitude of variability (e.g. Gehrels *et al.,* 2005, 2008, 2012; Gehrels and Woodworth, 2013; Barlow *et al.,* 2013, 2014).

Previous reconstructions from salt-marsh archives invariably utilise foraminifera and/or diatoms as sea-level proxies (e.g. Gehrels *et al.*, 2005, 2006, 2008, 2012; Long *et al.* 2003, 2010, 2012; Edwards and Horton, 2000, 2006; Kemp *et al.,* 2009, 2011a; Barlow *et al.* 2012, 2013, 2014). A handful of recent studies have pioneered the proxy potential of salt-marsh testate amoebae, culminating in the first testate amoebae-derived sea-level reconstructions (Charman *et al.* 2010; Barnett *et al.* 2013). Increased reconstructive precision, compared to the more established proxies, indicated by these recent studies demonstrate the value of testate amoebae to the sea-level scientist's toolkit.

The rationale of this PhD project is to develop a new high-resolution sea-level record at a key site for studies of Holocene sea-level change (the Falkland Islands) through further pursuit of the proxy potential of salt-marsh testate amoebae. Thus, this thesis will: (i) develop a novel testate-amoebae derived sea-level reconstruction for the Falkland Islands combined with reconstructions using established proxies (ii) increase the understanding of the modern ecology of salt-marsh testate amoebae (iii) develop the methodological approach applied in the process of establishing sea-level histories from salt-marsh testate amoebae.

1.2 Research location and hypothesis

Instrumental observations and proxy data indicate that, during the 20th century, sea-level rise in the North Atlantic Ocean accelerated compared to average late Holocene trends reconstructed by geological methods (**Figure 1.2**; Gehrels *et al*., 2004; Bindoff *et al*., 2007; Donnelly *et al.* 2004; Gehrels *et al*., 2005; Kemp *et al.* 2011; Gehrels and Woodworth, 2013; Kopp *et al.* 2016). Gehrels *et al*. (2008, 2012) recently documented the inflexion in proxy records from New Zealand and Tasmania (**Figure 1.2**), giving rise to the hypothesis that the 20th century sea-level acceleration was global in extent

(Gehrels and Woodworth, 2013). Curiously, the magnitude of change in the rate of sea-level rise at the beginning of the 20th century is larger in the Southern Hemisphere sites than in the North Atlantic (**Table 1.1**; Gehrels and Woodworth, 2013).

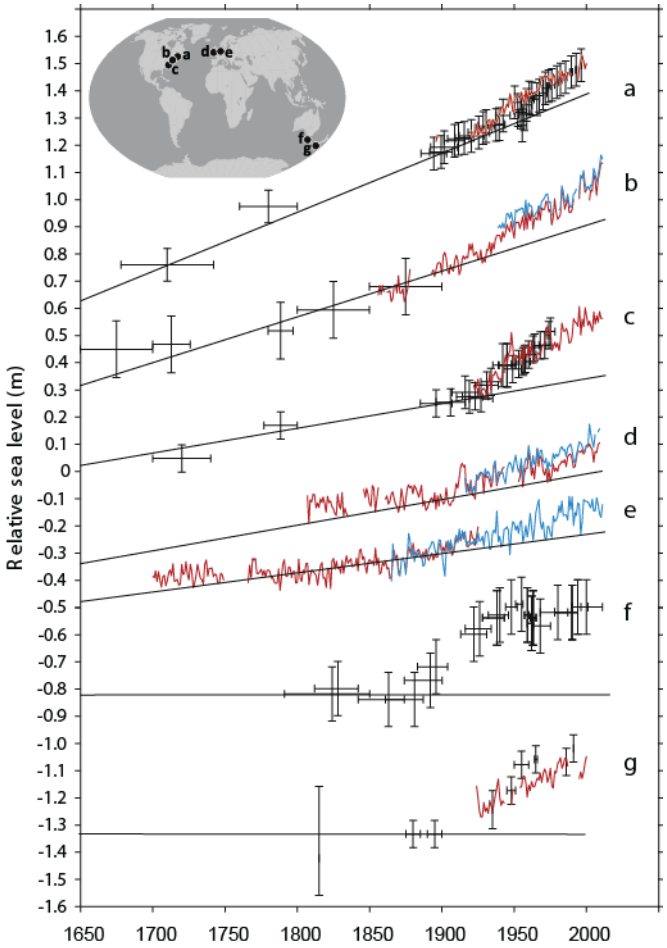

***Figure 1.2**: Recent sea-level changes (last 200-350 years) compared with late Holocene background trend of sea-level change (straight black lines) from five Northern Hemisphere and two Southern Hemisphere sites. Red and blue lines are tide-gauge records. Sea-level index points from proxy data are shown as crosses reflecting age and altitudinal uncertainties. a. Chezzetcook, Nova Scotia (Gehrels et al., 2005), with tide-gauge record from Halifax. b. Barn Island, Connecticut, USA (Donnelly et al., 2004), with tide-gauge records from New York City (red line) and New London (green line). c. Sand Point, North Carolina, USA (Kemp et al., 2009a, 2011), with tide-gauge record from Charleston, South Carolina. d. Tide-gauge records from Brest (red line) and Newlyn (green line) compared with late Holocene trend of relative sea-level change at Thurlestone, Devon, United Kingdom (Gehrels et al., 2011). e. Instrumental sea-level record from Amsterdam (red line) and tide-gauge record from Den Helder (blue line), compared with late Holocene trend of relative sea-level change at Schokland, the Netherlands (van de Plassche et al., 2005). f. Little Swanport, Tasmania, Australia (Gehrels et al., 2012). g. Pounawea southeastern New Zealand (Gehrels et al., 2008) with tide gauge data from Lyttleton.*

***Table 1.1**: Magnitudes of late 19th to early 20th century change in rate of sea-level change ('inflexion'). All data are from proxy records except the Permanent Service for Mean Sea Level (PSMSL) records which are from tide gauges (see www.psmsl.org). The differences between*

pre- and post-inflexion rates are greatest in the Southern Hemisphere, possibly indicative of a Northern Hemisphere ice melt source. From Gehrels et al. (2012).

Location	Latitude	Inflexion (Year AD)	Pre-inflexion (mm/yr)	Post-inflexion (mm/yr)	Difference (mm/yr)	Reference
SW Pacific						
SE New Zealand	46º29'S	1900-1940	0.3	2.8	2.5	Gehrels *et al.* (2008)
Tasmania	47º20'S	1800-1910	0.9	4.2(1900-1950) 0.7(1950-2000)	3.3	Gehrels *et al.* (2012)
NW Atlantic						
Nova Scotia	44º44'N	1900-1920	1.6	3.2	1.6	Gehrels *et al.* (2005)
Connecticut	41º20'N	1850-1900	1.0	2.8	1.8	Donnely *et al.* (2004)
N. Carolina	35º53'N	1879-1915	0.8	3.0	2.2	Kemp *et al.* (2009)
NE Atlantic						
N. Spain	30º23'N	1880-1920	0.3	1.9	1.6	Leorri *et al.* (2008)
Brest	48º28'N	1900	0.3	1.4	1.1	PMSL (2011)
Swinoujscie	55º55'N	1900	0.2	1.2	1.0	PMSL (2011)
Stockholm	59º19'N	1900	-0.5	-0.4	0.1	PMSL (2011)

Such spatial differences in the character of the onset of 20th century sea-level acceleration are potentially highly significant. Because the Earth is a rotating, self-gravitating planet ,sea-level change due to the melting of land-based ice is non-uniform (Farrell and Clark, 1976; Lambeck, 1989). Sea-level theory (Milne and Mitrovica, 1998; Mitrovica *et al.*, 2001; Thompson *et al.,* 2016) predicts that land-based ice melt produces increased rates of sea-level rise in the areas far from those which the melt source is located. The geometry of this spatial pattern of sea-level change is unique to each melt source and is known as a 'fingerprint'. The difference in the magnitude of sea-level change recorded in the North Atlantic Ocean compared to New Zealand and Tasmania is consistent with the fingerprint predicted from a Northern Hemisphere land-based melt source (Kopp *et al*., 2010; Thompson *et al.,* 2016). However, the greatest rates of sea-level rise as a consequence of Greenland melt are predicted to be in the South Atlantic Ocean, in the seas surrounding the Falkland Islands (**Figure 1.3a**). Furthermore, temporally-limited (continuous records are only

available since 1993) instrumental sea-level data from the Falkland Islands indicate a recent sea-level acceleration that is consistent with accelerations observed elsewhere (Woodworth *et al.,* 2010). The Falkland Islands are therefore a potentially important location for reconstructing recent sea-level rise that is derived from a northern (Arctic) melt source. Crucially, the Falkland Islands are in an area where any acceleration in the rate of SLR caused by Arctic land-based ice melt should be accurately detectable, because oceanographic processes that can obscure the signal are insignificant in this region (**Figure 1.3b**).

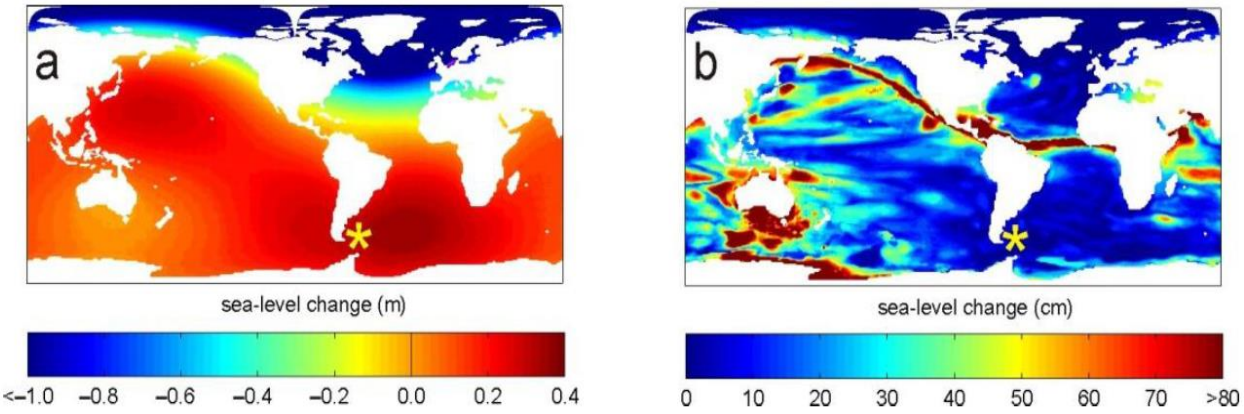

Figure 1.3*. (a) Pattern of additional sea-level change expected when 1 m of Greenland ice is melted.(b) Sea-level rise caused by Greenland ice melt required to exceed ocean 'noise' (static equilibrium and dynamic sea-level processes c.f. Kopp et al., 2010) and detect a fingerprint shown in (a) - this example is for a 0.1 Sverdrup model run, equivalent to 9 mm/yr sea-level rise. The Falkland Islands (yellow asterisk) occupy a strategic location because the Greenland melt signal is large (a) and ocean dynamical changes are small (b). Modified from Kopp et al. (2010).*

When considering longer (millennial) time scales, the Falkland Islands occupy a location in the South Atlantic Ocean that is key to understanding global Glacial Isostatic Adjustment (GIA) processes. Holocene relative sea-level (RSL) data from the

Falklands are not influenced by tectonics, local ice-loading effects and large tidal ranges, thus global GIA processes and ice-ocean mass flux are the dominant drivers of RSL change. The coastline of the Falkland Islands is in fact one of the few coastal locations in the world where the predicted middle and late Holocene RSL should be very close to the eustatic value and relatively insensitive to Earth model parameters (Milne and Mitrovica, 2008). The late Holocene RSL history of the Falkland Islands can therefore provide important information about sea-level variability during the Common Era, for example during the Medieval Climate Anomaly and the Little Ice Age. These data can be used to calibrate and test the validity of models that predict sea-level changes under scenarios of global climate change (e.g. Bittermann *et al*., 2013; Kopp *et al*., 2016).

A key deliverable of this project is a proxy-based (geological) reconstruction of Holocene sea-level change in the Falkland Islands, including a (sub-)centennial sea-level reconstruction for the late Holocene. These sea-level reconstructions will allow the testing of the following hypothesis: that the early 20th century acceleration in the rate of SLR had a significant contribution from Northern Hemisphere land-based ice melt.

1.3 Aims and objectives

In order to test the aforementioned hypothesis this project aims to establish a novel relative sea-level reconstruction spanning the late Holocene epoch, inferred from microfaunal salt-marsh proxies, for the Falkland Islands. Along with utilising the 'established' sea-level proxies (diatoms and foraminifera), a key focus of this project is on developing testate amoebae as proxy indicators of sea level. To achieve this, a modern 'training set' of testate amoebae is to be applied, using the transfer function (predictive palaeoecological model) methodology, to dated fossil assemblages from a

Falkland Islands salt marsh. Complementarily, this study investigates the modern ecology of testate amoebae and the seasonal factors influencing their distribution in surficial salt marsh sediments, in order to better understand their suitability as proxy indicators of sea level. To fulfil this, salt-marsh testate amoebae assemblages are to be monitored for seasonal influences on community compositions. The precise aims and objectives of this thesis are detailed in the following sections.

1.3.1 Aim 1 – To produce a high resolution relative sea-level record for the Falkland Islands inferred from intertidal salt-marsh litho-, bio- and chrono-stratigraphy.

Objectives:

- Establish the lithostratigraphic context of the salt marsh with a transect of sediment cores
- Interpret the cored strata through a combination of sedimentological analysis and micropalaeontological inference
- Collect surface (modern) samples encompassing the entire elevational gradient and core (fossil) samples
- Ascertain microfaunal (testate amoebae, foraminifera and diatom) assemblage compositions for each modern and fossil sample
- Quantitatively define the relationship between the modern assemblage data and sea level by developing predictive models (transfer functions) of this relationship
- Apply the transfer functions to the fossil assemblage data in order to reconstruct the contemporaneous sea level for each fossil sample

- Develop a chronostratigraphy to temporally resolve the reconstructed sea levels through the application of a suite of dating techniques to the sampled sediment core.

1.3.2 Aim 2 – (i) to investigate seasonal patterns in contemporary distributions of live and dead salt-marsh testate amoebae over one seasonal cycle; and (ii) to determine the implications of seasonality for future contemporary sampling strategies associated with sea-level studies

Objectives:

- Establish a set of sampling stations that are representative of all marsh sub-environments that testate amoebae inhabit
- Over one annual cycle, collect monthly surficial sediment samples from each station
- Record the live and deceased testate amoebae assemblages in surficial samples for each sampling period
- Discern variations in live and dead populations, species diversity and species concentrations over the seasonal cycle
- Develop transfer functions which comprise samples taken in each season

1.4 Synthesis

Detailed records of late Holocene sea-level variability are critical for understanding the climate-related impacts of sea-level rise. This understanding is fundamental for providing a plausible context from which to consider future scenarios of sea-level

change. To date, the majority of detailed sea-level records are from Northern Hemisphere locations, with a paucity of high-quality data from the Southern Hemisphere. However, the limited number of comprehensive late Holocene sea-level records from the Southern Hemisphere provide evidence of a recent climate-related acceleration in the rate of sea-level rise which is greater in magnitude than that observed in the Northern Hemisphere. Such spatial differences in the character of recent sea-level change are potentially highly significant as they provide crucial information on the response of Northern Hemisphere ice sheets to recent increases in global mean temperatures, yet, these differences remain relatively uninvestigated. The Falkland Islands present an ideal opportunity to investigate accelerated sea-level change in an important Southern Hemisphere location where a Northern Hemisphere ice-melt signal should be easily detectable. The primary focus of this PhD project therefore seeks to improve the understanding of recent sea-level changes in the Southern Hemisphere. To this end, this research pursues high-quality records of late Holocene sea-level change in the Falkland Island reconstructed by geological methods applied to salt-marsh sediments. Complementary to this, the secondary focus of this research intends to further develop the application of testate amoebae as sea-level indicators through better understanding of the environmental controls on contemporary salt-marsh distributions.

Chapter 2 – Literature Review

2.1 Introduction

Reconstructing sea-level histories from salt-marsh proxies is established upon research which spans numerous disciplines. This chapter comprehensively reviews the published literature relevant to the central aims of this PhD project. Sections are dedicated to: (1) reviewing recent sea-level changes in the Southern Hemisphere with particular focus on the Falkland Islands; (2) the virtues, challenges and application of salt marshes and their associated microorganisms (particularly testate amoebae) for reconstructing sea-level changes; (3) statistical methods for quantifying sea-level changes reconstructed from proxies; and (4) methods for dating Holocene sea-level records.

2.2 Recent sea-level changes in the Southern Hemisphere

Long tide-gauge records (e.g. Woodworth *et al.* 2009) and sea-level reconstructions (e.g. Gehrels and Woodworth, 2013) indicate a 20th century acceleration in sea-level rise (SLR) that is likely global in extent. In the Southern Hemisphere, the instrumental records (**Figure 2.1**) are invariably of insufficient duration for the identification of significant deviations from Holocene linear sea-level trends (e.g. Watson, 2011). In fact, only three tide gauges which span the late 19th/ early 20th century period were operational in the Southern Hemisphere (Fremantle, Australia (since 1897), Fort Denison, Australia (since 1886) and Dunedin, New Zealand (since 1900)). It is not possible to identify the presence (or absence) of an early 20th Century sea-level acceleration in these tide gauge records because the period of measurement before the turn of the 20th century (max. 14 years) is too short to account for decadal sea-level variability in the pre-20th century trends (c.f. Douglas, 2001).

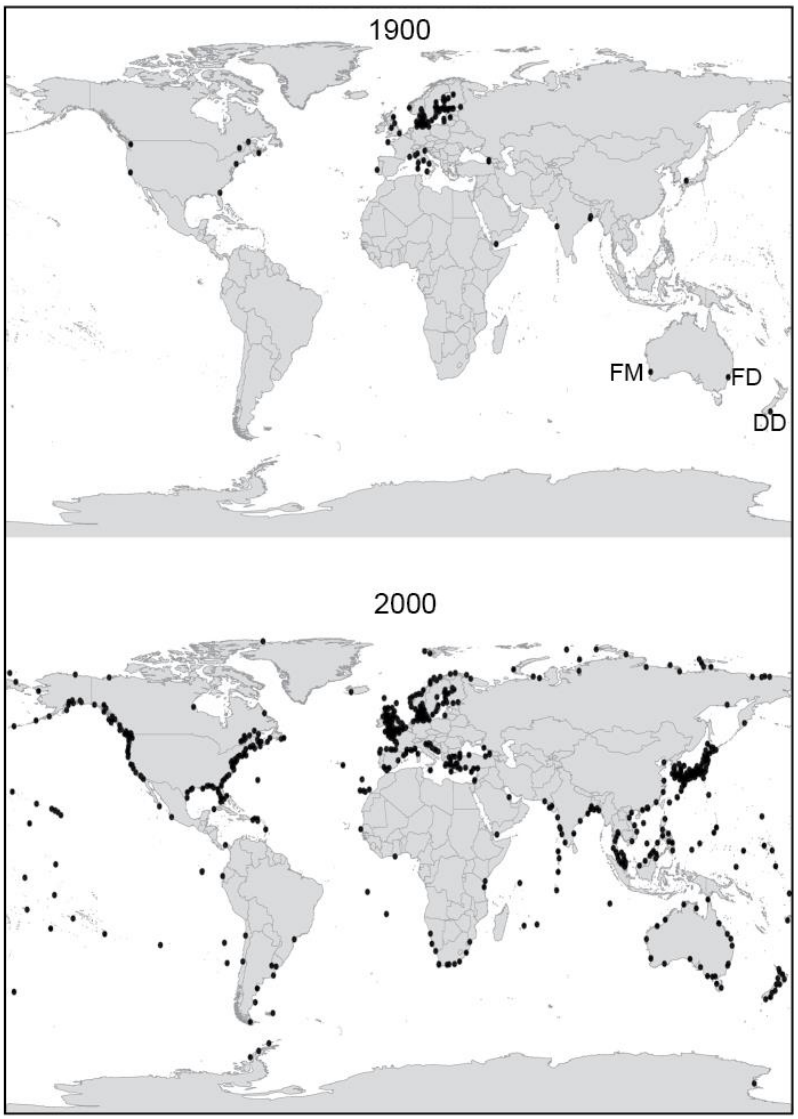

Figure 2.1: Map showing global distribution of tide gauges in 1900 (top) and 2000 (bottom). Note there are just three Southern Hemisphere tide gauges in 1900: Fremantle (FM), Fort Denison (FD) and Dunedin (DD). Data source: Permanent Service for Mean Sea Level (http://www.psmsl.org/data).

To date, there are no sea-level reconstructions (of sufficient resolution to detect an acceleration) from the south Atlantic or southwest Pacific regions which span the late 19th/ early 20th century period. However, a limited understanding of Southern Hemisphere sea-level changes during the last two centuries has been augmented by a few recent reconstructions from the southeast Pacific region (Smithers and Woodroffe, 2001; Gehrels *et al*. 2008, 2012; Godwin *et al.* 2008; Fadil *et al.* 2013).

The coral microatoll reconstruction of Smithers and Woodroffe (2001) indicated that for the eastern Indian Ocean there was little net change in SLR for the twentieth century with the rate over that period (0.35 mm/yr) significantly lower than that reflected in the globally aggregated instrumental records. However, in more southerly localities Gehrels *et al.* (2008, 2012) document clear inflexions in the rate of SLR at the turn of the twentieth century, based on salt-marsh reconstructions. Gehrels *et al.* (2008) recorded an acceleration in southeastern New Zealand from 0.3 ± 0.3mm/yr between AD1500-AD1900 to 2.8 ± 0.5mm/yr for the twentieth century. A similar pattern of sea-level change was documented in the Tasmania record of Gehrels *et al.* (2012) where sea level was stable (at slightly below present) for the mid- late Holocene followed by a significant acceleration at the onset of the twentieth century at rates of 4mm/yr from between 1880-1900 until the 1950s when the rate slowed significantly.

To date, the two studies of Gehrels *et al.* (2008, 2012) are the only Southern Hemisphere records which capture a twentieth century acceleration in the rate SLR. Both records observe a magnitude of acceleration significantly greater than that observed in the North Atlantic reconstructions (Donnelly *et al.* 2004; Gehrels *et al*., 2005; Leorri *et al.,* 2008; Kemp *et al.* 2011; Gehrels and Woodworth, 2013) which is consistent with a spatial pattern that would be expected for a significant contribution to GMSL rise from Northern Hemisphere ice melt in the early twentieth century (cf. Kopp *et al*., 2010). In New Zealand, Fadil *et al.* (2013) found that when the salt marsh sea-level reconstructions of Gehrels *et al.* (2008, 2012) were corrected for vertical land motion the 20th century rates of sea level rise in these records were twice the rates observed in tide gauge records for New Zealand. However, the reasons for these discrepancies are not understood. This highlights the importance of establishing more geological records of recent sea-level change for the Southern Hemisphere.

2.2.1 Holocene and recent sea-level change in the Falkland Islands

The Falkland Islands are an archipelago of islands located on the Patagonian continental shelf about 500 km east of mainland South America. Unlike coastal locations in southernmost South America (Rostami *et al*., 2000, Bentley and McCulloch, 2005; Milne *et al*., 2005), Holocene sea-level data from the Falklands are minimally influenced by tectonics, local ice loading effects and large tidal ranges. To date, there are no high-quality Holocene sea-level data for the Falkland Islands. Several raised beach deposits between 1 to 8 m above present mean sea level (MSL) have been reported from East Falkland (Adie, 1953; Roberts, 1984). The highest (6 to 8 m MSL) of the raised beaches identified by Roberts (1984) is dated with a single radiocarbon date at Stanley. Here, a cliff section comprising bedded quartz which coarsens upwards is overlain by a cobble layer and capped with peat. The base of the peat is dated 3680 +/- 40 BP at 7m above MHW. The peat is 0.5 m thick. Relating this date to a former sea level is very difficult, since the indicative meaning (the height relationship between the dated level and the contemporaneous tide level) is not known, but indicates sea levels were 6 to 8 m higher some time before 3.6 ka BP. However, the presence of Holocene sea-levels significantly above present is not in accordance with geophysical model RSL predications for the Falkland Islands (**Figure 2.2**.) Holocene RSL predictions for the Falkland Islands (**Figure 2.2**) are based on output from models by Peltier's lCE5G model (Peltier,2004), the Holocene ice-volume equivalent sea level (ESL) model of Bradley *et al*. (2016) and with predictions using the ocean mantle parameters (taB) of Lambeck *et al*. (2014) and a continental mantle model (cdB) of Lambeck *et al*. (in review). Predictions shown in **Figure 2.2** are based on the following 'plausible' mantle properties for the Falkland Islands (Kurt Lambeck, personal communication): the VM2 viscosity profile (Peltier, 2004) which has an

elastic lithosphere thickness of 90 km, and a multi-layer mantle viscosity profile with mean values of ~4-5 × 10^{20} Pa s in the upper mantle and ~2 × 10^{21} Pa s in the lower mantle; and the 120p510 viscosity profile (120 km lithosphere thickness, 1 x 10^{21} Pa s upper mantle viscosity and 50 x 10^{21} Pa s lower mantle viscosity) for the Bradley *et al.*(2016) model. Geophysical models predict a rapid early Holocene sea-level rise in the Falkland Islands which decelerates between ca. 7.5 to 5.5 ka, after which RSL generally rises until present. However, the Lambeck *et al.* (2014 [taB]) and ICE5G_VM2 (Peltier, 2004) models predict early Holocene RSL rise culminating in small highstands (<0.5m above present, around 5 and 4.5 ka respectively) and a gradual RSL fall until present.

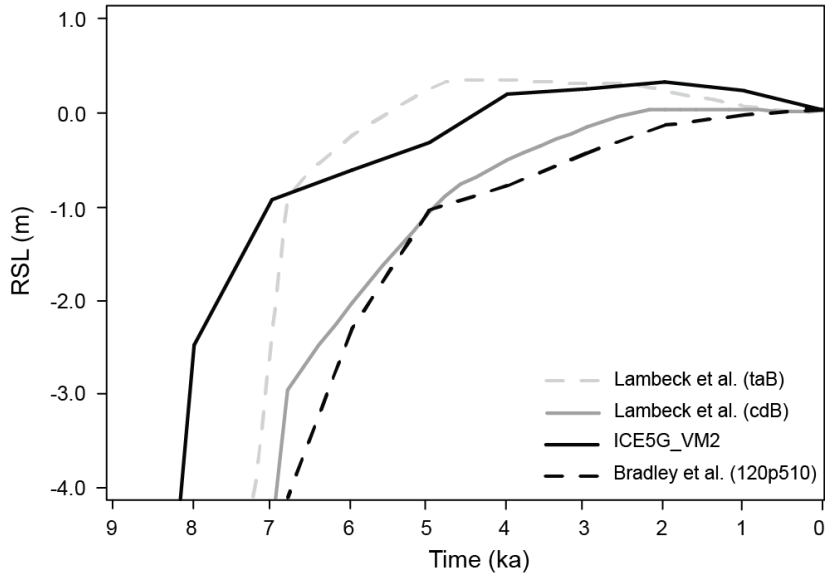

Figure 2.2: *Geophysical model predications of relative sea-level changes in the Falkland Islands from 8ka to present. Model parameters described in the text. Sources: Lambeck et al. (2014[taB], 2017[cdB]) Peltier (2004[ICE5G_VM2]), Bradley et al. (2016).*

There are no continuous instrumental records of sea-level change for the Falkland Islands prior to 1993. However, Woodworth *et al.* (2010, 2011) were able to determine the rate of sea-level change between historical measurements taken by James Clark

Ross at Port Louis, Eastern Falkland in 1842 and short tide gauge records from Berkeley Sound, Eastern Falklands in the early 1980s, in comparison with the rate of SLR observed since 1992 (**Figure 2.3**). It is suggested by Woodworth *et al.* (2010, 2011), that there has been a relatively recent acceleration in the rate of SLR indicated in the tide gauge and satellite altimetry records since 1992 which measure 2.60 ± 0.58 mm/yr and 2.79 ± 0.42 mm/yr. However, there is a lack of data before 1842 coupled with the large gap and paucity of data in the historical measurements from the Falkland Islands. Therefore it is a critical necessity that high-quality geological data is sought in order to determine the Holocene background rate of SLR and to identify with confidence any acceleration in the rate of SLR that is consistent with other records.

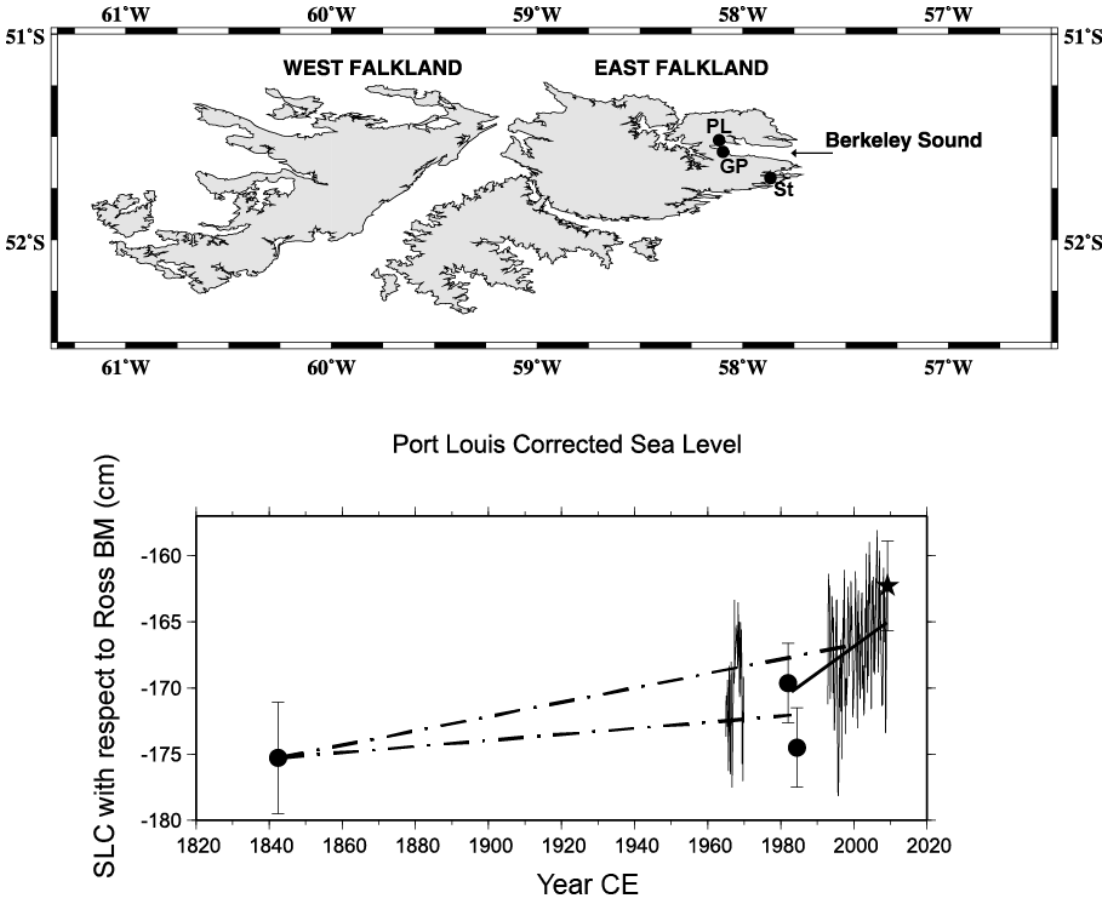

Figure 2.3*: Values of corrected sea level (SLC) in Berkeley Sound, Falkland Islands averaged over each period of measurement in 1842 (Port Louis [PL]), 1981–1982 (Green Patch[GP]), and 1984 (Port Louis) (dots). Values are shown relative to the height of the Ross benchmark (Port Louis) and are adjusted for the average seasonal cycle in SLC. The star indicates SLC*

during a fortnight measurement period at Port Louis in February–March 2009. Also shown are monthly mean values of SLC from tide gauges at Stanley. Stanley data have been aligned with those from Port Louis. The lower dash-dotted trend line connects the 1842 value to the 1981–1982 and 1984 values, whereas the upper dash-dotted line connects the 1842 value to the average of the Stanley SLC data since 1992. The solid line is a linear fit to the Stanley SLC data since 1992 extrapolated back to the early 1980s. See source paper for details of the methods employed and uncertainty derivations: Woodworth et al. (2010).

2.3 Reconstructing relative sea-level histories from saltmarsh sediments

Instrumental observations of sea-level change are limited in their spatial and temporal resolutions. Therefore reconstructions of relative sea-level change (RSL: the observed change in mean sea level at a particular locality relative to the level of the land) over recent geological time are crucial for placing modern rates of sea-level change into context and informing future predictions (e.g. Schaeffer *et al.* 2012; Gehrels and Woodworth, 2013). Salt marshes contain within their sediments a suite of flora and fauna which are intrinsically linked to sea level. Thus these organisms (e.g. testate amoebae, diatoms and foraminifera) serve as proxy indicators, providing a means to reconstructing RSL through time in order to address the gaps in the instrumental record (Shennan *et al.* 2015). This section reviews the surrounding literature on salt-marsh ecosystems, with emphasis on the application of salt marsh archives in studies of late Holocene sea-level change.

2.3.1 Saltmarsh geomorphology

Salt-marsh ecosystems are often found in mid to high latitude low-energy, coastal

environments and tidal estuaries (Allen and Pye, 1992; Allen, 2000). Geomorphological models show that in such sheltered environments, salt-marsh growth (by sediment accretion) initiates on top of an unvegetated mud or sand flat (Redfield, 1972; Allen, 2000). Following initiation the salt marsh develops characteristic halophytic, vascular vegetation patterns which mark the transition from marine to terrestrial environments. Due to the nature of this position between the marine and freshwater domains, salt marshes display a strong environmental gradient encompassing marine, brackish and freshwater realms related to marsh surface elevation and the tidal prism. Marsh surface height and the rate of vertical accretion are primarily controlled by the supply and characteristics of local tidal sedimentation, plant productivity and the nature of tidal inundation (Redfield, 1972; Allen and Pye, 1992; Allen, 2000).

Fundamentally, salt marshes exhibit an ability to maintain surface elevation in line with moderate rates of SLR as the vegetation reduces water turbulence, trapping suspended sediments and contributing organic matter to the sediment column (Redfield, 1972; Allen, 2000; Orson *et al.* 1998; French, 2006). This ability allows sea-level changes to be recorded within the stratigraphy of the salt-marsh sediments. If the rate of sedimentation is greater than the rate of SLR, marsh surface elevation increases relative to the tidal levels and a regressive sequence is recorded in the stratigraphy. Conversely, a transgressive facies is recorded when the rate of SLR is more rapid than the rate of accretion and the marsh surface is lowered relative to tidal levels (van de Plassche, 1991; Gehrels *et al.* 2005).

In the face of rapidly rising sea levels, the marsh elevation equilibrium may decline toward a lower limit. Also, the frequency and duration of tidal flooding may increase, negatively impacting the vegetation and increasing susceptibility to sediment erosion

as a result of increased wave action upon the flooded surface (Donnelly and Bertness, 2001; Mariotti and Fagherazzi, 2010). Notwithstanding this, if the character of the surrounding land permits, the salt marsh may migrate inshore as the lowermost elevations are replaced by open water or inter-tidal mudflats and the mid-upper marsh vegetation is replaced by low-marsh flora (Donnelly and Bertness, 2001). However, there remains concern surrounding the maximum threshold for the rate of RSL rise that a marsh can survive (e.g. Reed, 1995; Craft *et al.* 2009). Kirwan *et al.* (2010) use a modelling approach to determine the limits on marsh adaptability to rapidly rising sea level. The results of Kirwan *et al.* (2010) suggest that tidal range and suspended sediment concentrations play an important role in the ability of a marsh to survive rapid rates of SLR. Marshes with higher tidal ranges and suspended sediment concentrations may survive SLR rates of up to ~10mm/yr. However, for marshes with low tidal ranges and/or low suspended sediment concentrations the threshold rate of SLR is ~5mm/yr. Finally, the modelling results suggest that marsh drowning occurs ~30-40 years after the threshold rates are exceeded (Kirwan *et al*., 2010, 2013).

2.3.2 Saltmarshes as relative sea-level archives

In recent decades a standard method for reconstructing palaeosea-level positions from coastal sediments based on lithostratigraphic and biostratigraphic data has been established (van de Plassche, 1986; Shennan *et al.* 2015). This method establishes sea-level index points (SLIPs) which are data-points that fix the elevation of past sea level temporally and spatially; from a series of these data-points sea-level curves can be created (Tooley, 1978; van de Plassche, 1986; Shennan 1986; Shennan and Horton, 2002). In order to validate a SLIP the following requirements are essential: the sample requires a location, an age, a measured elevation and the elevation relative to

the relationship with modern tide level (termed ‘indicative meaning’): and a tendency (van de Plassche, 1986; Barlow *et al*. 2013). The tendency of a SLIP is the increase (positive sea level tendency) or decrease (negative sea level tendency) in marine influence demonstrated by the SLIP (Barlow *et al.* 2013; Shennan, 2015).

For example, as a result of early Holocene deglaciation, post-glacial RSL rise opened up new accommodation space on marsh surfaces, enabling the growth of thick transgressive sequences of salt-marsh sediments (Allen, 2000). Because of the mechanistic link between RSL and the accumulation of coastal sediments, the relationship between the altitude of sedimentary sequences and their age provides an initial stratigraphic set of SLIPs from such sequences (e.g. Kidson and Heyworth, 1976; Shennan 1986). However, due to the inherently large uncertainties associated with age and altitude determinations based on stratigraphic derivations of indicative meaning, it is only possible to produce a generalised curve of RSL over the period of study (see: Edwards, 2004; Waller *et al.* 2006). Therefore, the identification of subtle, sub-millennial scale, RSL variability necessitates the investigation of the changes in microfossil assemblages over- or underlying a SLIP in combination with the litho- and chronostratigraphical data, thus providing a continuous record of RSL.

2.3.3 Sources of error

It is important that all sources of error are recognised and, where appropriate, quantified as they have the potential to impinge the interpretation of a sea-level reconstruction. There are a number of inherent vertical errors associated with SLIPs (see: Shennan, 1986; Shennan *et al.* 2015) that should be accounted for. Contamination errors and compression of the sediment during penetration are associated with the coring equipment used. There are also vertical errors associated

with levelling; however, these can be reduced by using precise levelling equipment. Moreover, if samples are collected from one site and therefore levelled to the same datum (as if often the case in salt marsh sea-level studies) levelling errors are insignificant (Gehrels *et al.* 2008). The effect of tidal range change through time has the potential to impact the accuracy of the reference water level assigned to a SLIP as salt-marsh microfauna exhibit different vertical assemblages dependent on tidal regime (e.g. Barlow *et al.* 2013). Understanding palaeotides requires complex modelling (e.g. Uehara *et al.* 2006) however, for studies of recent (middle to late Holocene) sea-level change, tidal range chage is assumed to be minimal (e.g. Gehrels *et al.* 2005).

Autocompaction i.e. compression of a sedimentary unit under its own weight or the weight of overlying sediment (Kaye and Barghoorn, 1964; Brain *et al.* 2011; Tornqvist *et al.* 2008) is potentially a large source of error. If autocompaction is present and not corrected for, SLIPs will be lowered from their depositional elevation resulting in an overestimation of the inferred rate and magnitude of RSL change (Brain, 2006, 2015; Edwards, 2006; Long *et al.* 2006). The many variables involved in the process of compaction (Pizzuto and Schwendt, 1997; Allen, 2000; Brain, 2006) make quantification of, and subsequent correction for, autocompaction difficult. Measurements of sediment bulk density provide a means of identifying post-depositional compaction (Gehrels *et al.* 2008; Brain *et al.* 2011; Brain 2015). Furthermore, Brain *et al.* (2012) modelled the effects of sediment compaction on salt marsh reconstructions of recent SLR. The results of this modelling suggest that the effect of autocompaction is significant in transgressive sequences, particularly those >1m thick, but shallow (<0.5m thick) regressive sequences experience insignificant amounts of compaction.

2.4 Microfossils: the key to interpreting sub-centennial sea-level change

The application of microfossils to palaeosea-level reconstructions subscribes to the uniformitarian principle that understanding the present is the key to interpreting the past. As a result of the strong environmental gradient in intertidal environments, salt-marsh flora and fauna display a distinct vertical zonation on the salt-marsh surface relative to tidal datum (e.g. Redfield, 1972). Thus, the identification of characteristic intertidal sub-environments permits these organisms to serve as indicators of sea level. The microorganisms foraminifera, diatoms and testate amoebae are amongst the most valuable of these indicators as they are readily preserved ((sub)fossilised) in salt-marsh sediments (e.g. Scott and Medioli, 1978; Gehrels, 1994; Charman *et al.* 1998; Gehrels *et al.* 2001; Roe *et al.* 2009). The identification of the zones at which particular species exist makes it possible to assign an indicative meaning (IM) to a sample based on the microorganism assemblage contained within it. The IM has two components, the indicative range (the vertical range at which the sample may occur) and a reference water level within the tidal frame (mid-point of the indicative range). The IM of foraminifera coupled with vegetation zones has been applied to fossil sequences to produce detailed reconstructions of RSL (e.g. Gehrels, 1994). This approach has been extended in the light of statistical methods developed by Imbrie and Kipp (1971) applying palaoenvironmental transfer functions to fossil assemblages (e.g. Guilbault *et al.* 1995; Gehrels, 1999; Zong and Horton, 1999; Gehrels *et al.* 2005, 2006, 2012; Massey *et al.* 2006; Kemp *et al.* 2009b, 2011a). Transfer functions shall be discussed in more detail in subsequent sections.

2.4.1 Testate amoebae

A central aim of this project is to develop and improve the application of testate amoebae to quantitative reconstructions of RSL from salt-marsh sediments. Testate

amoebae (Protozoa: Rhizopoda) are microscopic (15-300 µm) test-forming organisms abundant in a variety of moist soils, freshwater and brackish environments. They have been recognised and applied as environmental indicators in lacustrine and peatland sediments for >100 years (Blytt, 1876; Lagerheim, 1902; Weber, 1900; Sernander, 1908). However, it was not until the latter half of the 20th century that interest in these organisms as palaeoenvironmental indicators advanced; stimulated by more recent ecological and statistical work (Charman and Warner, 1992, 1997; Woodland *et al.,* 1998; Charman *et al*., 2000a; Lamentowicz, 2007). This quantitative, statistical work focused on reconstructions of peatland hydrology. In the last decade or so, pioneering work on the salt-marsh ecology of testate amoebae has been conducted (e.g. Charman *et al.* 1998; Roe *et al*. 2002; Gehrels *et al.* 2006b; Charman *et al*, 2010; Ooms *et al*. 2011, 2012) with the intention to apply them as palaeo sea-level indicators. Despite this, recent focus on the distribution of salt-marsh testate amoebae, their robustness and practicalities for sea-level reconstructions are relatively unexplored. This section reviews the systematics, morphology, palaeoenviromental applications and pioneering investigations of salt-marsh testate amoebae; providing a context for the application of testate amoebae in reconstructing recent sea-level change, to fulfil the aims of this study.

2.4.2 Testate amoebae systematics

The classification of protozoa has changed often due to taxonomic revisions in light of new research over time (c.f. Tolonen, 1966; Whittaker, 1968 and; Pawlowski and Burki ,2009; Adl *et al.* 2012). Under the modern classification scheme (see: Sleigh, 1973; Pennisi, 2003) testate amoebae belong to the superclass Protozoa (**Figure 2.4**). The term Protozoa is of Greek origin meaning first (*proto*) animal (*zoion*) which alludes

to the fact that, like all Protozoa, testate amoebae display the simplest cellular organisation of the animal kingdom (although technically, under the modern classification system they belong to the kingdom Protista (Whittaker, 1969; Sleigh, 2003)). It is reported that there are ~80,000 species of Protozoa, of which ~50% have solely been described in the fossil record (Sleigh, 2003). Of this there are ~15,000 described species of amoebae and amoeboid protists (Adl *et al*. 2007). It should be noted that Protozoa are not an indigenous evolutionary group, but have previously been grouped together for amenity, hence why this group is almost constantly under revision (e.g. Adl *et al.* 2012; Kosakyan *et al.* 2013).

Testate amoebae belong to a polyphyletic group, meaning they derive from several ancestral types (Beyens and Meisterfeld, 2002), based primarily on pseudopodia morphology. Testate amoebae are distinguished from other amoeboid protozoa because they are encapsulated within a shell (test). Under the modern classification scheme, the majority of testate amoebae are classified within the new phyla Amoebozoa, Cercozoa or Rhizaria belonging to the subphyla *Lobosa* (class: *Testacealobosia*), *Filosa* (classes: *Imbricatea, Thecofilosea* and *Granofilosea*) and *Endomyxia* (class: *Gromiidea*) (Cavalier-Smith, 2002; Adl *et al*. 2005, 2012; Pawlowski and Burki, 2009;). However, there are a few exceptions, for example the genus *Amphitrema* (abundant in *Sphagnum* peat) is classified within the phylum Heterokonta. These subclasses are recognised as testate amoebae and are the only non-marine test-forming Protozoa where the shell (test) encapsulates the single-celled amoebae. Some earlier authors (e.g. Tolonen, 1966, 1986; Scott *et al*. 1991; Medioli *et al*. 1999) used the terms Rhizopods, Arcellaceans or Thecamoebians when describing these organisms in coastal and lacustrine sediments, because these terms allude to a single phylum or superclass, it is more appropriate to apply the name ‘testate amoebae’ which is the prevalent nomenclature in the more recent literature

(Charman, 2015; Barnett *et al.* 2017).

In light of the most recent taxonomic research utilising small subunit ribosomal RNA (SSU rRNA) genes to explore microbial taxonomy (e.g. Cavalier-Smith, 2010; Pawlowski and Burki, 2009; Adl *et al.* 2012) an attempt has been made to summarise the phylogeny of the major testate amoebae taxa (**Figure 2.4**). This is by no means a categorical taxonomy with some common taxa lying outside the phyla included (e.g *Amphitrema*, as previously mentioned), but it does account for the majority of species.

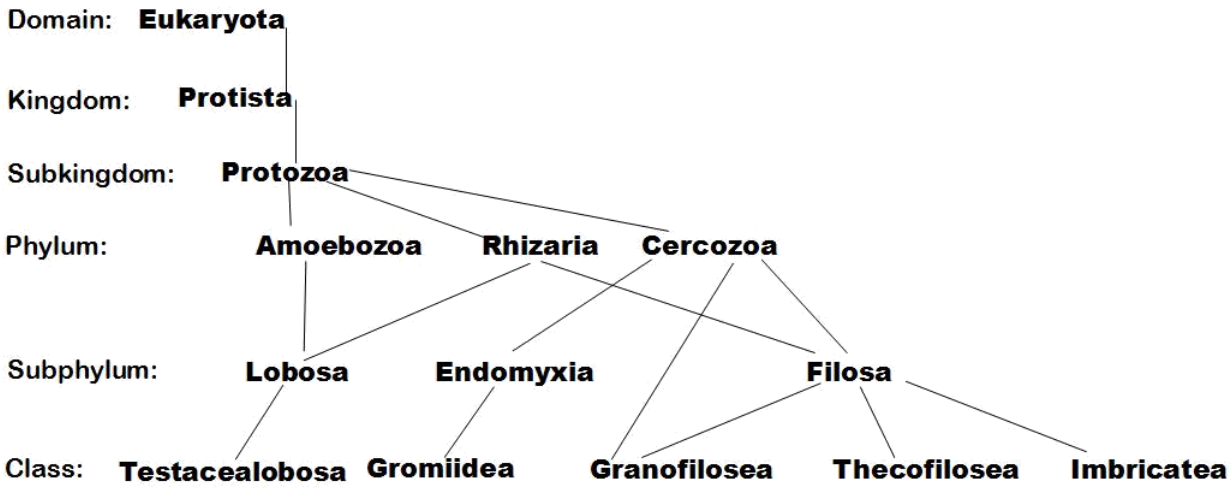

***Figure 2.4**: Taxonomic classification of testate amoebae to class level.*

2.4.3 Testate amoebae morphology

As the overview on the systematics has demonstrated, testate amoebae are not a straightforward taxonomic group. For palaeoenvironmental applications they are best defined as morphospecies (classified by the characteristics of the test). It is therefore pertinent to stress here that the use of the term 'testate amoebae' throughout this thesis refers to all test-forming non-marine taxa of single-celled protozoa. The 'test' is

reference to the shell that encapsulates the living cell which is composed of the nucleus and surrounding cytoplasm. Tests have at least one aperture from where the pseudopodium extends. The test is the most important element for palaeoenvironmental applications as this is the structure preserved in the fossil record. Several types of test exist, referred to as xenosomic (agglutinated) or idiosomic (autogenous), depending on the nature of materials used in their construction. Xenosomic tests are those which are constructed from materials sourced from the environment that the amoeba inhabits, which may include siliceous grains, pollen grains, diatom frustules, or any other available detritus *(*Charman *et al.*, 2000b; du Châtelet, 2010). Idiosomic tests are composed of materials secreted by the parent amoebae during reproduction (usually by asexual binary fusion). The test produced in the construction of idiosomic tests can be smooth proteinaceous, pre-formed siliceous plates (referred to as idiosomes), pseudochitinous or mucopolysaccharide material (Charman, *et al.* 2000). Some larger idiosomic taxa may consume smaller taxa and recycle the plates in the construction of their test. Medioli *et al*. (1987) demonstrated that some taxa that are usually considered xenosomic are able to produce tests entirely by secretion when starved of available construction materials.

Due to the versatility of testate amoebae in the production of their tests, adapting to the availability of materials in their environment, species definitions based on test material are inherently dubious; this is particularly problematic for the biological taxonomy described earlier. However, different test constructions are useful in defining morphospecies for palaoenvironmental applications. Moreover, as the availability of materials used in the assembly of tests is a function of environmental parameters, then species definitions based on test material can be of value when assemblages are used to interpret palaoenvironmental conditions in fossil studies (Charman *et al*., 2000b). Charman (1999) identifies five principal problems related to the morphology of testate

amoebae in fossil studies (summarised in Charman, 2001; Charman *et al.,* 2000b):

1. Effects of fossilisation on test preservation
2. Morphological variability within taxa
3. Identification is based solely on test characteristics, not on the pseudopodia (as in higher taxonomy), which can be critical
4. Visibility of distinguishing features on specimens mounted using standard techniques (e.g. Hendon and Charman, 1997). Orientation and lack of manoeuvrability under the coverslip may limit taxonomic precision.
5. Counting of statistically significant numbers of tests.

Some of these problems are easy to overcome if an advised methodology is implemented throughout the study. Some are inevitably perennial, affecting the environmental indicator-value of particular taxa and should be considered when making inferences from such proxy data. Perhaps the greatest problem is the poorly understood taphonomy of testate amoebae, especially in salt-marsh environments. *A priori* reasoning would lead one to assume that the degree of preservation, or lack thereof, would relate to the composition (idiosomic versus xenosomic) of the test. However, Medioli and Scott (1988) found that xenosomic tests were better preserved compared to idiosomic tests. Nonetheless, Hendon and Charman (1997) demonstrated that some idiosomic tests were better preserved than xenosomic when subjected to the harsh chemical treatment used in palynological studies. Mitchell *et al.* (2008) investigated the issue of fossil preservation for peatland and fenland testate amoebae. The results of the study were somewhat inconclusive, suggesting that differential preservation has little impact on palaeohydrological reconstructions from *Sphagnum*-dominated peatlands. Adversely, in minerotrophic peatlands, differential preservation lead to a consistent underestimation in the reconstructed

palaeohydrological values. The effect of differential preservation in salt marshes is not well known, owing to the comparatively limited research into fossil salt-marsh testate amoebae, which shall be discussed in more detail later.

Charman *et al.* (1998) report small spatial scale variability between the composition of living and deceased assemblages along a salt-marsh surface. This suggests that there is little post-mortem transportation of tests along the salt-marsh; although the taphonomic processes governing fossil assemblage composition require further investigation in order to confirm this. Roe *et al*., (2002) studied fossil testate amoebae from a range of coastal depositional environments. They found that results were mixed, with some sites displaying a fossil assemblage analogous to the contemporary assemblage, and some fossil assemblages having poor modern analogues. Furthermore, the majority of sites in the study had a sparsity of fossil tests, the implications of this shall be discussed further subsequently. Likewise, studies of salt-marsh foraminifera demonstrate that differential preservation of fossil tests, related to test composition, is common (e.g. Louiser and Parkinson, 1981; Jonasson and Patterson, 1992; de Rijk, 1995). In an attempt to overcome this problem, often only the deceased foraminiferal assemblages are included in the modern training set (e.g. Horton *et al.* 1999; Edwards *et al.,* 2004). Moreover, it has been demonstrated that selective preservation of agglutinated foraminifera (dominant in salt-marshes) has an insignificant influence on modern assemblage composition (Culver and Horton, 2005).

Morphological variability within taxa, if unchecked, has the potential to detrimentally affect the reliability of palaeoenvironmental reconstructions using testate amoebae if species are incorrectly identified. This is largely dependent on the intraspecific morphological variability accepted by the researcher (Charman, 1999). While the

development of SSU rRNA, discussed earlier, may go some way resolving morphological diversity versus genetic diversity in contemporary specimens, it does little to aid the assessment of fossil diversity as genetic material is rarely preserved. The best solution to overcome the problem of morphological diversity is the adoption of a practical taxonomic scheme for the identification of testate amoebae during routine counting (e.g. Charman *et al.* 2000b; Booth and Sullivan, 2007), the exact scheme used in this study shall be discussed in detail in later chapters. The methodology chapter shall also discuss adjustments made to the preparation and mounting procedures in the interest of improved fossil identification and reduced counting time. Another problem with morphological variability is the degree of change over evolutionary time, however, this is assumed to have an unappreciable affect in this study as the fossil records used in analysis only span the last few millennia. The problem of identification of fossil specimens based on test characteristics alone (as their pseudopodium is rarely preserved) is unavoidable, but as taxa are defined by the morphological characteristics of the test this does not pose an insuperable risk if caution is applied. In cases where there is a degree of morphological variability within a taxon but not so much that it constitutes the definition as a species then the names are given the suffix 'type' (e.g. Roe *et al.,* 2002). Reassuringly, it has been demonstrated by the review of Barnett *et al.* (2017) that salt-marsh testate amoebae taxa grouped by morphospecies classifications have consistent ecologies that can be used to precisely estimate marsh elevation over large geographic regions (i.e. the North Atlantic).

Finally, the problem of counting statistically significant test numbers has been investigated by Payne and Mitchell (2009). Traditionally, most studies targeted an arbitrary count of 150 individuals per sample. Payne and Mitchell (2009) found that a

count of 100 individuals is unnecessary for most samples if the intention is to reconstruct palaeoenvironments, yet, higher counts are more appropriate if the aim is to capture the full ecological diversity of an assemblage. Higher counts also allow the relative abundance of rare taxa to be identified with greater accuracy (Wall *et al*., 2009). In the absence of rare taxa, defined as those that account for <5% of the total count), a count of 50 individuals may be statistically significant (Payne and Mitchell, 2009). The issue has been investigated for salt-marsh testate amoebae from Norway by comparing the assemblages of replicate sub-samples, one being counted to 150 individuals and one to 100; the results suggest that a count of 100 is statistically significant (Barnett *et al.* 2013).

2.4.4 Using saltmarsh testate amoebae for palaeosea-level applications

Despite testate amoebae having long been recognised for their potential as palaoenvironmental indicators in peatland and lacustrine sediments, their potential to reconstruct sea level from salt-marsh sediments remains comparatively untapped. The earliest studies to report testate amoebae in salt marshes (e.g. Scott *et al.* 1977, 1991) described the larger specimens in sediments within the size range (63-500 µm) primarily processed for foraminiferal analysis. However, largely due to these studies employing a preparation procedure which is suboptimal for testate amoebae analysis (optimised for foraminifera), species richness and test concentrations were inherently low.

Charman *et al.* (1998, see also: Charman *et al.* 2000a) were the first to investigate the occurrence of testate amoebae in the <63µm range in salt-marsh sediments, which is where the maximum abundance is usually found in peat and lake sediments (Charman, 1999). This study aimed to develop a methodology for analysis of the

<63µm fraction and compare the results with the >63µm fraction. For the >63µm fraction the preparation remained the same as that routinely used for foraminiferal analysis, which yielded the limited testate amoebae previously reported in salt-marsh sediments. The <63µm fraction was prepared using an adapted method outlined by Hendon and Charman (1997). The results demonstrated that, as in peat and lake sediments, testate amoebae occur in greater abundance in the <63µm fraction. Furthermore, species richness in the <63µm fraction was comparatively higher than in the >63µm fraction reported in the study and that of previous studies which have reported testate amoebae in the >63µm fraction of samples. The surface distribution of the <63µm fraction displayed a vertical distribution of taxa related to the position within the tidal frame. Compared with foraminifera distributions along the same transect, testate amoebae showed a narrower vertical zonation in the upper high-marsh zone, also occurring in the supratidal zone (elevations above high water spring tide), opening up the possibility of analysis of supratidal sediments to improve the precision of sea-level reconstructions (cf. Allen, 1990). Testate amoebae were not found where the marine (polyhalobous) diatoms occurred on the same site but did occur in high numbers in the middle marsh where salinity levels were lower. This suggests that salinity (related to the frequency/duration of tidal inundation) is an important control on the distribution of salt-marsh testate amoebae, as is the case with other salt-marsh flora and fauna (e.g. Gehrels, 2000).

The pioneering investigation by Charman *et al.* (1998) set the context for future studies to broaden the understanding of salt-marsh testate amoebae with a view to applying them as a proxy for sea-level reconstructions. Gehrels *et al*. (2001) extended the work in a multiproxy study (testate amoebae, foraminifera and diatoms) combining the data from Charman *et al.* (1998) with data from two new sites. Testate amoebae were

analysed in the fraction between 15-300µm to include both the larger (>65µm), and most abundant, smaller (<65µm) specimens. Again the results suggest that contemporary testate amoebae display a tightly-constrained vertical zonation in the upper marsh as a result of a rapid turnover of taxa (see also: Charman *et al.,* 2002). Furthermore, the results showed that testate amoebae distributions were closely related to duration of tidal flooding; this implies that the other hydrological properties of the salt-marsh (see: Knott *et al.,* 1987) have an inappreciable effect on species distribution. Gehrels *et al.* (2006) describe the contemporary distribution of testate amoebae in North American salt marshes. The testate amoebae assemblages and vertical distribution in Gehrels *et al.*'s (2006) investigation were comparable with those from UK salt marshes (Charman *et al.* 1998, 2002; Gehrels *et al.* 2001) and recently, comparable assemblages have been described from Norwegian marshes (Barnett *et al*. 2013). This suggests that testate amoebae distributions in salt-marshes are spatially robust, giving opportunity for the use of regional scale, and/or trans-Atlantic transfer functions (Barnett *et al.* 2017).

Following on from the preliminary investigations which focused on the contemporary distribution of testate amoebae along salt-marsh surfaces, Roe *et al.* (2002) extensively investigated fossil testate amoebae from a range of coastal sediments. Despite tests being found in high diversity and concentration in surface salt-marsh sediments Roe *et al.* (2002) found that, on the whole, fossil tests were sparse. However, some sites yielded fossil assemblages analogous to contemporary assemblages. The implications of the variability between the fossil preservation of tests at different sites can potentially inhibit the application of testate amoebae for sea-level reconstructions; if fossil testate amoebae are not analogous to contemporary assemblages, or not preserved, then they are of reduced value for reconstructing past

sea levels. The reason(s) underlying the sparsity of fossil testate amoebae in salt-marsh sediments where they would be expected to occur is unknown. Roe *et al.* (2002) suggested several factors may account for this. It could be that the core samples analysed may not be analogous to the high-marsh zone where testate amoebae inhabit a tight vertical range, therefore testate were never there to be preserved. This inference is supported by the fact that where testate occurrences in core samples were greatest, foraminifera were sparse, demonstrating that the narrow range occupied by testate amoebae has little overlap with foraminifera. Thus it is important that coring for fossil assemblages should be optimised for testate amoebae occurrence. This shall be addressed in the methods section.

In previous investigations salt-marsh testate amoebae occurred in the greatest concentrations in the most recent (~last 100yrs) salt-marsh samples and were sparse in older sediments (Roe *et al.,* 2002; Charman *et al.,* 2010; Barnett *et al.,* 2015). This could be a function of test degradation, which is supported by evidence of differential preservation. Where testate amoebae were present in older samples they were generally dominated by xenosomic tests rather than, what have been perceived to be more fragile idiosomic tests (Lousier and Parkinson, 1981; Mitchell *et al.,* 2008). However, as discussed previously, some idiosomic tests have demonstrated a greater degree of preservation than xenosomic tests in some conditions (Hendon and Charman, 1997). This highlights the need for further research into the controls on the preservation potential of testate amoebae in salt-marsh sediments.

The culmination of this pioneering research resulted in the first testate amoebae-derived sea-level reconstructions. Charman *et al*. (2010) present two reconstructions for the past 100 years from two North American Atlantic sites (Maine, USA and Nova

Scotia, Canada). Testate amoebae concentrations, as has been the problem in the samples analysed by Roe *et al.* (2002) in the two cores were relatively low, with testate amoebae only being found in significant concentrations in the upper section (~20cm) of the cores. However, it is suggested that this is a result of the cores being taken for foraminiferal analysis and therefore only capturing the lower 'tail' of the range of testate amoebae distribution, i.e. the species occupying mid to lower zones of the marsh (Charman *et al*. 2010). This also means that the taxa that are associated with higher locations on the marsh, which should provide the most accurate reconstructions as this is where species zonation is most strongly defined (Charman *et al.* 1998, 2000, 2002; Gehrels *et al.* 2006b), were not sampled in the core. Nonetheless, Charman *et al.*'s (2010) sea-level reconstructions (particularly for Nova Scotia) agreed with instrumental records for same time period. This demonstrates the ability to reconstruct past sea levels using testate amoebae with high precision and accuracy. Furthermore, precision of the reconstructed values was equal to, if not better than, the precision of reconstructed values based on foraminifera from both sites (it should be taken into consideration that the precision of foraminifera values here were better than average). Moreover, the reconstructions conformed to the observed sea-level trends measured from tide gauges and foraminiferal reconstructions in the region.

Since the first sea-level reconstructions of Charman *et al*. (2010) a limited number of studies have furthered the development by applying testate amoebae as proxies for new sea-level reconstructions. Haynes (2011) reported fossil testate amoebae in salt-marsh sediments from Iceland which dated to approximately AD 1330 to 1620; the oldest fossil testate amoebae recorded in salt-marsh sediments. The sea-level curve was in agreement with the diatom-derived curve at the same site and indicated an average precision of ±5 cm, matching the precision of Charman *et al.* (2010).

Furthermore, the zonation of contemporary species in Iceland corresponded to the zonation displayed in UK and North American salt-marshes. Ooms *et al.* (2011, 2012) investigated testate amoebae as proxies for water-level changes in an inland, tidal freshwater marsh and a brackish tidal marsh respectively. In the tidal freshwater marsh water-levels were reconstructed with a precision which matched that of salt-marsh studies (Ooms *et al.* 2011). In the brackish marsh (Ooms *et al.* 2012) testate amoebae displayed a vertical zonation similar to that observed in salt-marshes. However, whilst species elevation was linked with flooding for samples taken within the inter-tidal zone, the results suggested that for the supratidal zone, species distributions were predominantly controlled by particle size and organic matter; displaying a weak correlation between frequency of flooding and testate amoebae vertical zonation.

2.4.5 Testate amoebae summary

Testate amoebae have proven to be a valuable proxy for palaeoenvironmental applications in terrestrial moist soils. Recent pioneering work investigating the potential of salt-marsh testate amoebae for palaeosea-level applications has laid the foundations for the use of salt-marsh testate amoebae for reconstructing past sea levels, which is the overall focus of this study. It has been demonstrated that testate amoebae display a tightly-constrained vertical zonation in high-marsh locations over a large spatial range. This is particularly promising for two main reasons: (i) zonation in the high marsh was more tightly constrained than for foraminifera and also extended into the supratidal zone; this area of the marsh has the greatest potential for high-precision reconstructions as this is the least dynamic geomorphological zone (Allen, 1990); and (ii) if the species-environment relationship and therefore species zonation is spatially robust this permits the development of regional, or potentially global-scale transfer functions to be developed. Also, this gives testate amoebae an advantage

over foraminifera which display a greater degree of vertical assemblage variation between sites (cf. Horton *et al*. 1999; Edwards *et al*. 2004). Despite this, as the results of Ooms *et al.* (2012) suggest, caution should be excised when drawing inferences from testate amoebae assemblages in the supratidal zone. Further investigation into the controls on testate amoebae distribution in the supratidal zone should be conducted before a decision is to be made on whether or not to include supratidal assemblages in sea-level studies. For example, it may be that in the supratidal zone, species distribution is a function of the hydrological properties of the underlying substratum, as is the case in peatlands (e.g. Woodland *et al.* 1998). This depends on whether groundwater level is coupled with sea level.

In spite of the virtues identified by investigations of salt-marsh testate amoebae, the preliminary research has also revealed a number of factors which can potentially inhibit sea-level studies. Most notable is the variability in preservation of tests in the fossil record, with testate amoebae only occurring in significant abundances in the uppermost sections of salt-marsh substrata. However, promise can be sought in the few studies which have reported testate amoebae at greater depth, and also the fact that these pioneering investigations mostly relied on the analysis of cores taken from sub-optimal locations for testate amoebae occurrence. Notwithstanding this, the greater degree of precision (as opposed to foraminifera) of testate-derived sea-level reconstructions, which themselves may be improved as understanding of the potential caveats develops, demonstrates the importance of applying testate amoebae as proxies in sea-level studies. The other concerns identified can largely be ameliorated by the adoption/development of a remedial methodology, which shall be outlined in more detail in the methodology **Chapter 3**.

2.4.6 Intertidal foraminifera as sea-level indicators

The potential and application of intertidal foraminifera to sea-level studies has long been established, and is not the primary focus of this study. However, as this study uses foraminifera as well as testate amoebae and diatoms it is necessary here to provide a brief overview of foraminifera as sea-level proxies (see Edwards and Wright, 2015 for a comprehensive review). Foraminifera are defined as microscopic (63–500 μm), shell-forming, marine unicellular protozoa. Foraminifera are separated from testate amoebae because they are predominantly marine organisms. Foraminifera are divided into agglutinated and calcareous taxa on the basis of test construction. Agglutinated taxa are dominant in the minerogenic, intertidal environment of salt-marshes (Scott *et al.* 2001). The vertical zonation of foraminifera in salt-marsh environments is predominantly, although not always (e.g. Barbieri, 2001), controlled by the marsh physicochemical conditions which are a function of the duration and frequency of tidal inundation relative to elevation (Scott and Medioli, 1978; 1980; Berkeley *et al.,* 2008). Applying the standardised methodology discussed earlier (i.e. van de Plassche, 1986; Shennan *et al.,* 2015) many studies have produced quantitative reconstructions of late Holocene RSL from fossil foraminiferal sequences (e.g. Gehrels, 1999; Gehrels *et al*. 2002, 2005, 2006, 2008, 2012; Long *et al*. 2003, 2010, 2012; Edwards and Horton, 2000, 2006; Kemp *et al.,* 2009, 2011a; Barlow *et al.* 2012). The precision of foraminifera-based reconstructions is at best ± 5cm (e.g. Southall *et al*. 2006) but often ~ ±10 cm or worse (references above).

2.4.7 Intertidal diatoms as sea-level indicators

As with foraminifera, diatoms are relatively well-established as proxy indicators of sea level. In addition to testate amoebae and foraminifera this project utilises diatoms as a tool for reconstructing sea-level changes. This section provides a short review of

diatoms and their utility as sea-level indicators (see Zong and Sawai, 2015 for a comprehensive review).

Diatoms are a group of microscopic (~5 µm to 200 µm in size) photosynthesising algae that form siliceous skeletons (the frustule: composed of two valves) and are abundant in almost any moist, naturally illuminated, environment - including intertidal mudflats and marshes (Stoermer and Smol, 2010). Their differing ecological tolerances to water salinity and duration of tidal inundation results in specific assemblage zonations as a function of marsh surface elevation (e.g. Zong and Horton, 1998, 1999) which may be used to infer changes in coastal environment (e.g. van de Plassche, 1986). This, coupled with diatom valves being identifiable to species (or sub-species) level based on morphology and also readily preserved in fine-grained intertidal sediments, makes diatoms an ideal tool for reconstructing sea level. Thus, diatoms have can be used to qualitatively define the indicative meaning component of SLIPs (e.g. Horton and Sawai, 2010). More recently, advances in statistical methods, using transfer functions, have resulted in quantitatively reconstructed sea-level records based on diatom proxy information (e.g. Szkornik *et al.,* 2006; Hill *et al.,* 2007)

In spite of their virtues as proxy indicators of sea level, diatoms are not without inherent problems which could potentially jeopardise the reliability of any diatom-inferred sea-level reconstruction. There are only minute morphological features which separate certain species so it is therefore important to exercise rigour when identifying diatom frustules if taxonomies are to be harmonised and compared between studies. Diatom distributions may be controlled by multiple or different environmental parameters (e.g. Zong and Horton, 1998). Disentangling this information requires quantitative analyses of diatom assemblages and environmental variables (e.g. Zong and Horton, 1998;

Skzornik *et al.,* 2006). Perhaps the greatest problem is determining diatoms deposited *in situ* (autochthonous) from those transported from elsewhere (allochthonous) within any sample assemblage. This can be somewhat prevented by not counting extensively damaged valves as these may be indicative of post-mortem transportation. However, it has been suggested that during post-mortem transportation species with weaker valve morphology may be broken while stronger valves survive to be deposited and therefore preferentially preserved (e.g. Flower, 1993). An understanding and consideration of the life form i.e. planktonic or benthic (Zong and Sawai, 2015) and/or valve fragmentation (Vos and de Wolf, 1993) may help to distinguish allochthonous from autochthonous diatoms in a sample. It is therefore of critical importance to evaluate the reliability of any diatom-derived reconstruction with these potential limitations in mind.

2.4.8 Cautionary factors: seasonality, patchiness, predation and infaunal habitation

The application and interpretation of testate amoebae, diatoms and foraminifera as sea-level indicators relies on the fundamental assumption that the contemporary assemblages accurately represent fossil assemblages in terms of composition and ecology. A number of factors have been identified which have the potential to nullify these assumptions. These have largely been identified and evaluated in foraminiferal and/or diatom studies but are equally applicable (with the exception of infaunal habitation) to salt-marsh testate amoebae.

The majority of studies which have utilized salt-marsh microorganisms as sea-level indicators use samples collected at only one time of year. As a result of seasonal reproduction blooms in foraminiferal populations (e.g. Scott and Medioli, 1980; Horton

and Edwards, 2003), assemblages from such samples may be unrepresentative of the time-averaged fossil assemblage (Horton and Edwards, 2003; Horton and Murray, 2006). However, using only the dead assemblage in the modern training set negates the influence of seasonal blooms (e.g. Horton and Murray, 2006). Oppenheim (1991) investigated seasonal changes in the assemblage structure of dominant diatoms along a transect crossing a salt-marsh, sandflat, and mudflat of an estuarine intertidal succession. The results of the study suggested seasonal changes in the structure of the salt-marsh and mudflat communities. However, there were no annual patterns in the succession of taxa repeated over time indicating that different combinations of environmental variables influence diatom distributions over time. Due to the sparsity of studies on salt-marsh testate amoebae there has been no investigation into the influence of seasonality on salt-marsh testate distributions. Warner *et al*. (2007) investigated seasonal influences on testate ecology from an open bog/fen community and swamp community. A clear species separation over the seasonal cycle was observed in the bog/fen community, however, no significant difference was observed in the swamp community. Uncertainty in the findings of Warner *et al*. (2007) highlight an important gap in the knowledge of the response of testate to seasonal changes, which requires further investigation, especially in salt-marsh communities.

Modern samples of salt-marsh microorganisms which comprise the training set are usually taken systematically along an approximately linear transect traversing the marsh perpendicular to the coastline. It is assumed that a sample taken from a given point on the marsh surface represents a microfossil assemblage indicative of the elevation from which it was taken. However, if the microfossils exhibit patchiness in their distribution then the reliability and precision of a reconstruction may be adversely affected. Notwithstanding this, studies of foraminifera have demonstrated that whilst

they display some small-scale variability, patchiness is infrequent and occurs only with rare taxa (Alye and Murray, 2000; Morvan *et al.* 2006). Moreover, the effect of patchiness may be reduced by only using the deceased assemblage which usually displays spatial homogeneity, or multiple samples from the same elevation but different marsh locations could be artificially homogenised (e.g. Buzas *et al.* 2002; Morvan *et al.* 2006). Future research is required in order to better understand the effect of patchiness within testate amoebae assemblages.

Diatoms, foraminifera and testate amoeba may be preyed on by marine and/or intertidal dwellers, other species of the same microorganism group and shore birds (Lipps, 1988; Culver and Lipps, 2003, Smith *et al.,* 1996). Murray (1991) suggests that the effect of predation would not have an insignificant impact on foraminiferal populations as there is no selective predation of species. The fact that both testate amoebae and foraminifera are encapsulated by protective tests and display rapid reproduction rates (Morvan *et al.* 2006; Charman, 2001) lessens further the influence of predation. For diatoms, however, in the presence of other certain microorganisms assemblage structure may be altered due to selective predation (e.g. Smith *et al.,* 1996) although the influence is negated by the limited presence of the predatory species.

Some infaunal foraminiferal species have typically been documented living within the top 20 cm, but this can be up to 60 cm depth in subtropical locations (Patterson *et al.* 1999; Hippensteel *et al.,* 2000, 2002). Consequently, routine analysis of the uppermost centimetre for modern surface samples (e.g. Wright *et al.* 2011) will not account for infaunal taxa living below the surficial sediments. Also, deep-infaunal habitation may contribute taxa to the fossil assemblage and are therefore not

contemporaneous deposits. This particular caveat is not applicable to testate amoebae as they are almost exclusively epifaunal dwellers (Neville *et al.* 2010) with only one species known to live infaunally (*Cryptodifflugia oviformis;* Heal, 1962). In any case, investigations at various sites have shown infaunal habitation is limited and has little impact for palaeoenvironmental applications which conduct analysis on only surficial (0-1cm) sediments (e.g. Patterson *et al.* 2004; Horton and Culver, 2005; Hawkes *et al.* 2010).

2.5 Geochronology: constraining the timing of sea-level fluctuations

In order to fulfil the age component of the standardised methodology for reconstructing RSL change from salt-marsh proxies, a precise age-depth profile of the stratigraphy is required in order to constrain the timing of changes and trends in RSL. Recent studies have demonstrated that high-resolution reconstructions may be obtained from continuous salt-marsh sequences. This section reviews the suite of dating and modelling techniques applied in these recent high-resolution reconstructions (e.g. Gehrels, 2000; Gehrels *et al.,* 2005, 2012; Kemp *et al.,* 2009, 2011; Barnett *et al.,* 2014).

2.5.1 Radiocarbon dating

Due to the high organic matter content in most salt marshes the most widely used technique for chronological control of late Holocene RSL studies is conventional radiocarbon dating of bulk organic material (e.g. van de Plassche, 1980, van de Plassche *et al.* 1989; Tooley, 1974, 1978; Shennan, 1986, 1989). Essentially, radiocarbon dating is a comparative dating technique that relies on a quantified relationship between the atmospheric concentration of stable carbon isotopes ^{12}C, ^{13}C and the radioactive (unstable) isotope ^{14}C, and the known rate of decay (expressed as half-life) of ^{14}C (see: Hua, 2009; Piotrowska *et al.* 2011). The conventional (raw)

radiocarbon age is expressed as yrs (years) BP (before present), with present being set by arbitrary convention at 1950 AD (Stuiver and Polach, 1977). Establishing the chronostratigraphy of a sequence based on this approach is limited by the large amount of bulk material necessary to acquire a date and contamination by allochthonous (derived from elsewhere) carbon (Hatte and Jull, 2007; Hua, 2009). Recent technological advances applying accelerator mass spectrometry (AMS) have led to the development of a method for more precise radiocarbon dating using significantly smaller samples i.e. discreet plant fragments (Törnquist *et al*. 1998; Jull, 2007; Kim *et al.,* 2009). The selection of organic material for radiocarbon dating requires a careful methodological approach. Poor decisions taken in the selection of datable material may result in spurious dates. The exact methodology employed in this investigation shall be detailed in the methodology section. The small amount of material required for radiocarbon measurement by AMS facilitates the dating of individual plant macrofossils, negating the risk of allochthonous contamination i.e. by penetrating plant roots/rootlets (Törnquist *et al*. 1998, Hatte and Jull, 2007).

In order to assign an age to a sample, the raw measurement of ^{14}C needs to be converted to a conventional radiocarbon age by comparing the measured ^{14}C to $^{12}C/^{13}C$ ratio with an absolute international radiocarbon standard (see: Stuiver and Polach, 1977). Due to fluctuations in atmospheric ^{14}C content over time, ages need to be calibrated in order to assign calendar dates (Reimer *et al.* 2004; Hua, 2009). Ages are then converted to calendar dates using a calibration curve (e.g. Reimer *et al*. 2004) displaying ^{14}C concentrations through time, derived from precise, independent dates on organic materials. Radiocarbon dating is limited by the immeasurably small amount of intrinsic ^{14}C remaining after ~ 60,000 years which is indistinguishable from background ^{14}C (e.g. Plastino *et al*. 2001). Other difficulties inhibit accurate dating of

recent sediments deposited in the last ~300 years (Scott, 2003). Plateaus in the calibration curve (i.e. CE1650-1950) as a product of the natural variability in atmospheric ^{14}C results in multiple calendar dates for the same sample; hence a broad range of calendar ages where the calibration curve flattens (Reimer and Reimer, 2007). Between CE 1950-1960 atmospheric ^{14}C concentrations were significantly altered due to above-ground nuclear weapons testing (Reimer *et al.* 2004; Hua and Barbetti, 2004). Recently, the 'bomb spike' approach (Turetsky *et al.* 2004) has been used in combination with 'high-precision' AMS radiocarbon dating to calibrate the date of organic salt-marsh sediments which were deposited around the period nuclear weapons testing which peaked in 1950 CE (Marshall *et al*. 2007).

2.5.2 Radionuclides: ^{210}Pb, ^{137}Cs and ^{241}Am

In order to produce detailed chronologies for recent sediments, deposited in the last ~100 years, a suite of other dating or age calibration techniques need to be used in combination with the radiocarbon technique. The most widely applied approach for dating of recent salt-marsh sediments is ^{210}Pb (e.g. Gehrels *et al.* 2005; Kemp *et al.* 2012). ^{210}Pb is a naturally occurring part of the Uranium (^{238}U) series and has a half-life of 22.3 years (Appleby and Oldfield, 1983). The parent isotope of ^{210}Pb is ^{226}Ra which decays (half-life: 1622 years) into the inert gas ^{222}Rn. As ^{222}Rn disperses into the atmosphere it decays (through four short-lived isotopes) into ^{210}Pb, known as unsupported ^{210}Pb (Gale *et al.,* 1995; Baskaran, 2011). The unsupported ^{210}Pb lead isotope then attaches to atmospheric aerosols and is deposited on the ground mainly by precipitation (~90%; Binford *et al.,* 1993) or dry fallout (Baskaran, 2011). Upon reaching the surface, ^{210}Pb binds to salt-marsh particles becoming buried as the surface accretes whilst continually decaying at the known half-life. Thus, sedimentary archives of ^{210}Pb do not provide direct age estimations; the age estimation is inferred

from a ^{210}Pb-derived estimated sediment accumulation rate.

Age determination from unsupported ^{210}Pb inventories is interpreted through the use of an accumulation model (e.g. constant rate of supply; Horton *et al.* 2006) which makes an assumption on the influx of atmospheric unsupported ^{210}Pb that is deposited on the Earth's surface (Appleby and Oldfield, 1992; Appleby, 2001). This model needs to be corrected for regional variations (Appleby, 2001). Thus, by combining the accumulation with the decay rate, an unsupported ^{210}Pb vertical profile can be established for the stratigraphic sequence. A number of factors reduce the validity of the assumptions on which the accumulation models are based; the relative contribution of ^{210}Pb from marine sources, variance in sedimentation rates, sediment reworking and ^{210}Pb diffusion (Smith, 2001; Kemp *et al.* 2012). Another limitation of this technique is that due to the short half-life of ^{210}Pb, chronologies can only be established for the last 100-120 years (Gale *et al.,* 1995; Kemp *et al.* 2012).

Chronologies based on ^{210}Pb thus require calibration by an independent technique in order to validate the derived age estimations (e.g. Goodsite *et al.,* 2001). One such technique, mentioned earlier, is the 'bomb spike' calibration method (Marshall *et al.* 2007). Other radionuclides e.g. ^{137}Cs and ^{241}Am (Dyer *et al.* 2002; Gehrels *et al.* 2005) or ^{207}Bi (Kim *et al.* 1997) may also be used as independent age markers which can constrain ^{210}Pb chronologies. As with the 'bomb spike' technique ^{137}C and ^{241}Am methods exploit the abrupt input of anthropogenic radionuclides into the atmosphere from nuclear events (e.g. Cambray *et al.* 1987) and thus appear as a 'spike' in

chronological profiles. However, the ^{137}Cs method may produce spurious results due to the post-depositional vertical translocation of caesium and/or discharge from nuclear facilities (Morris *et al*. 2000; Harvey *et al.* 2007).

2.5.3 Chronology construction

Sea-level studies using salt-marsh sequences (cores) are usually limited in the number of dated levels throughout the core. This often results in reconstructed sea-level positions within the core that do not have an age constraint. It is therefore necessary to infer the ages of all (undated) depths within the core along with associated uncertainty in order to fulfil the age component of non-directly dated SLIPs. Obtaining multiple dates, through several dating methods, spread along a core permits the development of composite chronologies (e.g. Parnell and Gehrels, 2015). Whilst there are uncertainties associated with individual dates, providing that a core is undisturbed then there should be an upcore progression from older to younger ages (monotonicity). This phenomenon can be exploited statistically by taking the depths and ages within a core and combining them with assumptions about the rate of sedimentation to create models of the age-depth relationship that preserve this monotonic function (e.g. Parnell *et al.,* 2008; Parnell and Gehrels, 2015). There are a number of different statistical models available (see: Parnell *et al.*, 2011) for constructing chronologies. The exact methods employed in this project are detailed in **Section 6.2.6**

2.5.4 Summary

By combining several of these dating methods it is possible to produce a detailed chronology for salt-marsh sediments. Thus, sea-level reconstructions can be temporally constrained. The results from the suite of dating techniques can be synthesised statistically to establish an age-depth model (e.g. Parnell *et al.* 2008;

Blaauw and Heegaard, 2012) which can then be used to estimate the ages of the undated sediments in a sequence. The age estimates are expressed with the 'associated error' inherent in the dating technique. The term 'error' can be defined here as either 'uncertainty' or 'mistake' which can be random or systematic (Maher *et al.* 2012; Blaauw and Heegaard, 2012). Random errors reflect the precision of an analytical method and are attributed to random processes in machine measurements e.g. a $^{14}C/^{12}C$ ratio only provides an inexact approximation of the actual value, with the estimated value varying with repeat measurements (Blaauw and Heegaard, 2012; Maher *et al.* 2012). Conversely, systematic errors (or bias) include error components which are constant or vary predictably over the course of repeat measurements (Maher *et al.* 2012). Human-induced errors from laboratory mistakes such as; contamination, mixing of samples, submission of the wrong material or sample preparation faults, can also impact the accuracy of measurements (Marshall *et al.* 2007; Blaauw and Heegaard, 2012).

2.6 Transfer functions

Quaternary palaeoecology was greatly advanced by the pioneering work of Imbrie and Kipp (1971) with the initial development of a quantitative method for reconstructing past environmental variables though the application of a 'transfer function'. A transfer function is an empirically-derived numerical equation applied in the generation of quantitative palaeoenvironmental reconstructions. This is principally achieved though correlation between contemporary biotic assemblages (their preference to the environmental parameter in question e.g. elevation) and a fossil assemblage i.e. a proxy dataset (Sachs *et al.* 1977; Birks, 1995, 2010). Through regression modelling of the contemporary species-environment data the environmental variable can be expressed as a mathematical function of the species data (Birks, 1995). Following the

pioneering work of Imrie and Kipp (1971), subsequent studies from a number of disciplines (e.g. palaeolimnology, palaeoclimatology, oceanography, sea-level studies) have applied the transfer function approach to quantitative palaeoenvironmental reconstructions. In essence, transfer functions model biological data as a function of the environment.

2.6.1 Transfer function development

The first step in the development of a transfer function is to establish a modern 'training set' which consists of biological and environmental data (Birks, 1995). Through analysis (ordination) of this data, the modern training set establishes the relationship between a biological group (***Y***), e.g. testate amoebae, and the environmental variable of interest (***X***) e.g. elevation (Birks, 1995; 1998). Detrended canonical correspondence analysis (DCCA) is a frequently applied ordination method for salt marsh training sets (e.g. Kemp *et al.* 2013; Barlow *et al.,* 2013). DCCA is a direct gradient analysis procedure applicable to data comprising multiple response variables (i.e. individual taxa in the modern assemblages) that are understood in relation to a measured explanatory variable (i.e. elevation). DCCA thus provides a quantification of the strength of the relationship between taxa and their environment i.e. the importance of marsh surface elevation in governing microfaunal distributions (Birks, 1995; Lepš and Šmilauer 2003; Kemp *et al*. 2013). Furthermore, DCCA ordination can help to determine whether the taxon response to the environmental variable is unimodal or linear; important for ascertaining the appropriate regression model used in the next step of transfer function development.

The next step is to model the species-environment relationship using regression analysis. In the case of a single environmental variable an inverse regression model

is often applied, where $\boldsymbol{X}$ is signified as an ecological response function ($\boldsymbol{U}$) of $\boldsymbol{Y}$ (ter Braak and van Dame, 1989; ter Braak, 1995). It is essential that $\boldsymbol{U}$ is empirically-derived ($\hat{\boldsymbol{U}}$) as for most taxa there is only a limited understanding of the environmental controls on their distribution (Birks, 1995). Thus, the modern training set is expressed by the following formula (ter Braak, 1987):

$$\boldsymbol{X} = \hat{\mathrm{U}}\,(\boldsymbol{Y})$$

Next it is necessary to evaluate the performance (predicative ability) of the modern training set. This can be assessed by calculating the root mean square error of prediction (RMSEP) which demonstrates how capable a model can be expected to operate as a predictive tool (Wallach and Goffinet, 1987) expressed in original measurement units of the environmental variable (i.e. elevation in meters). The strength of the relationship between measured and predicted values is determined as the correlation (r) and/or the coefficient of determination (r^2). However, RMSE and r/r^2 are consistently under- and over- estimated respectively, a cross-validation technique is necessary in order to achieve a more precise estimation of predictive uncertainty (see Birks, 1995 and references within). The most straightforward and commonly used cross-validation procedure is 'jack-kniving' (leave-one-out: LOO) where an individual sample is removed from the training set and the remaining samples are applied to predict the value of the excluded sample (Birks, 1995). As training sets are often constructed from data collected from multiple samples at a single site (e.g. Gehrels *et al.* 2012) LOO has a tendency to return overly optimistic results (Kemp *et al.* 2013). For training sets which combine data from a number of sites leave-one-site-out (LOSO) cross-validation offers an alternative to mitigate over-optimism associated with the LOO approach (Payne *et al.* 2012). With both procedures, the difference between the predicted value and the observed value gives the prediction error for the

sample expressed as $RMSEP_{(jack)}$ (ter Braak and Juggins, 1993). Additionally, r and r^2 values can be calculated for the excluded samples and are expressed as $r_{(jack)}$ and $r^2_{(jack)}$ (Birks, 1995).

An alternative, more complex and objective cross-validation method often employed is 'bootstrapping' which can derive sample-specific RMSEP values (Birks, 1995). Bootstrapping involves a random group of samples being removed from the training and being replaced by the remaining samples in the original training set; this becomes the bootstrap training set of equal size to the original training set. Unselected samples for the bootstrap training set comprise the boot test set. The bootstrap training set imitates sample variation within the training set and is used to estimate the values of the boot test set. This process is repeated over many cycles (n=1000+) with a different random subset of the original training set and a new replacement set (Birks *et al.* 1990; Birks, 1995). Moreover, it is suggested by Telford *et al.,* (2004) that the preferred method of performance assessment should be based on a range of techniques (e.g. RMSEP, r^2, bootstrapping and scatterplots of observed vs predicted values).

Once the analysis (ordination) of the modern training set and development of the transfer function is complete, the next stage is to apply the transfer function to the fossil assemblage. This permits an estimated value for the unknown environmental variable ($\mathbf{X_0}$) to be inferred from the modern data. The Modern Analogue Technique (MAT: Prell, 1985) may be used to assess the reliability of the value estimated for $\mathbf{X_0}$ by way of a dissimilarity measure between modern and fossil assemblages (Birks, 1995; Jackson and Williams, 2004). However, the MAT relies on the presence of the same taxa in both the contemporary and fossil assemblages. Thus, if there are no

analogues for some fossil species, spurious reconstructions are likely to arise (Overpeck *et al*. 1992; Birks, 1998). Therefore, the success of the MAT rests on the extensiveness of the modern training set. Reliability is maximised through the generation of a comprehensive modern training which accounts for a wide range of habitats (Horton and Edwards, 2005; Barlow *et al.* 2013).

Inherent in all transfer functions is the assumption that test sites are independent of modelling sites. Violations of this assumption and the impact on the predicative ability are often overlooked (Telford and Birks, 2005). Positive spatial autocorrelation – the propensity of spatially proximal sites to more closely resemble each other than randomly selected sites (Legendre and Fortin, 1989; Telford and Birks, 2005) is one such violation of this assumption. Consequently, the cross-validation procedures proposed above have a tendency to overestimate predication errors in autocorrelated datasets. The MAT model is particularly impinged by autocorrelation (Telford and Birks, 2009; Kemp *et al.* 2013), if applied the results should therefore be interpreted cautiously. The precise ordination procedure(s) and transfer function model used in this study shall be discussed in detail in later chapters.

2.6.2 Applying transfer functions to reconstructing sea levels

The transfer function approach has been widely adopted by the sea-level community since the late 1990s to provide quantitative relative sea-level histories (e.g. Guilbault *et al*. 1995; Zong and Horton, 1999; Horton *et al.* 1999, 2000; Gehrels, 2000; Gehrels *et al.* 2001, 2002, 2005). The application of transfer function derived RSL reconstructions involves the vertical zonation of salt-marsh microorganisms described previously. Thus, the initial stage of transfer function development is to gather a modern training set of samples, encompassing the entire range of sub-environments

which comprise indicative microorganism assemblages. The training set may be local; samples collected adjacent to the fossil assemblages (e.g. Gehrels *et al.* 2006a) or regional; the training set comprises samples collect from numerous nearby marshes (e.g. Kemp *et al.* 2009b, 2013) varying from marshes along a single estuary to marshes around an entire country or coastline (Barlow *et al.* 2013). The predictive ability of the transfer function is most efficient when the environmental gradient is evenly sampled (Telford and Birks, 2011a). However, modern training sets employed in sea-level studies often comprise a greater number of samples from high-tidal elevations than low-tidal and sub-tidal elevations (e.g. Callard *et al.* 2011; Gehrels *et al.* 2012). Particularly for foraminiferal-based investigations, where the environmental gradient extends well into the sub-tidal zone (Woodroffe, 2009), uneven sampling may produce bias in the results of cross-validation (Telford and Birks, 2011a). As testate amoebae are freshwater organisms, naturally, the environmental gradient they inhabit falls within the range of elevations routinely sampled in sea-level studies - negating the potential for bias caused by uneven sampling.

The ordination procedure(s) described earlier are applied to the modern training set to establish and quantify the relationship between the microorganism assemblages and the marsh surface elevation (tide-relative) that they inhabit. Following ordination and the selection of an appropriate model (e.g. WA; WA-PLS: Birks, 1995) the modern training set is applied to the fossil assemblages to derive an estimate of palaeo marsh surface elevation (PMSE) for each fossil sample taken from the core. Because elevation is used as a surrogate variable for sea level the PMSE values need to be converted to RSL following :

$$\boldsymbol{S = H - I}$$

where ***S*** is the former sea-level (i.e. mean tide level: MTL) ***H*** is the height at which the sample was taken relative to contemporary MTL, and ***I*** is the MTL-relative indicative

meaning calculated by the transfer function (Gehrels, 1999). The cross-validation procedures mentioned previously are applied in order to derive sample-specific vertical error values (RMSEPs). The final, critical, step is to evaluate the reliability of the reconstruction by performing 'transfer function reconstruction diagnostics' (Juggins and Birks, 2012; Kemp and Telford, 2015). The most commonly applied reconstruction diagnostic is an assessment of analogue quality using the MAT method (e.g. Barlow *et al.,* 2013) although there are a number of methods available (see: Juggins and Birks, 2012; Kemp and Telford, 2015). It is therefore good practice to perform a number of reconstruction diagnostics. Furthermore, accuracy and reliability of the reconstruction can be assessed through validation with instrumental tide gauge records (e.g. Gehrels *et al.* 2002, 2006; Kemp *et al.* 2009a, 2013). If the reconstructed RSL curve reproduces (within the range of associated errors) the instrumentally measured RSL curve then the reconstruction is deemed reliable. A first-order validation of reconstruction reliability can performed by testing whether the transfer function is capable of reconstructing the surficial elevation of the core (Barlow *et al*. 2013).

2.7 Summary

This chapter has reviewed the historical and most recent literature from multiple disciplines which provides a context for the rest of this thesis. The literature search identifies a lack of late Holocene sea-level records in the Southern Hemisphere generally and only very limited data for the Falkland Islands. Moreover, previous work suggests that Southern Hemisphere sites, particularly the Falkland Islands are strategically located to test hypotheses relating to recent accelerations in the rate of sea-level rise. The quantitative palaeoecological techniques from previous studies utilising testate amoebae, foraminifera and diatoms as sea-level indicators were

reviewed. The use of diatoms and foraminifera as sea-level proxies are well established and their limitations recognised and relatively well studied. However, there has been relatively little investigation into limitations associated with the use of testate amoebae.

Chapter 3 – Sites, materials and methods

3.1 Introduction

This chapter introduces the study sites, materials and methodologies central to this project. The first two sections provide descriptions of the two study sites along with detailed descriptions of the materials and methods that are specific to the study sites. This includes the fieldwork, sampling design and rationale, and site survey methods. The final two sections of this chapter present the broader methods employed throughout this project. This includes the detailed methods followed during laboratory work and the subsequent methods employed in the analysis of the data obtained. Particular emphasis is given to the methods used for the preparation of salt-marsh testate amoebae, as a novel approach is developed for this project.

3.2 Study site: Swan Inlet, Falkland Islands

The study area associated with **Aim 1** of this project is situated in the Falkland Islands. The Falkland Islands are an archipelago situated in the South Atlantic Ocean on the Patagonian continental shelf about 500 km east of mainland South America (**Figure 3.1**). The study site, on East Falkland, is the most extensive area (~1.5 km^2) of salt marsh in the Falkland Islands and is situated on the eastern edge of a tidal channel at Swan Inlet, ~9km from the open coast and ~50km from the capital Stanley (51°49’31’’S, 58°35’46’’W). This microtidal (mean tidal range: 0.7 m; spring tidal range: 1.1 m) salt marsh lies at the interface between the open estuary of Swan Inlet and extensive freshwater valley-bottom marshes (**Figure 3.2**). The eastern margin of the marsh comprises unvegetated mudflats at low tide. Photographs of the Swan Inlet site and fieldwork activities can be found in Appendix A.

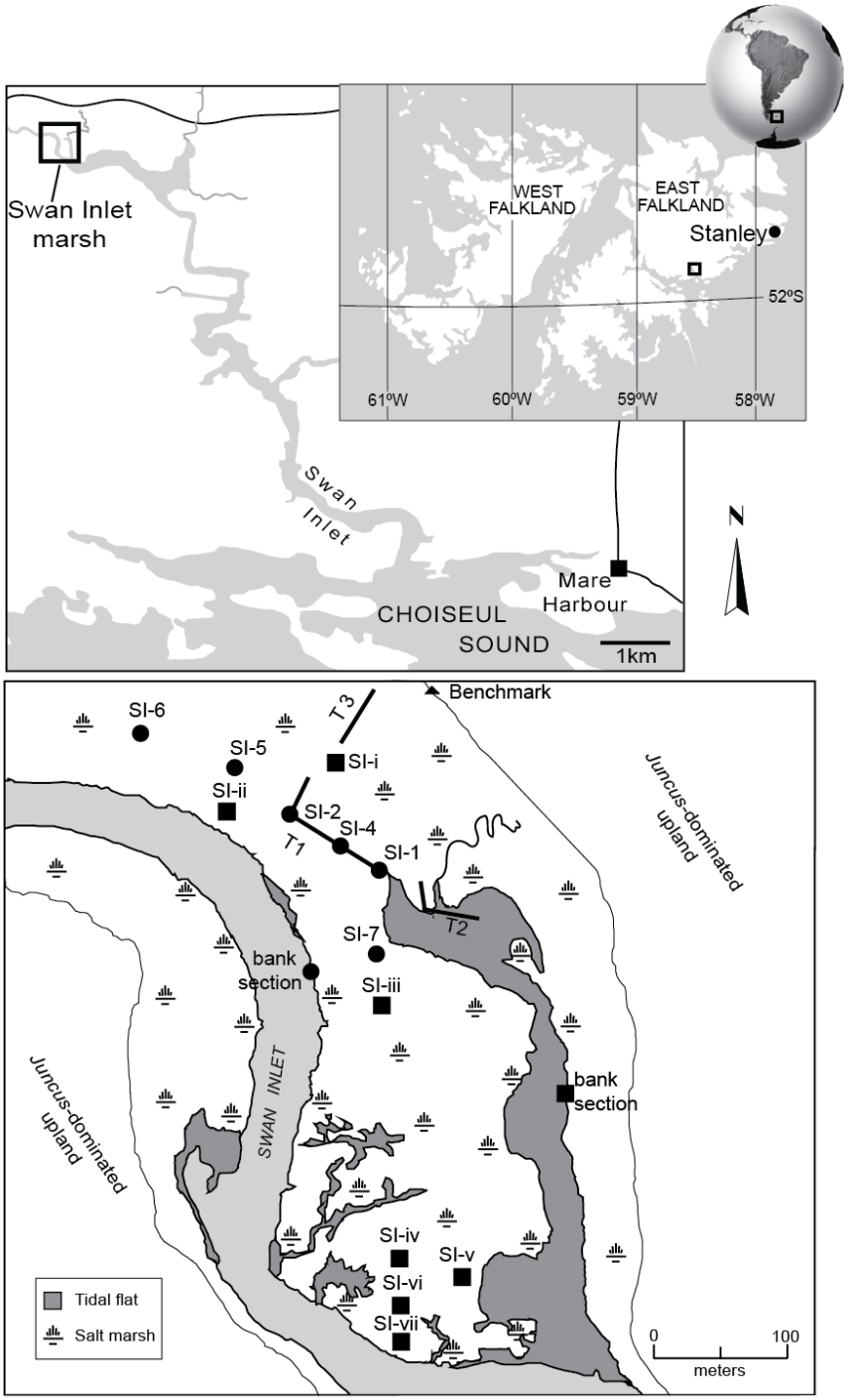

***Figure 3.1**: Location of Swan Inlet salt marsh and schematic diagram showing marsh sub-environments, locations of cores (SI- 1 – SI-7: red circles) and surface sampling transects (T1-T3: black lines) plus additional core samples taken in 2005 (SI-i – SI-vii: red squares (see **section 6.2**).*

3.2.1 Fieldwork: survey design and rationale

Fieldwork was conducted in February 2013. In order to establish the elevation gradient of the marsh surface profiles were surveyed. Heights were surveyed using a BOIF DSZ3-1 Auto Level (dumpy level) and levelling staff. No nearby geodetic benchmark is available at Swan Inlet. Therefore, a benchmark was established at the edge of the salt marsh by planting a survey pin into the ground where the substrate was resistant to compaction and elevations were measured relative to this. From here on this benchmark will be referred to as Swan Inlet Datum (SID). Tidal measurements were recorded with a pressure transducer submerged in the tidal inlet between 17/02/2013 and 24/02/13 which was compared with contemporaneous tide-gauge measurements from Stanley (Appendix C). This enabled marsh elevations (**Table 3.1**) defined for Mare Harbour at the mouth of Swan Inlet to be estimated for the Swan Inlet salt marsh (**Figure 3.1,** Admiralty Tide Tables, 2016).

Table 3.1*: Tidal datums at Swan Inlet relative to Swan Inlet Datum (m SID). MTL = mean tide level, MHHW = mean highest high water, MLLW = mean lowest low water, HAT = highest astronomical tide. HAT* was estimated from tidal predications (Admiralty Tide Tables, 2016) for Mare Harbour based on the difference between HAT and MTL predictions.*

MTL	MHHW	MLLW	HAT*
-1.89	-1.51	-2.09	-0.97

3.2.2 Fieldwork: modern sampling design and rationale

Three representative transects were established across the marsh surface that encompassed the entire elevation gradient and the range of salt-marsh sub-environments present at Swan Inlet (**Figure 3**). Transect 1 (T1), 130 m long, traverses

the mid-marsh and bridges the lower and upper limits of the freshwater and mid-marsh. Transect 2 (T2), 50 m long, runs from the mid-low marsh, across the low and into the tidal flats. Transect 3 (T3), 40m long, crosses the upper extent of the marsh close to the point where there is a bedrock outcrop at the valley wall. The elevation across the three modern sampling transects ranges from -1.47 to -0.01 m SID. Marsh vegetation was identified with the help of a local expert (Emma Edwards) and the keys of Moore (1968) and the full extent of each species along the sampling transects was recorded (**Figure 5.1**).

The modern environments were sampled to obtain appropriate modern analogues for the range of marsh palaeoenvironments present in cores. Surficial (uppermost 4cm) samples were collected at ~4cm elevation intervals along each transect. Where possible, care was taken not to sample in, or close to, disturbed areas (e.g. ponds, creek margins or bioturbated areas of mudflat) as fossil environments that show signs of disturbance are considered to provide unreliable proxy sea-level information. In total 51 surface samples were collected. Samples were sealed in airtight containers and shipped back to Plymouth, UK (1 week transit) where they were stored at 4^{o}C.

3.2.3 Fieldwork: fossil sampling design and rationale

In order to understand environmental changes over time, it is necessary to document the lithostratigraphy of Swan Inlet. A ~300 m coring transect was established stretching from the predominantly freshwater portion of the marsh into the salt-marsh zone, up to and including an exposed bank section at the edge of the main channel. A series of borehole samples were taken along the transect using an Eijkelkamp gouge auger (0.5 m barrel length, 50mm diameter) and the bank section was logged (**Figure 3.1**; SI-1 to SI-7). The vertical and horizontal characteristics of each sampled lithofacies, the lithological composition, the nature of contacts between lithofacies,

depositional and post-depositional structures, and weathering features were recorded in the field following the descriptive system of Tröels-Smith (1955). Sub-samples from each lithofacies of the sampled boreholes were examined in the laboratory of the Fisheries Department in Stanley for their microfossil content (or lack thereof). Informed by the results of the lithostratigraphic survey and microfossil analyses, a complete (and two replicates) sediment core of the entire marsh lithofacies (302 cm depth) was retained from the location of SI-2 for detailed laboratory analysis. This core was selected because it contained a relatively undisturbed and thick high marsh sequence (upper 90 cm). The core was recovered in 50 cm sections, wrapped in non-PVC plastic film and sealed in plastic casing. Additionally, 10 sediment subsamples were taken at the contacts between major stratigraphic units that were identified in the other cores for additional microfossil analyses and dating. All fossil samples were shipped along with the surface samples and also stored at 4ºC.

***Figure 3.2**: Overview of marsh environments at Swan Inlet and coring sites (SI-1 – SI-7) looking south from the top of the Juncus-dominated upland towards the open coast (see **Figure 3.1**).*

3.3 Study site: Fal-Ruan nature reserve, Cornwall, UK

The fulfilment of **Aim 2** requires frequent site visits which meant that site selection was limited by the proximity (accessibility) to Plymouth, UK. Reconnaissance of several salt marshes was undertaken to determine the presence and diversity of testate amoebae communities, and thus, their suitability for this study. Following this reconnaissance a salt marsh situated within the Fal-Ruan Estuary Nature Reserve, Cornwall, UK (50^0 14'26.87"N, 4^0 57'57.56"W) contained the most abundant and diverse testate amoebae assemblages and was therefore selected for this investigation. The reserve comprises undisturbed environments of woodland, salt marsh and mudflats covering approximately 41 hectares which has designated SSSI and AONB protection status. This area was the focus of a seminal study by Ranwell (1974). The area of salt marsh lies at the interface of the freshwater Fal-Ruan River (**Figure 3.3**) close to the tidal limit of the Fal Estuary near the village of Ruan Lanihorne, ~14.5 km channel distance from where the Fal reaches the English Channel at Falmouth). Tidal datums for the Fal-Ruan Nature Reserve are given in **Table 3.2**. Fieldwork was conducted between November 2013 and November 2014. Photographs of the Fal-Ruan site can be found in Appendix B.

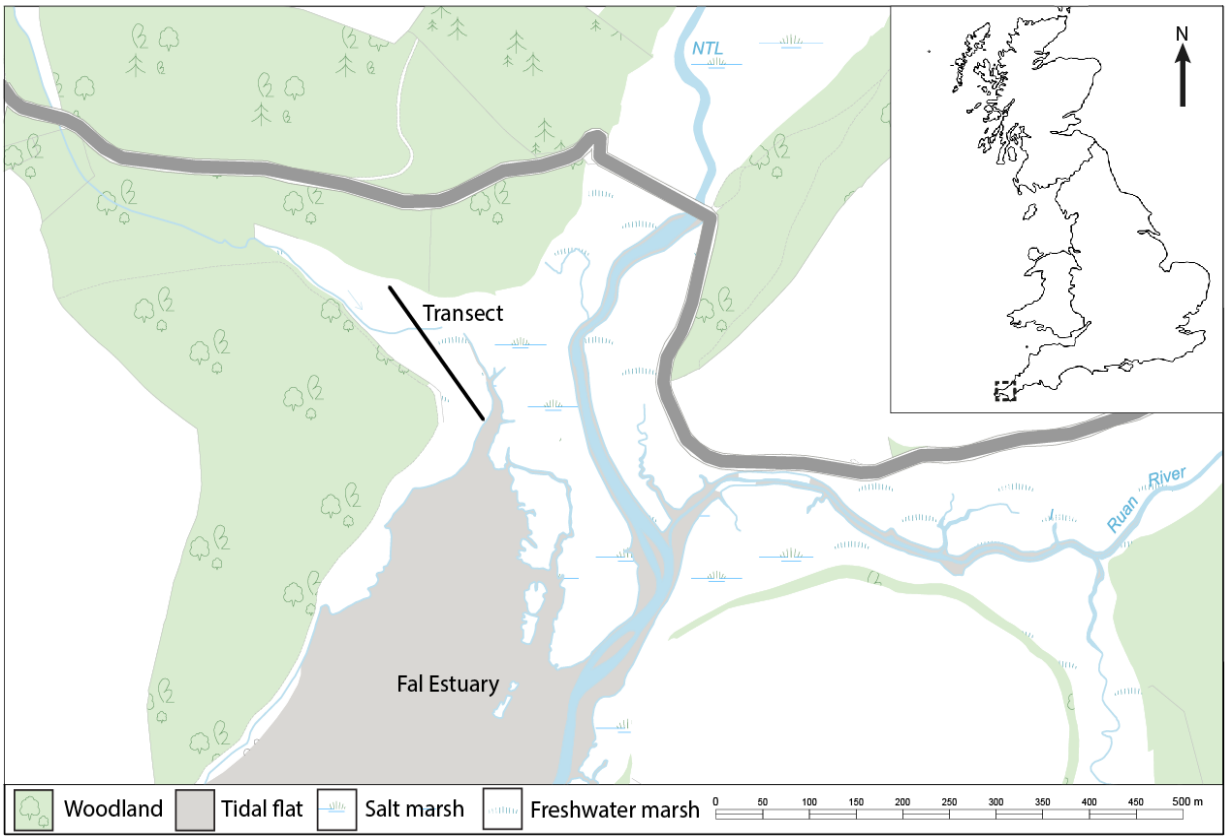

***Figure 3.3**: Location of Fal-Ruan salt marsh and sampling transect.*

***Table 3.2**: Tidal datums (m OD) at Fal-Ruan nature reserve inferred from Truro tidal information. MLWS/N – mean low water spring/neap tides, MHWS/N mean high water spring/neap tides, MSL – mean sea level, L/HAT – lowest/highest astronomical tide, MH/LWN – mean high/low water neap. Source: Admiralty Tide Tables vol. 1 (2015) * no data because this part of the Fal estuary falls dry at low tide.*

LAT	MLWS	MLWN	MSL	MHWN	MHWS	HAT
n/a*	n/a*	n/a*	2.6	3.2	4.2	5.0

3.3.1 Survey design and rationale

In November 2013 a surface transect was established running in the direction of slope, encompassing the intertidal zone and the full range of vegetation zones. In order to relate the marsh elevations to Ordnance Datum at Newlyn (OD) a benchmark was established and levelled using a Trimble DGPS RTK base station. The marsh surface elevations along the transect were measured to this benchmark using a Trimble SPS610 Total Station and Autolock precise measurement prism. Initially, surface samples were taken at ~5cm intervals along the entire marsh elevation gradient. These samples were analysed for testate amoebae and a subset of 10 samples were selected for detailed for detailed study based on their species richness and abundance. In each subsequent month up to, and including, November 2014 samples were taken from the same 10 'sampling stations' comprising the subset of initial samples. The 10 sampling stations were also purposefully chosen at elevations that mostly lie between HAT and MHWS to ensure testate amoebae populations predominantly governed by tidal influence were being monitored. Above HAT, the variance of testate amoebae populations explained by tidal influence declines (Ooms *et al.* 2012) and below MHWS testate amoebae diversity and abundance declines (Charman *et al.* 2010). In order to locate sampling stations each station was marked with an iron rod and located using a Trimble Geo 7 handheld GPS. To avoid sampling sediments disturbed by previous sample collections, samples were taken at progressive 15cm intervals along a transect (running perpendicular to the elevation gradient) measured from the iron rod at each station. For consistency all sampling dates coincided with the week succeeding the second Spring tide of each lunar cycle.

3.3.2 Species diversity measures

For each monthly sampling period species data from all 10 sampling stations were used to measure species diversity. Species diversity was measured using several commonly used indices, as follows:

Simpson's diversity index (D):

$$D = \frac{1}{\sum_{i=1}^{s} {p_i}^2}$$

where S is the total number of species and the p_i is the proportion of S made up of the ith species, and Simpson's evenness (E) is calculated as:

$$E = \frac{D}{D_{max}} = \frac{1}{\sum_{i=1}^{s} {p_i}^2} \times \frac{1}{S}$$

(Simpson, 1949)

Shannon-Wiener index (H), where proportion of species i relative to the total number of species (p_i) is calculated, and then multiplied by the natural logarithm of this proportion ($\ln p_i$). The resulting product is summed across species, and multiplied by -1:

$$H = -\sum_{i=1}^{s} p_i \, ln \, p_i$$

(Shannon, 1948).

3.4 Laboratory methods

This section presents the laboratory methods which are applied in the analysis and results generation of subsequent chapters. Where there are any slight modifications to this overarching methodology they will be described in the relevant section.

3.4.1 Testate amoebae analyses

All the modern surface samples and cored sediments were subsampled and prepared for testate amoebae analysis. The preparation procedure followed an adapted methodology to that developed by Barnett *et al.* (2013) for processing salt-marsh testate amoebae, which itself is adapted from Charman *et al.* (2000) as follows:

1. Take a $1cm^3$ subsample of sediment from the core or the upper 0.5cm of each surface sample. For surface samples only, soak in 2g/L Rose Bengal and deionised water solution (minimum 48hrs) to stain the testate amoebae protoplasm in order to differentiate between live and deceased populations (see: Walton, 1952).
2. Transfer the subsample to a 250ml Pyrex beaker, dilute with 150ml deionised (di) H_2O and add 1 *Lycopodium clavatum* tablet in order to calculate testate amoebae concentrations (see: Stockmarr 1971).
3. Warm the beaker on a hot plate at 80^oC for a minimum of 2 hours, agitating every 15 minutes, cool and leave to soak for a minimum of 12 hours in order to aid disaggregation.
4. Sieve the sample and retain the ≥15µm - ≤212µm fraction.
5. This stage calls for an *a posteriori* approach to be employed in order to make a better-informed decision of whether to apply a weak alkali treatment (cf. Barnett *et al.* 2013) to aid in the removal of detrital material which may obscure tests during routine counting. A minute fraction of the retained fraction is mounted (see step 9) and examined under light microscopy to determine the extent of detrital material.
6. a. If detrital material is not sufficient enough to significantly obscure tests continue to step 7.

b. If there is excessive detrital material then apply a [5%] KOH treatment (see: Barnett *et al.* 2013).

7. Transfer the retained fraction into a 30ml Sterilin tube and dilute with diH_2O for storage.
8. Prior to counting, centrifuge at 3000 RPM for 5 minutes and remove supernatant.
9. Pipette a small amount (1-2 drops) of the sample onto a 22x50mm glass microscope slide, add 1 drop of Glycerol and 1 drop of diH_2O, mix with wooden rod, cap with coverslip and seal with nail varnish.

Subsampling was performed scrupulously to prevent cross-contamination of samples. All equipment and surfaces were thoroughly rinsed with diH_2O before and between each sample was taken. For fossil sampling, the outermost sediment was removed from the core, cutting in a horizontal direction, to diminish the possibility of downcore contamination caused by the auger. The key adaptation of Barnett *et al.*'s (2013) methods is the addition of the *a posteriori* decision process. This is aimed at reducing the risk of test loss and/or test degradation associated with weak alkali treatments (see: Hendon and Charman, 1997; Haynes, 2011). The modified mounting procedure has the benefit of test manoeuvrability achieved by non-permanent diH_2O mounts; the addition of the glycerol- diH_2O solution prevents drying-out, enabling slides to be archived whilst not compromising the optical clarity
(cf. Charman *et al*. 2000). Test concentrations were calculated for each sample following the equation:

$$C = \frac{\left(\frac{\sum a}{\sum c}\right) * \sum t}{s}$$

where *C* represents the concentration of tests per cm^3, Σa and Σc represents the total number of *Lycopodium* spores added and total counted respectively, Σt represents the total number of tests and *S* the volume of the sample.

Tests were counted under light microscopy (400x magnification) until a minimum of 100 unstained (dead) individuals was reached. For the seasonal study (**Chapter 4**) exactly 150 individuals (live or dead) were counted in the combined interests of capturing full ecological diversity (cf. Payne and Mitchell, 2009) and maintaining even samples necessary for appropriate comparisons of species diversity indices. Identifications were made in accordance with the classification schemes of Charman *et al.* (2000) and Booth and Sullivan (2007) based primarily on test morphology. Certain taxa are not described in these keys, but have been described in recent studies of salt marsh testate amoebae (Gehrels *et al*. 2001; Charman *et al*. 2002; Gehrels *et al*. 2006b).

3.4.2 Foraminifera analyses

Modern surface material and fossil core material was subsampled and prepared for foraminiferal analyses following the method of Gehrels (2002) which itself is adapted from Scott and Medioli (1980b). Surficial (upper 0.5 cm) and core subsamples of $2cm^3$ volume were measured by water displacement. All the modern and fossil subsamples taken from the upper 20 cm of the core were stained using a 2g/L Rose Bengal and deionised water solution (for 24-48 hours). Rose Bengal stains live organic proteins pink and helps the identifier to differentiate between living and deceased foraminifera (Walton 1952; Murray and Bowser 2000). Following Murray and Alve (1999), tests

containing stained protoplasm within the last few chambers were assumed to be living at the time of collection. Subsamples were wet sieved with the ≤500 - ≥63μm fraction being retained for analysis. The entire 2cm^3 sample was counted, with all foraminifera contained being picked and archived in counting trays for subsequent identification.

Both the living and deceased assemblages were counted for all samples. Living populations exhibit seasonal variations in standing crops (e.g. Horton and Murray, 2006) thus introducing the risk of seasonal bias which may occur as a consequence of the timing of sample collection. It is assumed that deceased specimens represent a time-averaged assemblage that is immune from the effects of seasonality (Horton and Edwards, 2003). Therefore only the deceased assemblages from modern samples were included in the modern training set for foraminiferal transfer functions on the basis that these most closely resemble fossil assemblages (Murray 1976, 1982, 2000).

3.4.3 Diatom analyses

For modern and fossil diatom analyses, sample preparation followed a slight modification of the standardised procedures presented by Palmer and Abbott (1986) and Batterbee *et al.* (1988). For modern samples the upper 0.5 cm was sampled. The only modification was to replace the centrifugation stage with successive manual decantations (using a pipette) in the interest of reducing the risk of damage to valves (cf. Blanco *et al*., 2008). Diatoms were identified, where possible, to species and sub-species level under light microscopy (1000x magnification) primarily following the taxonomy of Krammer and Lange Bertalot (1991a, 1991b, 1997a, 1997b). For each sample a minimum of 300 diatom valves were counted following Zong (1997).

A representative proportion of each sample mounted beneath each cover slip was examined by counting individual fields of view along continuous traverses, ensuring that both central and edge sections of the cover slip were examined. Diatom preservation was variable with some samples containing many broken valves. All fragments that included the centre part of the valve were counted as one. For taxa which do not possess recognisable centres fragments where at least ca. 60% of the valve was present were also counted as one. Complete frustules were counted as two (Batterbee *et al.*, 2001). In this study it is assumed that the surficial diatom assemblage encompasses several seasonal cycles, thus negating bias related to seasonal blooms in diatom species (Zong and Horton, 1999). It is also assumed a mixture of both allochthonous and autochthonous valves occur in both modern and fossil sediments with no significant differences in the relative proportions (Zong, 1997), therefore, no attempt to separate allochthonous valves was made.

3.4.4 Lithology and sedimentalogical analyses

The sedimentalogical and lithological properties of intertidal sedimentary sequences can provide valuable additional information to aid palaeoenvironmental interpretations (see: Switzer and Pile, 2015; Plater *et al.,* 2015). This section describes the methods employed in various analyses performed on core SI-2 including; loss-on-ignition, organic content and particle size analysis.

Loss-on-ignition

Loss-on-ignition (LOI) was used to measure the organic matter (OM) and carbonate ($CaCO_3$) content of a sediment sample. The method is based on a two-step reaction whereby OM (carbon) is oxidised at 500-550^{o}C and lost from the sediment as carbon

dioxide (CO_2) and at 900-1000^oC CO_2 is released from $CaCO_3$ (Ball, 1964,1986). The estimated OM and $CaCO_3$ content of a sediment sample can therefore be determined by measuring the weight loss that occurs during these reactions which is proportional to the amount of organic carbon in a sample (Dean, 1974).

In this project the OM and $CaCO_3$ content of a sample were estimated following the recommendations of Heiri *et al.* (2001) based on evaluation of standard methods (Dean, 1974; Bengtsson and Enell, 1986) as follows:

- Sediment subsamples of roughly equal volume (ca. 5cm^3) were placed in crucibles of approximately equal volume and shape;
- The subsamples were oven-dried at 100^0C for a minimum of 12 hours (max 24 hours) , cooled to room temperature and their dry weights recorded (~0.5 – 1.3 g);
- The subsamples were then placed in a muffle furnace and combusted at a constant 550^oC for 4 hours and the subsequent weights recorded;
- Finally, samples were returned to the furnace and combusted at a constant 950^oC for 2 hours.

OM estimates were calculated following the equation:

$$LOI_{550} = ((DW_{100}–DW_{550})/DW_{100})*100$$

where LOI_{550} represents LOI at 550 °C (as a percentage), DW_{100} represents the dry weight of the sample before combustion and DW_{550} the dry weight of the sample after combustion at 550 °C.

$CaCO_3$ estimates were calculated following the equation:

$$LOI_{950} = ((DW_{550}–DW_{950})/DW_{100})*100$$

where LOI_{950} is the LOI at 950 °C (as a percentage), DW_{550} is the dry weight of the sample after combustion of organic matter at 550 °C, DW_{950} represents the dry weight of the sample after combustion at 950 °C and DW_{100} is the dry weight of the sample before the OM combustion. The weight loss by LOI at 950 °C multiplied by 1.36 theoretically equals the weight of carbonate in the original sediment sample (Bengtsson and Enell, 1986).

Particle size analysis

The measurement of particle sizes through salt marsh sequences can be used to aid palaeoenvironmental interpretations and is therefore often conducted in proxy studies of sea-level change (see: Switzer and Pile, 2015, for a review). In this project particle size analysis followed the methods outlined below.

Sediments were subsampled (ca. 5g), oven dried at 100^{o}C overnight, and disaggregated using a rubber pestle and mortar. Samples were weighed and then sieved to separate the sample into proportions >1mm and <1mm in dimension. The >1mm fraction was then weighed to determine the relative proportion >1mm of the initial sample. The <1 mm fraction was analysed to determine the relative proportions of clays, silts and sands. The <1mm fraction was split into three subsamples (ca. 0.5 cm^3), placed into 10 ml vials containing a 3% hydrogen peroxide (H_2O_2) solution and heated at 40^{o}C in a water bath. Samples remained heated in the H_2O_2 until there was no organic detritus remaining. A Malvern Mastersizer 2000 and autosampler were used to measure particle size distributions at half phi scale resolution for each subsample. The process was replicated 5 times for each subsample. The coefficient of variation (CV) between the results of each of the 5 replicates was used to identify outliers. Outliers were defined by a CV >15% and, where present, the outlying replicate result discarded. The averages of the outlier-

removed replicate results were then used to calculate the particle size distributions for a given sediment sample.

3.5 Data analysis

Prior to applying the modern species-environment data to perform palaeoenvironmental reconstructions based on the fossil assemblage data it must be thoroughly scrutinised quantitatively, but also qualitatively, to ensure quality and to enable informed decisions to be made during transfer function development. The various methods used in transfer function development are discussed in detail by Kemp and Telford (2015). This section describes the specific methods employed in this project in the generation and assessment of transfer functions and the analysis of species and environmental data.

3.5.1 Cluster zonation and ordination

Raw species counts were initially converted to relative abundances (%) for each sample. The relative abundances are used to illustrate species distributions. The modern assemblage data were assigned to hierarchical faunal zones inferred from the results of constrained cluster analysis (incremental sum of squares, Euclidean distance, unweighted, no transformation (Grimm, 1987) performed with CONISS in Tilia version 2.0.b.4 (Grimm, 1990). Detrended correspondence analysis (DCA: detrending by segments, no transformation) was performed in CANOCO for Windows version 4.56 (Jongman *et al*. 1995; ter Braak and Šmilauer, 2002) to supplement the cluster analysis and aid in defining boundaries between cluster groups.

3.5.2 Data screening

Prior to further analysis the raw modern assemblage data were subjected to screening to assure data quality and thus improved accuracy in the reconstruction. The intention

was to identify outlier samples and/or anomalous species data (i.e. taxa that did not have their entire environmental range sampled). For each taxonomic group, raw modern species counts were used to calculate the fractional abundance of each taxonomic unit in each sample (Patterson and Fishbein, 1989). Following Wright *et al.* (2011) the minimum fractional abundance was computed at the 95% confidence level for each sample using the following equation (Fatela and Toborda, 2002, pp. 170):

$$p = 1 - f\,(0.05)^{1/n}$$

Where p is the minimum fractional abundance acceptable for a species, n is the total number of individual specimens counted and f is the specified confidence level. All species within a sample were deemed to have been sufficiently detected if fractional abundances exceeded this level. Species with fractional abundances below this level are determined to be insufficiently captured and are therefore omitted from the sample for subsequent analysis. The remaining species data along with the sample elevations comprise the final training sets from which the transfer functions were developed from.

3.5.3 Transfer function development

An iterative approach was used to model the modern species-environment relationship and generation of transfer functions for each microfaunal group. For each microfaunal group the species relative abundances were used in the analyses employed in transfer function development. The first step was to explore the species distributions in response to elevation, as well as other environmental variables, through the process of ordination (e.g. ter Braak, 1995; Legendre and Birks, 2012). In order to determine the nature of the species-environment relationship (i.e. are species

collectively responding unimodally or linearly?) detrended canonical correspondence analysis (DCCA: ter Braak, 1986) was performed using elevation and species relative abundance (%) data. DCCA was performed in CANOCO for Windows version 4.56 (Jongman *et al*. 1995; ter Braak and Šmilauer,2002). Environmental variables are separated into axes with the response of each variable given for each axis. DCCA calculates gradient lengths for measured (canonical) and unknown environmental variables, measured in SD units (but not actual standard deviations) - full species turnover along an environmental gradient has a gradient length of 4 SD. As a general rule-of-thumb (following ter Braak and Prentice 1988) if a gradient length is >2 SD then a majority of the taxa in the training set are likely to have their optima along the sampled gradient implying a unimodal response; gradient lengths <2 SD therefore imply a linear species-environment response. Only one canonical environmental variable (elevation) was measured in this study owing to project limitations (time and budget constraints). DCCA also calculates the proportion of variance explained by the environmental variables (measured or unknown) calculated as eigenvalues for each axis. Because in this study there is only ever one measured variable (elevation) only the first axis is canonical and is representative of the species variation explained by the measured environmental variable – higher axes represent the 'residual' variation. Although the environmental variable(s) responsible for the residual variation is unknown they can be very useful in exploratory analyses; they quantify the effect of environmental variables other than elevation have on the species distributions. Ordination bi-plots are used in this study to visually assess the ordination results.

The next step of transfer function development is to apply multivariate regression to model the species-elevation relationship. Appropriate regression models were selected on the basis of the DCCA results e.g if species are responding unimodally

then the unimodal regression methods of weighted averaging (WA) and weighted averaging partial least squares (WAPLS) were explored. The bootstrapping cross-validation procedure (10000 iterations) was applied to all regressions. Initially, all samples and species remaining in the training set after data screening (**Section 3.5.2**) were used for the regression modelling to generate a series of transfer functions. A set of performance statistics were generated for each transfer function; root mean squared error (RMSE), coefficient of determination (r^2), root mean squared error of prediction (RMSEP), average bias and max bias. The RMSEPs of the initial set of transfer functions were used identify and remove any anomalous samples (outliers). There is no consensus approach to outlier removal (Barlow *et al*. 2013) but this study follows Edwards *et al*. (2004), deeming samples that exhibit a residual error (the difference between the observed value and the estimated value during cross-validation) greater than the standard deviation of the environmental gradient to be significant outliers and these were therefore removed. Where outliers were removed additional, qualitative, justification for their removal was sought based on field observations during sample collection and visual inspection of the data (e.g. Barlow *et al.* 2013). After removal of outlier samples (if identified) the regression models were run again on the outlier-removed training set. The final transfer functions to be applied in the generation of environmental reconstructions were selected on the basis of their performance statistics and visual inspection of scatterplots of observed and estimated values generated by cross-validation.

3.6 Chronology

A number of techniques were employed to date the salt-marsh sediments from Swan Inlet. This section explains the methods (radiocarbon and other short-lived

radionuclides) utilised to obtain age constraints in this project and the rationale followed.

3.6.1 Radiocarbon dating

Rationale

The radiocarbon dating in this project was conducted in two stages. The initial stage was aimed at establishing the chronostratigraphy of the millennial-scale sea-level history of Swan Inlet. 'Rangefinder' dates were obtained for 10 samples taken at the contacts between major stratigraphic units (full details in **Section 6.2.2**). This enabled the age of stratigraphic units (indicative of sea-level related changes in depositional environment) to be determined. With the exception of a grass fragment extracted from the exposed bank section, rangefinder dates were obtained from bulk sediment samples as no additional plant macrofossils were found at key stratigraphic transitions. The second stage was to develop a detailed radiocarbon chronology for the late Holocene toward fulfilment of **Aim 1**. The framework provided by the results of the rangefinder dates (**Section 6.2.2**) identified the upper 90 cm of core *SI-2* to be of late Holocene age. Therefore, this 90 cm section of core *SI-2* was meticulously dissected and 19 suitable plant macrofossils extracted for radiocarbon analysis (**Section 6.3.3**).

Samples being analysed for radiocarbon analyses should, ideally, remain unaltered by any process other than radioactive decay since interaction with the biosphere ceased. However, in intertidal environments there are many (post)depositional processes which can alter (contaminate) the radiocarbon content. In order to reliably constrain the depositional age of a sedimentary horizon it is, therefore, of critical importance that the dated material is representative of the depositional environment it is found i.e. *in situ*. With these factors in mind strict protocols for the selection of

suitable material and analytical (laboratory) procedures were observed to negate the risk of unreliable results.

Sampling protocol

Core samples were subsampled for bulk sediments (~1g wet weight) from the inner portion of the core in order to negate the risk of sampling sediments contaminated by penetration of the auger when coring. For the sampling of plant fragments the outer surface of the upper 90cm of core *SI-2* was removed (scraped horizontally). The core was dissected with stainless steel tweezers and a scalpel in search of suitable material for dating. The identification of suitable, *in situ,* material was based on the following criteria for plant fragments; being of terrestrial, above ground origin; being detrital in origin; being horizontally lain; showing few signs of damage (reworking); originating from the surrounding environment. The selected plant fragments were then rinsed with deionised water, examined under a low power microscope and removed of penetrating micro-roots. All samples were oven dried at 40^{o}C and stored in airtight glass vials.

Sample pretreatment

Pretreatment of all samples was conducted at the NERC Radiocarbon Facility (East Kilbride). Bulk sediment samples were digested in 2M HCl (80^{o}C, 8 hours), washed free from mineral acid with deionised water then digested in 0.5M KOH (80^{o}C, 2 hours). The digestion was repeated using deionised water until no further humics were extracted. The residue was rinsed free of alkali, digested in 1M HCl (80^{o}C, 2 hours) then rinsed free of acid, dried and homogenised. Plant fragment samples were digested in 2M HCl (80^{o}C, 8 hours), washed free from mineral acid with deionised water then dried and homogenised.

Analytical procedure

The AMS method of direct isotope counting was used to determine ^{14}C concentrations. The samples were prepared to graphite at the NERC Radiocarbon Facility (East Kilbride). The total carbon in a known weight of the pre-treated sample was recovered as CO_2 by heating with CuO in a sealed quartz tube. For high precision samples, the recovered sample CO_2 was split to provide multiple targets (duplicate or triplicates) when sufficient amounts of CO_2 were available. One graphite target was produced for each sample by Fe/Zn reduction. The graphite targets were analysed for ^{14}C at the Scottish Universities Environmental Research Centre (SUERC) AMS facility.

Calibrations

Conventional radiocarbon ages were calibrated to calendar ages using the SHcal13 calibration curve (Hogg *et al.,* 2013) in the Calib program (v7.1; Stuiver and Reimer,1986). Modern (post nuclear weapons testing) ages were calibrated with the SH Zone 1-2 bomb curve extension using the CaliBomb program (Reimer *et al.*, 2004).

3.6.2 Short-lived radionuclide dating

To provide additional age constraints for the most recent RSL reconstruction, core SI-2 was analysed for ^{137}Cs and ^{210}Pb concentrations. The methods used in this project follow those described by Appleby (2002). The upper 20 cm of core SI-2 was subsampled contiguously at 0.5 cm resolution. The bulk density of each subsample was calculated and then the samples were ground with a pestle and mortar in order to disaggregate into a homogenised sample. The homogenised samples were packed into 4 ml vials and the weight of the packed sample was recorded. The packed sample vials were sealed and stored for 25 days to the allow ^{214}Pb and ^{226}Ra to reach equilibrium. Analyses were performed at the Consolidated Radioisotope Facility (CoRIF) at Plymouth University using the EGandG Ortec well (GWL-170-15-S) HPGe Gamma spectrometry system. The instrument was calibrated using sediments spiked

with a traceable, certified, mixed radioactive standard. Samples were counted for a minimum of 48 hours for activity concentrations of ^{210}Pb, ^{214}Pb, ^{137}Cs and ^{241}Am.

3.6.3 Age-depth modelling

In order to provide a temporal framework for considering sea-level changes in the Falklands it was necessary to model the age-depth relationship throughout dated core sections. This was achieved following a flexible Bayesian age-depth modelling approach using the program Bacon v.2.2 (Blaauw and Christen, 2011). Cores were divided into contiguous 1cm segments and linear accumulation rates were calculated for each segment sequentially through the core. Age-models were developed based on several million iterations, followed by thinning to remove any autocorrelation between individual model runs. More specific details of the age-depth modelling approach can be found in **Section 6.2.6**.

Chapter 4 - Seasonal distributions of salt-marsh testate amoebae

4.1 Introduction

This chapter presents the results of the monthly monitoring of salt-marsh testate amoebae distributions at the Fal Ruan salt marsh in fulfilment of **Aim 2** of this project. The chapter begins with a description of the marsh topography, dominant vegetation zones and the location of the monthly monitoring stations. Summary and statistical comparisons of the monthly testate amoebae assemblages are presented. This chapter finishes by presenting a suite of seasonal transfer functions based on different combinations of sampling timing in order to determine the optimal sampling strategy for developing salt marsh testate amoebae transfer functions.

4.2 Marsh topography and vegetation cover

The 10 monthly monitoring stations were situated along a single surface transect (**Figure 3.2**) which covered the entire woodland-mudflat succession of the marsh. The marsh topography, dominant vegetation cover and the location of each sampling station are shown in **Figure 4.1**. The upper, northern, extent of the marsh is marked by a steep transition to an *Alnus-Quercus* woodland which encroaches on to the high marsh. The high marsh vegetation is dominated at its upper limit by *Phragmites australis.* This transitions to a *Festuca rubra*-dominated zone with pockets of *Juncus maritimus* from the high-marsh to the upper mid-marsh. At the transition between upper mid-marsh to lower mid-marsh the vegetation transitions from *Festuca rubra* to *Puccinellia maritima.* The *Puccinellia maritima* zone extends from the mid-marsh into the low-marsh. The low-marsh transitions from the *Puccinellia maritima* zone to a zone dominated by *Spartina maritima* which extends across the low marsh to the sharp transition to mudflat. The extensive mudflats are mostly unvegetated but there are

isolated patches of *Salicornia sp.* at the upper limit. The details of monitoring stations, dominant vegetation cover, and marsh sub-environments are summarised in **Table 4.1**.

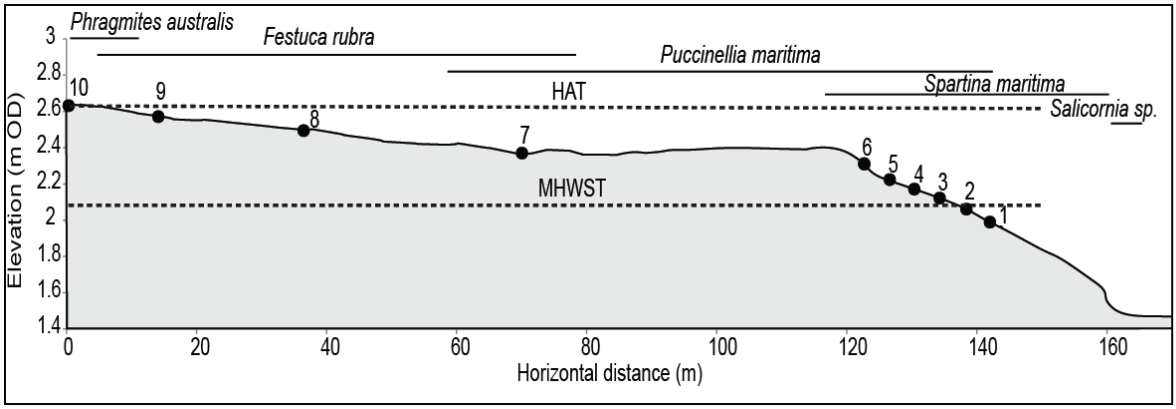

***Figure 4.1**: Topographic profile of the surface sampling transect, dominant vegetation and locations of monitoring stations.*

***Table 4.1**: Dominant vegetation cover, elevation and marsh sub-environment for each monthly sampling station.*

Station number	Dominant vegatation	Elevation (m OD)	Sub-environment
1	*Spartina maritima*	2.03	low marsh
2	*Spartina maritima*	2.10	low marsh
3	*Puccinellia maritima/Spartina maritima*	2.19	lower mid-marsh
4	*Puccinellia maritima/Spartina maritima*	2.26	lower mid-marsh
5	*Puccinellia maritima/Spartina maritima*	2.30	lower mid-marsh
6	*Puccinellia maritima/Spartina maritima*	2.35	mid-marsh
7	*Festuca rubra/Puccinellia maritima*	2.42	mid-marsh
8	*Festuca rubra/Puccinellia maritima*	2.48	upper mid-marsh
9	*Festuca rubra*	2.55	high-marsh
10	*Phragmites australis/Festuca rubra*	2.63	high-marsh

4.3 Seasonal testate amoebae distributions

This section presents the results of the monthly monitoring of testate amoebae populations at the 10 sampling stations over one annual cycle. The first part of this section summarises the testate amoebae count data for each monthly sampling. The second part of this section explores seasonal variations in the live and death assemblages. The dataset for which subsequent analyses is based on comprises 130 samples (10 samples from each of the 13 sampling periods), 36 species (19,500 individuals)

4.3.1 Summary of testate assemblages over one annual cycle

In total 30 taxa were recorded across all monitoring stations during the annual cycle. A summary of the total live and dead testate amoebae surface distributions recorded at all sample stations between November 2013 and November 2014 is presented in **Table 4.2**. Excluding rare species (< 2% relative abundance) from the 26 taxa present only 12 taxa remain (**Figure 4.2**). These 12 taxa were also recorded in every sampling month. The average number of taxa recorded in a single sampling month was 21.1. The maximum number of taxa recorded in a single month was 26 in May 2014 and the minimum was 16 in November 14. May 2014 also saw the greatest abundance of testate amoebae with 2200 ± 600 tests per cm^3. The lowest testate abundance (rounded to the nearest 100) was in December 2014 with 600 ± 200 tests per cm^3; the annual average was 1200 ± 500 tests per cm^3.

***Table 4.2**: Total number of live and dead testate amoebae taxa recorded along with mean and standard deviation of abundance for each sampling month (to the nearest 100).*

	Number of taxa	Abundance (tests per cm^3)
Nov-13	16	700 ± 300
Dec-13	18	600 ± 200
Jan-14	23	800 ± 200
Feb-14	21	900 ± 300
Mar-14	19	1600 ± 500
Apr-14	22	1500 ± 400
May-14	26	2300 ± 600
Jun-14	24	1000 ± 400
Jul-14	25	1100 ± 500
Aug-14	23	900 ± 400
Sep-14	22	800 ± 500
Oct-14	19	900 ± 500
Nov-14	16	700 ± 100
Annual average	21.1	1200 ± 500

Figure 4.2a-d shows the relative abundances of the testate amoebae taxa for representative seasonal populations over the annual cycle (absolute live and dead testate amoebae counts can be found in **Appendix D**). For each sampling period,12 taxa dominate, 6 taxa (*Pseudodifflugia fulva* type*, Tracheleuglypha dentata,*

Centropyxis cassis type*, Centropyxis delicatula, Centropyxiella* sp*.* and *Cyphoderia ampulla*) reach individual relative abundances over 10% for each month. Combined, these taxa account for at least 47% (max 75%) of the testate amoebae death assemblage for each month. The number of taxa recorded at each monitoring station between November 2013 and November 2014 is presented in **Table 4.3.**

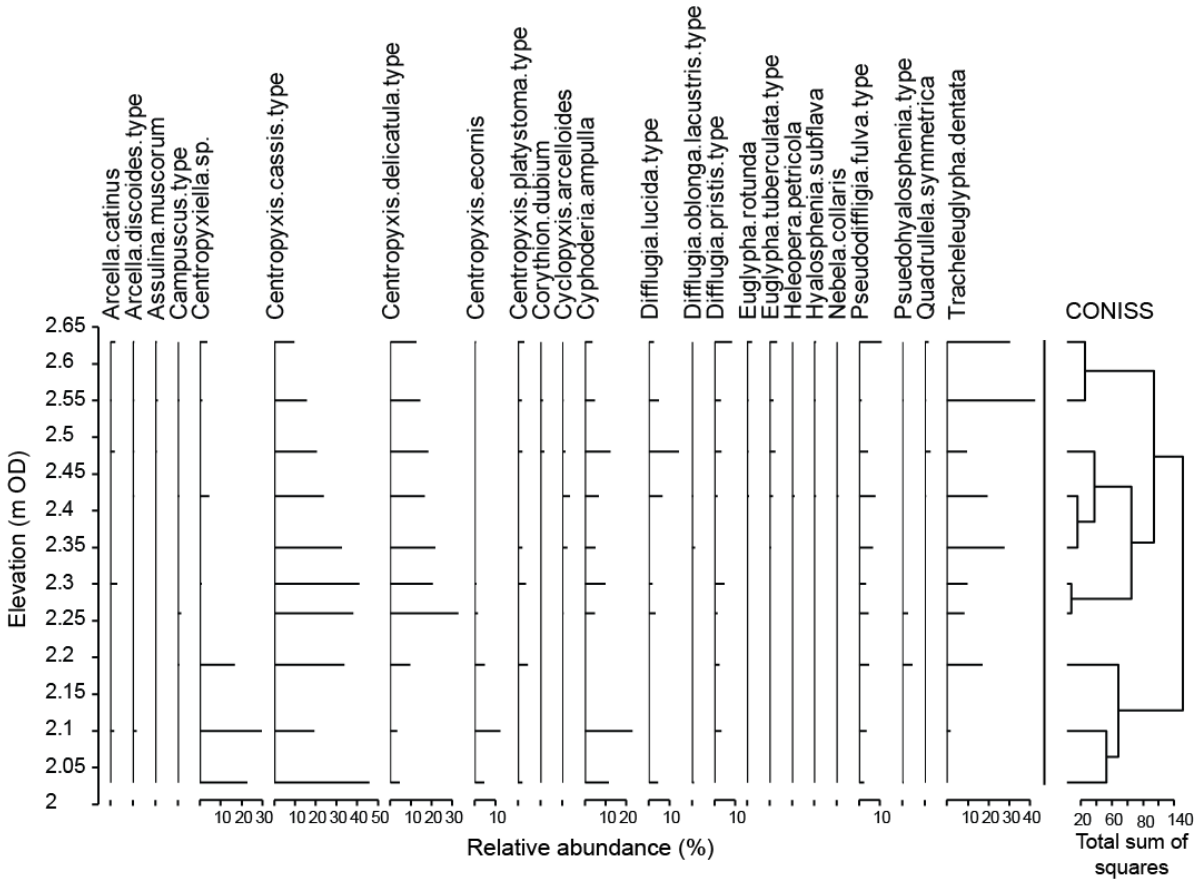

Figure 4.2a*: Constrained cluster analysis (CONISS) of total (live and dead) testate amoebae assemblages from a representative winter sampling (January 2014).*

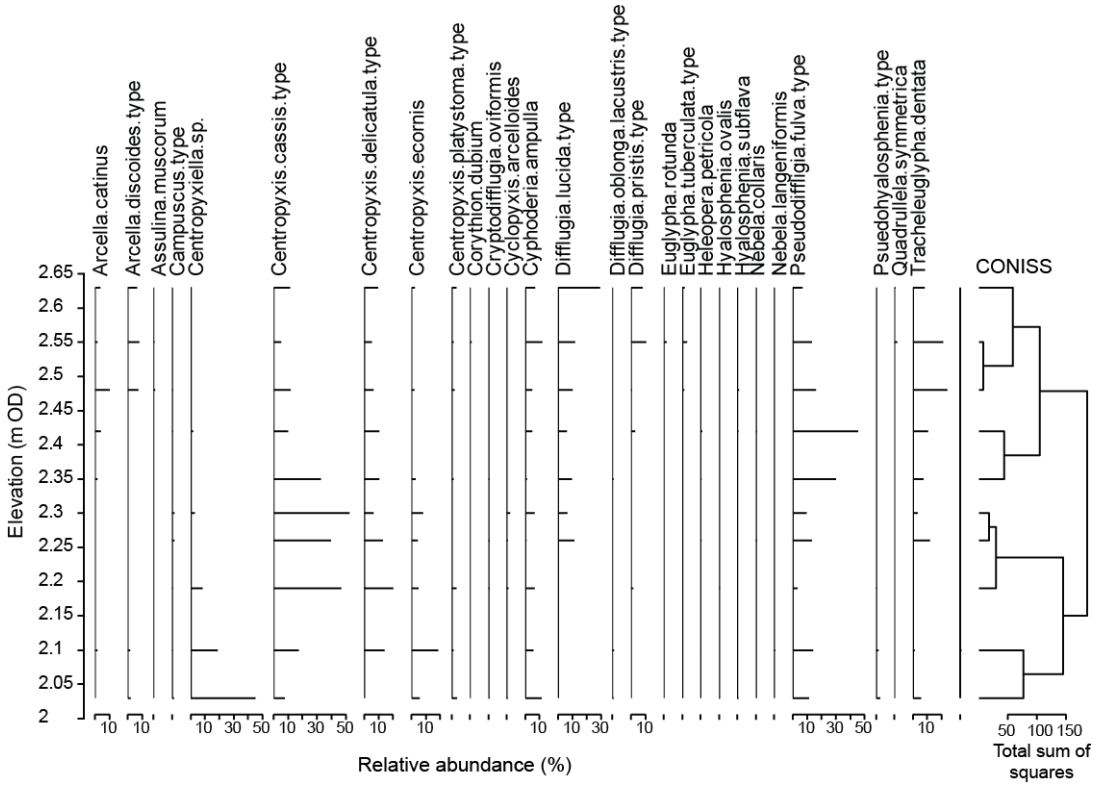

***Figure 4.2b**: Constrained cluster analysis (CONISS) of total (live and dead) testate amoebae assemblages from a representative spring sampling (May 2014).*

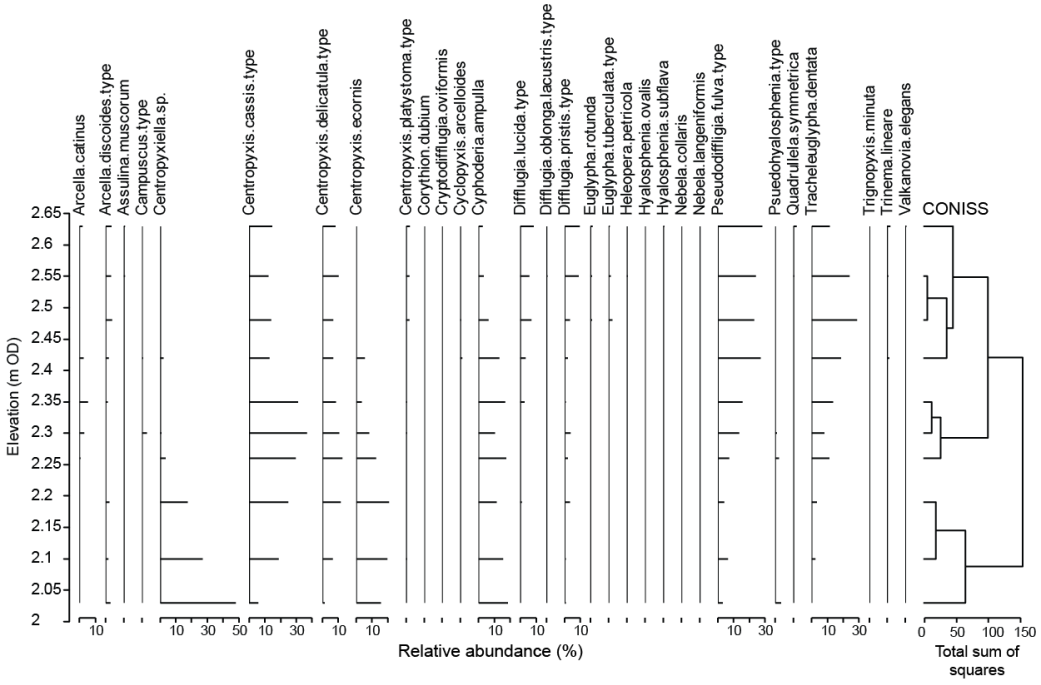

***Figure 4.2c**: Constrained cluster analysis (CONISS) of total (live and dead) testate amoebae assemblages from a representative summer sampling (August 2014).*

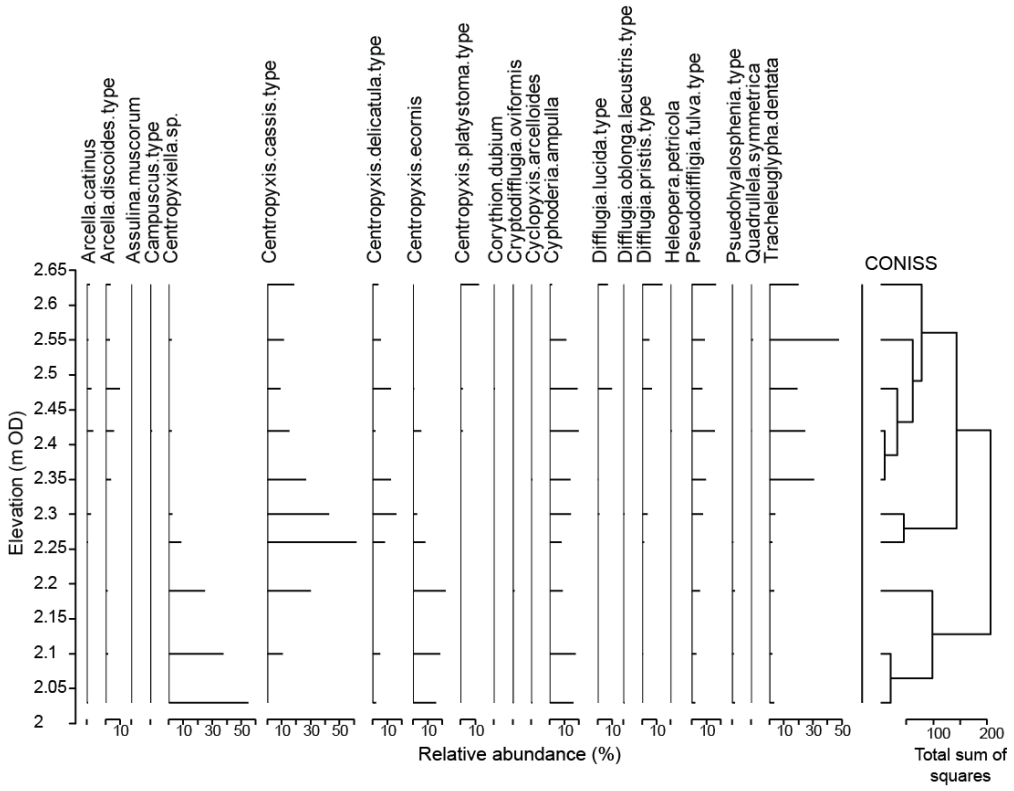

***Figure 4.2d**: Constrained cluster analysis (CONISS) of total (live and dead) testate amoebae assemblages from a representative spring sampling (November 2014).*

In general species richness (i.e. number of taxa present) is greatest at the higher marsh sampling stations and declines toward the lower limit of the testate amoebae tolerance zone. The transition between the higher marsh and lower marsh testate amoebae assemblages also corresponds to a decrease in relative abundance of *Pseudodifflugia fulva* type*, Tracheleuglypha dentata* and *Centropyxis cassis* type and an increase in relative abundance of *Centropyxiella* sp*., Centropyxis delicatula,* and *Cyphoderia ampulla* (**Figure 4.2a-d**). Over the annual cycle there is little variance in the number of taxa present at each station (min SD = 1.12: Station 4; max SD = 3.13 : Station 7). Although, at the highest elevations (Stations 6-10), where the number of taxa is greatest there is generally greater variance. Variance in the number of taxa

present in a given sampling month is greater than for number of taxa present at monitoring stations (min SD = 1.6 : November 2014; max SD = 5.2 : January 2013). There tends to be a greater mean number of taxa present during months with the greatest total number of taxa present and highest concentration of testate amoebae.

***Table 4.3**: Number of taxa recorded at each monitoring station over the annual cycle*

	Month													Mean	SD
	N	**D**	**J**	**F**	**M**	**A**	**M**	**J**	**J**	**A**	**S**	**O**	**N**		
Station 10	14	17	19	18	16	17	18	19	14	17	15	16	9	16.1	2.69
Station 9	13	15	21	19	15	14	16	17	18	16	19	15	11	16.1	2.72
Station 8	10	19	17	15	13	15	16	15	17	12	10	13	12	14.2	2.92
Station 7	10	18	20	20	17	13	19	17	15	14	13	16	14	16.1	2.90
Station 6	5	13	9	10	13	12	13	16	17	11	10	11	9	11.5	3.13
Station 5	10	12	11	9	14	13	11	13	12	13	10	10	12	11.5	1.51
Station 4	12	11	11	10	12	13	12	11	10	10	12	9	11	11.1	1.12
Station 3	10	9	10	10	10	9	14	15	12	10	14	13	9	11.0	2.31
Station 2	6	10	7	10	11	12	16	14	10	10	11	12	10	10.7	2.59
Station 1	9	9	10	11	11	10	15	11	13	10	9	12	10	10.8	1.74
Mean	10	13	14	13	13	13	15	15	14	12	12	13	11	12.9	1.42
SD	2.8	3.7	5.2	4.5	2.3	2.5	2.5	3	2.9	2.6	3.1	2.4	1.6	-	-

4.3.2 Seasonal variations of testate amoebae assemblages

Sea-level studies using foraminifera as proxies often use the microfossil death assemblages on the assumption that this is a time-averaged assemblage that negates seasonal blooms. This assumption requires testing for salt-marsh testate amoebae.

This section explores how both the death and live testate assemblages respond over the seasonal cycle. **Table 4.4** and **Figure 4.3** present seasonal variations of species diversity, species evenness and test concentrations in the death assemblages. There are many ways (indices) to measure species diversity, each with their own criticisms (e.g. Molinari, 1996; Tuomisto, 2010). Because the purpose of this study is not to measure 'true' species diversity *per se*, but is to understand testate amoebae assemblage changes over an annual cycle, several commonly used indices are used to provide quantitative estimates of biological variability in order to aid comparisons between sampling periods. Pielou's index measures only evenness (i.e. how evenly individuals in the community are distributed over the different species) and the other indices used here are heterogeneous indices (i.e. they measure both species richness and evenness). Indices which measure only richness were discounted as they only account for the number of taxa and not the abundances of each taxon; since changes in species abundances over an annual cycle can affect the proxy value of that species, richness indices are not useful for these comparisons.

In general species diversity varies little over the study period with all indices having a SD < 1. Evenness remains almost constant throughout the seasonal cycle (SD = 0.04). Simpson's index, which is generally considered more robust (Magurran, 2013), shows the most variance (SD = 1.0) and shows species diversity to be greater between May and November 2014 (**Figure 4.3**). Species diversity does not closely relate to changes in testate amoebae concentrations although peaks in diversity correspond to peaks in concentration. The concentration of dead testate amoebae varies from 493 tests per cm^3 in December 2014 to a maximum of 2023 in May. Testate amoebae concentration is characterised by a maximum between March and June.

***Table 4.4**: Species diversity calculated using, Simpson's and Shannon-Wiener indices, and Simpson's evenness index for the testate amoebae deceased assemblages for each sampling month*

	Nov-13	Dec-13	Jan-14	Feb-14	Mar-14	Apr-14	May-14	Jun-14	Jul-14	Aug-14	Sep-14	Oct-14	Nov-14	SD
Simpson's	5.8	7.5	7.8	6.7	6.6	6.2	8.2	7.8	7.7	7.8	8.5	9.2	8.7	0.17
Shannon-Wiener	2.2	2.3	2.3	2.3	2.3	2.2	2.4	2.4	2.3	2.3	2.3	2.4	2.2	1.00
Pielou's index	0.7	0.8	0.8	0.7	0.8	0.7	0.8	0.8	0.8	0.8	0.8	0.8	0.8	0.07
Simpson's evenness	0.7	0.8	0.8	0.7	0.8	0.7	0.8	0.8	0.8	0.8	0.8	0.8	0.7	0.04

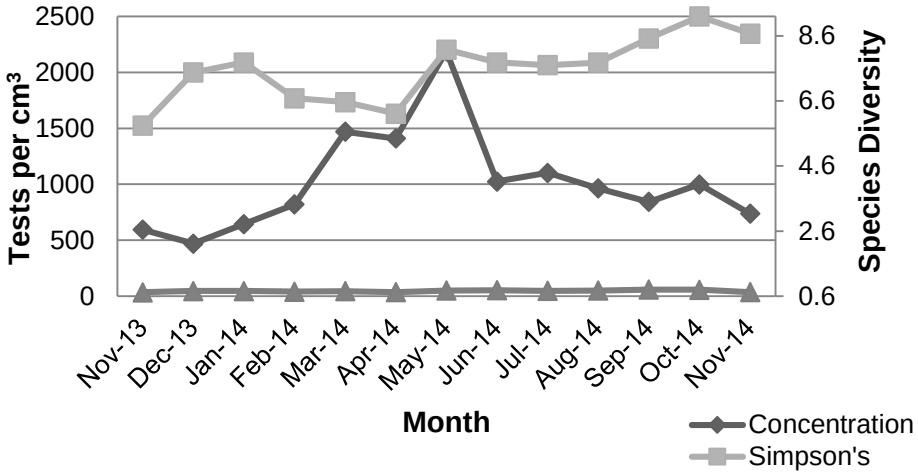

***Figure 4.3** Seasonal variations in testate amoebae species diversity (Simpson's index), Pielou's evenness and testate amoebae concentration for dead assemblages from all stations over the study period.*

Analysis of the live and dead proportion of the twelve most dominant testate amoebae species (**Figure 4.4**) identifies distinct seasonal blooms in the living populations which are species-specific. For all species the live proportion is never greater than the dead proportion. *Pseudodifflugia fulva* type has the greatest live proportion of all species accounting for ca. 40% of the total in January and February. Several species (*Tracheleuglypha dentata, Difflugia lucida type, Centropyxis delicatula type, Centropyxis cassis* type and *Pseudodifflugia fulva* type) have a live population >5% for most of the seasonal cycle. Increases in the ratio of living:dead for a species tends to precede increases in the relative abundance of the deceased assemblage for the

subsequent months (**Figure 4.4** and **Figure 4.5**). For example, a peak in the live proportion of *Pseudodifflugia fulva* type in January and February 2014 is followed by a sharp increase the *Pseudodifflugia fulva* type relative abundance for the deceased assemblage from February-April 2014. With the exception of *Tracheleuglypha dentate,* the relative abundance for all species within the deceased population displayed significant dispersion of between 24 to 81 % from the annual mean (**Figure 4.5**). Within the dead populations of the most abundant taxa (*Centropyxis cassis* type*, Centropyxis delicatula, Centropxis ecornis Centropyxiella sp, Pseudodifflugia fulva* type*, Tracheleuglypha dentata,* and *Cyphoderia ampulla*), there is a trend of increased relative abundance in some species corresponding with decreased relative abundance in another species. For example, the relative abundances of *Centropxis delicatula* type*, Centropyxis cassis* type and *Pseudodifflugia fulva* type generally decline as the relative abundances of *Cyphoderia ampulla* and *Centropyxis ecornis* increase.

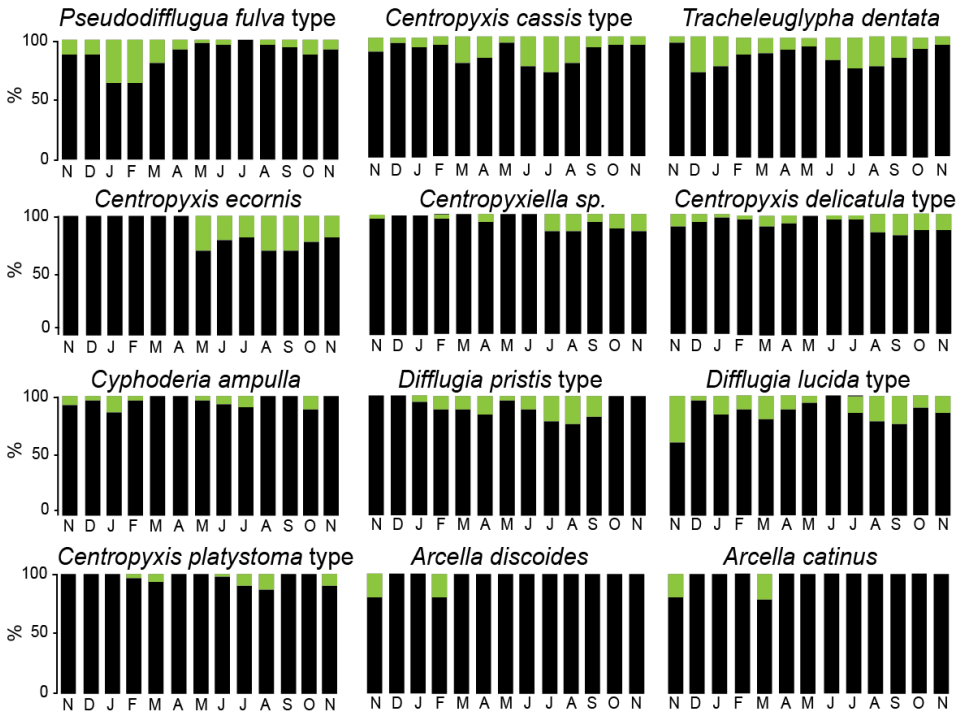

***Figure 4.4** : Relative proportions of live (green) and dead (black) specimens for the 12 most dominant testate amoebae species between November 2013 and November 2014.*

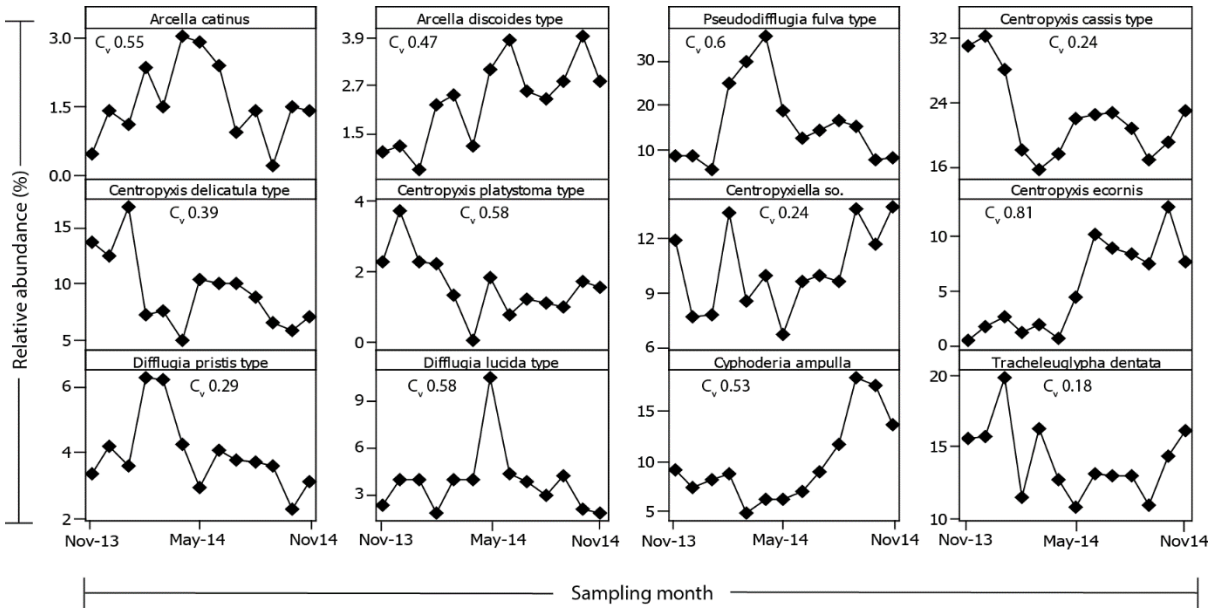

Figure 4.5*: Relative abundances and coefficient of variation (C_v) in the death populations of the 12 dominant testate amoebae taxa over the seasonal cycle.*

Cluster analysis was performed on the testate amoebae death assemblages for each month (following **Section 3.5.1**). For each month three main cluster zones were determined, from highest to lowest; zone I (sub-clusters Ia and Ib), zone II and zone III (**Figure 4.6**). It should be taken into consideration that the landward and seaward limits of the vertical zonation are not determined by the cluster analysis but by the upper end of the transect and the lowest limit of the saltmarsh occupied by testate amoebae respectively. The highest marsh zone Ia is distinguished from the other zones by comprising the greatest number of species each month. Zone Ia is dominated by varying abundances of *Psudodifflugia fulva* type*, Tracheleuglypha dentata* and to a lesser extent *Difflugia pristis* type, *Difflugia lucida, Centropyxis platystoma* and *Centropyxis cassis* type. Zone Ib has a similar composition to zone Ia but can be distinguished by an increase in dominance of *Psudeodifflugia fulva* type which reaches peak relative abundance in this zone and a decline in the relative abundance of *Difflugia pristis* type *and Centropyxis platystoma*. Zone II is

characterised by a dominance of *Centropyxis cassis* type and *Centropyxis delicatula* type, which both reach their greatest relative abundance in this zone, and a decline in the relative abundances of the dominant species in zone Ia and Ib. The lowermost zone III is characterised by an overall reduction in species richness and sharp increase in dominance of *Centropyxiella* sp. and to a lesser extent *Cyphoderia ampulla* and *Centropyxis ecornis.* The vertical cluster zonation varies throughout the annual cycle (**Figure 4.6**) in response to fluctuations in the relative abundances and species diversity, as described previously, of the dominant taxa in each cluster zone. The lower boundary between zones I and II reaches a maximum elevation of 2.43m OD in January 2014 and fluctuates between February and June 2014 reaching a minimum elevation of 2.3m in May 2014. There is generally greater variation in the elevation of each cluster zone between November 2013 and June 2014 (**Figure 4.6**). From June 2014 until the end of the study period the elevation of all cluster zones remains relatively stable with only the boundary between zone IIa and IIb shifting by 3 cm in July and October 2014. It should, however, be taken in to consideration that the elevation gradient was not particularly well nor evenly sampled in this study with only 10 elevations sampled at height intervals of between 5-9 cm.

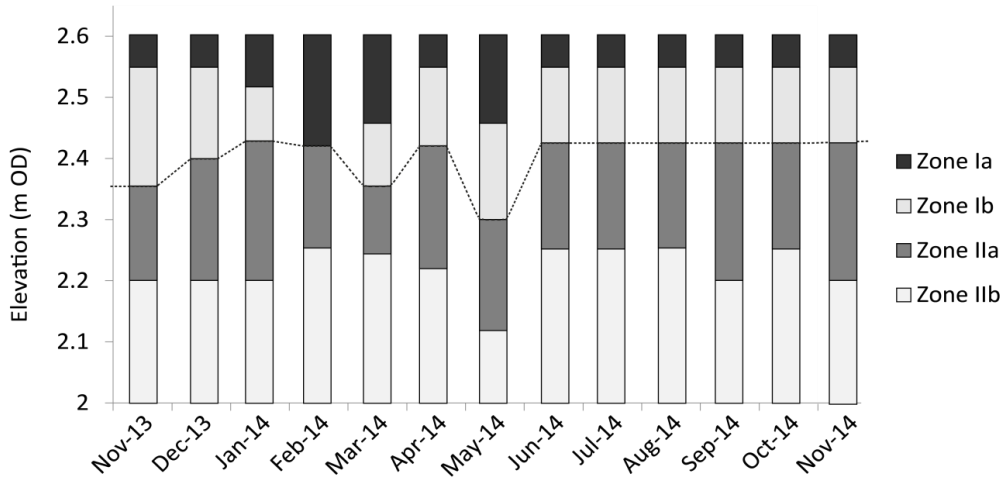

Figure 4.6*: Elevation of CONISS-defined cluster zones throughout the seasonal cycle.*

4.3.3 Effect of sampling strategy on transfer function performance

The primary purpose of this investigation of seasonal testate amoebae distributions is to determine the implications of seasonality with respect to utilising testate amoebae as a proxy for sea level. Because modern samples are usually only taken at one time of year it is pertinent to investigate how sampling at different times of the year affects the predictive ability of salt-marsh testate amoebae transfer functions. To this end, a number of transfer functions, based on several different seasonal 'training sets' were developed for comparison. The small number of samples taken each month (n=10) makes it unfeasible to develop reliable transfer functions for each monthly assemblage. Thus, amalgamations of the monthly assemblage data were used to create larger (≥ 30 samples) training sets that represent individual seasons (i.e. sampling at one time of year), all possible combinations of seasons (i.e. two samplings each at different times of the year) and a full season (i.e. samplings throughout the annual cycle) (**Table 4.5**).

Table 4.5*: Composition of seasonal training sets based on amalgamated samples taken throughout the seasonal cycle.*

Training set	Samples included	No. of samples
Winter	Dec-'13, Jan and Feb '14	30
Spring	Mar, Apr and May '14	30
Summer	Jun, Jul and Aug '14	30
Autumn	Nov '13, Sep, Oct and Nov '14	40
Autumn and Spring	combination of above	70
Autumn and Summer	combination of above	70

Table 4.5 continued

Autumn and Winter	combination of above	70
Spring and Summer	combination of above	60
Spring and Winter	combination of above	60
Summer and Winter	combination of above	60
Full season	All	130

Gradient analysis (see **Section 3.5.3**) performed on the full season transfer function determined that the testate amoebae are responding unimodally to elevation with a gradient length of 2.49. Therefore the unimodal regression models of weighted averaging (WA) and weighted averaging partial least squares (WAPLS) were used to generate transfer functions for the full season training set. Based on the assessment criteria outlined in **Section 3.5.3** the WAPLS component 2 model was determined to be the best performing transfer function. In the interest of consistency, only the WAPLS component 2 model performance is considered for the comparisons of all the seasonal transfer functions (**Table 4.6**).

***Table 4.6**: Summary performance statistics of WAPLS component 2 seasonal transfer functions. RMSEP % change represents the percentage increase or decrease of each transfer function relative to the RMSEP of the full season transfer function.*

Transfer function	RMSEP (m)	$r^{2(boot)}$	Max. bias (m)	RMSEP % change
Full season	0.07	0.87	0.08	n/a
Winter	0.08	0.87	0.10	-12.39
Spring	0.08	0.85	0.13	-8.95
Summer	0.06	0.91	0.08	16.55
Autumn	0.06	0.91	0.07	17.37
Autumn and Spring	0.07	0.86	0.11	-2.27
Autumn and Summer	0.06	0.90	0.07	15.35
Autumn and Winter	0.07	0.87	0.07	0.16
Spring and Summer	0.07	0.87	0.09	2.37
Spring and Winter	0.08	0.85	0.13	-8.90
Summer and Winter	0.07	0.87	0.07	-0.26

Overall, all models have a similar reconstructive performance in terms of RMSEP (0.07 ± 0.01 m) but the maximum bias and correlation between observed and predicted elevation varies depending on the season (max. bias: 0.07 – 0.13 m and $r^{2(boot)}$: 0.87 – 0.91). Although the full season transfer function comprises many samples that were taken throughout the seasonal cycle, with a RMSEP of 0.07 m it is not the most precise transfer function. The overall best performing transfer function was for the autumn

which has RMSEP >17% less than the full season transfer function, the smallest maximum bias (0.07 m) and strongest correlation between observed and estimated elevation ($r^{2(boot)}$ = 0.91). The summer transfer function performs almost on a par with the autumn transfer function with only a ca. 1% reduction in RMSEP and slightly greater maximum bias (0.08 m). The winter and spring transfer functions were associated with RMSEPs >12 % and >8 % greater than the full season transfer function respectively and maximum bias of 0.10 and 0.13 m. Transfer function performance appears to relate to species diversity (**Table 4.4**; **Figure 4.3**) which is generally higher in the summer and autumn months than in winter and spring. Transfer functions sampled over multiple seasons (i.e. two sampling periods) have lower RMSEPs than the full season RMSEP only when at least one of the best performing training sets (summer and autumn) is used. The performance of the winter and spring transfer function in terms of RMSEP is only marginally improved compared with either of the once-sampled transfer functions for these seasons.

4.4 Summary

Testate amoebae distributions over one annual seasonal cycle from November 2013 to November 2014 were investigated. A total of 36 species of dead testate amoebae taxa were encountered over the annual cycle. There was a clear seasonal pattern in testate amoebae concentration which peaks in the spring (max concentration in May 2013). Species evenness displayed minimal variation with 12 dominant taxa occurring in every sampling month (n=13) over the season. There was no clear seasonal pattern in the live and dead proportions of the 12 dominant taxa, although, for some individual taxa seasonal blooms in the living proportion were observed. The blooms in the live population of a species tended to precede increases in the dead proportion of the same species in subsequent months. Species diversity remained relatively stable

throughout the season but was greatest from May to November 2014. Increased species diversity coincided with increased stability in the vertical position of species zonation defined by cluster analysis (June to November 2014). Furthermore, transfer functions performed best, with a predictive ability of ± 0.06 m, when generated for training sets obtained in the summer and autumn.

Chapter 5 - Results: Modern environments, Swan Inlet

5.1 Introduction

This chapter presents the results of the contemporary intertidal marsh investigations at Swan Inlet outlined in **Section 3.2**. This includes descriptions of the marsh topography, dominant vegetation cover, modern distributions of testate amoebae, diatoms and foraminifera and the development of local transfer functions for reconstructing past sea-level changes at Swan Inlet.

5.2 Marsh topography and vegetation cover

There is a 1.49 m elevation range across the three modern sampling transects (**Figure 3.1; Figure 5.1**). The highest point, in the supratidal zone above HAT, lies on Transect 3 (T3) at -0.64 m SID and the lowest point is situated on Transect 2 (T2) between MLHW and MHWS at -1.94 m SID. Four dominant vegetation zones were identified at Swan Inlet (**Figure 5.1**). The uppermost zone, encompassing the supratidal extent of the high marsh is dominated by *Cortaderia pilosa* (Whitegrass) below the limit of HAT until ca. -1.12 m SID. The *Cortaderia pilosa* zone transitions to a *Festuca magellanica* (Fuescan fescue) dominated zone toward the open estuary as the elevation decreases up to the point of MHHW at -1.51 m SID. The level of MHHW is marked by a break in slope at which point the marsh gradient flattens. At this break in slope the mid-marsh zone is dominated by *Deschampsia antarctica* (Antarctic hair-grass) which extends from MHHW to MLLW. The low marsh is characterised by a steep gradient dominated by *Rostokovia magellanica* (Short or Brown Rush). The low marsh gradient flattens and the cover of *Rostokovia magellanica* decreases, marking the transition from low salt marsh to unvegetated mudflat. A schematic diagram of the topography across the three modern transects, dominant vegetation cover, sampling points and tidal datums is provided in **Figure 5.1**.

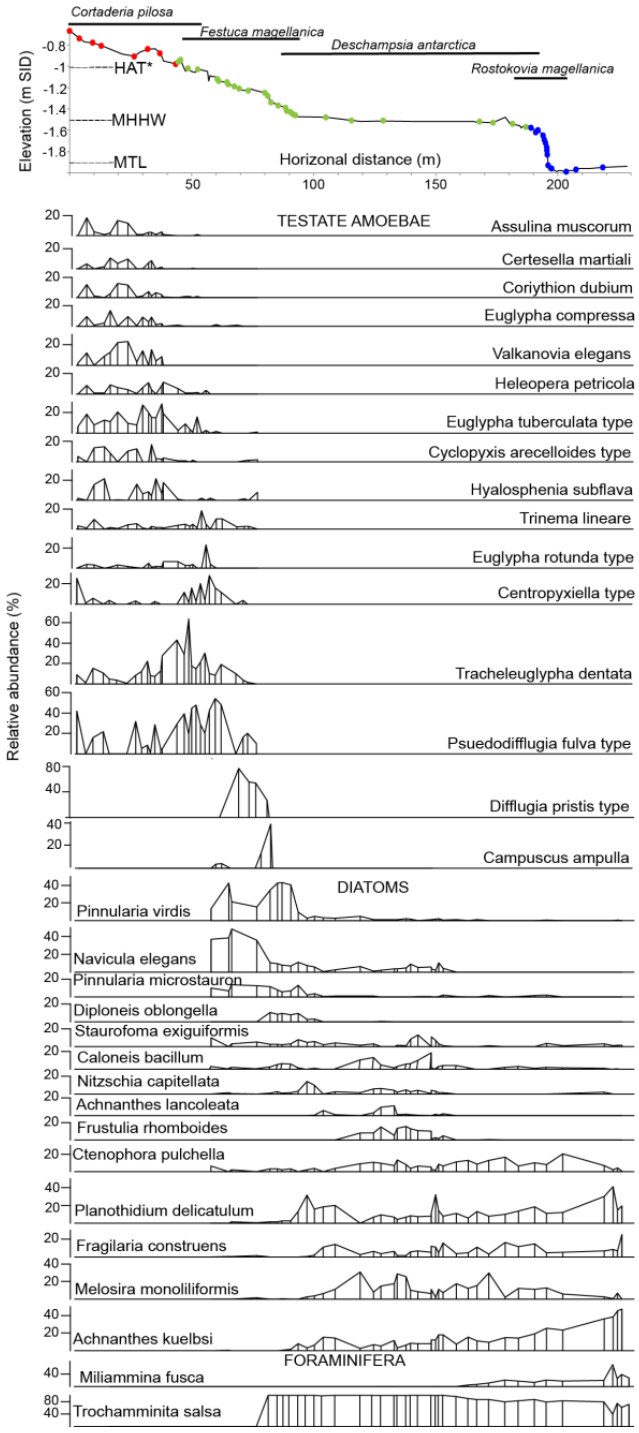

Figure 5.1*: Swan Inlet marsh topography with dominant vegetation and distributions of dominant testate amoebae, diatoms and foraminifera. Points (black circles) along the topographic profile represent the modern sampling locations.*

5.3 Modern microfaunal distributions

An overall vertical succession of testate amoebae, diatoms and foraminifera, from highest marsh to the mudflat elevations, is observed at Swan Inlet

(**Figure 5.1**). Testate amoebae demonstrate a narrow vertical zonation but only occupy the highest elevations of the marsh above the level of MHHW. For unknown reasons diatoms are scarce in the zone where testate amoebae are most abundant. However, diatoms occupy the greatest elevation range encompassing the mid-marsh and low-marsh zones and extending into the tidal flats. The diatom distributions overlap with the lowest zone of testate amoebae close to the level of MHHW and the entire range of foraminifera which extends from MHHW to lowest sampled elevations in the tidal flats. The next three sections present, in detail, the modern distributions for testate amoebae, diatoms and foraminifera at Swan Inlet.

5.3.1 Modern testate amoebae assemblages

A total of 24 testate amoebae taxa were present in significant counts (where it was possible to reach a count >100) in 28 samples from -0.64 m SID to -1.4 m SID (0.76 m range). Samples below -0.64 m SID contained very low concentrations of testate amoebae (<100 tests per cm^3), it was therefore not possible to achieve optimal counts. The raw testate amoebae count data can be found in Appendix E. The contemporary testate amoebae assemblages are shown in **Figure 5.2**. The results of the cluster analysis identified four major ecological zones within the testate amoebae distributions (*TZ*).

The uppermost high-marsh zones group into two clusters (*TZ-I* and *TZ-II*). These zones comprise the most diverse assemblages with 17 taxa having occurrences > 2% in these zones. No taxa have a particular dominance within zones *TZ-I* and *TZ-II* with the assemblages being characterised by

varying abundances of *Euglyphid* taxa (*Euglypha tuberculata* type*, Euglypha compressa, Assulina muscorum, Valkanovia elegans and tracheleuglypha dentata*); and *Hyalosphenisa subflava, Heleopera petricola, Cyclopyxis arcelloides* type*, Corythion dubium, Trinema complantanatum, Pseudodifflugia fulva* type *and Certesella martiali.* With the exception of *Pseudodifflugia fulva* type*,* which has not previously been reported in salt marshes, and *Certesella martiali* (Certes, 1888)*,* which is restricted to the Southern Hemisphere (Loeblich and Tappan, 1961; Meisterfeld and Mitchell, 2008) these are assemblages broadly similar to high-marsh testate amoebae zones described from North Atlantic salt-marshes (Charman *et al.,* 1998, 2002; Gehrels *et al.,* 2001, 2006, Barnett *et al.,* 2013, 2015, 2017).

There is a general reduction in species diversity toward lower elevations. The lowest elevations of testate amoebae group into two clusters (*TZ-III* and *TZ-IV*) and are characterised by a decline in species diversity and a reduction in the relative abundances of the dominant taxa in zones *TZ-I* and *TZ-II*. Zone *TZ-III* is dominated by *Tracheleuglypha dentata and Pseudodifflugia fulva* type*,* which reach their peak abundances, accounting for a combined ca. 90% relative abundance, in the middle of this zone. The lowermost zone, *TZ-IV*, is characterised by declining relative abundances of *Tracheleuglypha dentata* and *Psuedodifflugia fulva* type and a dominance of *Difflugia pristis* type*, Cyphoderia ampulla* and *Psuedohyalosphenia* sp*.* which have their distributions almost entirely within this zone. These lowermost taxa are also typically found in the lowest zone of testate amoebae occurrence in salt-marshes in the North Atlantic region (references above).

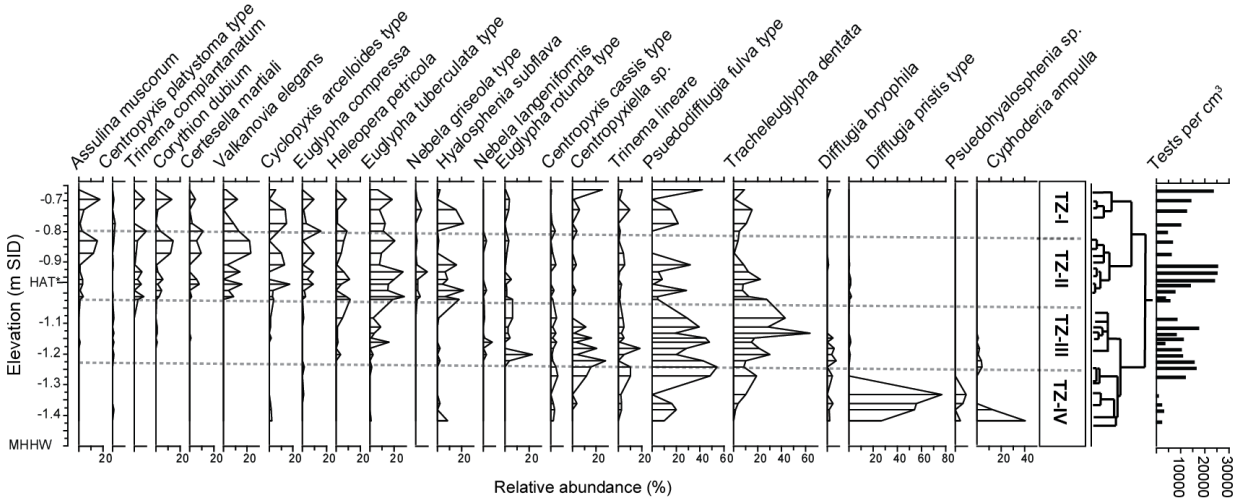

Figure 5.2*: Dominant (taxa accounting >2% relative abundance) modern testate amoebae assemblages from Swan Inlet and CONISS cluster zones.*

5.3.2 Modern diatom assemblages

A total of 60 diatom taxa were recorded with 32 species being present in significant counts (> 2 % relative abundance) in 39 samples (Appendix F) spanning an elevation range of 0.99 m from just above HAT at -0.95 m SID on transect 2 down to the lowest sampled sub-environment, just above MSL at -1.94 m SID on transect 1. The contemporary diatom assemblages are presented in **Figure 5.3**. The cluster analysis identified three distinct cluster zones (DZ); *DZ-I, DZ-II* and *DZ-III*. The zone of the highest occurrence of diatoms (*DZ-I*) is dominated by the typically freshwater-brackish *Pinnularia* taxa and *Navicula elegans*. These taxa count for up to 90% of the total assemblages within zone *DZ-I*, which is characterised by relatively low species diversity compared to other zones. The largest zone, in the middle marsh is *DZ-II* from -1.17 – -1.67 m SID and comprises the most diverse and species rich diatom assemblages. A total of 32 taxa occur in significant numbers in zone *DZ-II*. This zone is dominated by five taxa: *Ctenophora pulchella, Melosira monililiformis, Planothidium delicatulum, Fragilaria construens* and *Achnanthes kuelbsii*, which fluctuate in relative abundance throughout but account for up to 85% of the total assemblages within this

zone. There are also a number of non-dominant taxa that have their entire distribution within zone *DZ-II* e.g. *Frustulia rhomboides* and *Achnanthes lanceolata*. The low-marsh zone *DZ-III* is characterised by a decline in overall species diversity, although, the same five dominant taxa from zone *DZ-II* also dominate this zone. The brackish species *Planothidium delicatulum* (ca. 45%) and *Achnanthes kuelbsii* (*ca.* 48%) reach their peak abundances toward the lower limit of zone *DZ-III* where tidal influence is greatest.

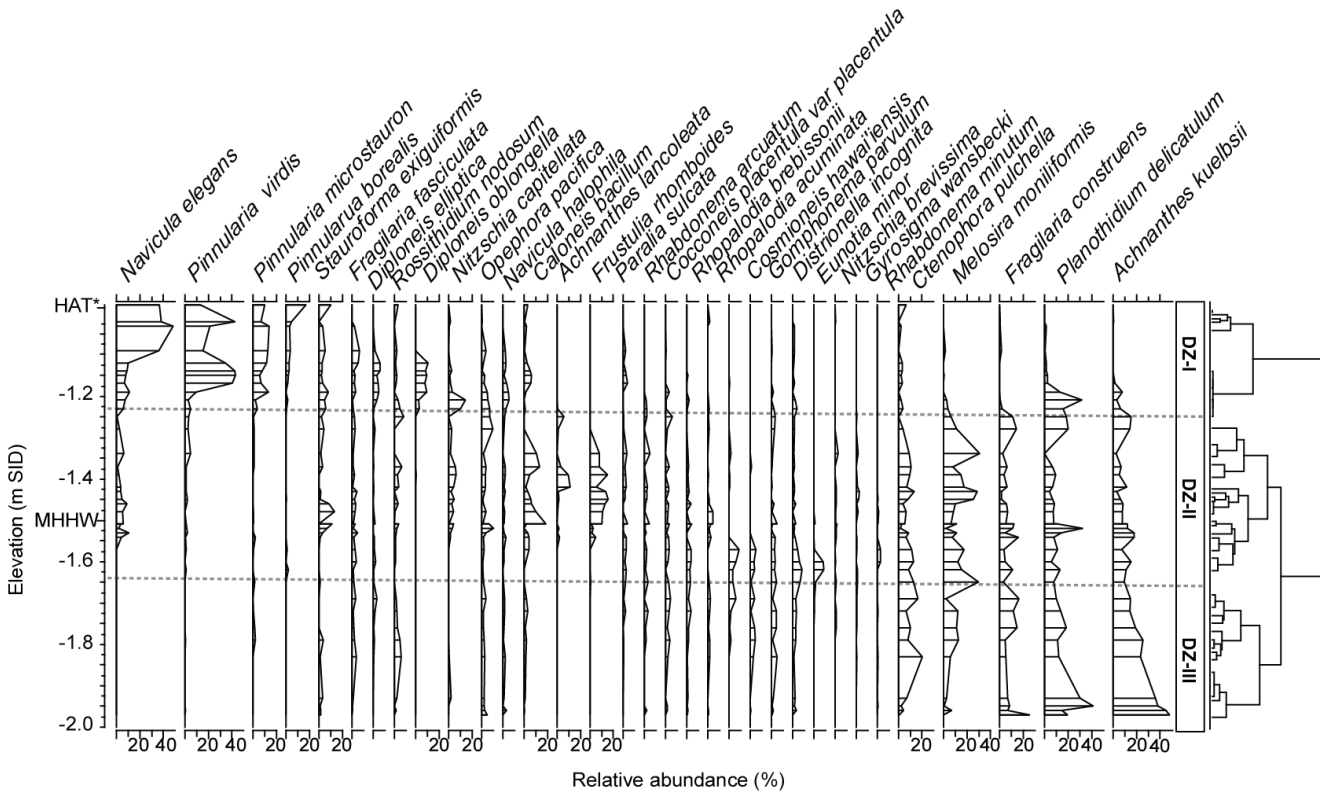

Figure 5.3*: Dominant (taxa accounting >2% relative abundance) modern diatom assemblages from Swan Inlet and CONISS cluster zones.*

5.3.3 Modern foraminiferal assemblages

Foraminifera were present in significant concentrations (> 50 individuals per cm^3) in 35 samples from the lowest mudflat environment up to the upper salt

marsh to around the limit of MHWS (**Figure 5.1**). Across the 35 samples only 4 taxa were present. The salt marsh is dominated by two species *Trochamminita salsa* and *Miliammina fusca.* In some samples there were occasional occurrences of *Trochammina inflata* and *Jadammina macrescens* but these two taxa combined never amounted to >2% relative abundance in any sample. The low species diversity limits the dataset from being used as a training set for developing a reliable foraminiferal transfer function. However, there still remains a clear vertical zonation between these two dominant taxa. From -1.57 m SID to the upper limit of foraminiferal occurrence just above MHHW (-1.51 m SID) *Trochamminita salsa* accounts for virtually 100% of the sample assemblages making it a useful high marsh indicator. *Trochamminita salsa*-dominated high-marsh assemblages have also been described in previous Southern Hemisphere studies from Chilean Patagonia (Fernandez and Zapata, 2010; Jennings *et al.,* 1995, 2012) New Zealand (Hayward *et al.,* 1996; Gehrels *et al.,* 2008) and Australia (Callard *et al*., 2011). Below -1.57 m SID down to -1.96 m SID the monospecific assemblage is broken by the occurrence of *Miliammina fusca* which reaches peak relative abundance of ca. 40% in the tidal flat samples. There is a clear vertical zonation between the two dominant taxa which may serve as a useful indicator of low marsh elevations.

5.4 Transfer function development

This section presents the results of the data screening, ordination, and modelling of the modern testate amoebae, diatom and foraminiferal species data and associated environment (elevation) data used in the generation of several transfer function

models. Following the iterative methods of transfer function development outlined in **Section 3.5.3**, the most appropriate 'final' models are presented in this section. In addition to developing single proxy transfer functions for testate amoebae and diatoms, this section also presents the results of combining the testate amoebae, diatom and foraminiferal data into a single 'synthetic' transfer function. The best performing transfer function models selected in this section, based on the assessment criteria outlined in **Section 3.5.4**, are the final models used to reconstruct the past sea-level changes presented in **Chapter 6**.

5.4.1 Testate amoebae transfer function

Following the data screening outlined in **Section 3.5.2,** two taxa, *Arcella discoides type* and *Sphenoderia lenta,* were deemed to be insufficiently detected and their data removed from the training set prior to subsequent analyses. The results of the DCCA ordination (**Table 5.1**) suggest that the testate amoebae transfer function should be based on unimodal regression. This is because the gradient length for axis 1 (elevation) is > 2 SD which is generally considered to demonstrate a unimodal response of species the environmental variable i.e. taxa have an optimal occurrence along the elevation gradient and their abundance declines either side of that optimum (Birks, 1995). In addition to enabling decisions regarding the type of regression model(s) to apply to the training set, DCCA ordination also quantifies the proportion of variance explained by the measured environmental variable (elevation: axis 1) and unmeasured environmental variables (axes 2-4). These results demonstrate that the dominant environmental control on the overall testate amoebae distributions at Swan Inlet is elevation which explains 59.6% of the variance (**Table 5.1**). The additional axes (**Table 5.1**: 1-4) show the proportion of variance explained by extraneous (lesser dominant) environmental controls. Although the actual environmental variables are unknown, it

could be these environmental variables may be correlated with marsh surface elevation e.g. pH and salinity or vegetation (Alvarez-Rogel *et al.,* 2000; Ooms *et al.,* 2011). Other (unknown) dominant controls on testate amoebae distributions at Swan Inlet explain 24.4% of the variance (**Table 5.1**: axis 2). Whilst it is important to recognise the effect of other controls on species distribution, the DCCA results suggest that the relationship between testate amoebae and marsh surface elevation is robust.

Table 5.1*: Results of DCCA analysis on the testate amoebae training set. The canonical axis (Axis 1) represents the species response to elevation (gradient length measured in SD units) and the amount of assemblage variation explained by elevation (proportion of variance). All other axes show the species response and amount assemblage variation related to other (unmeasured) environmental variables.*

	Axis 1	Axis 2	Axis 3	Axis 4
Gradient Length	3.417	2.499	1.565	1.536
Proportion of variance	0.596	0.244	0.098	0.076

Number of samples	28
Number of taxa	24
Significance (p value)	0.002

The CCA results are displayed graphically in **Figure 5.4** as an ordination bi-plot. The species and sample relationship with elevation (CCA axis 1) is plotted on the horizontal axes and the vertical axes represent residual variation not explained by elevation (CCA axis 2). Species are plotted as estimates of their optima. There is a clear pattern (positive correlation) in the species plot related to elevation (**Figure 5.4a**) with high marsh taxa plotting high on axis 1 and low on axis 2 mid-low marsh taxa plot low on axis 1 and high on axes 2. Three species (*Cyphoderia ampulla, Difflugia pristis* type

and *Pseudohyalosphenia* sp. (c.f. 'Wrinkled flask type' Charman *et al.,* 2002) do not follow this same pattern. These three species plot low on both axes (negative correlation) but these species are all dominant in the lowest limit of testate amoebae occurrence (along transect 1) demonstrating there is still a consistent relationship between species distribution and elevation. The ordination of samples (**Figure 5.4b**) exhibit the same general pattern as the species indicating that samples in the training set are representative of the species-environment relationship along the elevation gradient of the salt-marsh.

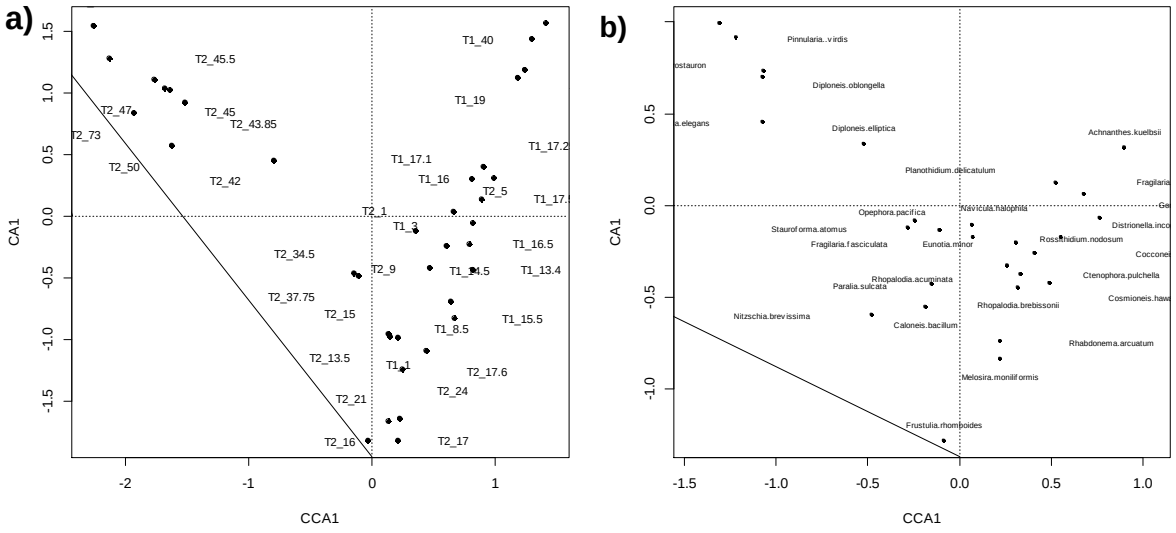

Figure 5.4*: Testate amoebae CCA Ordination bi-plots showing species (a) and sample (b) variance related to elevation (Axis 1: horizontal axis) and residual variation (Axis 2: vertical axis)*

Several applicable unimodal regression models are available for developing a transfer function. Both the modern analogue technique (MAT) and correspondence analysis (CA) models were disregarded. MAT would be particularly prone to autocorrelation due to the nature of the modern sampling (at one site) so was omitted on that basis.

CA was not the most appropriate model for this dataset as it is primarily designed for indirect ordination where the environmental variable is unknown (Birks, 1995). Only weighted averaging (WA) and weighted averaging partial least squares (WAPLS) were considered appropriate to model the species-environment relationship of the modern testate amoebae training set. These unimodal models are widely used in sea-level studies (Barlow *et al*., 2013) and are considered simple, robust and ecologically plausible (Birks, 1995, 2010). WA applies the abundance-weighted average distribution of taxa along the environmental gradient to estimate the position of a species assemblage with no measured environmental variable (i.e. fossil assemblages) along the environmental gradient (i.e. elevation). The WAPLS model follows the same protocol adding additional statistical components which consider correlations in the residuals to improve fit between species data and the environmental variable in the training set (Birks, 1995, 2010). With each component the statistical complexity increases with component 4 being the most complex.

Both models were applied to the testate amoebae training set and run using the bootstrapping cross-validation technique (1000 iterations) in order to quantify the prediction error (RMSEP). Following the method outlined in **Section 3.6.2**, the three highest occurring samples (-0.27, -0.67 and -0.64 m SID) were identified as significant outliers and removed. As these samples occur at the 'freshest' (highest elevation) part of the marsh, in the supratidal zone (above MHWS), it may be that these samples demonstrate a greater response to variables other than elevation e.g. proximity to the water table or potentially reflect disturbance in the upper reaches of the marsh; Ooms *et al.* (2012) found that testate amoebae were controlled by particle size and organic matter in the supratidal zone. The screened testate amoebae training set, with outliers removed, comprises 22 taxa and 25 samples. This training set was then used to create

the WA and WAPLS transfer functions. Summary statistics for all models are presented in **Table 5.2**. Scatterplots of observed and transfer function-estimated elevations and of the spread of the residuals for each WAPLS and WA models are presented in **Figure 5.5** and **Figure 5.6** to aid interpretation of model performance through visual inspection.

***Table 5.2**: Summary performance statistics of weighted averaging (WA) and weighted averaging partial least squares (WAPLS) regression models applied to the testate amoebae training set.*

Model	RMSE (m)	r^2	$r^{2(boot)}$	RMSEP (m)	RMSEP % change	Av. bias (m)	Max. bias (m)
WAPLS Component 1	0.06	0.90	0.86	0.08	n/a	0.00	0.12
WAPLS Component 2	0.06	0.91	0.83	0.09	-6.06	0.00	0.10
WAPLS Component 3	0.05	0.93	0.80	0.10	-20.52	0.00	0.09
WAPLS Component 4	0.05	0.93	0.77	0.12	-16.21	0.00	0.04
WA (inverse deshrinking)	0.06	0.89	0.85	0.08	n/a	0.00	0.12
WA (classical deshrinking)	0.06	0.89	0.85	0.08	n/a	0.00	0.13
WA (tol., inverse deshrinking)	0.06	0.89	0.85	0.08	n/a	0.00	0.10
WA (tol., classical deshrinking)	0.06	0.89	0.85	0.08	n/a	0.00	0.10

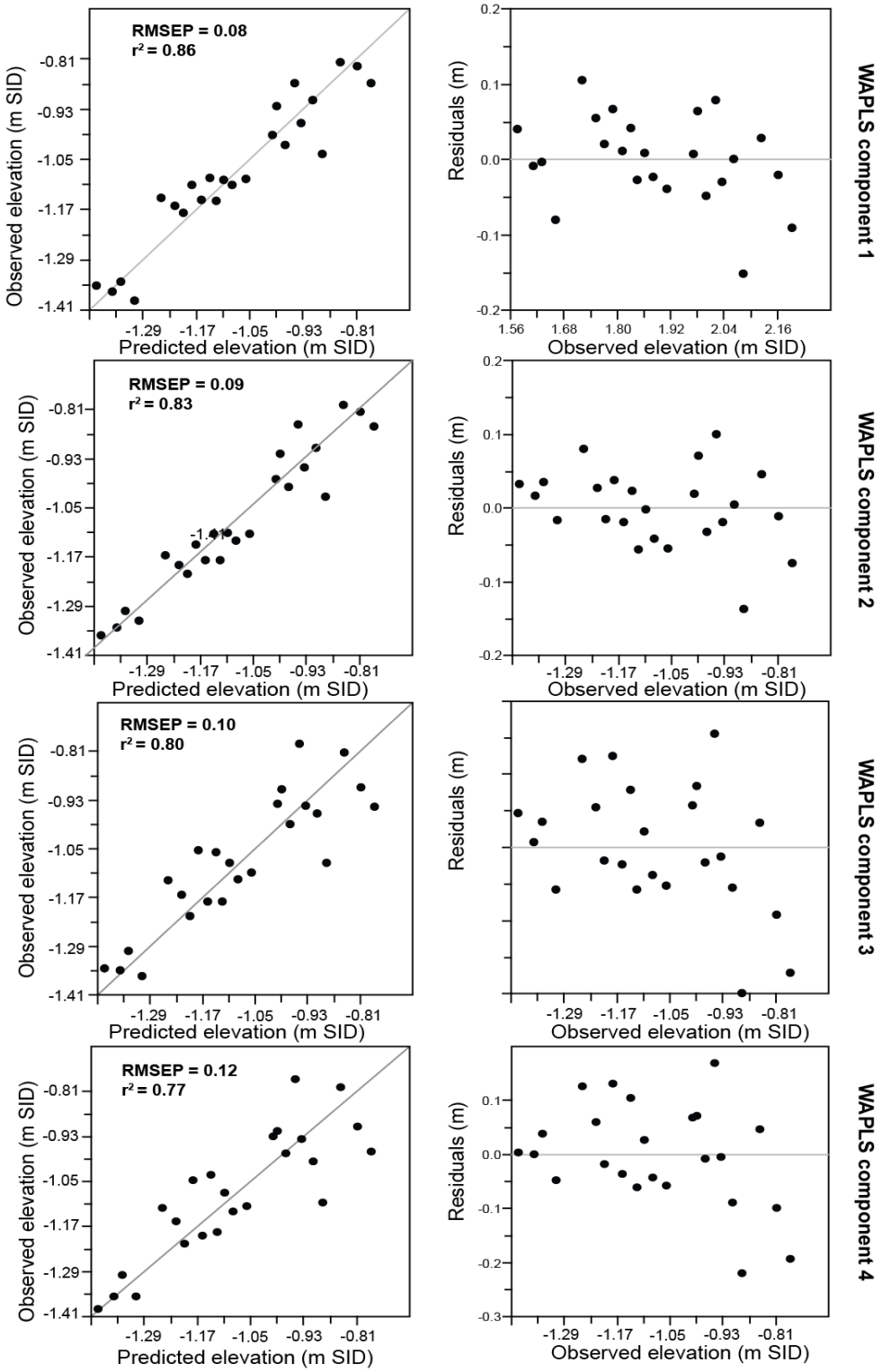

Figure 5.5 *Scatterplots of observed sample elevations against WAPLS (components 1-4: top – bottom) elevation estimates on the bootstrapped testate amoebae training set (left panel) and residuals of estimated sample elevations against observed sample elevations (right panel).*

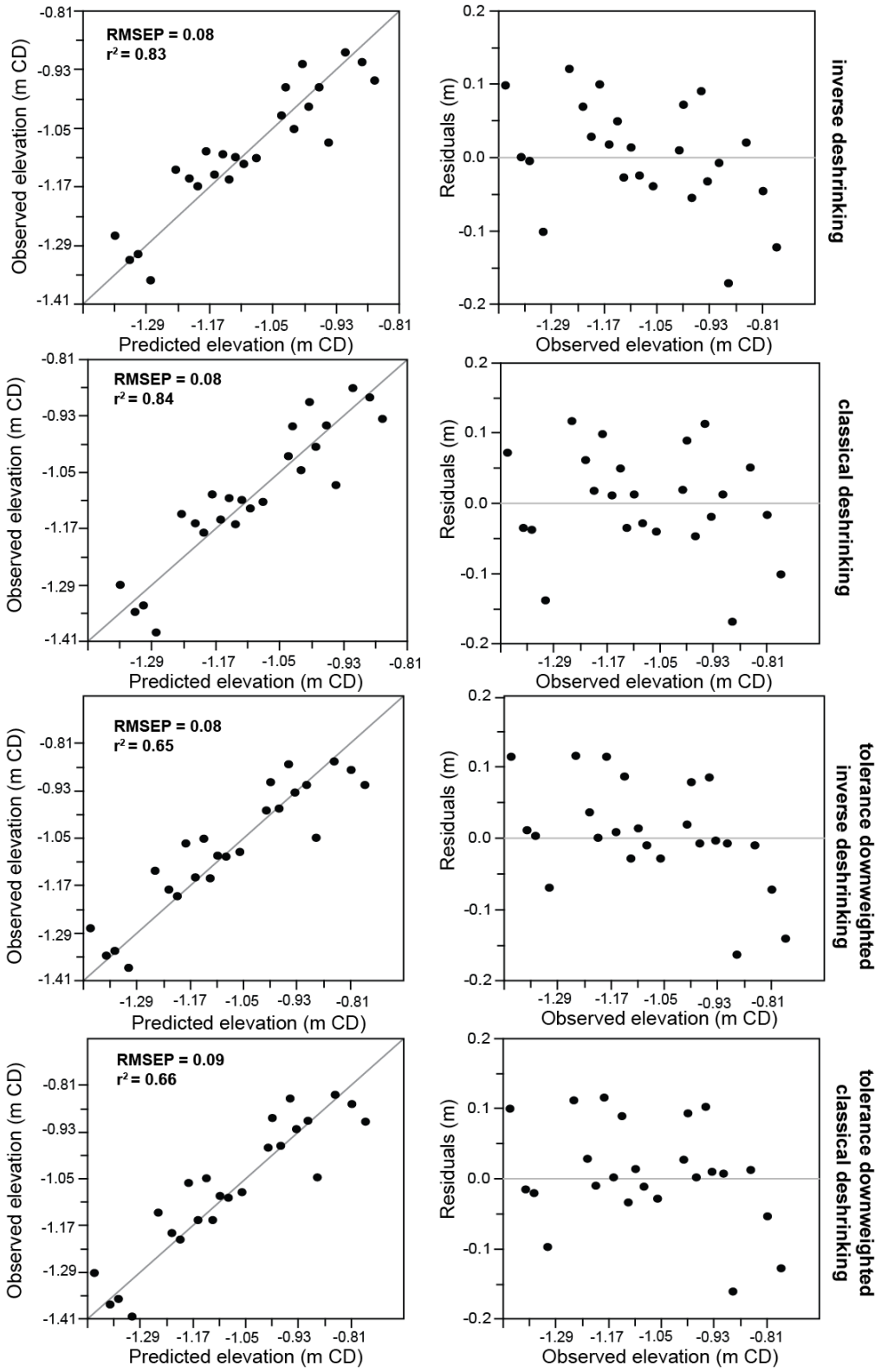

Figure 5.6 *Scatterplots of observed sample elevations against WA (model variants from top-bottom) elevation estimates on the bootstrapped testate amoebae training set (left panel) and residuals of estimated sample elevations against observed sample elevations (right panel).*

Table 5.3 presents the relative ability of WAPLS component 1 and WA models to reconstruct the observed elevation of the surficial testate amoebae assemblage of core SI2. All models perform well in this assessment, predicting the observed elevation to within 0.06 m but the WA (inverse deshrinking) model is the least accurate.

***Table 5.3**: Performance of selected testate amoebae transfer functions at reconstructing the observed elevation of the master core surface.*

Model	observed elevation (m SID)	predicted elevation (m SID)	difference (m)
WAPLS component 1	-1.03	-1.05 ± 0.09	-0.02
WA (inverse deshrinking)	-1.03	-1.09 ± 0.14	-0.06
WA (classical deshrinking)	-1.03	-1.05 ± 0.09	-0.02

5.4.2 Diatom transfer function

Following the data screening protocol no species occurring in >2% relative abundance in any sample were determined to be insufficiently detected so all 32 dominant taxa remained in the training set. The results of the DCCA (**Table 5.4**) indicate that the diatoms exhibit a unimodal response to elevation with a gradient length of 3.373 SD units. The canonical axis score for elevation (Axis 1; **Table 5.4**) demonstrates that elevation is the dominant environmental variable governing the diatom assemblage distributions, explaining 61.4% of the variance. The next most significant (unknown) environmental controls on diatom distributions accounts for just 14.3 % of the species variation (Axis 2; **Table 5.4**). Thus, diatoms are an excellent proxy for elevation at Swan Inlet and unimodal regression models are most appropriate for generating transfer functions from this training set. The ordination bi-plot presented in **Figure 5.7** presents the DCCA results. Species and samples in the ordination bi-plot display similar patterns of correlation with the elevation axis (DCCA axis 1: horizontal axis

Figure 5.7a). Species dominant in high marsh samples (*Pinnularia* sp*.* and *Navicula elegans*) plot together high on axis 1. Low-marsh taxa group low on axis 1 (e.g. *Achnanthes kuelbsii, Planothidium delicatulum, Opephora pacifica* and *Navicula halophila)*. Generally samples from higher-marsh elevations (T1) and lower-marsh elevations (T2) group together in the same positions as high-marsh and low-marsh species. Three samples from transect 2 (T2_16, T2_17 and T2_21) group in a cluster separate from other samples in the middle of the elevation gradient. These samples do, however, plot in a position similar to the species *Frustulia rhomboides* which has a sharp peak in relative abundance in these samples. These relationships observed in the bi-plot suggest that diatom species and samples in the training set are representative of changes in the elevation and therefore suitable indicators of sea-level.

Table 5.4*: Results of DCCA analysis on the diatom training set. The canonical axis (Axis 1) represents the species response to elevation (gradient length measured in SD units) and the amount of assemblage variation explained by elevation (proportion of variance). All other axes show the species response and amount of assemblage variation related to other (unknown) environmental variables*

	Axis 1	**Axis 2**	**Axis 3**	**Axis 4**
Gradient Length	3.373	1.550	1.180	0.095
Proportion of variance	0.614	0.143	0.056	0.027

Number of samples	39
Number of taxa	32
Significance (p value)	0.002

a) **b)**

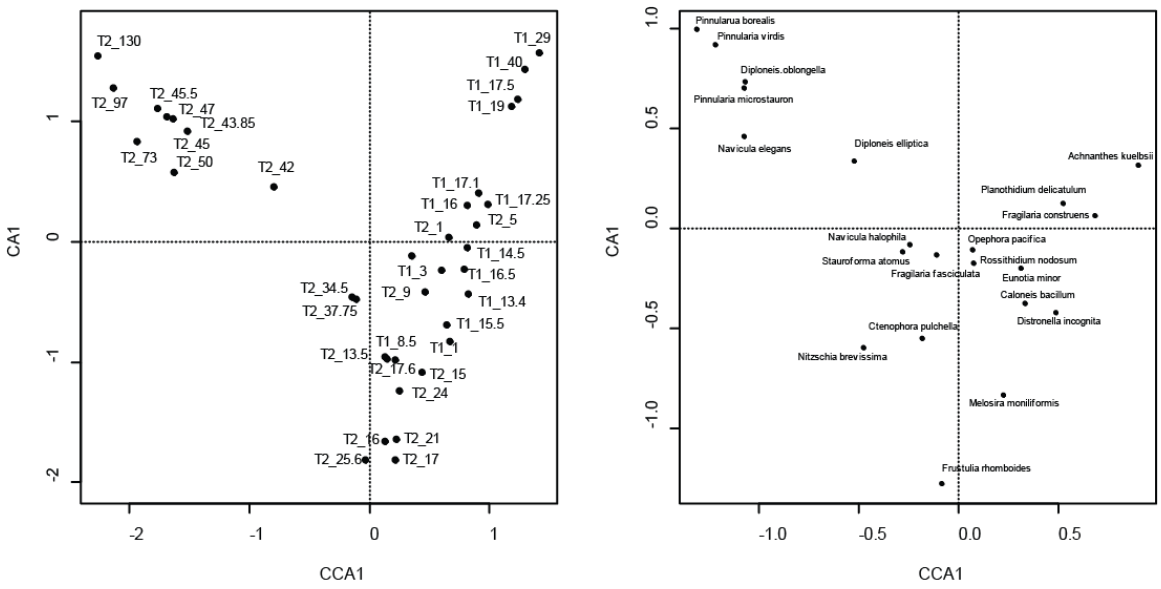

Figure 5.7*: Diatom CCA Ordination bi-plots showing samples (a) and species (b) variance related to elevation (Axis 1: horizontal axis) and residual variation (Axis 2: vertical axis)*

WA and WAPLS transfer functions were generated for the diatom training set. Following the first iteration of transfer functions two outliers were identified (following **section 3.6.2**). The two outlier samples were from 1.72 and 1.75 m on transect 1. These samples were removed from the training set based on being statistical outliers but it was also noted that these two sampled were taken either side of small marsh creek which intersects transect 1. Consequently, the diatom assemblages in these samples may be responding more strongly to environmental variables associated with the creek sub-environment and are therefore anomalous of the species-elevation relationship governing diatom assemblages in the rest of the training set. With these two outliers removed, the final diatom training set comprising 37 samples to generate a final suite of WA and WAPLS models. Summary performance statistics for all models are presented in **Table 5.5**. Scatterplots of observed and transfer function-estimated elevations and of the spread of the residuals for each WAPLS and WA models that were used to aid interpretation of model performance through visual inspection are

presented in **Figure 5.8** and **Figure 5.9.**

Table 5.5: *Summary performance statistics of weighted averaging (WA) and weighted averaging partial least squares (WAPLS) regression models applied to the diatom training set.*

Model	RMSE	r^2	$r^{2(boot)}$	RMSEP (m)	RMSEP % change	Av. bias (m)	Max. bias (m)
WAPLS Component 1	0.1	0.86	0.83	0.12	n/a	0	0.17
WAPLS Component 2	0.06	0.96	0.93	0.08	33.27	0	0.1
WAPLS Component 3	0.04	0.98	0.95	0.07	11.83	0	0.06
WAPLS Component 4	0.04	0.98	0.96	0.07	1.08	0	0.05
WA (inverse deshrinking)	0.1	0.86	0.83	0.12	n/a	0	0.17
WA (classical deshrinking)	0.11	0.86	0.83	0.13	n/a	0	0.15
WA (tol., inverse deshrinking)	0.08	0.92	0.89	0.1	n/a	0	0.14
WA (tol., classical deshrinking)	0.09	0.92	0.89	0.1	n/a	0	0.14

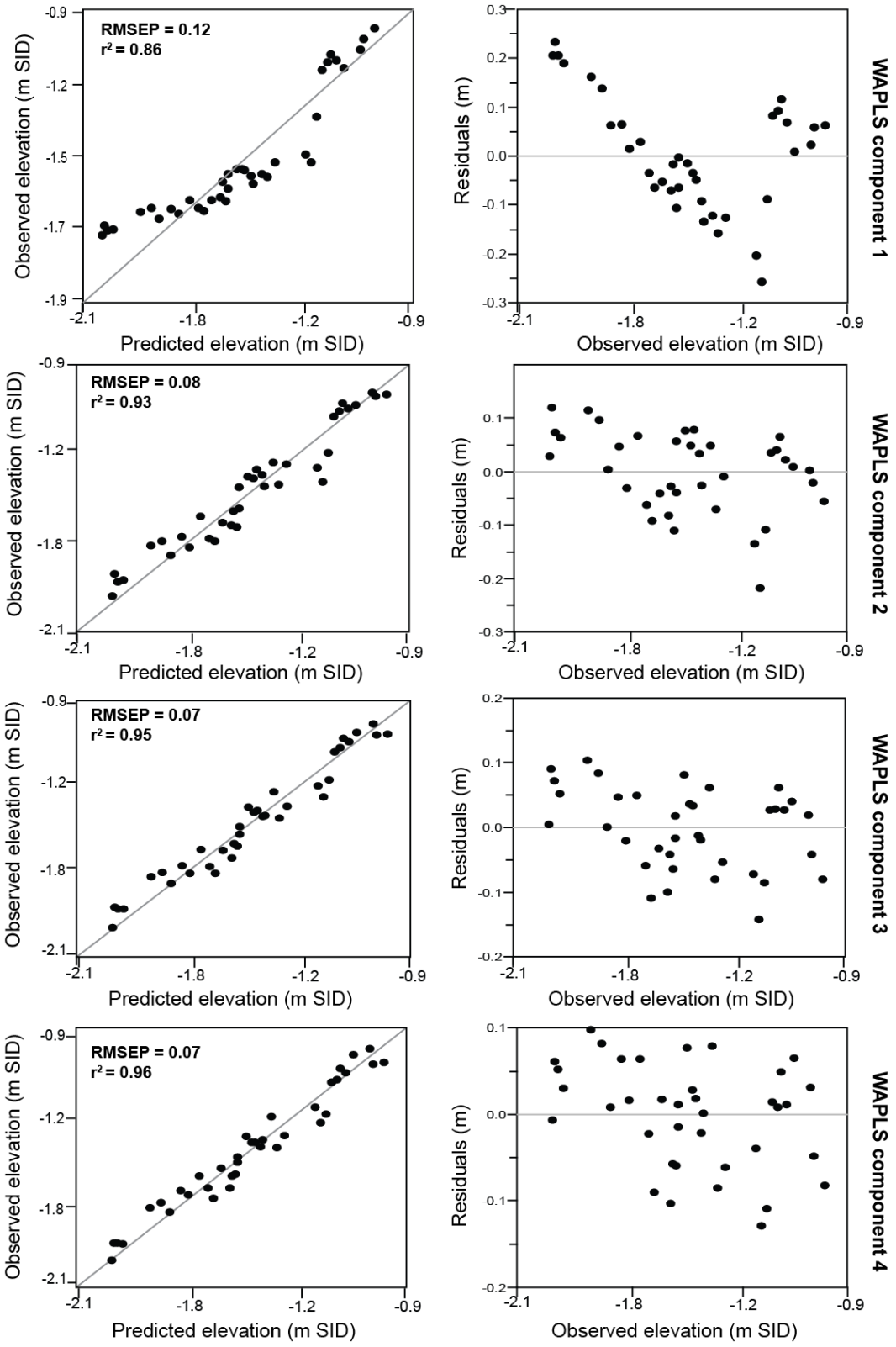

Figure 5.8*: Scatterplots of observed sample elevations against WAPLS (components 1-4: top – bottom) elevation estimates for the bootstrapped diatom training set (left panel) and residuals of estimated sample elevations against observed sample elevations (right panel).*

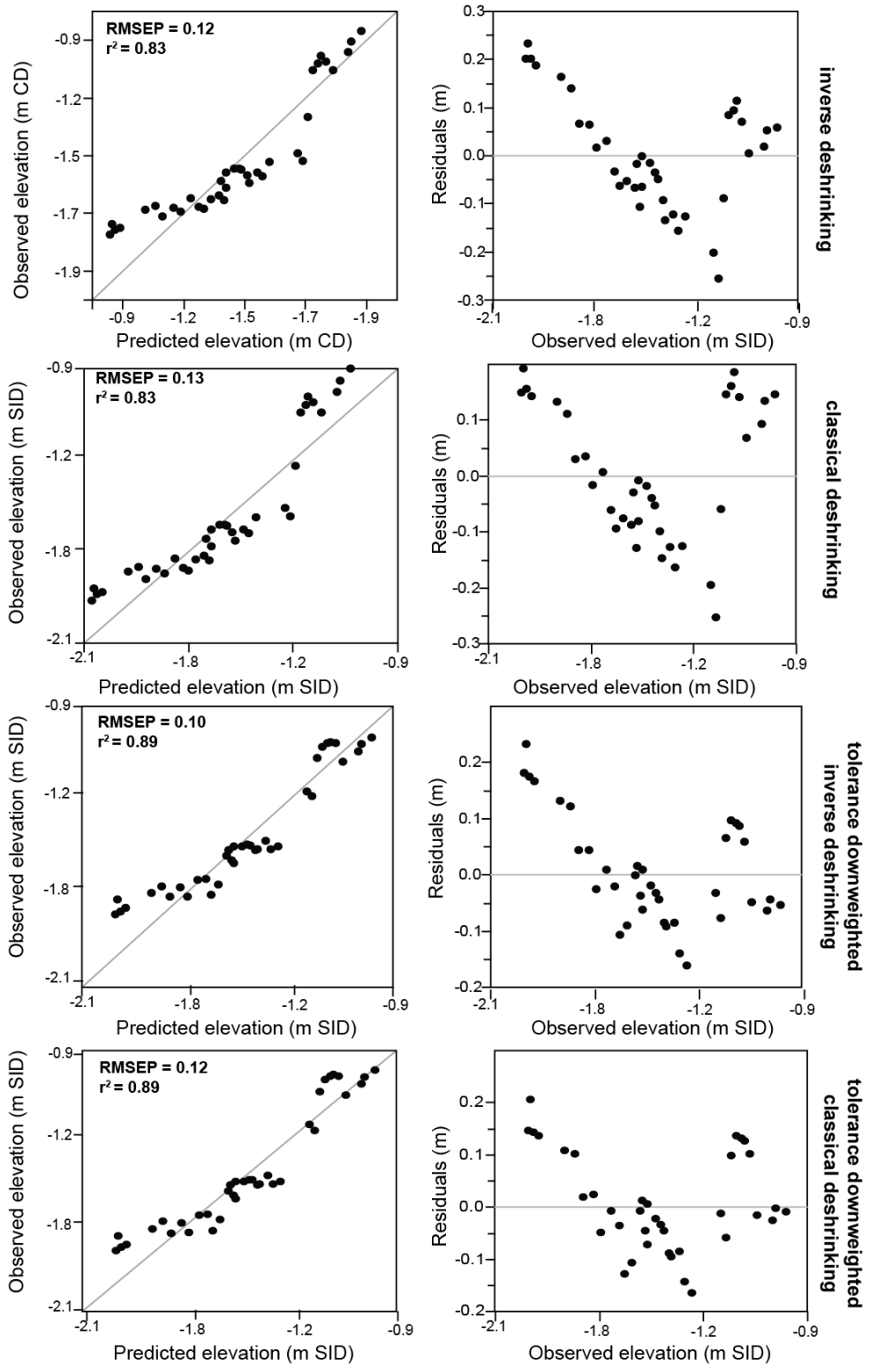

Figure 5.9: *Scatterplots of observed sample elevations against WA (model variants from top-bottom) predicted elevation on the bootstrapped diatom training set (left column) and residuals of estimated sample elevations against observed sample elevations (right column).*

Upon consultation of the summary performance statistics and visual inspection of the scatterplots for WAPLS and WA diatom transfer functions it is evident that WAPLS transfer functions perform best. The exception to this is the WAPLS component 1 model, which performs on par with WA models (RMSEP ≥ 0.10 m; $R^{2\,(boot)}$ ≥ 0.83). It is unsurprising that the WAPLS component 1 model performs similarly to WA models as the first component of a WAPLS model is simply a weighted average of the original environmental property i.e. the same as the base WA model without the addition of deshrinking, tolerance downweighting or weighted residual averages (additional WAPLS components). WA based models (including WAPLS component 1) tend to systematically over-predict elevation at the upper and lower limits, and under-predict elevation in the middle of the gradient. This is most evident in the structure of the residuals. On this basis, the WA and WAPLS component 1 models were not considered appropriate transfer functions. Model performance is improved for additional components in WAPLS regression (components 2-4; RMSEP ≤ 0.08 m; $r^{2(boot)}$ ≥ 0.93). There is little difference in the performance of WAPLS components 1-3, and all three models would likely produce similar reconstructions. There is almost a 12% increase in model precision (RMSEP) for component 3 over component 2 but only an addition 1% gain for component 3. **Table 5.6** presents the relative ability of WAPLS component 2-4 models to reconstruct the observed elevation of the surficial diatom assemblage of core SI2. All models perform better than the average RMSEP for each model but WAPLS component 3 performs best despite the performance statistics suggesting WAPLS component 4 is the most precise model. It may be due to the increased complexity of component 4 is less direct measure of the species-elevation relationship (e.g. Wright *et al.* 2011). Therefore, in the interest of achieving the best reconstructive precision with the least amount of statistical complexity, the WAPLS component 3 model is selected as the final diatom transfer function.

***Table 5.6**: Performance of selected diatom transfer functions at reconstructing the observed elevation of the master core surface.*

Model	observed elevation (m SID)	predicted elevation (m SID)	difference (m)
WAPLS component 2	-1.03	-0.99 ± 0.08	0.04
WAPLS component 3	-1.03	-1.00 ± 0.07	0.03
WAPLS component 4	-1.03	-0.98 ± 0.07	0.05

5.4.3 Combined transfer function

This section explores the applicability of a mulitiproxy transfer function combining the modern testate amoebae, foraminifera and diatom data. Although the foraminiferal distributions were unsuitable for quantitative modelling, in combination with testate and diatoms they may provide valuable proxy information. In order to test the combined utility of these proxies the relative species abundances (%) were calculated in each sample, treating the three groups as a single species quasi- assemblage distribution. The same anomalous species removed from the testate amoebae and diatom training sets were removed from the combined training set. No prior weighting of species was conducted as individual species are weighted by the WA and WAPLS regression models based on their number of occurrences and relative abundance (ter Braak and Looman, 1986). By combining the three proxies the elevation range is extended to 1.27 m compared to 0.99 m and 0.76 m for diatoms and testate amoebae respectively. DCCA ordination demonstrates that in combination there remains a unimodal species response to elevation with a gradient length of 3.632 (**Table 5.8**: axis 1). Elevation explains 58.2 % (axis 1) of the species variation although unknown environmental variables explain 25.1% (axis 2), which is greater than axis 2 scores for

either of the single proxy training sets. The initial set of WA and WAPLS identified no statistical outlier samples so the final set of models for consideration is based on regression of 48 samples and 59 taxa. Performance statistics and scatterplots for the combined transfer function are presented in **Table 5.7** and **Figures 5.10** and **5.11**.

Table 5.7: *Results of DCCA analysis on the combined training set. The canonical axis (Axis 1) represents the species response to elevation (gradient length measured in SD units) and the amount of assemblage variation explained by elevation (proportion of variance). All other axes show the species response and amount of assemblage variation related to other (unknown) environmental variables*

	Axis 1	**Axis 2**	**Axis 3**	**Axis 4**
Gradient Length	3.632	2.837	2.121	1.526
Proportion of variance	0.582	0.251	0.091	0.065

Number of samples	48
Number of taxa	59
Significance (p value)	0.002

As with the single-proxy testate amoebae and diatom transfer functions, the added statistical complexity included in WAPLS components 2-4 generally increases the predictive performance in terms of RMSEP (**Table 5.8**: WAPLS components 2-4 ≤ 0.09 m ; WA ≥ 0.11 m). Visual inspection of the model performances (**Figures 5.10** and **5.11**) show that WA models (including WAPLS component 1) have a general tendency to over-predict and under-predict elevation at the lower and upper limits of the elevation gradient respectively. This tendency is particularly evident in the residuals for these models which show a systematic structure. This systematic

structure is still evident in the WAPLS component 2-4 models but is significantly reduced. For these reasons the WA and WAPLS component 1 models are not considered as suitable for reconstructing the full range of elevations captured by the combined dataset. As an additional test the WAPLS component 2-4 models were used to predict the known elevation of the surface assemblages of core SI-2 (**Table 5.9**). WAPLS component 3 performed best with an ability to predict the core top elevation to within 0.06 m. Based on this and overall performance, best RMSEP, strongest r^2, lowest max bias, the WAPLS component 3 model was selected for the final combined transfer function model.

***Table 5.8**: Summary performance statistics of weighted averaging (WA) and weighted averaging partial least squares (WAPLS) regression models applied to the combined training set.*

Model	RMSE	r^2	$r^{2(boot)}$	RMSEP (m)	RMSEP % change	Av. bias (m)	Max. bias (m)
WAPLS Component 1	0.12	0.87	0.86	0.13	n/a	-0.02	0.33
WAPLS Component 2	0.07	0.96	0.94	0.09	32.61	0	0.18
WAPLS Component 3	0.04	0.98	0.96	0.07	17.45	0	0.12
WAPLS Component 4	0.04	0.99	0.96	0.07	-0.21	0	0.13
WA (inverse deshrinking)	0.12	0.87	0.85	0.13	n/a	0	0.32
WA (classical deshrinking)	0.13	0.87	0.85	0.14	n/a	0	0.28
WA (tol., inverse deshrinking)	0.09	0.93	0.91	0.11	n/a	0	0.25
WA (tol., classical deshrinking)	0.09	0.93	0.91	0.11	n/a	0	0.22

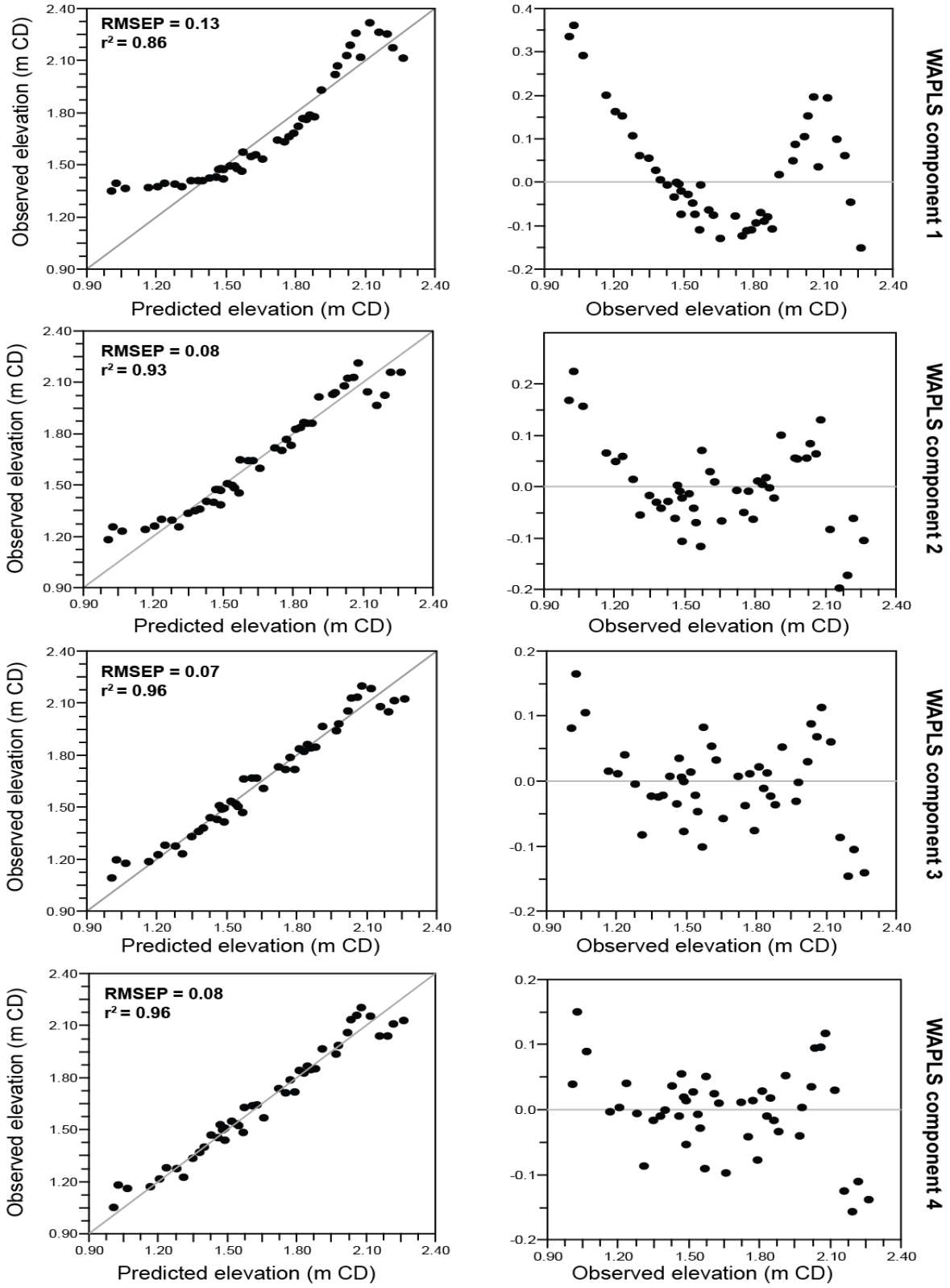

Figure 5.10*: Scatterplots of observed sample elevations against WAPLS (components 1-4: top – bottom) elevation estimates for the bootstrapped combined training set (left panel) and residuals of estimated sample elevations against observed sample elevations (right panel).*

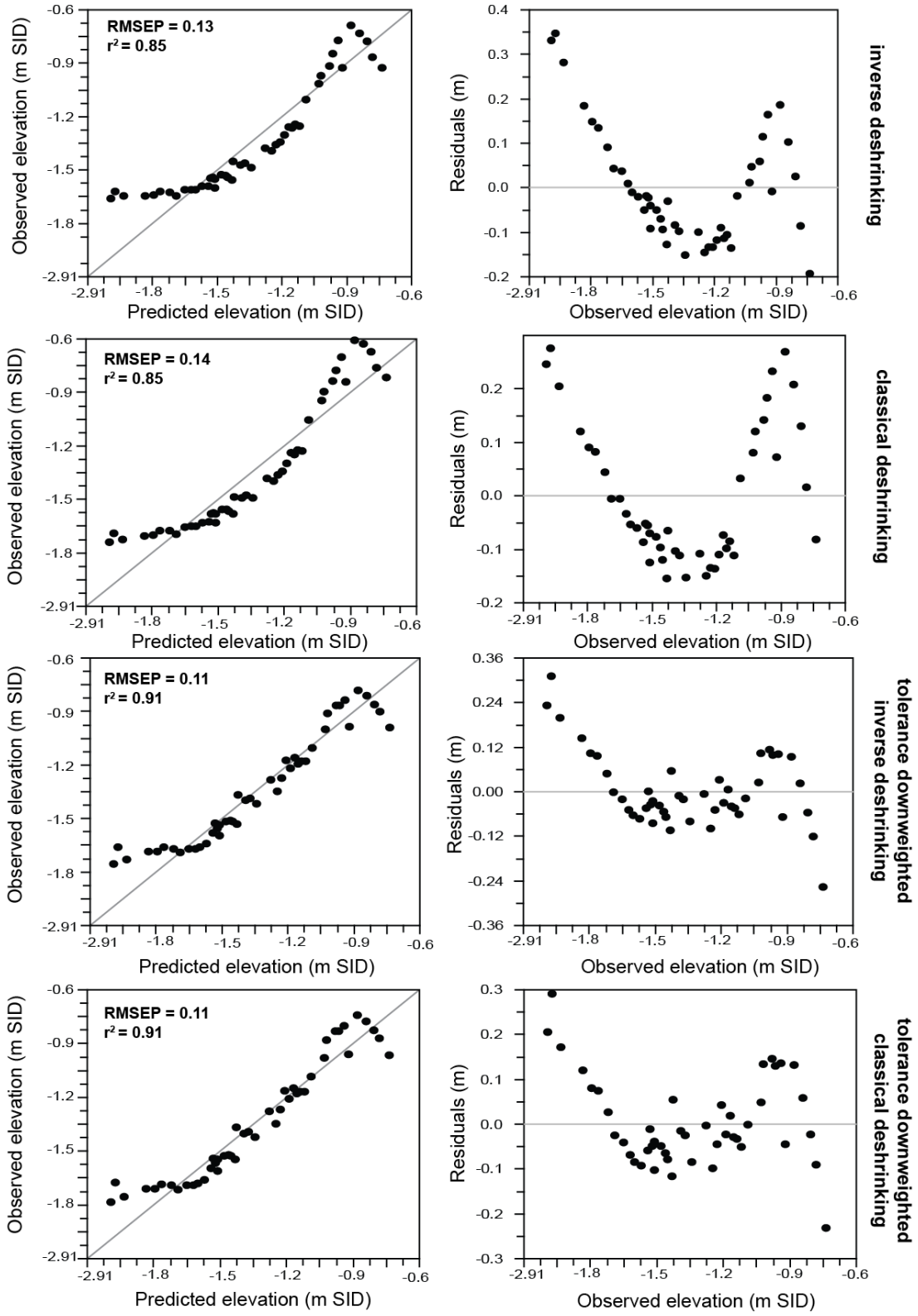

Figure 5.11 *Scatterplots of observed sample elevations against WA (model variants from top-bottom) elevation estimates on the bootstrapped combined training set (left panel) and residuals of estimated sample elevations against observed sample elevations (right panel).*

***Table 5.9**: Performance of selected combined transfer functions at reconstructing the observed elevation of the master core surface.*

Model	observed elevation (m SID)	predicted elevation (m SID)	difference (m)
WAPLS component 2	-1.03	-0.96 ± 0.08	+0.07
WAPLS component 3	-1.03	-0.07 ± 0.07	+0.06
WAPLS component 4	1.94	-0.96 ± 0.07	+0.07

5.5 Summary

This chapter has demonstrated that there is an overall vertical succession of vegetation, testate amoebae, diatoms and foraminifera at Swan Inlet that can be related to relative sea level. Through the application of a suite of quantitative techniques the nature of this relationship has been established and modelled to create a number of transfer functions. Transfer functions were developed for testate amoebae, diatoms and a combination of testate amoebae, diatoms and foraminifera using weighted averaging (WA) and weighted averaging partial least square (WAPLS) regression. Overall, all the transfer functions performed well although WAPLS-based models generally out-performed WA models in terms of predictive ability. Following statistical, qualitative and independent tests of predictive ability, three models were selected for their ability to predict elevation as final (optimal) transfer functions for testate amoebae, diatoms and a combined mulitiproxy transfer function. For the testate amoebae transfer function, a WAPLS component 1 model with an average predictive ability of ± 0.08 m was selected as the final transfer function. The final diatom and combined transfer functions selected were WAPLS component 3 models, both being capable of, on average, reconstructing elevation to within ± 0.07 m. These

three transfer functions will be applied to microfossil assemblages recovered from Swan Inlet to develop the sea-level reconstructions presented in **Chapter 6**.

Chapter 6 – Palaeoenvironmental interpretations and sea-level reconstructions

6.1 Introduction

This chapter presents the results of the analyses applied toward fulfilment of **Aim 1** of this thesis, to reconstruct palaeoenvironmental and sea-level changes in the Falkland Islands. The results described in this section are based on litho- bio- and chrono-stratigraphic analyses undertaken on the fossil sediment samples described in **Section 3.2.3**. This chapter can be separated into two parts. The first part presents the lithostratigraphic and biostratigraphic results which are used to interpret the Holocene development of the Swan Inlet marsh. The transfer functions presented in **Chapter 5** are used to quantitatively estimate palaeo-marsh surface elevations (PMSEs) contemporaneous to the deposition of fossil sediment samples. The results of rangefinder radiocarbon dates (**Sections 3.6.1**) are combined with PMSE estimates (converted to RSL) to produce a series of SLIPs documenting the Holocene sea-level history of the Falkland Islands. The second part of this chapter focuses on developing high resolution sea-level reconstructions for the Common Era. The results are presented for high resolution microfossil and chronological analyses of the most recent salt-marsh sediments (upper 90 cm core *SI-2*) and the final late-Holocene sea-level reconstruction for the Falkland Islands is presented.

6.2 Holocene palaeoenvironments and sea-level changes

This section details the results of investigations conducted on the sediment cores sampled at Swan Inlet, described in **Section 3.2.3.** This includes detailed sedimentological descriptions of each core, along with a presentation of the age determinations of radiocarbon dated samples described in **Section 3.6.1.** The sedimentology, chronology and biostratigraphy of the cores are used to interpret

palaeoenvironmental changes at Swan Inlet. Finally, a Holocene RSL curve for the Falkland Islands is presented based on SLIPs established from the analyses at Swan Inlet.

6.2.1 Litho- and biostratigraphy of Swan Inlet

Sedimentological analyses of the six cores and exposed bank section sampled at Swan Inlet in 2013 revealed a relatively consistent stratigraphy across the marsh. The detailed stratigraphy of each core is presented graphically in **Figure 6.1** and described using the Troels-Smith classification scheme (**Table 6.1**: Troels-Smith, 1955) in **Table 6.2**. The investigation identified four distinct lithological units which are indicative of the contemporaneous environment these sediments were deposited in. All cores reached the bedrock basement. The basement at Swan Inlet is a Permian black shale (Aldiss and Edwards, 1999) which is successively overlain by the following major units (identified by lithological analyses):

Unit 1 – grey-brown organic clay

Unit 2 – grey coarse-sands with occasional pebbles

Unit 3 – grey-brown organic clayey peat

Unit 4 – dark brown fibrous peat

***Table 6.1**: Description of notation used to record sediment cores in this study. After Troels-Smith (1955).*

Abbreviation	Name	Description
As	*Argilla steatodes*	*Clay (<0.002mm)*
Ag	*Argilla granosa*	*Silt (0.002-0.06mm)*
Ga	*Grana arenosa*	*Fine to medium sand (0.06-0.6mm)*
Gs	*Grana suburralia*	*Coarse sand (0.6-2mm)*
Sh	*Substantia humosa*	*Humified organics beyond identifiaction*
Th	*Turfa herbacea*	*Herbaceous roots, stems and rhizones*
Nig	*Nigror*	*Degree of darkness (0 = lightest, 4 = darkest)*
Strf	*Stratificatio*	*Degree of stratification (0 = homogenous, 4 = clearly defined layers)*
Sicc	*Siccitas*	*Degree of dryness (0=liquid, 4= air dry)*
Elas	*Elasticitas*	*Degree of elasticity (0 = plastic, 4= rigid)*
Lim	*Limnetica*	*Sharpness of boundary/contact (0= >10mm,<0.5mm)*

Table 6.2: *Sedimentary composition of core sediments from Swan Inlet following the Troels-Smith (1955) classification scheme.*

Core	Depth (cm)	Facies composition	Physical Description
SI-1	0-25	Sh3 As1 Th++ Nig2+ Strf0 Sicc2 Elas0 Lim-	Grey-brown clayey peat
	25-65	As2 Sh2 Th+ Nig2 Strf0 Sicc2 Elas0 Lim0	Grey-brown peaty clay
	66-178	Ag4 Gg+ Nig2 Strf0 Sicc2 Elas0 Lim3	Grey sand with occasional pebble
	179-240	As4 Ag+ Nig2 Strf0 Sicc2 Elas0 Lim1	Grey organic clay with sand bands
SI-2	0-70	Sh3 Th1 As+ Nig2 Strf0 Sicc1Elas1Lim-	Dark brown muddy peat
	71-92	As2 Sh2 Th+ Nig2 Strf0 Sicc2 Elas0 Lim0	Brown-grey organic clay
	93-150	Ga4 Gg+ Nig1 Strf0 Sicc2+ Elas0 Lim1	Grey sand
	151-180	As2 Ag1 Ga1 Th+ Nig3 Strf0 Sicc2 Elas0 Lim0	Brown-grey sandy-gravelly clay
	181-225	Ag2 Ga2 Sh+ Gg+ Nig2 Strf0 Sicc2 Elas0 Lim0	Brown-grey silty sand
	225-303	As3 Sh1 Th+ Nig2 Strf0 Sicc2 Elas0 Lim2	Grey-brown organic clay
SI-3	0-18	As2 Th2 Nig2+ Strf0 Sicc2 Elas0 Lim-	Fibrous grey-brown clayey peat
	18-55	As1 Sh2 Th1 Nig2 Strf0 Sicc2 Elas0 Lim2	Grey-brown peaty clay
	56-110	Ga2 Gg1 As1 Nig2 Strf0 Sicc2 Elas0 Lim2	Gravelly grey sand with clay and angular gravel
	111-200	As3 Sh2 Th1 Nig2 Strf0 Sicc2 Elas0 Lim0	Grey sandy clay with gravel
	201-260	As3 Gg1 Ga+ Nig2 Strf0 Sicc3 Elas0 Lim0	Brown-grey gravelly clay
SI-4	0-15	Sh2 Th2 Nig2 Strf0 Sicc3 Elas0 Lim-	Brown fibrous peat
	16-85	Sh2 As2 Th++ Nig2 Strf0 Sicc2 Elas0 Lim0	Grey-brown organic peaty clay
	86-120	As2 Ga1Gs1 Ag+ Nig2 Strf0 Sicc2 Elas0 Lim2	Grey sandy clay
	121-200	Ag2 Gg1 Gs1 Nig2 Strf0 Sicc2 Elas0 Lim2	Grey gravelly sand
	201-220	As3 Sh1Ga+ Th+ Nig2 Strf0 Sicc2 Elas0 Lim0	Grey-brown organic clay
	221-240	Sh2 As2 Th++ Nig2 Strf0 Sicc2 Elas0 Lim0	Grey sand with gravel
	241-278	Ga2 Gg1 Gs1 Nig2 Strf0 Sicc2 Elas0 Lim0	Grey gravelly sand with clay bands
SI-5	0-40	As2 Th2 Nig2+ Strf0 Sicc3 Elas0 Lim-	Dark brown fibrous peat
	41-80	As2 Th1 Sh1 Nig2 Strf0 Sicc2 Elas0 Lim0	Grey-brown organic peaty clay
	81-185	As3 Ga1 Nig2 Strf0 Sicc2 Elas0 Lim0	Grey sandy clay
	186-235	As4 Th+ Nig2+ Strf0 Sicc2 Elas0 Lim4	Grey-brown organic clay
	236-286	As4 (Ag3 Ga1) Nig2 Strf0 Sicc2 Elas0 Lim0	Brown clay interbedded with fine silty sand
SI- 6	0-40	As2 Th2 Dh+ Nig2+ Strf0 Sicc2 Elas0 Lim-	Dark brown fibrous peat
	40-100	Sh2 As1 Th1 Dh+ Nig2 Strf0 Sicc2 Elas0 Lim0	Peaty organic clay
	100-146	Ga2 As2 Nig2 Strf0 Sicc2 Elas0 Lim0	Grey sandy clay with gravel
SI-7	0-25	As2 Th2 Dh+ Nig2 Strf0 Sicc2 Elas0 Lim-	Brown fibrous clayey peat
	26-66	As3 Th1 Dh+ Nig2 Strf0 Sicc2 Elas0 Lim0	Brown-grey peaty clay
	67-122	Gs2 Ga1 As1Gg+ Nig2 Strf0 Sicc2 Elas0 Lim3	Grey clayey coarse sand
	122-160	As2 Ag2 Ga+ Nig2 Strf0 Sicc2 Elas0 Lim1	Grey silty clay
	161-210	As4 Sh+ Nig2 Strf0 Sicc2 Elas0 Lim2	Brown grey clay

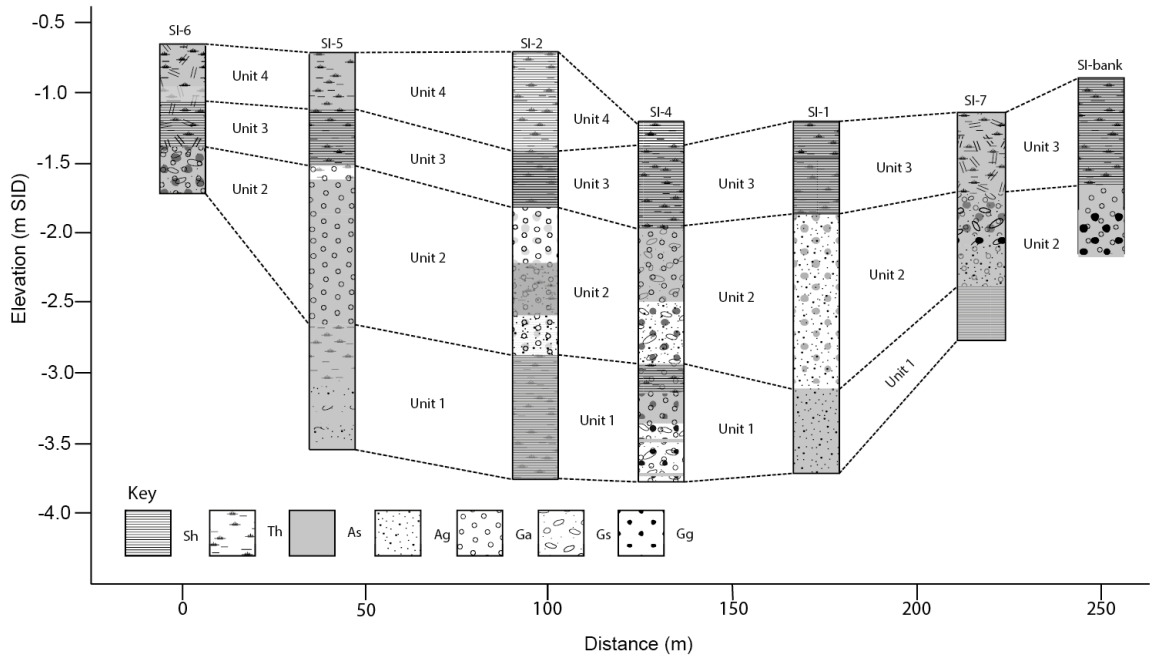

Figure 6.1 *Stratigraphic logs and major lithological units of cored samples described in the text, following the Troels-Smith (1955) descriptions in* ***Table 6.1****. Core locations are shown in* ***Figure 3.1****.*

Microfossil analyses for testate amoebae, diatoms and foraminifera were conducted on spot samples taken from each major unit identified in the core samples. The microfossil data aided palaeoenvironmental interpretations by supporting the presumption that the sediments in each unit were deposited under similar prevailing environmental conditions (see below). The results of the microfossil analyses supported the sedimentological interpretations which identified four major units. However, the basal organic unit (unit 1) in core SI-5 was interpreted as being reworked based on the microfossil assemblages (see below). The final facies interpretations based on the sedimentological properties and microfossil content of each unit are presented in **Figure 6.2**.

Summary of facies interpretations and justifications

This section provides a final summary of the facies interpretations of the Swan Inlet stratigraphy based on the sedimentalogical analyses presented above (**Table 6.1** and

Figure 6.1). This is combined with the justifications for the palaeoenvironmental interpretations of each unit presented in **Figure 6.2** inferred from the microfossil assemblages observed in each unit**,** as follows:

Unit 1a, Reworked organic clay: This unit was composed of grey-brown organic clay interbedded with fine silty sand. This unit was dominated by freshwater-brackish diatom taxa most notably *Navicula elegans* (ca.50%) and *Pinnularia sp.* (ca.30%). However, diatom concentrations were low in this unit and, compared to other samples, there were many broken valves which could not be identified. Testate amoebae were not present in significant numbers although the occasional fragmented test was identified. No foraminifera were found in this unit. This unit is likely of freshwater-brackish origin inferred from the presence of testate amoebae, the predominantly freshwater-brackish diatom assemblages and absence of foraminifera. The large number of broken diatom valves and fragmented testate amoebae tests supports the interpretation of this unit being reworked (**Section 6.2.2**).

Unit 1b, Salt-marsh clay: This unit consisted of grey-brown organic clay. There is a dominantly brackish (ca. 55%) and marine (ca. 35%) diatom assemblage most notably *Fragilaria spp., Paralia sulcata, Opephora* spp. and *Stauroforma* spp. The foraminiferal assemblages in this unit consist of typical salt-marsh taxa dominated by *Trochamminita salsa* (ca. 80%) and *Miliammina fusca* (ca. 20%). Testate amoebae concentrations were generally very low throughout this unit but isolated occurences of *Centropyxiella* sp.*, Cyphoderia ampulla, Arcella discoides* and *Difflugia pristis* were observed. These taxa typically occupy the lowest elevations of salt-marsh testate amoebae distributions in the modern salt marsh at Swan Inlet. The microfossil content of this unit suggests this clay unit is of salt marsh origin.

Unit 2, Tidal flat sands: This unit consits of medium-to-coarse sands with occasional pebbles. This unit is dominated by the foraminifera *Miliammina fusca* (ca. 95%) which is also dominant in the modern tidal flat environment at Swan Inlet. The diatom assemblages in this unit are diverse but generally dominated by brackish and nearshore/marine diatom taxa, most notably the tidal flat diatom *Paralia sulcata* (ca. 60-80%). Other indicatively tidal flat taxa include *Achnanthes kuelbsii, Cocconeis spp.* and *Planothidium delicatulum.* No testate amoebae were found in this unit. This unit is therefore interpreted as being of tidal flat origin inferred from the sandy sedimentology (characteristic of tidal flats) and the predominantly tidal flat/marine microfauna preserved in these sediments.

Unit 3, Salt-marsh peat: This unit consists of brown-grey organic peat. The foraminiferal assemblages in this unit were dominated by *Trochamminita salsa* (95-100%) with *Miliammina fusca* (<5%), which resembles the assemblages found in the middle to low modern salt-marsh envrionment at Swan Inlet. Testate amoebae assemblages in this unit were of relatively low diversity and dominated by *Centropyxiella* sp.*, Psuedodifflugia fulva* type*, Difflugia bryophilia* and *Difflugia pristis* type*.* These testate amoebae taxa are common at the lower tolerance limits of salt-marsh testate amoebae occurance. The diatom assemblage in this unit is dominated by brackish taxa (ca. 80%) most notably *Planothidium delicatulum, Stauroforma atomus, Opephora pacifica* and *Fragliaria construens.* Across most of the marsh this unit extends up to the modern day surface. This, coupled with the characteristically salt-marsh microfossil assemblages, supports the interpretation of this unit being a salt-marsh peat.

Unit 4, Upper-marsh peat: This unit comprises dark-brown fibrous peat and is confined to the portion of the marsh most distal of the sea. Testate amoebae assemblages are at their most diverse in the upper reaches of this unit but are overwhelmingly dominated by *Hyalosphenia subflava* and, to a lesser extent, *Euglyphid* taxa*.* The testate amoebae taxa encountered are typical of assemblages at the upper reaches of the contemporary marsh. The diatom assemblage in this unit is dominated by brackish-freshwater taxa (ca. 80%) most notably *Navicula elegans* and *Pinnularia* spp. No foraminfera were present in this unit. This unit is distinguished from the salt-marsh peat based on testate amoebae and diatom assemblages and the absence of foraminifera.

6.2.2 Chronology of marsh development at Swan Inlet

This section describes the radiocarbon age determinations of sea-level related palaeoenvironmental changes at Swan Inlet. The results of the 10 'rangefinder' radiocarbon dates (**Section 3.6.1**) obtained from samples taken close to the contacts between each of the major units described above are presented in **Table 6.3** and **Figure 6.2**. The oldest age dates to the late Pleistocene (11.75 – 12.05 ka BP). However, this age, at the contact between the bottommost unit and the tidal flat sands in core *SI-5* appears to be chronostratigraphically out of sequence as the basal date for core *SI-5* is younger (10.24 - 10.49 ka BP). This supports the interpretation of this unit being reworked i.e. material dated was not deposited *in situ,* therefore the two lowest dates in core *SI-5* are deemed unreliable. The basal date of core *SI-1* at 227-229 cm (8.39 – 8.58 ka) is also younger then the overlying date at the contact between the salt-marsh clay and tidal flat sands (8.73 - 9.01 ka BP). Because this date was obtained close to the erosive contact between these two units the dated material could

potentially have been washed in with the tidal sands. This date is therefore also deemed unreliable.

***Table 6.3**: Radiocarbon dates obtained from sampled sections of the Swan Inlet stratigraphy*

Sample location	Depth (cm)	Laboratory code	C14 age (yrs BP ± 1σ)	Min. 2σ cal. age	Max. 2σ cal. age	Stratigraphic context
SI-1	80-83	SUERC-47991	4730±37	5315	5580	salt-marsh peat/ tidal flat sands contact
SI-1	198-200	SUERC-50086	8087±38	8728	9080	tidal flat sands/salt-marsh clay contact
SI-1	227-229	SUERC-48880	7724±45	8391	8576	base of sequence
SI-2	87-89	SUERC-50458	1860±37	1614	1866	salt-marsh peat/ tidal flat sands contact
SI-2	232-233	SUERC-47992	7759±38	8419	8584	tidal flat sands/salt-marsh clay contact
SI-2	298-299	SUERC-48884	7672±45	8368	8540	base of sequence
SI-5	81-83	SUERC-50459	2639±37	2499	2788	salt-marsh peat/ tidal flat sands contact
SI-5	187-188	SUERC-50089	10256±41	11754	12050	tidal flat sands/reworked clay contact
SI-5	269-270	SUERC-47993	9229±40	10242	10491	base of sequence
Bank section	70	SUERC-47994	948±35	910	740	salt-marsh peat/ tidal flat sands contact

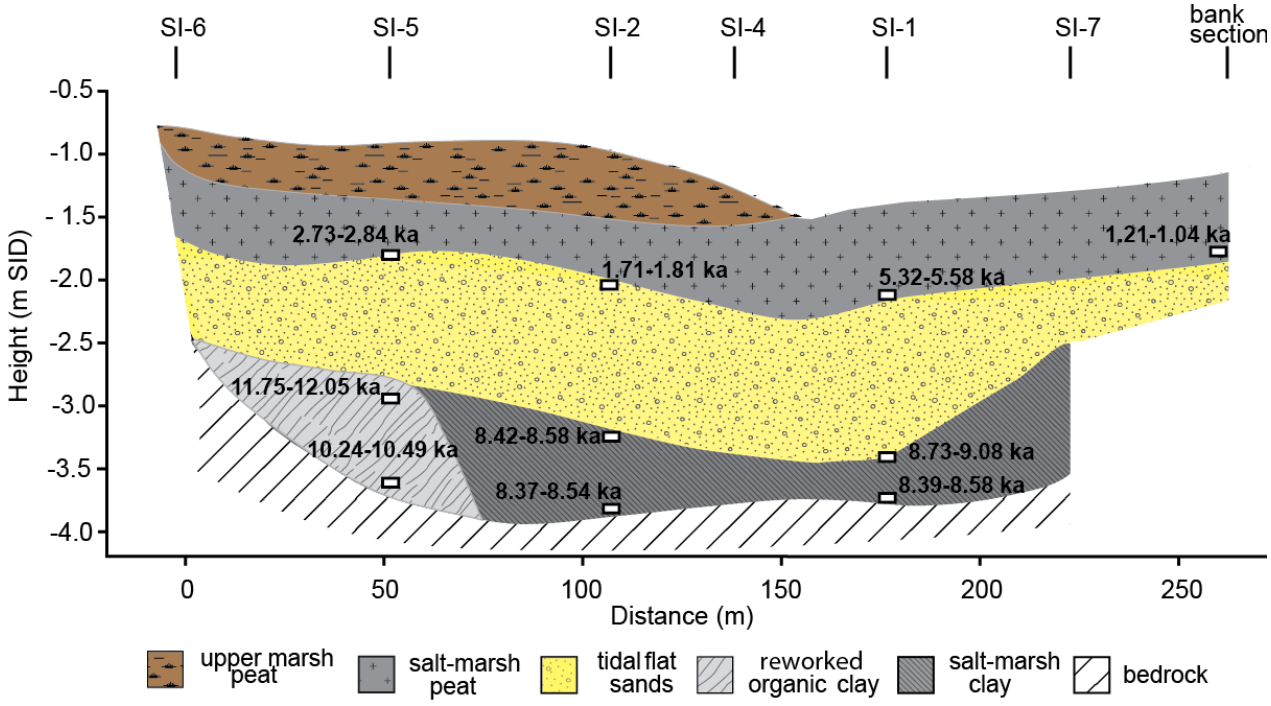

***Figure 6.2**: Palaeoenvironmental interpretations of the stratigraphy of Swan Inlet based on the sedimentology and biostratigraphy with positions of radiocarbon dated samples (**Table 6.3**) described in the text, core locations are shown in **Figure 3.1**.*

The stratigraphy of Swan Inlet in this study is consistent with the stratigraphy observed by the earlier reconnaissance of Bentley *et al.* (2005). The stratigraphy recorded by Bentley *et al.* (2005) is presented in **Figure 6.3** and the same four units can be identified. Although, a large section of the marsh was not sampled, no microfossil analyses were conducted and core elevations were not surveyed. Additionally, three radiocarbon dates (SUERC – 9984, 9986 and 9988; allocation no. 1138.1005) were obtained on detrital plant fragments recovered from an exposed bank section sampled in 2005 (**Figure 6.3**). These dates provide additional constraints for the upper (6.74 - 6.97 ka BP) and lower (6.79 – 7.03 ka BP) contacts of the tidal flat sands. However, the date obtained from an interbedded plant fragment within the tidal flat sands (9.15 – 9.52 ka BP) is out of chronostratigraphic sequence and much older. It is deemed to be unreliable based on the interpretation that the dated material was likely washed in with the sands and is therefore not *in situ*.

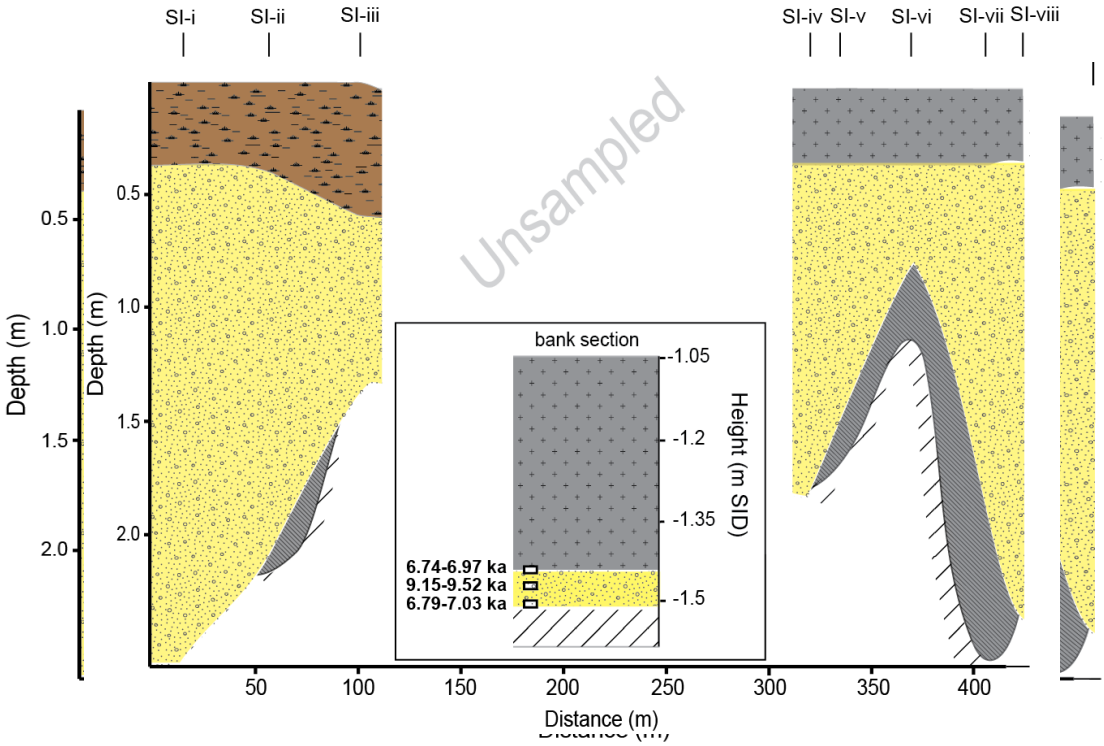

***Figure 6.3**: Stratigraphy of Swan Inlet described by Bentley et al. (2005), black lines at the top of the diagram indicate coring locations shown in **Figure 3.1**. Key as in **Figure 6.2**. Inset: stratigraphy of exposed bank section sampled for radiocarbon dating in 2005, sample heights inferred from marsh survey in 2005 (see Appendix C).*

6.2.3 Holocene sea-level reconstruction for the Falkland Islands

The radiocarbon dates and their associated microfossil assemblages were used to provide SLIPs documenting the Holocene sea-level history of the Falkland Islands (**Table 6.4, Figure 6.5**). The transfer functions presented in **Chapter 5** were used to derive the indicative meaning component for each SLIP based on the microfossil content associated with dated samples (**Table 6.5**). Although 14 radiocarbon dated samples were available (**Table 6.4**), only 9 samples were used to produce the Holocene SLIPs as 4 samples were unsuitable due to the following reasons. One sample from SI-1 at 198-200 cm was not used as a SLIP because the date of 9.08 – 8.73 ka (older than the date lower down in the core) is deemed unreliable and there were no microfossils preserved (**Table 6.5**) from which an indicative meaning could be derived. This sample was taken close to the erosive contact between the salt-marsh clay and the tidal flat sands and is therefore likely to contain reworked sediments of unknown origin. Two samples from SI-5 at 187-188 cm and 269-270 cm were not used as SLIPS as the peat unit from which these samples were taken was interpreted as being reworked (**Section 6.2.1**). One sample from the 2005 bank section at 41 cm was not used as a SLIP as this date (9.52- 9.15 ka), based on a plant fragment, was much older than the dated samples above and below it in the sequence. The plant fragment was therefore most likely reworked from an older deposit.

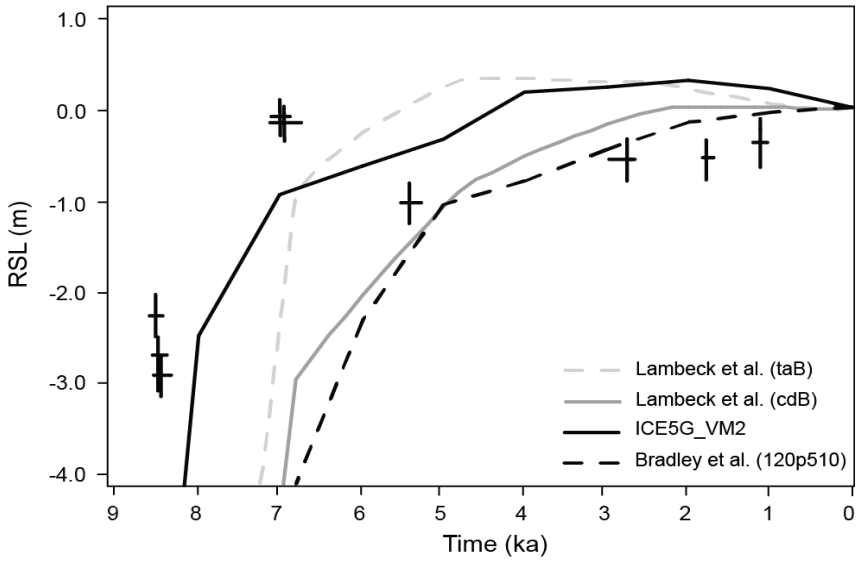

***Figure 6.4**: Holocene SLIPs (crosses) from Swan Inlet compared with GIA model predictions of RSL (lines) GIA models described in the text. Sources: Lambeck et al. (2014; 2017), Peltier (2004), Bradley et al. (2016).*

***Table 6.4**: Holocene sea-level index point information. Relative sea-level (RSL) values are calculated by subtracting the indicative meaning (IM) from the sample height. IMs were derived from microfossil data (**Table 6.5**) Samples without IM and RSL values were not used as SLIPs for the reasons described in the text (above).*

Sample	Height	median age	2σ cal. age error		IM	RSL	Error 2σ
	(m SID)	cal. Yrs BP	+ yrs	- yrs	(m SID)	(m)	(m)
SI-1 80-83	-2.305	5407	92	173	-1.3	-1.005	0.22
SI-1 198-200	-3.48	8915	187	165	-	-	-
SI-1 227-229	-3.77	8473	82	103	-1.12	-2.65	0.4
SI-2 87-89	-1.91	1756	142	110	-1.38	-0.53	0.22
SI-2 232-233	-3.355	8495	76	89	-1.12	-2.235	0.22
SI-2 298-299	-4.0	8426	58	114	-1.105	-2.895	0.22
SI-5 81-85	-1.81	2736	237	52	-1.27	-0.54	0.22
SI-5 187-188	-2.865	11898	144	152	-	-	-
SI-5 269-270	-3.685	10346	104	145	-	-	-
2012 bank section	-1.89	819	91	79	-1.8	-0.09	0.14
2005 bank section 37	-1.455	6852	114	122	-1.39	-0.06	0.28
2005 bank section 41	-1.495	9385	235	135	-	-	-
2005 bank section 45	-1.535	6935	36	221	-1.175	-0.36	0.19

***Table 6.5**: Dominant microfossil assemblages and indicative meaning derivations for Holocene sea-level index points from the Falkland Islands.*

Sample	Testate amoebae										Foraminifera		
	Difflugia pristis type	*Pseudodifflugia fulva type*	*Difflugia bryophila*	*Centropyxis platystoma type*	*Centropyxiella sp.*	*Centropyxis arcelloides*	*Cyphoderia ampulla*	*Centropyxis cassis type*	*Tracheleuglypha dentata*	*Assulina muscorum*	*Trochaminita salsa*	*Miliammina fusca*	**Idicative meaning derivation**
SI-1 80-83													
	46	8	10	3	13	3	0	10	2	0	91	9	testate amoebae transfer function
SI-1 198-200	NIL	NIL	NIL	NIL	NIL	NIL	NIL	NIL	NIL	NIL	NIL	NIL	N/A
SI-1 227-229	0	0	0	0	0	25	0	33	0	17	100	0	upper limit of foraminifera
SI-2 87-89	76	11	4	0	3	2	2	2	0	0	97	3	testate amoebae transfer function
SI-2 232-233	0	0	0	0	7	0	15	15	0	15	80	20	upper limit of foraminifera
SI-2 298-299	25	0	0	0	0	75	0	0	0	0	100	0	upper limit of foraminifera
SI-5 81-85	39	4	6	15	2	0	0	33	0	0	79	19	testate amoebae transfer function
SI-5 187-188	NIL	NIL	NIL	NIL	NIL	NIL	NIL	NIL	NIL	NIL	NIL	NIL	N/A
SI-5 269-270	NIL	NIL	NIL	NIL	NIL	NIL	NIL	NIL	NIL	NIL	100	0	N/A
2012 bank section	1	42	7	0	28	0	4	0	9	0	100		testate amoebae transfer function

	diatoms													
	Planothidium delicatulum	*Achnanthes kuelbsii*	*Diploneis elliptica*	*Eunotia minor*	*Opephora pacifica*	*Stauroforma exiguiformis*	*Navicula halophila*	*Caloneis bacillum*	*Stauroforma atomus*	*Frustulia fasiculata*	*Paralia sulcata*	*Ctenophora pulchella*	*Rhopalodia brebissonii*	
2005 bank section 37	13	4	5	1	8	7	5	1	4	10	7	10	3	diatom transfer function
2005 bank section 41	11	4	1	1	15	13	3	0	2	7	23	9	2	N/A
2005 bank section 45	8	4	4	4	14	16	2	4	3	1	16	7	4	diatom transfer function

The stratigraphy of Swan Inlet described in **Section 6.2.2** can be directly related to the Holocene sea-level history of the Falkland Islands reconstructed by the 9 SLIPs. The data indicate that before ca. 8 ka BP, RSL was several metres below present MSL with the shale basement at Swan Inlet being exposed and above the tidal limit. Under rising sea levels in the early Holocene, the shale basement began to be inundated at high tide permitting the development of a salt marsh. This salt marsh persisted until ca. 8.4 ka BP when it was suddenly drowned, indicated by the tidal flat sand unit. At this time the salt marshes were transformed to tidal flats. Sea level continued to rise until ca. 7 ka BP reaching a position between 0.5 and 1.0 m below present. Sea level

fell gradually from ca. 7 ka BP marking the end of rapid early Holocene rise, before gradually rising from ca. 6 ka BP up to its present position. These 9 SLIPs were compared with output from Glacio-isostatic adjustment (GIA) models by Peltier (2004) and Bradley *et al.*, (2016) and with predictions using ocean mantle parameters (taB) of Lambeck *et al.* (2014), and a continental mantle model (cdB) of Lambeck *et al.* (2017) (**Figure 6.4**). Overall the Lambeck *et al.* (2017) and Bradley *et al.* (2016) predications have the best fit for the sea-level data of the past 6 ka. The oldest data are best captured by the ICE5G model with the VM2 viscosity profile (Peltier, 2004). But there is not a unique GIA model prediction that agrees with all SLIPs. The implications of this new Holocene sea-level curve for GIA models and understanding of Holocene sea-level changes in the South Atlantic region are discussed in **Chapter 7**.

6.3 Late Holocene sea-level changes in the Falkland Islands

This section focuses on the late Holocene, presenting results obtained from high-resolution chrono- and bio-stratigraphical analyses of the upper 90cm of core *SI-2*. Analyses were confined to the upper two units (upper-marsh peat and salt-marsh peat) of core *SI-2* as these units represent the late Holocene. The sedimentological properties and microfossil assemblages of testate amoebae, diatoms and foraminifera are described. Applying the transfer functions presented in **Chapter 5,** the RSL associated with each microfossil assemblage is reconstructed. The reliability of these reconstructions is evaluated through assessment of a suite of reconstruction diagnostics. The results of the chronological analyses conducted on core *SI-2* (described in **Sections 3.6.1** and **3.6.2.**) and modelled age-elevation profile of the core are presented. Finally, the age-depth profile is combined with the RSL reconstructions

that were deemed reliable to produce a late-Holocene sea-level curve for the Falkland Islands.

6.2.4 Sedimentology of late Holocene deposits, Swan Inlet.

This section presents detailed analyses of the sedimentological properties on the upper 95 cm of core *SI-2.* Loss-on-ignition (LOI), particle size and bulk density analyses were conducted (following **Section 3.4.4**) on contiguous subsamples taken at 1 cm intervals through the upper 95 cm of core *SI-2.* A total of 95 samples were analysed. The results of these analyses are presented in **Figure 6.5.**

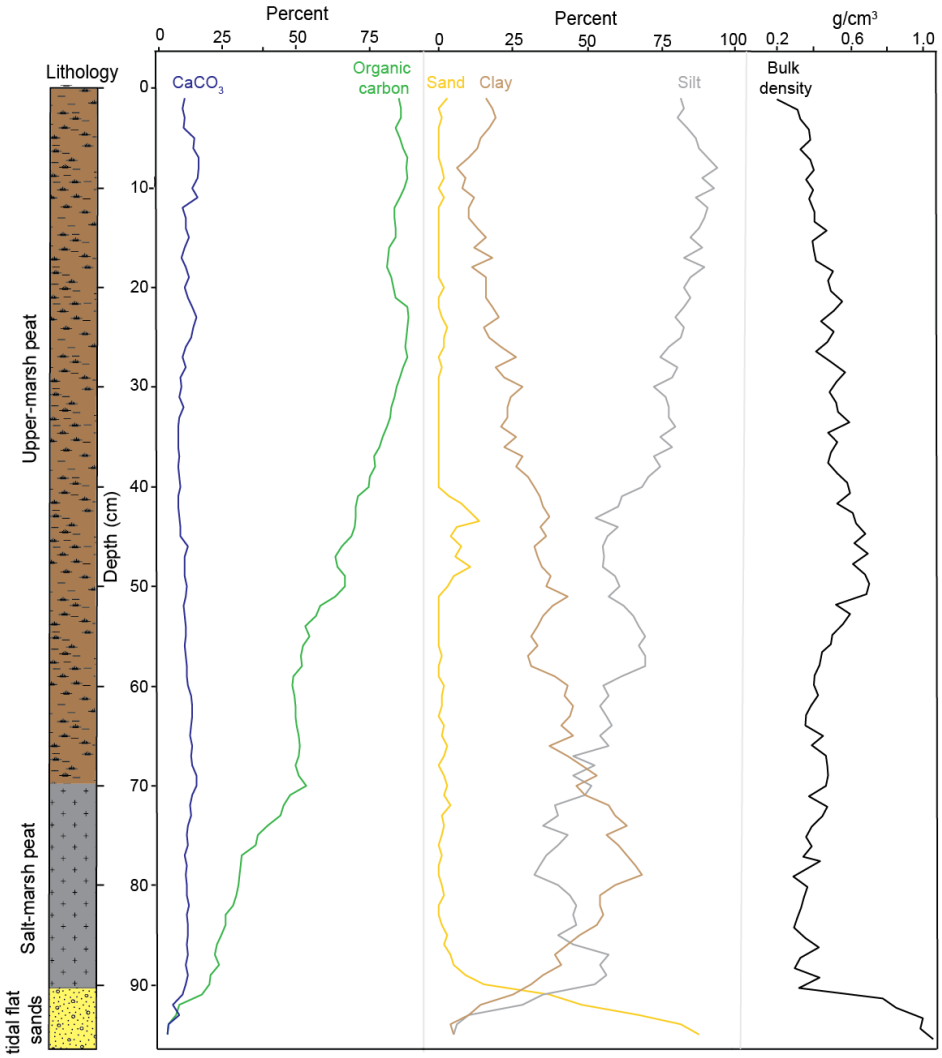

Figure 6.5*: Sedimentology of core SI-2 (0-95 cm) showing results of loss-on-ignition ($CaCO_3$ and organic carbon), particle size (sand, silt, clay) and dry bulk density analyses.*

LOI - organic carbon and calcium carbonate

The organic carbon content exhibits an overall increasing trend upcore. The amount of calcium carbonate ($CaCO_3$) is comparatively stable throughout the entire sequence. At the base of the sequence, in the tidal flat sands (below 90 cm), the $CaCO_3$ content is below 3% then generally increases upcore, in the salt-marsh and upper-marsh peats, comprising 9 – 14 % of the dry sediment mass between 90 - 0 cm. Organic carbon is low at the base of the sequence, comprising between 2 – 5% of the dry sediment mass in the tidal flat sands. The organic carbon content steadily increases at a rate of ca. 1% per cm from 17% at the contact between the salt-marsh peat and tidal flat sands (90 cm) up to 46% at the contact between the salt-marsh and freshwater peats (71cm). The organic carbon content continues to increase upcore in the upper-marsh peats. In the upper 34 cm organic carbon consistently accounts for >80% of the dry mass of the sediments, reaching a maximum of ca. 88% between the depths of 22-27 cm.

Particle size

In the tidal flat sands unit (90-95 cm) the relative proportion of sand is greatest (87%) at 95 cm as the clay and silt proportions are at their minimum (5 %) at the base of the sequence. This trend reverses toward the contact between the tidal flat sands and salt-marsh peats (90 cm) highlighted by a rapid decline in the sand fraction (<5%). At the base of the salt-marsh peat unit, silt is the dominant sediment fraction (max. 57%) between 90 - 85 cm. The clay fraction (ca. 60%) becomes dominant over the silt proportion (ca. 40%) in the salt marsh peat unit from 85 - 74 cm. This general trend is punctuated by a small peak (max. 15%) in the sand fraction between 50 - 40 cm. Upcore of 70 cm the silt fraction decreases as the clay fraction increases with both reaching virtually equal proportions around the contact between the upper-marsh peat

and the salt-marsh peat (68-73 cm). The upper marsh peat (70 - 0 cm) is predominantly composed of silt which increases toward the top of the unit as the clay fraction decreases, the sand fraction is largely absent throughout this unit (max. 3%). In the upper 40 cm the silt fraction accounts for over 70% (max. 93% at 8cm) with the remaining fraction being predominantly composed of clay particles.

Dry bulk density

Throughout the upper-marsh peat and salt marsh clay units (90-0 cm) the bulk density remains relatively consistent, fluctuating by around 0.4 g/cm^3. Although large-scale changes in bulk density are not observed throughout these two units there are identifiable trends. At the contact between the salt marsh peat and the tidal flat sands, around 90 cm depth, the bulk density rapidly decreases from ca. 1 g/cm^3 to ca. 0.4 g/cm^3 which coincides with the rapid decline in sand content observed in the particle size analysis. From the base of the salt-marsh peat at 90cm, up to around 50 cm, bulk density gradually increases from ca. 0.3 g/cm^3 to ca. 0.4 g/cm^3. Between 50 and 40 cm bulk density reaches a peak of 0.7 g/cm^3 which coincides with a peak in the sand fraction observed in the results of the particle size analysis. From 40-0 cm bulk density exhibits a gradually decreasing trend from 0.6 – 0.2 g/cm^3.

6.2.5 Biostratigraphy of late Holocene deposits, Swan Inlet

In this section the results of microfossil analyses of testate amoebae, diatoms and foraminifera conducted through the upper 90 cm of core *SI-2* are presented. Preparation, counting and identification procedures, and data analysis for all three microfossil groups follows the methods detailed in **Chapter 3**.

Testate amoebae

The upper 90 cm of core *SI-2* was initially sampled at 4 cm resolution for testate amoebae analysis. Based on the initial results two sections were sampled at higher resolution; from 0-6 cm at 1 cm resolution and from 60-90 at 2 cm resolution. The assemblages of dominant (>2 % relative abundance) testate amoebae through *SI-2* are presented in **Figure 6.6**. A total of 21 taxa were recorded in 33 samples. The total sum of all rare taxa (defined as any taxon with a relative abundance no greater than 2 % in any sample) was < 2 % relative abundance in the majority of samples and therefore not presented in **Figure 6.6**.

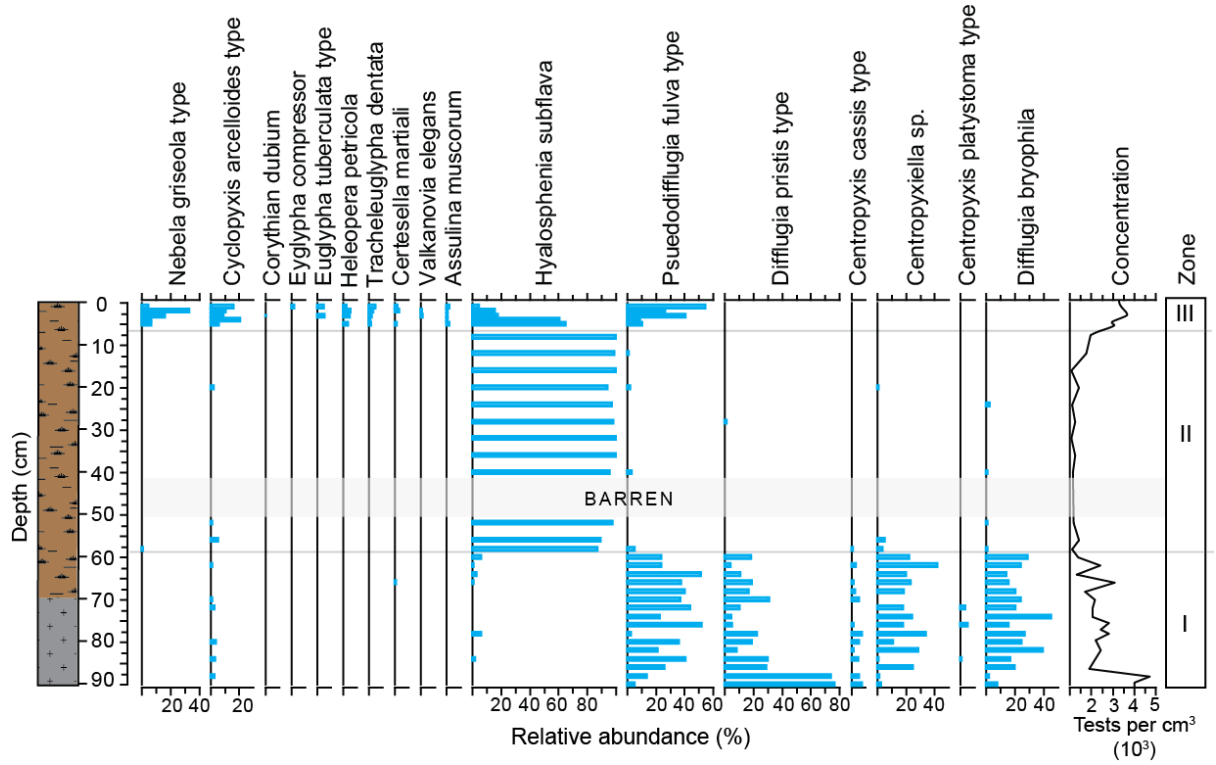

***Figure 6.6**: Dominant fossil testate amoebae and total testate amoebae concentrations in core SI-2.*

To aid interpretation, the fossil testate amoebae assemblages have been divided into zones (I, II and III; **Figure 6.6**) based on the similarities in assemblage compositions.

Species richness and test concentrations were within z*one I* (60-90 cm). The assemblages within this bottommost zone contain taxa which are typical of the lower limits occupied by testate amoebae in the contemporary salt marsh (**Section 5.3.1**). The dominant taxa in *zone I* are *Psuedodifflugia fulva* type, *Centropyxiella* sp., *Difflugia bryophila* and *Difflugia pristis* type. Except *Difflugia pristis* type, all these dominant taxa reach their peak abundances between 80 and 60 cm, with *Difflugia pristis* type alone accounting for ca. 80% of the relative abundance at the base of the sequence. *Zone II* spans the largest depth range in the core (58-6 cm). There is a virtually monospecific assemblage within this zone with *Hyalosphenia subflava* comprising between 86 % (58 cm) and 100 % relative abundance of the assemblages. The concentration of tests is relatively low throughout *zone II* and between 50 and 40 cm depth no testate amoebae were found. *Zone III* is the smallest and uppermost (5-0 cm) zone. The testate amoebae assemblages in *Zone III* are the most species rich of the three zones. The dominant taxa in this zone are *Psuedodifflugia fulva* type (up to 55 % relative abundance), *Hyalosphenia subflava* (up to 65 % relative abundance) and to a lesser extent *Nebela griseola* and *Cyclopyxis arcelloides. Hyalosphenia subflava* decreases in abundance upcore in *zone III* as the other dominant taxa increase in abundance. Notably, assemblages in *zone III* are the only part of the core with significant abundances of *Euglyphid* taxa (*Euglypha*, *Corythian*, *Tracheluglypha*, *Valkanovia* and *Assulina* genera) which are characteristic of the upper-marsh testate amoebae assemblages observed in the contemporary distributions (**Section 5.3.1**). However, no *Euglyphid* taxon has a relative abundance >6% in any sample within this zone.

Diatoms

In order to provide the high-resolution information necessary for detecting the onset and rate of recent sea-level acceleration, the upper 25 cm of core *SI-2* was analysed for diatoms at 1cm resolution. From 25-90 cm, diatom samples were taken at 4 cm intervals. The results of the diatom analyses are presented in **Figure 6.7**. Throughout the sampled section (0-90 cm) of *SI-2,* a total of 25 taxa were recorded in significant abundance (>2% relative abundance in a sample). An additional 17 taxa were recorded that never reached a relative abundance greater than 2% in any sample, the combined sum of these taxa in a sample has been recorded as 'Undifferentiated taxa' (**Figure 6.7**).

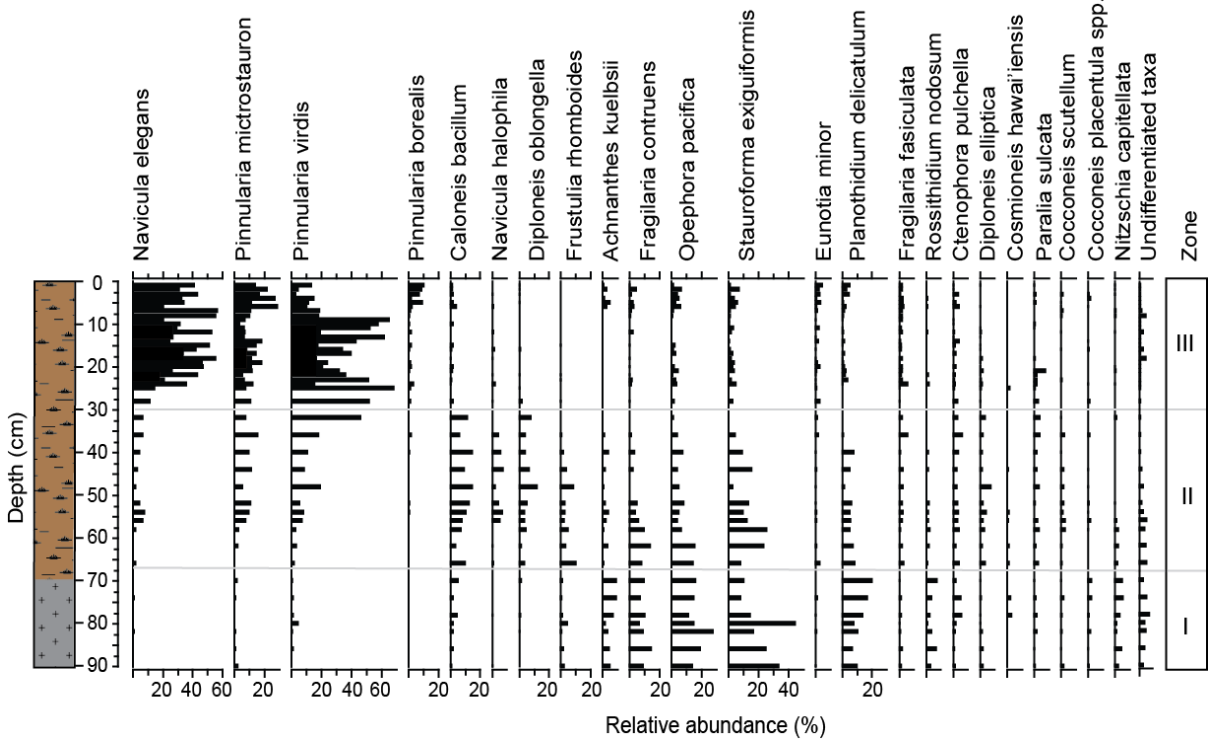

***Figure 6.7**: Dominant fossil diatom assemblages in core SI-2.*

The diatom assemblages have been divided into three zones based on assemblage differences/similarities throughout the core (I,II and III; **Figure 6.7**). The diatom assemblages in *zone II* (68-30 cm) are the most species rich of the three zones with

all of the 25 dominant taxa in the core having occurrences in this zone. In *zone I* (90 – 68 cm) overall species richness declines as the typically low marsh taxa: *Achnanthes kuelbsii, Fragilaria construens* and *Opephora pacifica,* reach their peak abundances. Notably, the undifferentiated taxa peak in this zone (max. 8% relative abundance) many of which were specimens <15 µm which were not able to be identified under light microscopy. It was also noted that samples from the contemporary tidal flats also had an abundance of unidentifiable <15 µm specimens. Within *zone II* several taxa that are typically found in the contemporary middle marsh reach their peak abundances; *Caloneis bacillum, Frustulia rhomboides, Navicula halophila, Cosmioneis hawai'iensis, Diploneis sp.* and *Ctenophora pulchella*). The relative abundances of taxa which occupy the upper zone of the contemporary diatom distributions (*Navicula elegans, Pinnularia microstauron* and *Pinnularia virdis*) gradually increase upcore through *zone II*. The most recent diatom assemblages in the upper core are dominated by *Navicula elegans, Pinnularia microstauron* and *Pinnularia virdis* which account for a combined 60-97 % of the relative abundances in *zone III* (30-0 cm). These same three taxa are dominant in the contemporary upper marsh sediments at Swan Inlet (**section 5.3.2**). Other, less abundant, taxa in *zone III* are also indicative of upper marsh assemblages in the contemporary distributions (*Pinnularia borealis* and *Eunotia minor*).

Foraminifera

Samples for foraminifera were analysed through the upper 90 cm of core *SI-2*. The results are presented in **Figure 6.8.** Probably owing to the coring location (upper marsh) being optimised for capturing testate amoebae assemblages, foraminifera were absent in much of the upper core. In all the core samples that foraminifera were present there were mostly monospecific assemblages of *Trochamminita salsa* with

only one sample towards the base of the sequence (88 cm) having a small proportion (3%) of *Milliamina fusca.* Monospecific assemblages of *Trochamminita salsa* were present from the base of the salt-marsh clay unit (90 cm) up to the contact between the upper marsh peat and salt-marsh clay (68 cm). The concentration of foraminifera generally decreases upcore within this unit. In the modern marsh *Milliamina fusca* occur in greatest abundance (ca. 40%) at the lowest marsh and tidal flat elevations, thus the lack of *Milliamina fusca,* except in only low abundance (3%) at the base of the sequence, suggests that the foraminifera in the core most likely represent a middle-low marsh environment. Foraminifera were absent in the upper-marsh peat unit below 50 cm. Between 50 and 40 cm, assemblages of *Trochamminita salsa* (100%) were present, albeit in relatively low-concentrations. From 40-0 cm, in the upper marsh peat, there were no foraminifera present.

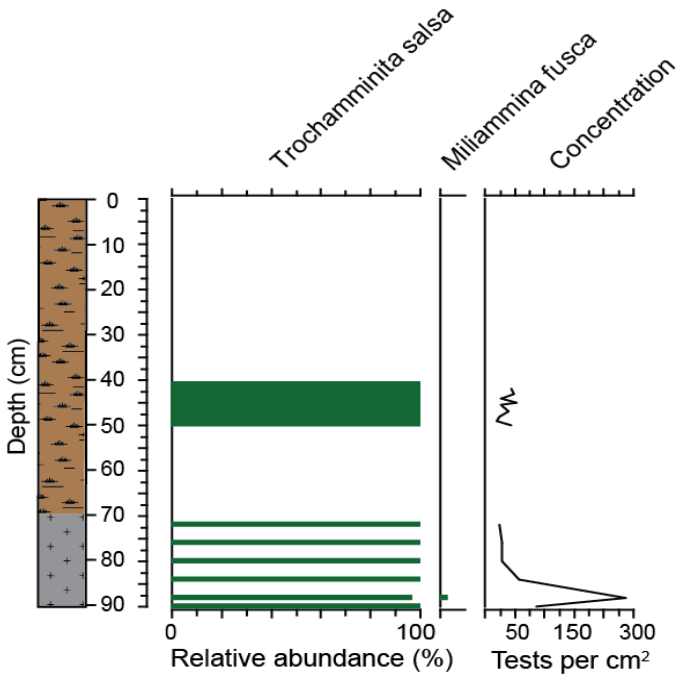

***Figure 6.8**: Foraminiferal assemblages and concentrations in core SI-2.*

Synthesis

The microfossil assemblages of testate amoebae, diatoms and foraminifera in core *SI-2* (**Figure 6.9**) contain mid-low marsh assemblages at the base which transition toward high-marsh assemblages upcore, indicative of an overall regressive trend. However, the absence of testate amoebae and the isolated peak of foraminifera between 40 and 50 cm is indicative of a small transgression which interrupts the overall regressive trend.

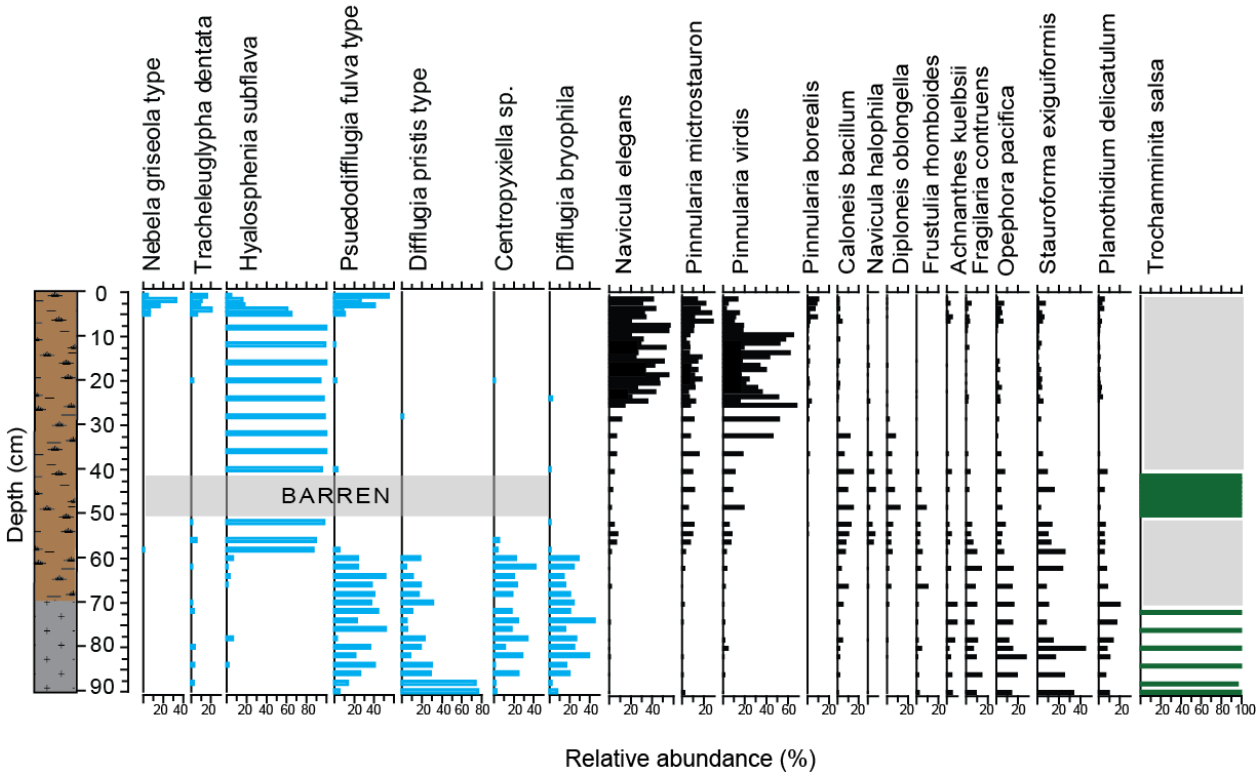

Figure 6.9*: Summary of dominant testate amoebae (blue), diatom (black) and foraminifera (green) in core SI-2.*

6.2.6 Chronostratigraphy of late Holocene deposits, Swan Inlet

This section presents the results of the geochronological analyses conducted on the upper 90 cm of core *SI-2*. The results here are for both the radiocarbon analyses

conducted on 19 plant macrofossils sampled in the upper 90 cm and the short-lived radionuclide analyses conduced on the upper 15 cm of core *SI-2*. Finally, the reliability of the age determinations are assessed before the final age-depth model is presented.

Short-lived radionuclide chronostratigraphy

Compared with Northern Hemisphere inventories (e.g. Corbett and Walsh, 2015) the detection of both ^{137}Cs and ^{210}Pb activity in the upper 15 cm of core *SI-2* (**Table 6.6**) was generally low or below the minimum detection limit (MDA) under gamma spectrometry (despite the increased count time of 48 hours rather than the standard 24 hours). This is a well-known limitation to applying this dating method to Southern Hemisphere sediments due to lower rates of fallout, particularly in remote locations such as the Falkland Islands (Longmore, 1982; Preiss *et al.* 1996). Due to the low fallout, radio-peaks in ^{210}Pb (and ^{214}Pb) were too weak to enable the signal to be separated from noise. The ^{210}Pb profile of core *SI-2* could therefore not be modelled to provide reliable age determinations. Although ^{137}Cs concentrations were generally low, the profile in core *SI-2* reveals a peak between 6-8 cm (**Figure 6.10**) that can be related to the maximum deposition (1964-1965 CE) of ^{137}Cs produced in atmospheric nuclear weapons testing (UNSCEAR, 2000). These results are broadly similar to those of Gehrels *et al.* (2008) who also found ^{210}Pb to be too low for reliable determination but found there to be a clear ^{137}Cs peak in New Zealand salt marshes.

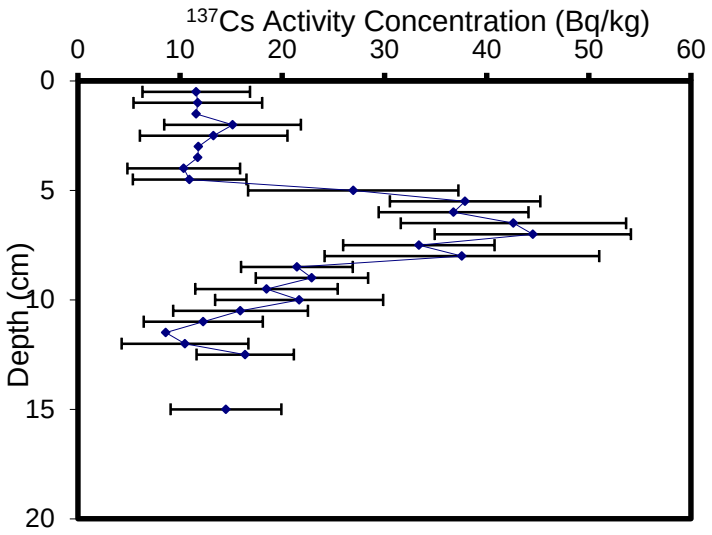

Figure 6.10 *Profile of ^{137}Cs activity in upper 15cm of core SI-2.*

Table 6.6*: Profiles of short-lived radionuclides in core SI-2*

Depth (cm)	^{137}Cs	2-sigma	^{210}Pb	2-sigma	^{214}Pb	2-sigma
0.5	11.6	5.3	135.8	62.5	29.4	11.1
1.0	11.7	6.3	162.4	86.5	23.5	13.9
1.5	MDA	MDA	129.3	67.3	MDA	MDA
2.0	15.2	6.7	141.1	70.7	MDA	MDA
2.5	13.3	7.2	MDA	MDA	MDA	MDA
3.0	MDA	MDA	MDA	MDA	MDA	MDA
3.5	MDA	MDA	MDA	MDA	MDA	MDA
4.0	10.4	5.5	116.6	64.6	21.3	11.1
4.5	10.9	5.6	MDA	MDA	MDA	MDA
5.0	27.0	10.3	MDA	MDA	25.6	15.0
5.5	37.9	7.4	MDA	MDA	MDA	MDA
6.0	36.8	7.3	MDA	MDA	22.1	10.7
6.5	42.6	11.0	129.9	74.0	MDA	MDA
7.0	44.5	9.6	MDA	MDA	29.9	15.4
7.5	33.4	7.4	MDA	MDA	42.9	13.1
8.0	37.6	13.4	MDA	MDA	MDA	MDA
8.5	21.4	5.5	MDA	MDA	MDA	MDA
9.0	22.9	5.5	MDA	MDA	14.0	8.4
9.5	18.5	7.0	MDA	MDA	MDA	MDA
10.0	21.7	8.2	MDA	MDA	MDA	MDA
10.5	15.9	6.6	MDA	MDA	MDA	MDA
11.0	12.3	5.8	MDA	MDA	25.5	13.9
11.5	MDA	MDA	MDA	MDA	MDA	MDA
12.0	10.5	6.2	MDA	MDA	MDA	MDA
12.5	16.4	4.8	MDA	MDA	MDA	MDA
15.0	14.5	5.4	MDA	MDA	19.7	8.3

Radiocarbon chronostratigraphy

A total of 19 radiocarbon ages were obtained on detrital plant fragments sampled throughout the upper 90 cm of core *SI-2*. The dates are summarised in **Table 6.6** including the core depth for each sample, radiocarbon ages (yrs BP) with 1 sigma uncertainties and calibrated ages with 2 sigma uncertainties. The radiocarbon ages were calibrated using the SHcal13 calibration curve (Hogg *et al.* 2013) with post 1950 CE ages (represented here as negative ages relative to 1950) calibrated using the postbomb SH zone1-2 calibration curve (Hua *et al.,* 2013). Calibrated ages given in **Table 6.7** represent the full 2-sigma (95 % confidence) range of age probabilities for each sample. All radiocarbon ages in this section are from NERC allocation number 1885.0415.

The basal date, in the lowest section of the salt-marsh clay unit in core *SI-2*, at 89 cm, has a calibrated age of 1428-1499 CE, which is more modern than other dates stratigraphically higher in this unit. At 87 cm the calibrated age ranges from 893 to 1025 CE, above this at 74 cm the calibrated age is 988-1148 CE. The sample taken close to the contact between the salt-marsh clay and upper-marsh peat units at 70 cm was dated at 1023 – 1176 CE. The lowest date in the upper-marsh peat unit at 64.5 cm dates to 1049-1270 CE. The next age upcore (57 cm) has a relatively large range of 1697-1957 CE, although the most probable (p=0.65) calibrated age for this sample is 1877-1917 CE. However, the next two dates upcore at 42 cm and 38 cm are most likely older (1468-1636 cal. CE and 1665-1956 cal. CE) than the date at 57 cm. The radiocarbon dates in the upper-marsh peat unit upcore of 57 cm suggests these sediments were deposited in the last ca. 60 years as the majority of calibrated ages are post 1955 CE. The age at 21 cm has a large range of probable ages (1672 - 1955 CE), this could be because this date was obtained on an aggregated sample of small

leaf fragments and more robust (woody) plant stems , some of which may have derived from reworked older material. Three dates at 34, 30 and 28 cm all fall within the same calibrated age range of 1955-1957 CE and should therefore be interpreted cautiously. The dates toward the top of core *SI-2* are generally in good agreement with the ^{137}Cs peak (1964-1965 CE) between 6-8 cm. The topmost age at 6.5 cm (1963-1980 cal. AD) postdates the nuclear weapons peak. However, the date at 7.5cm (1958-1999 cal. CE) is most likely (p=0.89) to be post 1994 CE and is therefore out of sequence. This age outlier at 7.5 cm could be due to the material dated being unreliable, possibly because the dated material had been deposited in an infilling crack on the contemporary marsh surface or may have been root material rather than a detrital plant fragment and therefore out of stratigraphic context .

Table 6.7*: Summary of radiocarbon dates for upper 90cm of core SI-2. Bold font denotes dates obtained through high precision analyses.*

				cal. CE age (2 sigma)	
Publication code	Depth (cm)	C^{14} Age (yrs BP)	± 1 sigma (yrs BP)	min	max
SUERC-61825	6.5	-2209	37	1963	1980
SUERC-61887	**7.5**	**-879**	**16**	**1958**	**1999**
SUERC-61888	**10**	**-1218**	**16**	**1959**	**1993**
SUERC-61889	**13.5**	**-985**	**16**	**1959**	**1996**
SUERC-61891	**15**	**-116**	**16**	**1955**	**1957**
SUERC-61892	**20**	**-3072**	**16**	**1964**	**1974**
SUERC-61897	**21**	**180**	**15**	**1672**	**1955**
SUERC-61898	**23**	**-737**	**15**	**1959**	**2003**
SUERC-61899	**28**	**-70**	**14**	**1955**	**1957**
SUERC-61900	**30**	**-2**	**14**	**1955**	**1957**
SUERC-61826	34	-6	35	1955	1957
SUERC-64937	**38**	**141**	**35**	**1665**	**1956**
SUERC-64938	**42**	**314**	**37**	**1468**	**1636**
SUERC-64939	**57**	**51**	**37**	**1697**	**1957**
SUERC-61833	64.5	897	37	1049	1270
SUERC-61834	70	990	36	1023	1176
SUERC-61835	74	1045	36	988	1148
SUERC-61836	87	1113	35	893	1025
SUERC-61837	89	471	25	1428	1499

Age-depth chronology

The chronology for the upper 90cm of core *SI-2* combines the ^{137}Cs and radiocarbon ages presented above into a model of the age-depth relationship. This enables the probabilistic estimation of age for sections of the core that were not directly dated. In order to achieve a robust age-depth relationship, a careful, critical assessment of the sample dates was undertaken to identify and appropriately deal with outliers. In an ideal situation, the oldest date will be the lowest in the core with upcore dates being sequentially younger. This situation, known mathematically as 'monotonicity', is used as a constraint when modelling the age-depth relationship. The calibrated radiocarbon results described above (**Table 6.7**) indicate a number of potential violations of the monotonicity constraint (age reversals). However, the 2-sigma age ranges are not necessarily a good summary of the age of the sample (Telford *et al.* 2004). Owing to the non-Gaussian probability distributions of calibrated ages (Bennett, 1994), these apparent age reversals may still be reliably modelled based on the range of relative probabilities of calibrated ages. Here a 'flag and shift' approach is applied when modelling the age-depth relationship (Christen,1994). In this approach the prior probability of a sample being an outlier is defined (i.e. 0.05 for a 1 in 20 chance), the model then estimates outliers (flagging them) and then attempts to 'shift' them into a position that conforms to the monotonicity assumption (Bronk-Ramsey, 2009). In instances where outlying dates could not be somehow shifted to satisfy the monotonicity constraint, the dates were removed and the model was re-run. An initial age-depth chronology modelled on all the dates revealed three extreme outliers that could not be shifted into a position that could be modelled**.** The three outliers were as follows; the date at the base of the sequence at 89 cm depth (SUERC-61837), the date at 57 cm depth (SUERC-64939) and at 20 cm depth (SUERC-61892).

The final chronology, with these outlying ages removed, is presented in **Figure 6.11** which encompasses many iterations (n=19.8 million) to provide an age-depth chronology modelled with 95% confidence. This is the model used to estimate the age at 1 cm resolution for depths between 0-87 cm of core *SI-2*, inclusive of depths which were not directly dated. The model uses a probabilistic approach to age estimation which therefore produces a unique uncertainty for each 1 cm core section which ranges from ± 6.1 yrs (minimum) to ± 241.8 yrs (maximum). Generally the smallest chronological uncertainties were in the uppermost, most recent, sections of the core where high-precision ^{14}C dates were focused. In total, over 90 % of samples had uncertainties less than ± 100 yrs.

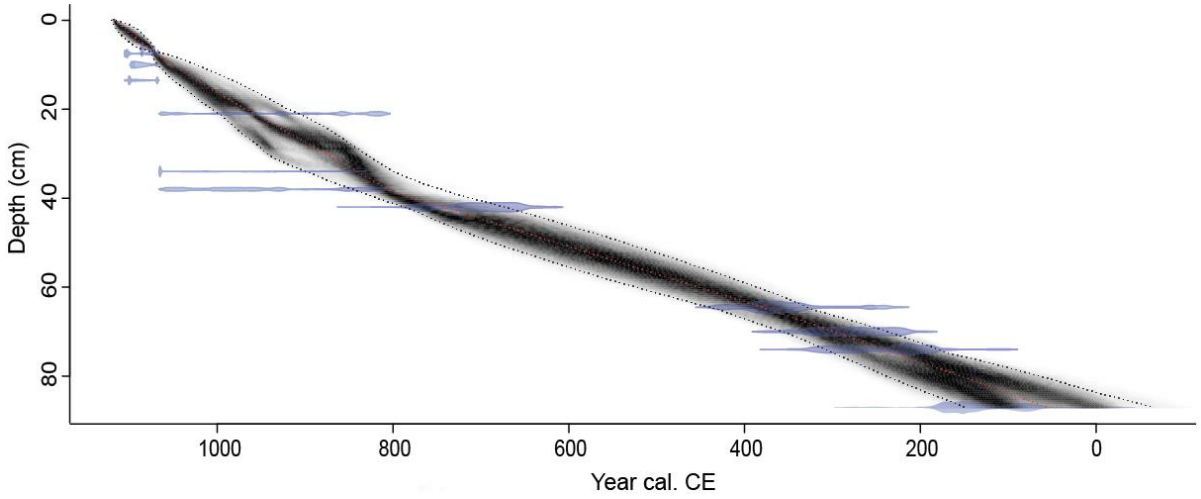

Figure 6.11*: Modelled age-depth chronology for core SI-2 (0-87cm) showing calibrated ^{14}C probability distributions (transparent blue). Darker greys indicate more likely calendar ages; grey stippled lines show 95% confidence intervals; red curve shows single 'best' model based on the weighted mean age for each depth.*

6.2.7 Late Holocene environmental reconstructions

This section presents the final late Holocene environmental reconstructions for Swan Inlet. The transfer functions presented in **Chapter 5** are applied to the microfossil assemblages presented in **Section 6.3.2** to provide PMSE estimates for each sampled section of core *SI-2*. The reconstructed PMSEs are then evaluated through assessment of reconstructive performances using a number of statistical tests. The most reliable PMSE reconstructions are converted to RSL and the final sea-level reconstruction is presented.

Transfer function PMSE estimations

All the transfer function models developed in **Section 5.4** were calibrated on the fossil species data described in **Section 6.3.2** to generate PMSE estimates for each sample. For each group of transfer functions (diatom, testate amoebae and combined), all reconstructions based on both WAPLS and WA models showed the same broad patterns. In the absence of an independent means of validating the reconstructions, the fact that these multiple reconstructions using different numerical procedures and different proxies have comparable trends immediately gives some confidence in the reliability of the reconstructions. Only the reconstructions based on the best-performing models selected in **Section 5.4** are presented in this section, these also tended to have the lowest reconstruction uncertainties. These are: WAPLS component 3, WAPLS component 1 and WAPLS component 3, for the diatom, testate amoebae and combined transfer functions respectively. The PMSE reconstructions for these models are presented in **Figure 6.12** which shows each reconstruction individually and a combined plot of the overlain 1-sigma uncertainties for each reconstruction. Between 5 and 52 cm it was only possible to generate reconstructions for four testate amoebae samples due to a lack of modern analogue for most of the samples in this

section of the core which is dominated by a monospecific assemblage of *Hyalosphenia subflava* (**Section 6.3.2**). However, with diatom and foraminifera assemblage data included, the combined transfer function was able to generate reconstructions for these samples. The general trends of all three reconstructions show a similar pattern. The reconstructions are characterised by an overall regressive sequence with an upcore trend of increasing PMSE. The 1-sigma ranges of all three reconstructions are overlapping for most samples which gives some confidence in the reliability of the reconstructions. Generally there is a better match between reconstructions towards the top of the core, however, at the very top of the core (0-5cm) and between 70 and 80 cm the aggregated 1-sigma uncertainty is greatest as the overlap between the three reconstructions is smaller.

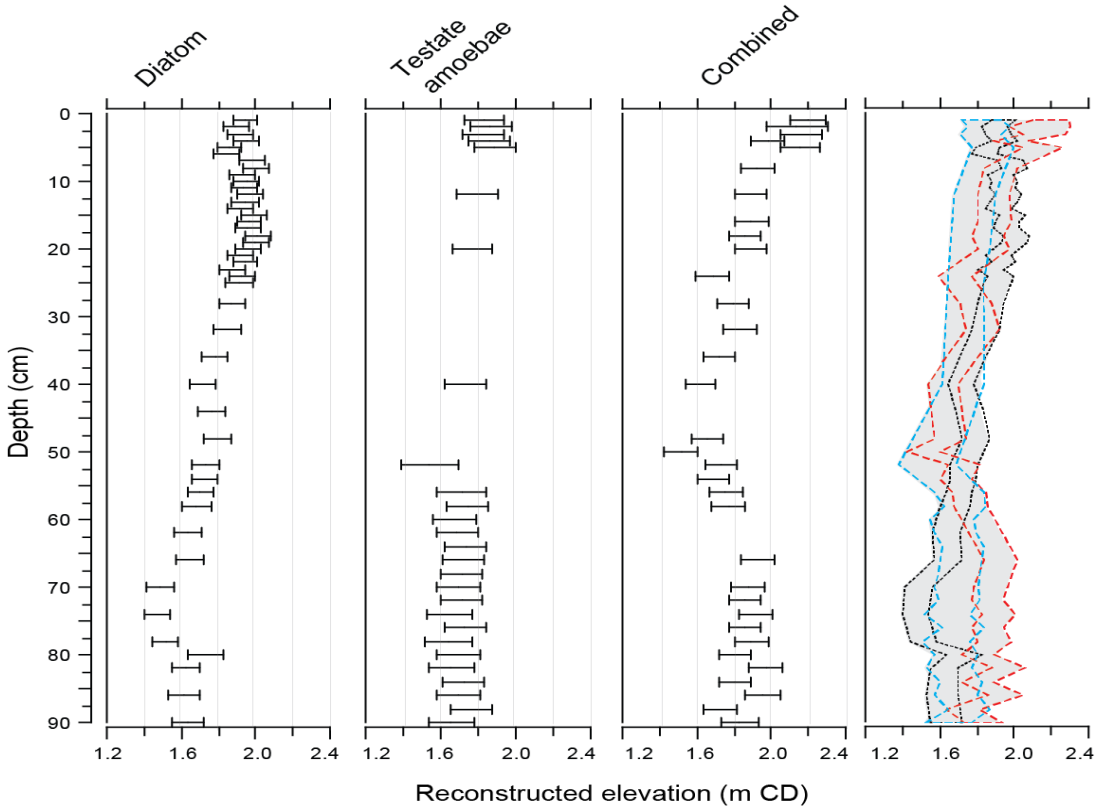

Figure 6.12 *Reconstructed palaeo-marsh surface elevation (PMSE) of microfossil samples in core SI-2. The far right panel shows the aggregated range of 1-sigma uncertainties for all reconstructions (grey) and the 1-sigma uncertainties for testate amoebae (blue dashed lines) diatom (black dashed lines) and combined (red dashed lines) transfer function reconstructions.*

Reconstruction diagnostics

Providing there is at least one common taxon between a fossil sample and the training set, the transfer functions will produce a quantitative reconstruction. However, common taxa between the training set and fossil biostratigraphy does not necessarily equate to comparable assemblages as the relative abundances and species compositions may be significantly different. Therefore, it is crucial to evaluate the reliability of the reconstructions presented above. To this end, a suite of reconstruction diagnostic tests (statistical evaluations) were performed on each reconstruction in order to give a better indication of the reliability of the reconstructions (*cf.* Juggins and Birks, 2012). The first diagnostic presented here is an assessment of analogue quality. Analogue quality, defined as the taxonomic distance between a fossil assemblage and the most similar modern assemblage is assessed using a goodness-of-fit measure (Birks, 1998). For samples where fossil assemblages are not well-described by the modern training set, due to weak-analogue situations, environmental reconstructions are likely to be unreliable and/or the sample-specific error (RMSEP) to be an underestimate of the true uncertainty (ter Braak, 1995). Here a MAT model is fitted to the modern and fossil species data (expressed proportionally) to calculate the taxonomic distance from each fossil sample to the most similar modern assemblages (*cf.* Telford, 2014). The maximum distance possible here is 2, using a squared chord distance metric. The absolute distance values give little indication of the goodness-of-fit, however, fossil samples with distances close to the upper bound represent weaker analogues. However, there are no strict statistical criteria for defining the thresholds between good and bad analogues (c.f. Juggins and Birks, 2012). The thresholds here are defined (arbitrarily) following Jones and Juggins (1995) with the 20^{th} and 5^{th} percentiles of the distribution of dissimilarities calculated between all modern samples

marking the intercept between ‘close’ and ‘poor’, and, ‘good’ and ‘close’ modern analogues respectively.

The results of the analogue quality assessment for all three reconstructions (above) are presented graphically in **Figure 6.13**. For single-proxy transfer functions, the diatom fossil samples were overall best represented by the modern assemblages with the least amount of non-analogues (11%) compared to testate amoebae (36%). In total, 75% of the diatom fossil samples are of close (30%) or good (45%) analogue quality. This compares to 63% of the testate amoebae fossil samples having close (48%) or good (15%) analogues. Generally the diatom samples had better analogue quality in the upper part of the core and testate amoebae samples demonstrate better analogue quality toward the base of the core. The majority of the non-analogue situations for the testate amoebae fossil samples were between 5 and 50 cm depth, in the zone dominated by *Hyalosphenia subflava.* This is unsurprising as there are no such monospecific assemblages observed in the modern training set. The analogue quality is generally not improved for the combined fossil assemblages which have the least amount of close (16%) or good (39%) analogues. The combined assemblages tend to result in a reduction of analogue quality for samples which demonstrate good/close analogue in either of the single-proxy datasets**.** Moreover, none of the non-analogue samples in either the testate amoebae or diatom fossil samples show a significant improvement in analogue quality in the combined samples.

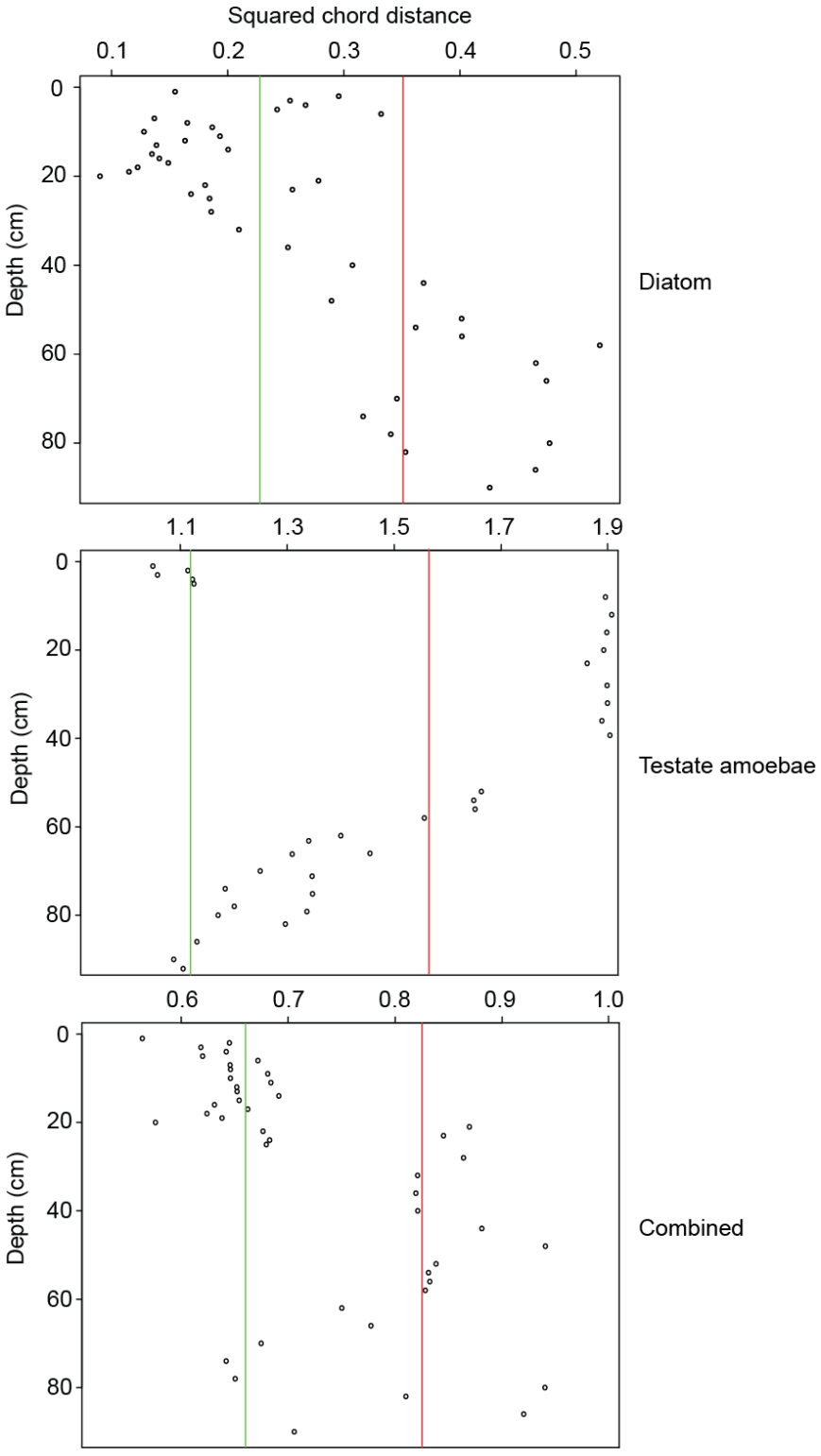

***Figure 6.13**: Squared chord distance from each fossil assemblage to the nearest modern analogue for the diatom (top), testate amoebae (middle) and combined (bottom) reconstructions. Green and red lines mark the 5th and 20th percentile cut-offs explained in the text.*

In order to have confidence in the reliability of the reconstructions the majority of the fossil taxa should be present in the modern training set and these taxa should have well defined optima (i.e. constrained environmental niches). Therefore the second reconstruction diagnostic employed evaluated the definition of the species optima and species coverage in the modern and fossil data. Here the Hill's N2 diversity index (Hill, 1973) is used to calculate the effective number of occurrences of each taxon in the modern training sets; taxa with fewer than 5 effective occurrences are presumed likely to have poorly defined optima. The results of this evaluation are presented graphically in **Figure 6.14**.

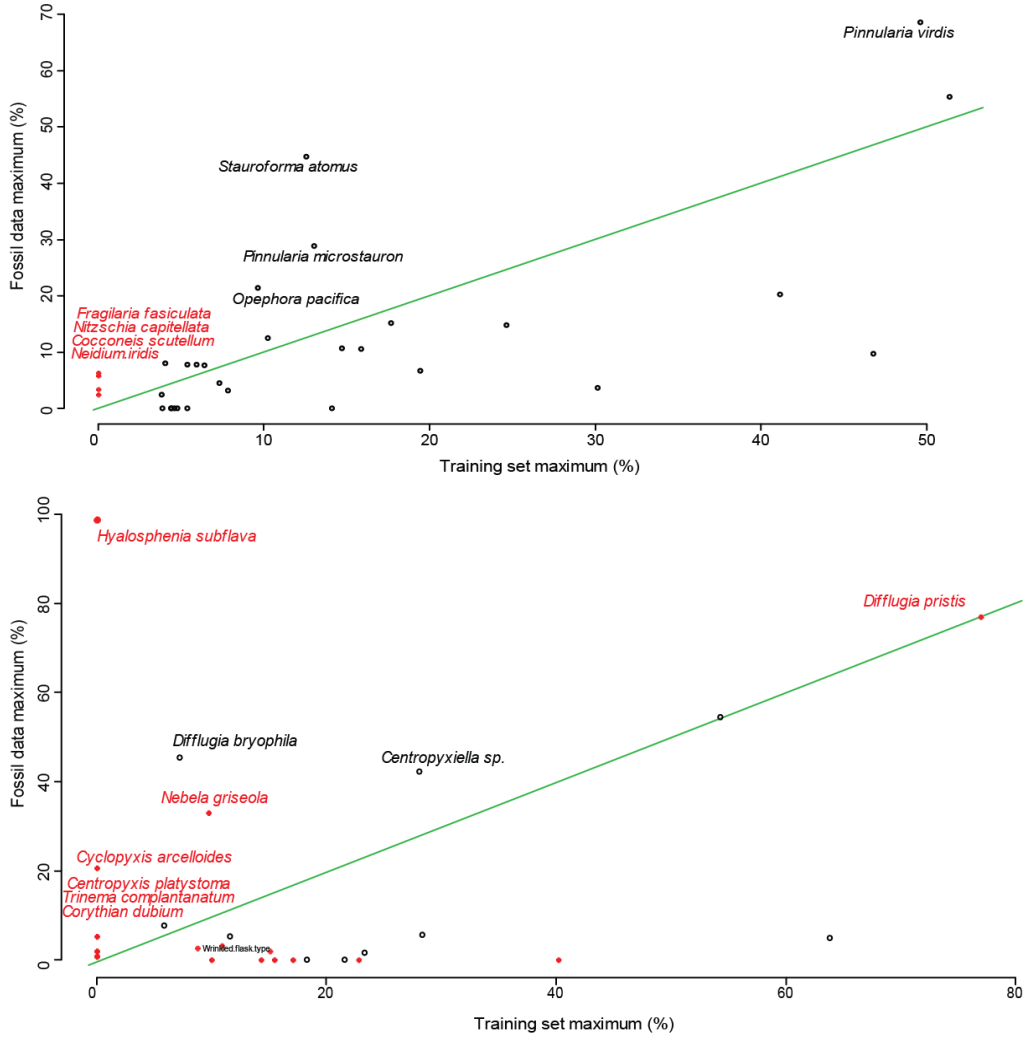

***Figure 6.14**: Maximum relative abundance of taxa in the fossil and modern data sets for diatoms (top) and testate amoebae (bottom). Taxa with poorly defined optima are shown in red and the 1:1(modern:fossil) is represented by the green line.*

The assessment for the combined datasets demonstrates that the foraminiferal taxa do not suffer from poorly defined optima or uneven representation between modern and fossil taxa; therefore, these results are not presented in **Figure 6.14**. For the diatom data, four taxa (*Pinnularia virdis, Pinnularia microstauron, Opephora pacifica* and *Stauroforma atomus*) have maximum occurrences in the fossil data which are considerably greater than in the modern training set. The greater representation of fossil taxa which have clearly defined optima (e.g. *Pinnularia microstauron* and *Pinnularia virdis*, which are dominant in the fossil samples at the top of the core (0-20 cm) does not appear to result in poor-analogue situations for these samples (**Figure 6.13**). Three diatom taxa (*Fragilaria fasiculata*, *Nitzschia capitellata* and *Cocconeis scutellum*) have poorly defined optima and also have greater maximum occurrences in the fossil data, albeit it low relative abundance (<8 %). The testate amoebae data suffers from a number of taxa with poorly defined optima but many of these taxa occur only in the modern training set and therefore do not affect the reliability of the reconstruction. However, six taxa that have poorly defined optima (*Hyalosphenia subflava, Nebela griseola, Cyclopyxis arcelloides, Centropyxis platystoma* type, *Trinema complantanatum* and *Corythian dubium*) also have their greatest abundance in the fossil data. It appears that the presence of these taxa in the fossil data in high abundance causes analogue problems. For example, *Hyalosphenia subflava,* which in the modern training set has a low maximum abundance and poorly defined optima, and is abundant in the core (5-50 cm), causes poor-analogue situations.

Finally, the sample-specific uncertainties for each reconstructed PMSE are evaluated. Calculating sample-specific RMSEPs is the best method available for quantitatively estimating reconstruction uncertainties. However, this method may lead to over- or under-estimation of errors (Juggins and Birks, 2012). Using the training set RMSEP

as a measure of reconstruction uncertainty assumes there are no additional sources of error as a result of poor-analogue situations and that fossil taxa are well described by the modern training set. As demonstrated above, there are several potential violations of this assumption for both the diatom and testate amoebae reconstructions. Sample-specific RMSEPs comprise two components (S_1 and S_2) which represent the errors in the reconstructed PMSEs as a result of uncertainty in the estimates of model parameters (S_1) and the errors in the observed and model-estimated elevations (S_2). These components are calculated by bootstrap resampling: S_1 is the standard deviation of the estimated values at each bootstrap cycle and S_2 is difference between model estimated and observed values calculated as the RMSEP for the training-set samples. Therefore, S_1 is variable between samples, whereas S_2, which usually dominates sample-specific uncertainty (Juggins and Birks, 2012), remains constant. A stratigraphic plot of S_1 calculated for fossil diatom and testate amoebae samples is presented in **Figure 6.15**. In non-analogue situations, where abundant fossil taxa have low abundance and poorly defined optima in the modern training set, S_1 may reach magnitudes close to or greater than S_2 (Juggins and Birks, 2012). This is evident in the diatom reconstructions where samples towards the base of the core have S_1 magnitudes close to, and exceeding, S_2. This trend reflects the trends observed in the analogue quality evaluation where the weakest analogues for the diatom samples were also toward the base of the core (**Figure 6.13**). For the testate amoebae reconstructions, however, S_1 does not reach magnitudes close to S_2 despite several non-analogue situations and abundant fossil taxa with poorly defined optima being observed in the above evaluations (**Figures 6.13** and **6.14**). This suggests that, for the testate amoebae data, the modern training set comprises noisy data and that the true reconstruction uncertainties may be substantially smaller than the training set RMSEP indicates (cf. McCune, 1997; Juggins and Birks, 2012), providing fossil

samples are well-represented in the modern training set. This is likely due to a relatively large number (15) of testate amoebae taxa in the modern training set having poorly-defined optima (**Figure 6.14**).

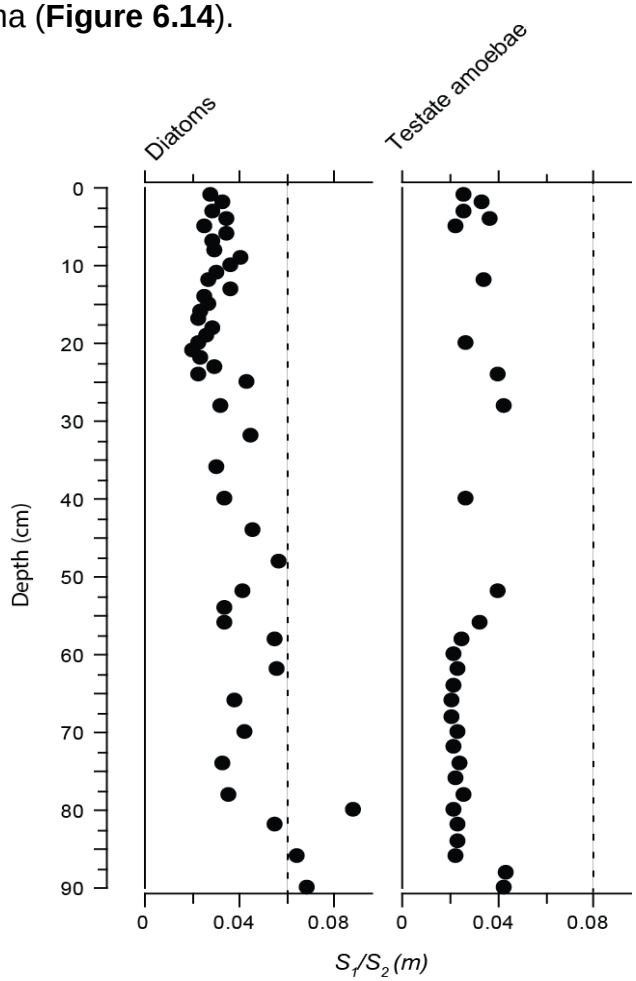

Figure 6.15*: Plot of decomposed sample-specific RMSEP for the diatom and testate amoebae reconstructions.* S_1 is represented as circles and S_2 is marked by the dashed line.

Final PMSE reconstructions

Based on the evaluations of reconstructive performances described above, the final PMSEs to be used in the sea-level reconstruction use only PMSE estimates based on either diatom or testate amoebae reconstructions. The combined reconstructions were not considered as these offered little or no improvement when compared with diatom or testate amoebae reconstructions. In order to achieve the most reliable sea-level

curve, several reconstructed PMSEs were not included in the final reconstruction set. These are summarised, along with the justification for excluding them, in **Table 6.8**

***Table 6.8**: List of fossil samples excluded from the sea-level reconstructions.*

Depth (cm)	Proxy	Justification
12	Testate amoebae	Non-analogue. Dominance of fossil *Hyalosphenia subflava,* poorly described in modern training set.
20	Testate amoebae	Non-analogue. Dominance of fossil *Hyalosphenia subflava,* poorly described in modern training set.
24	Testate amoebae	Non-analogue. Dominance of fossil *Hyalosphenia subflava,* poorly described in modern training set.
28	Testate amoebae	Non-analogue. Dominance of fossil *Hyalosphenia subflava,* poorly described in modern training set.
40	Testate amoebae	Non-analogue. Dominance of fossil *Hyalosphenia subflava,* poorly described in modern training set.
52	Testate amoebae	Non-analogue. Dominance of fossil *Hyalosphenia subflava,* poorly described in modern training set.
56	Testate amoebae	Non-analogue. Dominance of fossil *Hyalosphenia subflava,* poorly described in modern training set.
58	Testate amoebae	Non-analogue. Dominance of fossil *Hyalosphenia subflava,* poorly described in modern training set.
70	Diatom	Weak analogue. High S_1:S_2. Dominance of taxa poorly described in the modern training set.
74	Diatom	Weak analogue. High S_1:S_2. Dominance of taxa poorly described in the modern training set.
78	Diatom	Weak analogue. High S_1:S_2. Dominance of taxa poorly described in the modern training set.

In total 8 testate amoebae and 3 diatom fossil samples were excluded, the remaining 23 testate amoebae and 46 diatom samples are used for the final RSL reconstruction. Included in the final set are a number of samples that performed poorly in one or more of the reconstruction diagnostic assessments but their inclusion (or non-exclusion) can be justified as follows. Several samples contained taxa that have poorly defined optima

in the modern training set, however, it is clear from the reconstruction diagnostics that taxa with poorly defined optima are only a problem if they are dominant in the fossil species data e.g. *Hyalosphenia subflava*. For example, the diatom *Fragilaria fasiculata* has poorly defined optima and is present in relatively low abundance throughout the core but does not appear to cause an appreciable reduction in analogue quality as it is not dominant in any fossil samples. Therefore only samples that contain taxa with poorly defined optima, that are also present in greater maximum abundance in the fossil data and are dominant in the sample, were removed. Several samples that were deemed to be of poor analogue quality were not excluded because, whilst in general poor analogues cause unreliable reconstructions, the arbitrary definition of a 'poor' analogue may not necessarily indicate an unreliable reconstruction. The rationale for including these samples identified as poor analogues was as follows. Their reconstructed values were in good agreement with independently reconstructed values. For example, the 'poor analogue' diatom samples between 50 and 90 cm of core SI-2 (**Figure 6.13**) have reconstructed values within the same range of uncertainty of the testate amoebae reconstructions based on 'good' analogues (**Figure 6.15**). Moreover, experiments with simulated data suggest that there is not a strong relationship between poor analogue samples (defined by the distance between fossil and modern assemblages) and increased unreliability (Juggins and Birks, 2012). In fact, reconstructions based on weighted averaging regressions have been shown to perform well under mild non-analogue situations (ter Braak *et al.,* 1993; ter Braak, 1995). Thus, the analogue quality evaluation in this study is used to indicate potential issues rather than to determine unreliable reconstructions. Therefore, only samples that performed poorly on all diagnostic tests and with reconstructed PMSEs considerably different to independent reconstructions from the same core depth were excluded. With the above samples removed, the final reconstructed RSL values for

core *SI-2* are presented in **Figure 6.16**. Both the diatom and testate amoebae records show the same trend and have overlapping uncertainties for the reconstructed RSL values. The RSL reconstruction shows an overall rising RSL trend from the base of the core at 90 cm to 0 cm with a maximum of ca. 1 m of RSL rise throughout the record. Towards the present, from around 20 cm there is a positive inflexion evident in the record up to the present (0cm) which may represent the 20th century sea-level acceleration observed in previous studies (cf. Gehrels and Woodworth, 2013).

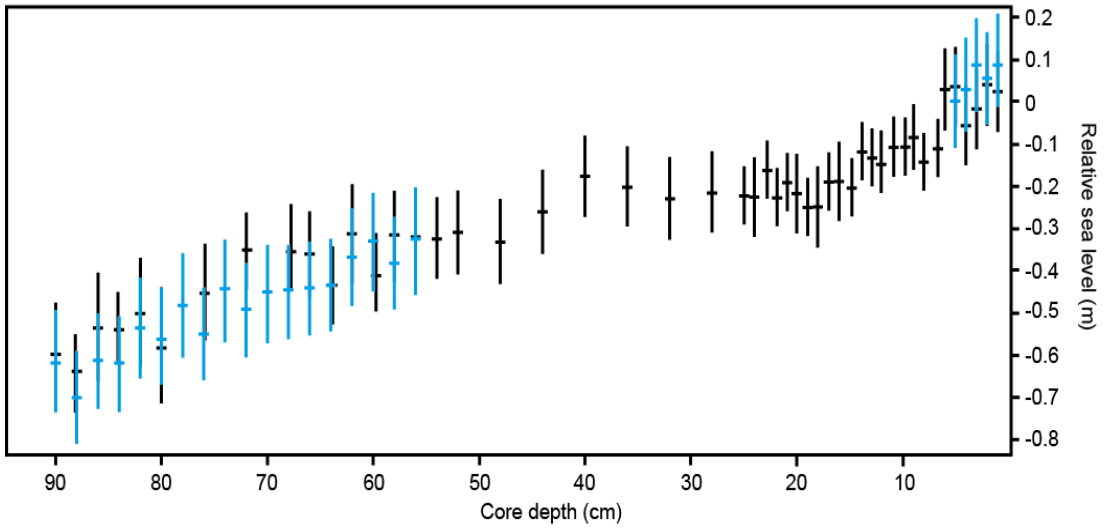

***Figure 6.16**: Relative sea-level reconstructions showing 1-sigma uncertainty ranges, derived from fossil diatom (black) and testate amoebae (blue) assemblages in the upper 90cm of core SI-2.*

Because quantitative reconstructions based on common fossil and modern taxa are possible irrespective of whether or not they are ecologically plausible, it is necessary to statistically test the overall significance of each reconstruction as a whole. To this end, a final assessment of reconstruction reliability was performed on the reconstructions presented in **Figure 6.16** in the form of a global significance test (Telford and Birks, 2011, Birks *et al.,* 2011). This test uses transfer functions trained on random environmental variables (the species data of the modern training set used for the reconstruction combined with randomly generated environmental data) to

generate PMSE reconstructions (n = 999) calibrated on the same fossil data used for the reconstruction. In order to be deemed significant (95% probability) any reconstruction as a whole should explain a greater amount of the variation in the fossil data than 95% of the reconstructions calibrated on randomly-trained transfer functions (Kemp and Telford, 2015). Here an ordination based on redundancy analysis (RDA) was applied to calculate the variance explained. In this test, both the diatom and testate amoebae reconstructions were shown to explain a greater proportion of variance than >95% (actually 100%) of the transfer functions trained on random data (**Figure 6.17**). It can therefore be stated with confidence that the reconstructions are statistically significant (95% confidence).

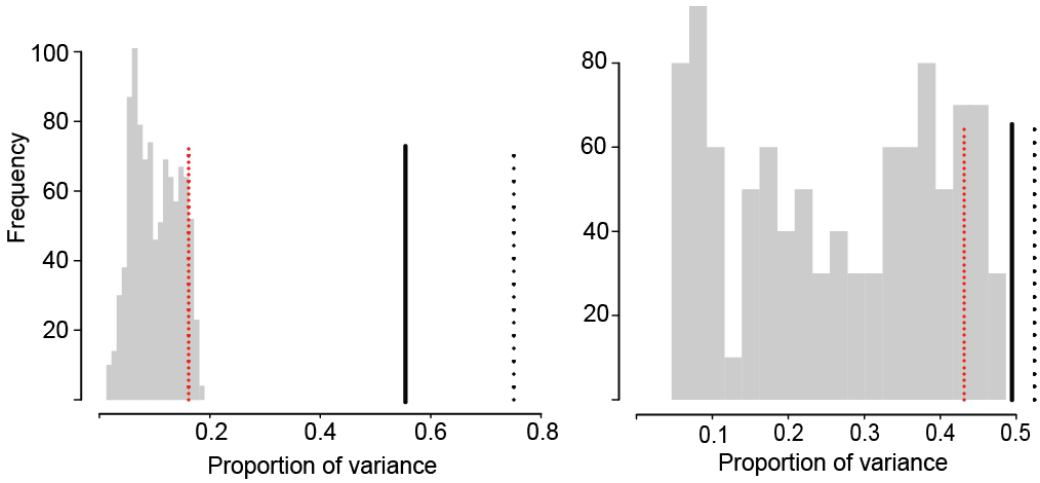

***Figure 6.17**: Results of global significance tests of the final diatom (left) and testate amoebae (right) reconstructions. Histograms show the proportion of the variance in the records explained by reconstructions of 999 random environmental variables and the PMSE reconstruction (black line). The dashed red line represents the 95th percentile of the null distribution. The dashed black line marks the amount of variance explained by the first axis of the RDA.*

6.2.8 Late Holocene sea-level reconstruction for the Falkland Islands

In this section the final late Holocene sea-level reconstruction for the Falkland Islands is presented. The section also details the processes of error quantification and corrections applied to the final sea-level reconstruction.

Errors and corrections

Inherently SLIPs are uncertain and should therefore be considered a best approximation of the former position of sea level in both time and space. In order to achieve the most accurate SLIPs, a conservative estimation of all potential sources of error was calculated for each sample. By assigning conservative errors to each SLIP the risk of over- interpretation of the final sea-level curve is reduced (e.g. Hijma *et al.,* 2015). The uncertainty associated with the temporal (horizontal) position of each SLIP encompasses the 2-sigma analytical errors reported for ^{137}Cs ages. For ^{14}C ages the reported 1-sigma errors were replaced by point-wise error estimates calculated by a student's-t distribution following Christen and Pérez (2009). These errors have been incorporated into the age-depth model (**Section 6.3.6**) to calculate the probable age (with 95% confidence) for each sample. The RSL (vertical) uncertainty combines several potential sources of error related to sampling processes and regression model uncertainties, expressed as:

$$E_t = \sqrt{\left(e_{thick}^2 + e_{samp}^2 + e_{core}^2 + e_{vert}^2 + e_{surv}^2 + e_{tfun}^2\right)}$$

where E_t is the total error and $e_{thick} \ldots e_{tfun}$ are component errors. Component errors are defined as follows. Thickness error (e_{thick}) relates to potential sub-sampling errors associated with measuring the thickness of samples, here this is defined as half of the measured thickness, following Shennan (1986). Sampling errors (e_{samp}) may arise from difficulties in accurately measuring the sample depth relative to the core top, this is conservatively estimated as ± 0.01 m, following Shennan (1986). Core shortening or stretching (e_{core}) may be caused during the manual coring operation (Emery and Hulsemann, 1964; Morton and White, 1997). Following Woodroffe (2006), e_{core} is set

at ± 0 - 0.02 m based on the ratio between the known barrel length of the coring auger (0.5m) and the length of core extracted. Slight non-vertical drilling of the core results in greater apparent depths for samples than the true sample depths, Törnqvist *et al.* (2004) suggest this causes discrepancies which increase with depth of up to -0.02 m per metre. On this basis a unidirectional error of -0.02 m m^{-1} depth for non-vertical coring (e_{vert}) was adopted here. An error of ± 0.06 m was adopted for the levelling errors (e_{surv}) based on the difference observed between repeat surveys. The uncertainties associated with transfer function estimates of sample elevation (e_{tfun}) uses the sample-specific RMSEPs. With the exception of the non-vertical coring error (e_{vert}) these errors are assumed to be the mean vales with normally distributed uncertainty (*sensu* Parnell, 2005) so are multiplied by 1.96 to give the 95% uncertainty interval.

Additional vertical errors associated with post-depositional lowering as a result of sediment compaction may result in the reconstructed rate of sea-level rise to be overestimated, if not corrected for. The base of the late Holocene units (upper 90 cm) of SI2 sits atop a sand unit which is assumed to be an incompressible surface (e.g. Shennan and Horton, 2002). It is also assumed that the compaction of the units below these sands had been completed before the late Holocene units were deposited. Therefore the sediments at the base of the salt-marsh peat unit (ca. 90 cm depth) are considered as 'basal' peats with samples taken from this depth assumed to have not been significantly lowered from their depositional position (e.g. van Asselen *et al.,* 2009). However, the sediment column above this basal deposit, from where the majority of the samples were taken, is susceptible to the effects of compaction especially considering organic peats (which comprise the upper 70 cm of core SI-2; **Figure 6.6**) are highly compressible (van Asselen *et al.* 2009). Brain *et al.* (2011)

modelled sediment compaction in salt-marsh stratigraphies with the results suggesting that for short (<1m) uniform successions (upper 70cm of *core SI-2*) and regressive stratigraphies (upper 90cm of core SI-2) errors associated with compaction are small (<0.01m) with peak post-depositional lowering occurring toward the middle of individual stratigraphic units with little effect at the top and base of the sediment column. Post-depositional lowering may therefore have a contribution to the observed inflexion in the RSL reconstruction (**Figure 6.16**). Furthermore, the modelled contribution of compaction in such stratigraphies equates to an additional 0.0 – 0.1mm yr^{-1} of RSL rise to a reconstruction (Brain *et al.* 2011). Such a small value may seem insignificant; however, if the upper estimate is considered (0.1 mm yr^{-1}) this is an equivalent sea-level contribution of ca. 40 km^3 yr^{-1} of land-based ice melt (Brain *et al.*, 2011). It is therefore critically important to account for post-depositional lowering caused by compaction when quantifying the rates of reconstructed sea-level changes.

An initial assessment of the influence of compaction is performed by comparing reliable sea-level positions (basal SLIPs and instrumental measurements) that cover the same time period with the non-basal SLIPs from core *SI-2* that may have experienced post-depositional lowering (**Figure 6.18**). The reliable sea-level positions used in this comparison were as follows: from 88 cm of core *SI-2,* which is considered here as basal due to it sitting 2 cm above the tidal flat sands; the *2012 bank section* (**Section 6.2**), which overlies the tidal flat sand unit and therefore considered basal; historic measurements from 1842 (Ross, 1847; assessed for accuracy by Woodworth *et al.,* 2010) and recent tide-gauge data (Holgate *et al*., 2013; PSMSL, 2016a, 2016b; Woodworth *et al.* 2005). Because the basal SLIPs lie below (-1 cm) the lowest dated late-Holocene depth at 87cm of *core SI-2* the age had to be interpolated from the age-depth chronology (**Section 6.3.3**). With recognition of the limitations associated with

interpolation, this was performed parsimoniously following Blaauw and Heegaard (2012, p.394-396) by fitting a 4th order polynomial regression. Full SLIP information is presented in **Table 6.9.**

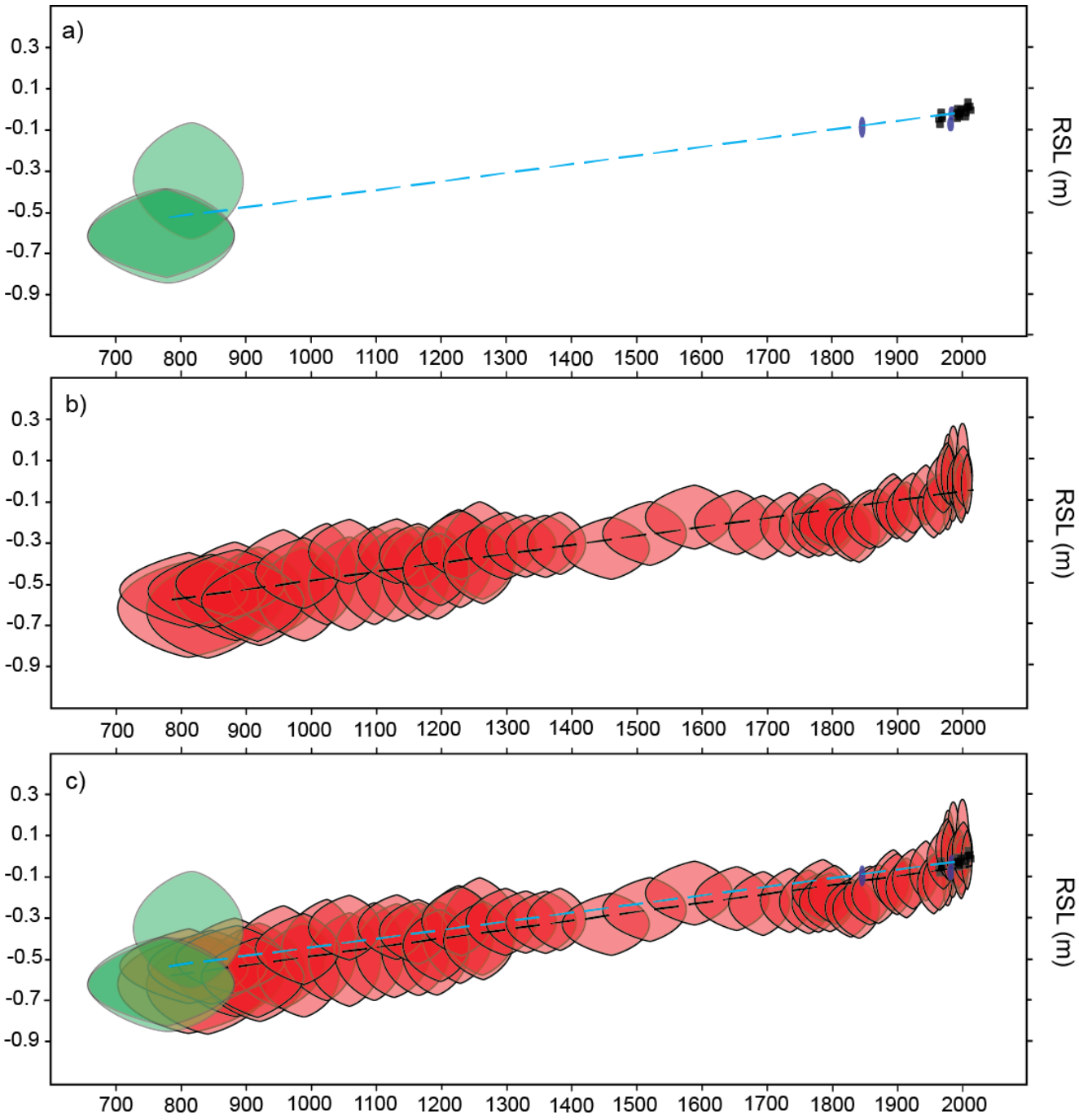

***Figure 6.18**: Comparison of reliable (non-compacted) sea-level data and SLIPs that are susceptible to compaction. a) Basal SLIPs (green ellipses), historic measurements (blue*

ellipses) and tide gauge measurements (black points), b) all other SLIPs susceptible to compaction (red ellipses), c) juxtaposition of a) and b). Blue and black dashed lines represent linear trends for the reliable and susceptible sea-level data respectively.

SLIPs illustrated in this thesis from this point onwards are represented by ellipses which reflect the 95% age and altitudinal uncertainty intervals described above. It is important, however, to note that it is unlikely that the point of maximum probability density is precisely at the centres of these ellipses because the age uncertainties are often asymmetric. The RSL (vertical) uncertainty is assumed to be normally distributed (*sensu* Parnell, 2005). The average rate of change (linear function, **Figure 6.18a**) between the basal SLIPs and the historic and tide gauge measurements is 0.42 mm/yr. The SLIPs that are susceptible to compaction (**Figure 6.18b**) yield a rate of 0.43 mm/yr. Considering the basal SLIPs and the historical and tide gauge measurements as 'true' RSL positions, these differences are assumed to be due to sediment compaction and consequent post-depositional lowing of the susceptible SLIPs. The difference (<0.01 mm/yr) between the average rates of the reliable and susceptible sea-level data (**Figure 6.18c**) suggests that, overall compaction is small and is therefore unlikely to cause significant 'artificial' trends in the long-term rate of RSL change (cf. Brain *et al.* 2015). Because compaction is usually greatest toward the middle of stratigraphic units (Brain *et al.,* 2011) it is, however, pertinent to consider differences between different segments of the reconstruction.

The 1842 CE sea-level measurements plot toward the upper limit of the uncertainty of the SLIP ages which overlap with this date (**Figure 6.18c**), which suggests these SLIPs have been lowered due to compaction. This suggestion is supported by the difference (0.07 mm/yr) between the average rate of change observed for the reliable sea-level data for the period 781-1842 CE (0.43 mm/yr) and susceptible SLIPs with

mean ages which are within the same period (0.36 mm/yr). The most recent SLIPs (1842 CE to present) are all sampled from the upper 16 cm of core *SI-2*. Based on the modelling results of Brain *et al.* (2012) the SLIPs from these shallow core depths are assumed to have experienced no significant sediment compaction. On this basis, a first-order 'decompaction' routine was performed for SLIPs with mean ages between 781-1842 CE, following Gehrels (1999), by adding the difference between the reliable and susceptible sea-level data (0.07 mm/yr).

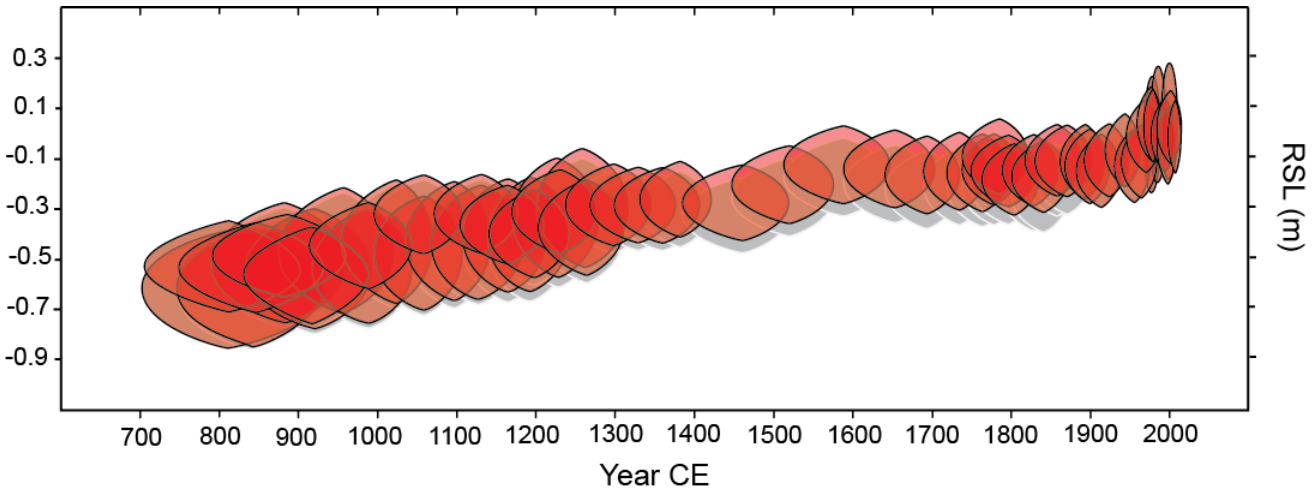

***Figure 6.19**: Susceptible SLIPs (red ellipses) decompacted by applying a correction based on differences in the linear trends between reliable and susceptible sea-level data. Grey ellipses show original positions from **Figure 6.18b**.*

***Table 6.9**: Common Era sea-level index information. All samples from core SI-2. All ages and age errors are the optimal modelled ages obtained from the age-depth model (**Section6.3.3**). Sea-level was calculated from either the testate amoebae or diatom transfer function (TF) presented in **Chapter 5**. Sea-level errors (E^t) calculated as described in the text (above).*

Depth (m)	Age (CE)	Age error+	Age error -	Indicative Meaning derivation	Sea level (m)	Error (m)
0.01	2007	10	6	Diatom TF	0.00	0.14
0.01	2007	10	6	Testate amoebae TF	0.09	0.22
0.02	2000	11	9	Testate amoebae TF	0.07	0.22
0.02	2000	11	9	Diatom TF	0.04	0.15
0.03	1993	11	10	Diatom TF	0.01	0.15
0.03	1993	11	10	Testate amoebae TF	0.06	0.23
0.04	1996	10	11	Diatom TF	-0.04	0.15
0.04	1986	10	11	Testate amoebae TF	0.05	0.23
0.05	1979	8	11	Testate amoebae TF	0.01	0.23
0.05	1979	8	11	Diatom TF	0.04	0.14
0.06	1972	6	9	Diatom TF	0.05	0.15
0.07	1965	4	3	Diatom TF	-0.10	0.14
0.08	1956	16	8	Diatom TF	-0.13	0.15
0.09	1945	21	13	Diatom TF	-0.06	0.15
0.1	1935	24	18	Diatom TF	-0.10	0.15
0.11	1924	27	21	Diatom TF	-0.09	0.15
0.12	1914	30	24	Diatom TF	-0.14	0.14
0.13	1903	32	26	Diatom TF	-0.12	0.15
0.14	1893	33	28	Diatom TF	-0.10	0.14
0.15	1882	34	31	Diatom TF	-0.19	0.14
0.16	1870	33	33	Diatom TF	-0.17	0.14
0.17	1857	93	31	Diatom TF	-0.17	0.14
0.18	1844	106	29	Diatom TF	-0.24	0.15
0.19	1832	28	42	Diatom TF	-0.24	0.14
0.2	1819	29	45	Diatom TF	-0.20	0.14
0.21	1806	30	45	Diatom TF	-0.17	0.14
0.22	1796	30	45	Diatom TF	-0.21	0.14
0.23	1786	31	47	Diatom TF	-0.15	0.15
0.24	1775	32	48	Diatom TF	-0.21	0.14
0.25	1764	32	49	Diatom TF	-0.21	0.16
0.28	1730	32	49	Diatom TF	-0.20	0.15
0.32	1692	47	47	Diatom TF	-0.21	0.15
0.36	1644	59	55	Diatom TF	-0.19	0.15
0.4	1583	61	69	Diatom TF	-0.16	0.15
0.44	1518	59	73	Diatom TF	-0.25	0.16
0.48	1453	63	69	Diatom TF	-0.32	0.16
0.52	1388	63	69	Diatom TF	-0.30	0.15
0.54	1356	63	68	Diatom TF	-0.31	0.15

0.56	1324	62	66	Diatom TF	-0.31	0.15

Table 6.9: Continued

Depth (m)	Age (CE)	Age error+	Age error -	Indicative Meaning derivation	Sea level (m)	Error (m)
0.58	1292	58	64	Diatom TF	-0.31	0.16
0.6	1259	55	63	Testate amoebae TF	-0.32	0.24
0.6	1259	55	63	Diatom TF	-0.40	0.19
0.62	1227	53	59	Testate amoebae TF	-0.35	0.23
0.62	1227	53	59	Diatom TF	-0.30	0.16
0.64	1194	48	55	Testate amoebae TF	-0.42	0.22
0.64	1194	48	55	Diatom TF	-0.42	0.18
0.66	1161	49	53	Testate amoebae TF	-0.43	0.23
0.66	1161	49	53	Diatom TF	-0.35	0.15
0.68	1127	50	55	Testate amoebae TF	-0.44	0.23
0.68	1127	50	55	Diatom TF	-0.33	0.15
0.7	1093	50	57	Testate amoebae TF	-0.44	0.24
0.72	1059	48	63	Testate amoebae TF	-0.48	0.23
0.72	1059	48	63	Diatom TF	-0.33	0.16
0.74	1024	45	70	Testate amoebae TF	-0.43	0.25
0.76	989	54	77	Testate amoebae TF	-0.54	0.22
0.76	989	54	77	Diatom TF	-0.44	0.17
0.78	954	63	80	Testate amoebae TF	-0.47	0.25
0.8	918	71	87	Testate amoebae TF	-0.54	0.23
0.8	918	71	87	Diatom TF	-0.57	0.20
0.82	883	77	91	Testate amoebae TF	-0.52	0.24
0.82	883	77	91	Diatom TF	-0.49	0.17
0.84	847	85	98	Testate amoebae TF	-0.61	0.23
0.84	847	85	98	Diatom TF	-0.53	0.18
0.86	811	91	105	Testate amoebae TF	-0.60	0.23
0.86	811	91	105	Diatom TF	-0.52	0.17
0.88	781	103	122	Diatom TF	-0.63	0.19

It is important to note, that this decompaction routine assumes a linear rate of compaction across this section of the core. Because modelling work suggests that compaction is in fact a non-linear process, with the greatest rates of compaction towards the middle of susceptible sedimentary units, it is likely that many of the decompacted SLIPs remain displaced (albeit closer) from their 'true' positions. Applying a linear method of decompaction such as this likely over-corrects the

younger SLIPs (shallower in the core) and under-corrects SLIPs from the middle of the core where compaction is likely greatest. But, in the absence of a geotechnically-modelled compaction correction (e.g. Brian *et al.,* 2011), this first-order method offers a best attempt at negating the influence of compaction.

Two late-Holocene sea-level curves for the Falkland Islands are presented in **Figure 6.20**. These reconstructions combine the final diatom and testate amoebae RSL reconstructions (**Section 6.3.4**) with the age-depth chronology (**Section 6.3.3**) and associated errors. The sea-level curve in **Figure 6.20a** includes the compaction corrections presented above, whereas the curve in **Figure 6.20b** is not corrected for compaction. The detailed SLIP information used to construct these curves are presented in **Table 6.9**. Hierarchal change-point analysis (Carlin *et al.,* 1992) was used to identify discrete changes in the rate of sea-level change for both sea-level curves. Three significant change-points (95% probability) were identified which provided four successive segments (periods) of RSL change for the non-corrected curve (**Figure 6.20b**). For the corrected curve (**Figure 6.20a**) two change points and three segments of RSL change were identified. Linear regressions were calculated for each segment to calculate the rate of sea-level change (95% confidence interval) for each time period. It should be noted that this method does not take into account age and altitude uncertainties associated with each SLIP (cf. Parnell and Gehrels, 2015) and also implies that rate changes between change-points are instantaneous rather than gradual.

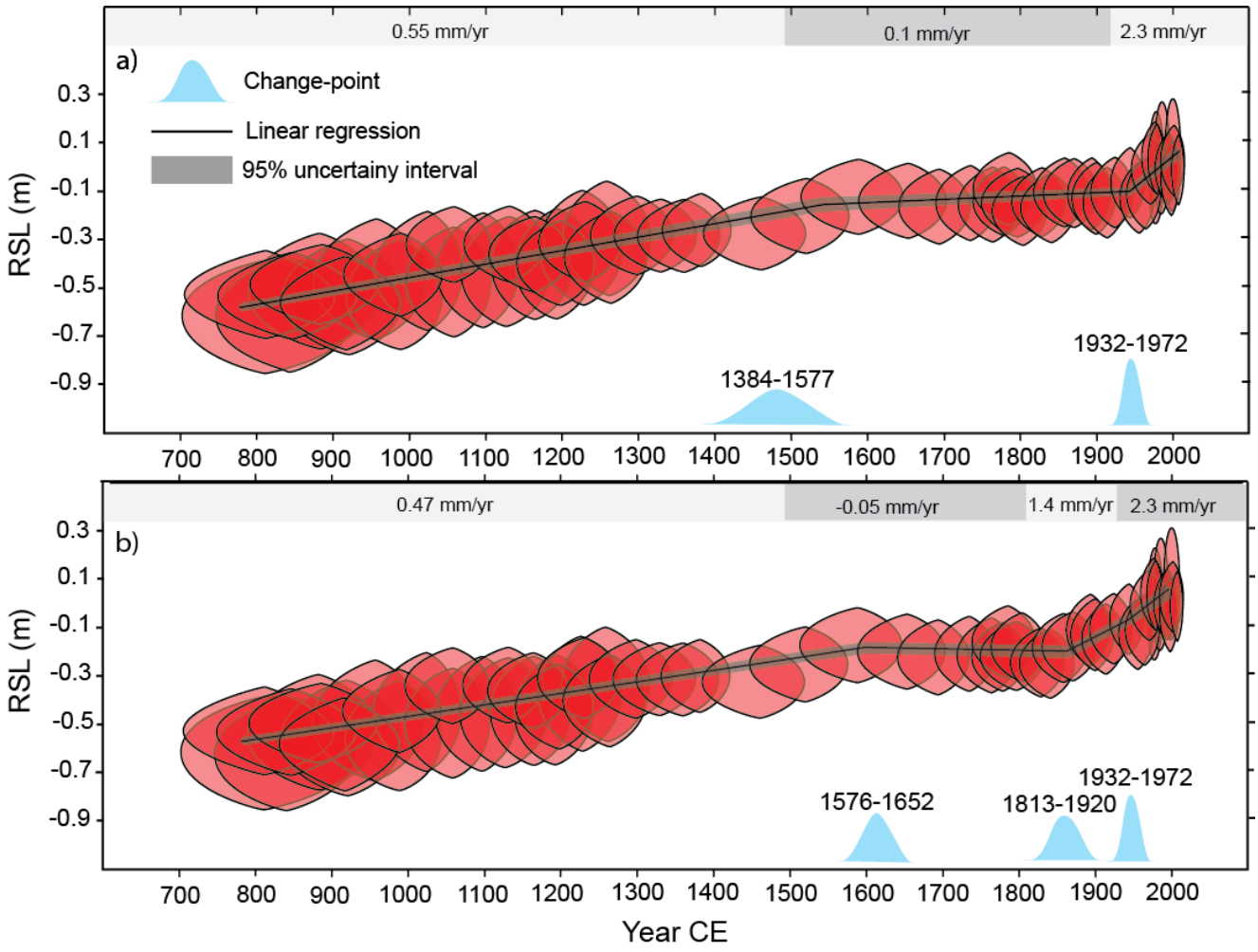

***Figure 6.20**: Sea-level trends for the Falkland Islands reconstruction a) Compaction-corrected RSL reconstruction for Swan Inlet. b) non-corrected reconstruction. Change-points (blue curves) identify periods (segments) of RSL change with rates and 95% uncertainty intervals calculated by linear regressions for each segment.*

The corrected RSL reconstruction (**Figure 6.20a**) shows a continually rising trend for the last ca.1200 years. Prior to the first change-point (1384-1577 CE), an average rate of change of 0.55 ± 0.08 mm/yr (95% confidence) is observed. The rate slows between the first (1384-1577 CE) and second (1932-1972 CE) change-points to 0.1 ± 0.13 mm/yr (95% confidence). After the second change-point (1932-1972 CE) until present the rate of change accelerates to 2.3 ± 0.62 mm/yr (95% confidence). The non-corrected curve (**Figure 6.20b**) yielded an 0.47 ± 0.08 mm/yr (95% confidence)

average rate of change up the first change point (1576-1652 CE). Between 1576-1652 CE and the second change point (1813-1920 CE) the non-corrected curve shows a slight RSL fall of -0.05 ± 0.21 mm/yr (95% confidence). The period after the second change point detects an acceleration to 1.4 ± 0.61 mm/yr (95% confidence) after 1813-1920 CE which increases after the third change point (1932-1972 CE) to 2.3 ± 0.62 mm/yr (95% confidence) until present. Whilst the patterns of change in the two curves are broadly similar, there are differences in the timing and magnitude of rate changes. Despite these differences, a recent acceleration in the rate of RSL rise is observed in both curves.

6.4 Summary

This chapter has presented the palaeoenvironmental results obtained from analyses of intertidal sediments collected from Swan Inlet, Falkland Islands. Microfossil assemblages of testate amoebae, diatoms and foraminifera, along with sedimentological and chronological analyses were used to inform interpretations regarding Holocene environmental and sea-level changes at Swan Inlet. Nine new sea level index points were established which document, for the first time, the broad-scale Holocene sea-level history of the Falkland Islands. These sea-level data present a challenge for sea-level models as no unique modelled prediction is able to explain all the data that currently exists. A high-resolution sea-level reconstruction spanning the last ca. 1200 years based on detailed microfossil (testate amoebae and diatoms) and chronological and analyses was presented. This reconstruction revealed an overall rising sea-level trend in the Falkland Islands during the late Holocene with an accelerated rate of RSL rise occurring in the 20th Century. However, the influence of compaction and lack of a precise decompaction routine makes it difficult to accurately determine the onset of accelerated RSL rise. The significance and wider implications

of these results along with comparisons with other studies are discussed in **Chapter 7**.

Chapter 7 – Discussion

7.1 Introduction

The previous three chapters have presented the results of the investigations of this PhD project which have culminated in the first Southern Hemisphere salt-marsh testate amoebae transfer function and first detailed, multiproxy sea-level reconstructions in the Falkland Islands and, more broadly, the South Atlantic region. This chapter will discuss the wider significance, implications and limitations of these results. Furthermore, the results will be critically examined by comparison with the results of previous studies. In light of the results presented in this thesis, the discussion includes recommendations for future research.

7.2 Developments in the application of testate amoebae to sea-level studies

This project has placed much emphasis on better understanding the proxy potential of salt-marsh testate amoebae as sea-level indicators (**Aim 2**). In this section the results of the investigations of seasonal influences on testate amoebae distributions and methodological recommendations are discussed.

7.2.1 Seasonal influences on testate amoebae distributions

Because the use of testate amoebae in sea-level studies is a relatively recent development, to date, little attention has been given to understanding environmental influences governing their modern distributions in salt-marshes. **Chapter 4** presented the results of the first investigation of seasonal influences on salt-marsh testate amoebae. Seasonal influences are important to consider because sea-level studies routinely sample the modern environment only once and assume samples to be ecologically representative of the sub-environment from which they are sampled.

Barnett *et al.* (2013) used only the dead testate amoebae assemblages on the assumption that these assemblages are time-averaged and therefore negate any potential seasonal bias. Additionally, sea-level studies rely on the statistically significant relationship between marsh surface elevation (a surrogate variable for the frequency and duration of tidal inundation) and variation in testate amoebae assemblages. This relationship with elevation is assumed to be consistent irrespective of seasonal influences. The results of the seasonal investigation of testate amoebae distributions can be used to better inform sampling strategies by testing the validity of these assumptions.

The results in **Chapter 4** suggested there were no clearly defined seasonal influences on live or deceased testate amoebae populations when considered collectively. However, there were pronounced seasonal blooms in the live populations of different individual taxa which were asynchronous. This suggests that testate amoebae taxa may respond differently to environmental factors and these factors may not be related to the seasonal cycle. The feeding habits of testate amoebae have been observed to differ between taxa (Schroeter, 2001; Jassey *et al.,* 2012) and also seasonally for individual species (Gilbert *et al.,* 2003). The differing seasonal peaks of live testate amoebae taxa may therefore, in part, be explained by the availability and/or seasonal preferences of food sources. The individual feeding preferences of many of the taxa observed over the seasonal study (**Chapter 4**) are not known. But, the results of Schroeter (2001) suggest that, in general, smaller species (e.g. *Pseudodifflugia fulva* type, *Cypohderia ampulla, Centropyxiella* sp. and *Traceleuglypha dentata*) predominantly feed on cyanobacteria, algae and fungi and that larger 'predatory' taxa (e.g. *Difflugia* sp., *Centropyxis* sp. and *Arcella* sp.) feed additionally on other protists including smaller testate amoebae taxa. Furthermore, 'predatory' taxa have been

observed to preferentially prey on smaller testate amoebae during the summer season (Gilbert *et al.,* 2003). This may explain the general decline in the living populations of the smaller taxa observed in the seasonal investigation (**Figure 4.4**). Increasing temperatures have been observed to increase reproductive rates in testate amoebae (e.g. Laybourn and Whymant, 1980), which could be a factor responsible for the summer peaks in live species observed for some species (e.g. *Difflugia pristis* type, *Centropyxis cassis* type). There are likely many other environmental factors (e.g. moisture content, preferential-predation, geochemistry etc.) which may account for the different timings of peaks in live testate amoebae populations but without more detailed investigations it is not possible to determine precisely what these factors are.

Although the environmental factors responsible for the species-specific seasonal peaks in living testate amoebae populations are not known, species-specific trends observed in this study are broadly consistent with observations of peatland testate amoebae by Sullivan and Booth (2010) and Lamentowicz *et al.* (2013). However, Camacho *et al.* (2015) compared intertidal testate amoebae assemblages from a single summer and a single winter sampling and observed a significant synchronous increase in the living assemblages of all species in the summer. Camacho *et al.,* (2015) suggested this increase was related to diminished salinity and hydrodynamics over the summer season. The results of the investigations in this study do not support such a pronounced seasonal peak, however, it could be that the resolution of the seasonal sampling (only one sampling in either season) of Camacho *et al.,* (2015) failed to capture the full seasonal variability.

The observed peaks in the abundance of living testate amoebae assemblages were observed to precede peaks in their respective concentrations in the death assemblages. This suggests that variations in the living populations are quickly

transferred to the death assemblage. Also, all species recorded in the live assemblages were observed in the death assemblages. Thus, in terms of preservation, the taxa observed in the seasonal study can be deemed robust and variations in the life assemblage are readily transmuted to the death assemblage. Furthermore, these observations do not support the interpretation of Camacho *et al.,* (2015) who suggested that winter peaks in species diversity and concentration of the death assemblages were the result of post-mortem transportation of tests. The variations observed in the living assemblages were not observed to have an impact on species evenness which remained relatively constant throughout the seasonal cycle. However, significant variability in the species diversity of the death assemblages were observed which coincided with increases in test concentrations which were greatest in the spring and summer seasons. The fact that species diversity and test concentrations demonstrate such variability over the seasonal cycle challenges the assumption that the death assemblage represents a time-averaged assemblage.

7.2.2 Seasonal influences on transfer function performance

Seasonal transfer functions were generated (**Section 4.3.3**) which simulated single (one season) and repeat (two or more seasons) sampling strategies to investigate the implications of the seasonal variability, observed in the death assemblages, for sea-level studies. These results suggested that in terms of precision (RMSEP), all the transfer functions had similar performances but reconstructive bias was greatest in the spring and winter seasons. The RMSEP for all transfer functions was < 2% of the tidal range of the Fal-Ruan salt marsh which is relatively small compared to the RMSEP of testate amoebae transfer functions from other mesotidal marshes which are often > 10% of the tidal range (Charman *et al.* 2002, Barnett *et al.,* 2017). However, comparisons between RMSEP of this and other studies, as well as between the

different transfer functions generated in **Section 4.3.3,** may be limited because sample sizes differ between the seasonal training sets. It has been shown that transfer function RMSEP generally improves as the number of samples increases (Kemp and Telford, 2015), so this may account for some of the differences between the seasonal transfer functions. However, Kemp and Telford (2015) demonstrate that training sets with > 30 samples and transfer functions using weighted-averaging models (as is the case for all those in **Chapter 4**) there is generally little change in RMSEP with additional samples. The best performing seasonal transfer functions (**Section 4.3.3**) were both based on single sampling periods (Winter-only, Summer-only) which coincided with the periods with greatest species diversity (**Section 4.3.2**), and the worst performing transfer functions coincided with periods with the least species diversity. This suggests that species diversity may influence transfer function performance and that greater bias in transfer function performances are caused by lower species diversity. This suggestion is supported by the performance of the full season transfer function which has comparable RMSEP (17 % less precise) than the best performing transfer function, but with maximum bias being slightly lower (1 % less).

It is important to recognise that the precision of transfer functions measured by the model RMSEP gives little indication of reconstruction accuracy (c.f. Wright *et al.*, 2011). A lack of fossil testate amoebae data from the Fal-Ruan site prevents statistical assessments of reconstruction accuracy (e.g. **Section 6.3.4**) or validation with instrumental data (e.g. Gehrels *et al.,* 2005). In any case, the purpose of the seasonal study was not to produce accurate reconstructions but rather to investigate the influence of seasonal bias on transfer functions. To this end, an assessment of the relative accuracy of the seasonal transfer functions is sufficient. The relative accuracy

of each of the seasonal transfer functions is assessed here by calibrating each transfer function on independent samples of species data and comparing each reconstructed sample elevation with its independently measured elevation (residual). The independent (validation) samples used in this test include two samples from the modern testate amoebae training set from the Falkland Islands (**Section 5.4.1**), two samples from Norway (Barnett *et al.,* 2013) and fourteen from the UK (Gehrel *et al.,* 2001; Charman *et al,* 2002). These samples were selected because they offered the best analogues for the dominant species assemblages, and their (normalised) elevations were within the range sampled, from the Fal-Ruan salt marsh. Because this method uses datasets from multiple sites, elevations were normalised to account for differences in tidal range between sites. The standardised water level index (SWLI) approach (Horton *et al,.* 1999) was used for this normalisation:

$$SWLI_n = \frac{100(h_n - h_{LOT})}{h_{HAT} - h_{LOT}} + 100$$

where $SWLI_n$ is the standardised water-level index for sample n, h_n is the sample elevation, h_{LOT} is the elevation of lowest occurrence of testate amoebae and h_{HAT} is the elevation of highest astronomical tide. The taxonomy between the samples from different studies was harmonised following the revised salt-marsh testate amoebae taxonomy of Barnett *et al.* (2017).

***Table 7.1**: Residual difference (Res.) between the observed elevations of the validation samples and the elevations estimated by the seasonal transfer functions, measured in SWLI units, and sample-specific 1-sigma uncertainties for each estimate (RMSEP) represented relative (%) to the sampled elevation range. Bottom row shows mean values.*

Full season		Spring		Summer		Autumn		Winter		Spr.& Sum.		Spr. & Win.		Aut. & Spr.		Aut. & Sum.		Aut. & Win.		Sum. & Win.	
Res.	RMSEP %	Res.	RMSEP %	Res.	RMSEP %	Res.	RMSEP %	Res.	RMSEP %	Res.	RMSEP %	Res.	RMSEP %	Res.	RMSEP %	Res.	RMSEP %	Res.	RMSEP %	Res.	RMSEP %
-0.10	12	3.23	20	-1	12	0.04	11	2.36	17	0.14	16	1.70	20	0.06	12	-0.67	12	-0.25	14	0.09	13
-3.46	14	2.30	24	-5.52	16	-2.05	16	-1.20	18	-2.45	20	-1.16	24	-0.37	14	-3.42	14	-2.30	16	-5.28	14
0.86	11	1.31	14	-0.45	10	-1.33	10	4.13	14	0.82	12	3.10	14	-0.59	10	-1.15	10	0.77	12	3.29	13
-2.48	12	-5.21	19	-4.19	12	-7.23	10	-3.89	22	-5.79	15	-4.70	19	-8.59	11	-6.69	11	-7.24	12	-3.32	14
1.22	11	6.15	16	4.43	11	2.85	11	4.97	13	6.17	13	5.90	16	4.36	11	3.99	11	4.26	12	5.53	12
8.29	11	10.30	16	10.93	10	9.14	10	10.34	19	9.22	13	9.87	16	7.82	10	9.32	10	8.51	12	10.77	12
11.56	11	14.88	14	13.00	10	12.76	10	16.52	15	13.69	12	15.67	14	13.09	10	12.61	10	13.97	12	15.57	12
11.91	12	13.62	14	9.87	12	11.13	10	17.67	17	12.35	13	15.92	14	12.70	10	10.55	10	14.28	13	15.21	14
7.07	11	7.80	14	4.55	11	5.72	10	8.86	16	6.47	13	8.38	14	7.03	10	5.37	10	7.33	12	7.47	13
17.70	12	17.28	14	13.80	12	14.72	10	22.03	17	16.44	13	20.14	14	16.48	10	14.31	10	18.39	13	19.69	14
8.65	13	9.21	15	5.95	12	6.80	10	13.65	19	8.65	14	12.13	15	8.69	10	6.39	10	10.27	13	11.79	14
10.84	12	11.47	15	7.97	12	9.12	10	15.90	19	10.80	14	14.29	15	11.11	10	8.69	10	12.71	13	13.80	14
11.18	13	11.57	15	7.57	13	9.45	11	17.31	18	10.40	14	14.74	15	11.24	11	8.72	11	13.57	14	14.07	14
0.40	14	-1.09	19	-2.45	13	0.24	11	9.95	18	-1.86	15	4.13	19	0.12	11	-0.89	11	5.36	16	5.19	17
8.72	13	9.28	16	5.12	13	6.28	11	14.79	21	8.80	15	12.95	16	8.89	11	5.83	11	10.83	14	12.34	15
1.16	13	4.60	19	-1.82	14	1.00	14	3.96	19	0.92	17	3.34	19	2.50	13	0.09	13	2.29	15	0.49	14
-5.31	13	-3.07	17	-9.12	13	-6.48	12	-1.58	19	-6.03	15	-2.78	17	-4.65	12	-7.44	12	-4.13	14	-5.08	14
5.19	12	6.68	17	3.47	12	4.25	11	9.16	18	5.22	14	7.86	17	5.29	11	3.86	11	6.39	13	7.16	14

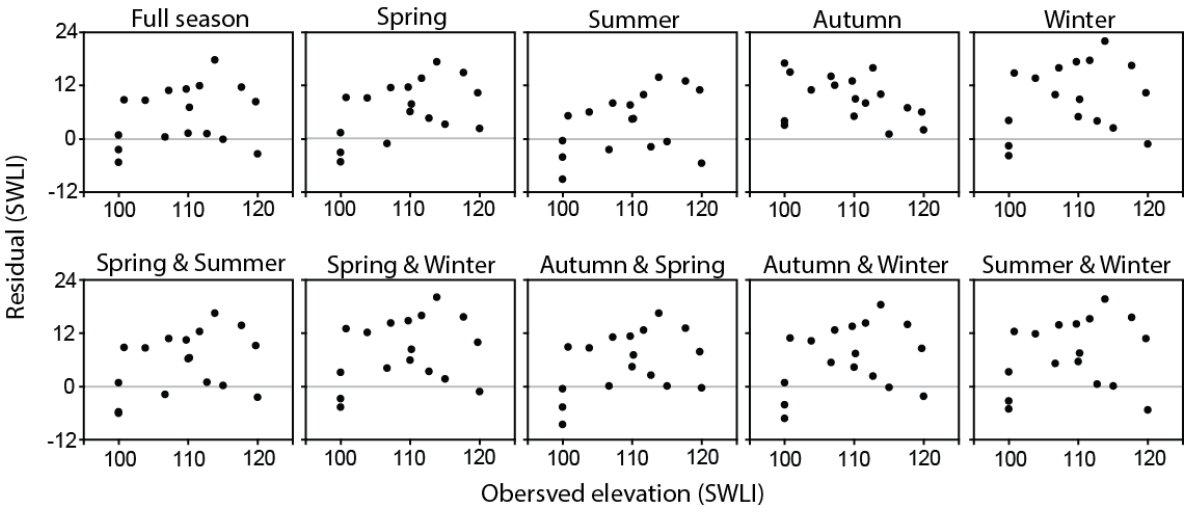

***Figure 7.1**: Residual difference between the observed elevations of the validation samples and the elevations estimated by the seasonal transfer functions from Fal-Ruan.*

The results of the relative accuracy assessment (**Table 7.1**; **Figure 7.1**) showed that, with the exception of the Autumn transfer function which consistently overestimated

the observed elevation, all the seasonal transfer functions demonstrated similar trends in the residuals. In terms of overall performance, the most precise transfer functions in terms of the internally cross-validated RMSEP (Autumn- only, Summer – only and Autumn and Summer), produced the most accurate elevation estimates with the least error when calibrated on the validation set. The Full Season transfer function, which captures the full seasonal variability, demonstrated overall accuracy only slightly less and mean sample-specific RMSEP error <1% greater than either of the most accurate transfer functions. In fact, the Full Season transfer function had the most estimates (5) within ca. 1 SWLI of the observed SWLI. These greater precisions for the most accurate estimates generated by the Full Season transfer function may be a result of the greater species diversity and more realistic time-averaged assemblages captured, making the model more robust by providing better analogues for the samples on which it is calibrated on. If this is the case then the sample-specific RMSEPs generated by the Full Transfer function are likely to be more realistic than for any single-season transfer function because they are more ecologically plausible.

7.2.3 Implications for sea-level studies and future recommendations

Seasonal variations in both the living and dead assemblages of salt-marsh testate amoebae have been observed. Variations in the live assemblages did not occur simultaneously for all species which suggests that this variance may not be related to environmental factors that are correlated with the seasonal cycle (e.g. temperature). Charman *et al.* (2002) describe intra-site variability of salt-marsh testate amoebae distributions and associate this variability to a number of environmental factors. Intra-site comparisons (which include the sites of Charman *et al.* 2002) by Barnett *et al.* (2017) found that whilst there are many taxa in common between sites (that also demonstrate a common relationship with elevation), there are also many, often rare,

taxa which are uncommon and/or demonstrate variable relationships with elevation between sites. However, the assemblages investigated by these studies were collected from a single sampling at each site and, for most sites, live and dead specimens were not differentiated. It therefore follows, based on the results of the seasonal investigations in this study, that some of the intra-site variability may be caused by variations in live and dead assemblages over time. Future investigations which measure a range of environmental variables and their relative effects on live testate amoebae over seasonal cycles may prove valuable in better understanding the factors influencing this variability.

Significant variations in both the relative abundances of individual taxa and the overall concentration of testate amoebae were observed over the seasonal cycle. These observations violate the assumption that death assemblages are time-averaged and therefore negate variations in live assemblages. However, further analyses testing the relative accuracy between different sampling periods suggested that seasonal variations in the testate amoebae death assemblages do not have a significant impact on the predictive power of transfer functions. Thus, transfer functions generated on modern testate amoebae death assemblages sampled at any one time of year may yield similarly accurate reconstructions providing there are suitable analogues between modern and fossil samples. Despite this, greater accuracy was clearly demonstrated by transfer functions generated from training sets that were collected through repeat sampling (i.e. sampling at multiple times of the year). It can be inferred from this that repeat sampling captures the observed variations in the death assemblage, offering a more realistic time-averaged training set that should result in more robust transfer functions and therefore more accurate reconstructions. This is consistent with studies of foraminiferal seasonal variability which suggest repeat

sampling improves transfer function performance (Horton and Edwards, 2003; Horton and Murray, 2006).

In reality it is often not logistically feasible for modern sampling in sea-level investigations to conduct repeat sampling, therefore an optimal season for sampling may be sought (e.g. Horton and Edwards, 2003). The seasonal investigations of this study were limited to only one annual cycle, and the assemblage variability throughout the observation period was asynchronous between species. It is therefore unwise to make recommendations regarding the optimum season for sampling. The recent work of Barnett *et al.,* (2017) offers an alternative to repeat sampling whilst capturing at least some of the variability in species assemblages by combining multiple sites into a regional transfer function. Future work can improve the robustness of this method by adding training sets obtained though repeat sampling to regional transfer functions, which could improve reconstruction accuracy for future sea-level studies.

It is important to recognise that the seasonal investigations in this study have several limitations. Because the study was undertaken for only one annual cycle it is unknown whether the variability observed is representative of long-term variations in testate amoebae assemblages (i.e. over several seasonal cycles). It should also be noted that some of the observations were based on samples taken in the winter of 2013/14. During this winter the region experienced anomalously high rainfall (Met Office, 2014) and several extreme tidal surge and storm events (Palmer *et al.,* 2014; Sibley *et al.,* 2015). The anomalous nature of these events implies that the testate amoebae assemblages may have, at least in part, been affected by anomalous environmental conditions. Additional investigations over multiple seasonal cycles and at multiple sites are required to test the representativeness of these results in time and space. Furthermore, it has been postulated that the Rose Bengal staining of living cells

(protoplasm) used to differentiate live and dead specimens may be inaccurate because cell material is lost through the test aperture of larger specimens during the preparation procedure (Booth *et al.,* 2010). This was not apparent in this study as the smaller taxa were not disproportionally stained compared with larger taxa, although this was not objectively tested. It can, however, be said on the basis of this investigation that the death assemblage does not represent an appropriately time-averaged assemblage. It is therefore recommended that for transfer function development both living and dead tests should be counted as these better represent the assemblages that become incorporated into the fossil record. If it is necessary for live specimens to be accurately identified (e.g. in future seasonal investigations) then it is recommended the Rose Bengal method of staining is evaluated in combination with other methods (e.g. Berhnard *et al.*, 2006; Figueira *et al.,* 2012).

7.3 Multiproxy approaches to sea-level reconstruction

This section discusses the modern and fossil analyses of testate amoebae, diatom and foraminifera from Swan Inlet presented in **Chapter 5** and **Chapter 6**. An important requirement for **Aim 1** of this thesis is to accurately reconstruct sea-level in the Falklands Islands with adequate precision to detect subtle trends in the long-term record of sea level change. To this end, the ability of each microorganism group to reconstruct sea-level in the Falkland Islands is evaluated. Additionally, the wider practical feasibility of a multiproxy approach to sea-level reconstruction with emphasis on the suitability of the relatively novel proxy of testate amoebae is discussed.

7.3.1 The relative suitability of testate amoebae, diatoms and foraminifera as sea-level indicators

In **Chapter 5** the results of the investigations of modern salt-marsh distributions of testate amoebae, diatom and foraminifera from Swan Inlet, Falkland Islands were

presented. The focus of these investigations was to evaluate the suitability of each of these microorganism groups for reconstructing past sea levels from the Falkland Islands (**Aim 1**). All three microorganism groups were observed to occupy distinct vertical niches along the elevation gradient of the Swan Inlet marsh. Moreover, species-specific vertical zonations were observed in the assemblages of each microorganism group. Testate amoebae demonstrated the narrowest species zonations and were the only microorganism group that occupied the highest marsh elevations as brackish-freshwater diatom flora were not present in the upper marsh. Diatoms occupied the greatest elevation range which overlapped with the lowest zone of testate amoebae and the entire range of foraminifera (which occupy the low marsh and tidal flat elevations). These zonations indicated that testate amoebae, diatoms and foraminifera may be suitable indicators of marsh surface elevation (a surrogate variable for sea level). However, foraminiferal diversity was low with only two dominant species present which prevented them from being used to quantitatively predict elevation (as a standalone proxy). But, in combination with diatoms and testate amoebae, the foraminifera may be used in a multi-proxy transfer function approach.

Previous studies have suggested that multi-proxy transfer functions are more robust than single-proxy transfer functions (Gehrels *et al.,* 2001; Mitchell *et al.,* 2013) and can therefore provide more accurate sea-level reconstructions (Elliot, 2015). Therefore, in **Chapter 5** a combined training set using all microorganisms was compared with diatom and testate amoebae training sets. Gradient analysis (DCCA) performed on each training set demonstrated that collectively the majority of species variance for testate amoebae, diatoms and combined testate amoebae, diatom and foraminifera assemblages is explained by elevation. In the UK salt-marsh investigations of Charman *et al.* (2010) other environmental variables explained as much variability in

testate amoebae assemblages as tidal parameters (frequency and duration of tidal flooding). Despite this, Charman *et al.* (2010) demonstrated that testate amoebae transfer functions were capable of producing accurate sea-level reconstructions. At Swan Inlet the proportion of variance explained by other (unknown) environmental variables explained 36% less variance in testate amoebae assemblages than elevation (**Table 5.2**). On this basis the testate amoebae distributions at Swan Inlet can be considered suitable proxies for sea level and reconstructions utilising these indicators need not consider other environmental variables (assuming elevation is an accurate surrogate for tidal parameters and the influence of elevation was also dominant for fossil assemblages).

When the CCA axis 1 (elevation) scores were plotted against the axis 2 (unknown environmental variables) scores it was generally suggested that elevation is the dominant control on variance for individual taxa as well as species assemblages in each modern sample of diatoms and testate amoebae (**Figures 5.5** and **5.8**). Whilst this was generally the case for most species and most samples there were some exceptions to this indicated in these plots. In the testate amoebae ordination bi-plot (**Figure 5.4**) several characteristically low-marsh taxa (*Cyphoderia ampulla*, *Difflugia pristis* type and *Pseudohyalosphenia* sp.) and the lowest marsh samples within the zone of testate amoebae distributions did not follow the same pattern as the other species and samples. This suggests that at the lowest marsh zones occupied by testate amoebae, elevation may have diminished influence on assemblages (i.e. extraneous environmental variables have increased influence). Previous studies have also observed greater variability in species compositions at lower marsh elevations compared with high marsh assemblages which supports this interpretation (Charman

et al., 2002; Camacho *et al.,* 2015). This could potentially introduce inaccuracies when calibrating the testate amoebae transfer function on low-marsh fossil assemblages.

In general a multi-proxy approach to sea-level reconstruction is desirable and should be more robust than a single-proxy approach because multiple reconstructions make for better evaluations of reconstruction accuracy. Sea-level reconstructions often have limited instrumental data available against which to assess the validity of the reconstruction (e.g. Gehrels and Woodworth, 2013). But if multiple, independent reconstructions show the same trends then the validity of the reconstructions can be assumed with greater confidence. Conversely, possible reconstruction inaccuracies can be elucidated where trends differ between independent reconstructions. In practice, however, the value of a multi-proxy approach is a trade-off between the gained degrees of accuracy and precision versus the amount of time required to undertake the analyses. The results in **Chapter 5** show that diatoms were the most accurate and precise indicators of marsh surface elevation based on the assessment of r^2 (boot) and RMSEP values as well as the scatterplot of observed vs predicted values. Diatoms are particularly useful as their distributions cover the greatest range of sub-environments at Swan Inlet. However, the scarcity of diatoms at the uppermost elevations hinders the recovery of the most accurate sea-level information; this is because the most accurate sea-level reconstructions are derived from samples formed in the uppermost reaches of the intertidal zone (Allen, 1990). Charman *et al.* (2010) recommend that cores are taken within the main zone of testate amoebae occurrence in order to achieve the most accurate sea-level reconstructions. Compared with foraminifera, analyses of diatoms and testate amoebae are considerably more time consuming (e.g. Gehrels *et al.,* 2001). Although foraminifera from Swan Inlet are not suitable for developing a transfer function, many previous sea-level studies have

successfully developed and applied foraminifera transfer functions (c.f. Edwards and Wright, 2015). The relatively quick and straightforward analysis they require, and their usefulness as indicators of mid-to-low marsh sub-environments, make it a worthwhile investment to include them in addition to other (more precise) proxies. Moreover, foraminifera are useful as indicators that can potentially delimit segments of the intertidal zone because they occupy the lowest marsh elevations with a well-defined upper limit after which they do not occur. This raises the question: for which additional proxy (diatoms or testate amoebae) should microfossil analyses be undertaken, in the interest of achieving the most accurate sea-level reconstructions, with the least investment of time?

Based on the results in **Chapter 5,** arguments could be made in support of conducting either diatom or testate amoebae microfossil analysis. Testate amoebae analysis is the most time efficient of the two proxies and could potentially produce the most accurate reconstructions because their occurrences are entirely within the uppermost intertidal zone where the most precise sea-level information can be obtained. Additionally, the lowest limit of testate amoebae occurrence is well-defined in this and previous investigations (c.f. Barnett *et al.,* 2017) which, as with foraminifera, provides a useful indicative constraint. At Swan Inlet and in previous marshes where both microorganism groups were studied (e.g. Gehrels *et al.,* 2001), the upper zone of foraminifera overlaps with the lowest zone of testate amoebae which enables straightforward intertidal constraints to be obtained through simple analysis of these two groups. By simply recording the upper and lower limits of foraminifera and testate amoebae respectively, it is possible to quickly determine three ‘indicative meanings’ delimited by marsh elevation zones that are occupied by: testate amoebae only, testate amoebae and foraminifera, and foraminifera only. Such analysis would require

little expertise as it simply requires a straightforward distinction between testate amoebae and foraminifera genera and no species-level identification. The indicative meanings for delimited testate amoebae and foraminifera zones could be readily applied to fossil zones through a saltmarsh core to reconstruct palaeo-sea level. Assuming the upper and lower limits of the testate amoebae and foraminifera zones are unchanged over time then such a reconstruction would likely be accurate. However, this method of reconstruction would inevitably be relatively imprecise because each zone occupies an elevation zone 'indicative range' on the order of several decimetres. The introduction of which would make it difficult to detect subtle trends in the record. Another limitation of this method is that, unlike transfer function derived reconstructions, it is not possible to apply rigorous statistical assessments of reconstruction accuracy such as those in. **Chapter 6**.

If greater analytical time is afforded then greater precisions and more robust assessments of reconstruction accuracy are generally achieved by sub-genera level analysis of testate amoebae or diatoms applying the transfer function methodology. However, it is difficult to determine *a priori* which microfossil group would produce the most accurate reconstructions. In fact, it is unlikely that either diatoms or testate amoebae would consistently produce the most accurate reconstructions at all sites because local factors e.g. tidal range, preservation etc. are variable between sites. In this study (**Chapter 5**) the diatom transfer function produced the most precise model in terms of RMSEP (0.07 m) although testate amoebae precision was only slightly worse (0.08 m). Furthermore, the diatom training set encompasses a greater environmental range, increasing the likelihood of providing modern analogues for the range of environments within the fossil samples. But, testate amoebae have more constrained elevation tolerances and occupy the high-marsh zone so have the

potential to produce precise and accurate reconstructions providing the sampled fossil environments encompass the same marsh zone. On this basis it may be possible to make an *a priori* decision by deciding whether to conduct analysis for the microorganism group whose modern distribution fits within the elevation range defined by the palaeoenvironments observed in the fossil core (e.g. Gehrels *et al.,* 2006).

In practice it is unrealistic to determine *a priori* which transfer function will perform best at predicting PMSE from microfossil assemblages simply on the basis of modern distributions and transfer function performance statistics. Although a single proxy transfer function (e.g. diatoms) may have the greatest precision in terms of RMSEP, it may not necessarily perform best on microfossil assemblages in terms of accuracy. This is in part because transfer function precision measured by RMSEP is an artefact of the length of the gradient sampled i.e. the maximum bias of the transfer function prediction is limited by the range of elevations sampled. With short gradients, the magnitude of error that is possible decreases, so lower RMSEPs are expected. Thus, RMSEP of the combined and the diatom transfer functions (**Chapter 5**) being the same (0.07m) despite a 30% increase in the size of the gradient sampled gives confidence that the species-elevation relationship is robust. The RMSEP in this case may suggest a reliable estimate of model predictive performance. The combined transfer function therefore could potentially produce the most accurate reconstruction because it reflects a greater range of sub-environments than either single-proxy transfer function without a reduction in precision. The accuracy of a transfer function, however, is largely dependent on the nature of the fossil data that are used for calibration. Transfer function reconstructions are most accurate when there are close analogues between the fossil assemblages and the contemporary assemblages in the training set. For 'local' training sets (composed of samples from a single site) such as those in this

study, close analogues between the test set and removed subset used in model cross-validation are often inherent due to spatial autocorrelation (Telford and Birks, 2009). A reconstruction therefore requires strong similarities in species assemblages between the fossil and modern data to achieve accurate reconstructions of comparable precision to the RMSEP of the transfer function. Provided that there are species in common between the training set and the fossil calibration set a reconstruction will be generated, whether environmentally plausible or not. Although sample-specific errors are calculated by the transfer function for each reconstructed variable the precision gives little indication of the accuracy of the reconstructions.

The inability to determine *a priori*, deduced from the modern microorganism distributions and transfer function performances, whether a testate amoebae, diatoms or combined transfer function (testate amoebae, diatoms and foraminifera) produces the most accurate reconstructions was illustrated in **Chapter 6**. The best-performing transfer functions from **Chapter 5** were calibrated on microfossil assemblages from *core SI-2* to reconstruct PMSE at Swan Inlet. Where there were good analogues for fossil assemblages in the modern training sets, testate amoebae, diatom and combined reconstructions were in good agreement. However, because sections of the core contained no fossil foraminifera and only monospecific assemblages of testate amoebae it was therefore not possible to accurately reconstruct PMSE. The statistical assessments of the reconstruction accuracy in **Chapter 6** demonstrated that there were no benefits to be gained by combining proxies into a single dataset. This result is consistent with that of Barnett *et al.* (2016) who found no improvement in transfer function performance when combining salt-marsh testate amoebae and foraminifera data in a unified dataset.

The fossil assemblages of testate amoebae at Swan Inlet highlighted preservation issues which reduces the reconstructive value of this proxy. For example, the monospecific assemblage of *Hyalosphenia subflava* within zone II and a lack of comparable monospecific assemblages in the modern distributions suggests that *Hyalosphenia subflava* may be preferentially preserved. In the modern testate amoebae distributions at Swan Inlet (**Chapter 5**) *Hyalosphenia subflava* is distributed in the upper zone of testate amoebae occurrence in association with assemblages comprising predominantly idiosomic (e.g. *Euglyphid*) and to a lesser extent xenosomic taxa (e.g. *Difflugia, Centropyxis*). The taphonomy of testate amoebae in salt-marsh deposits is poorly understood, but previous studies from upland and peatland environments indicate that idiosomic tests are highly susceptible to decomposition (Lousier and Parkinson, 1981; Ruzicka, 1982; Tolonen, 1986; Swindles and Roe, 2007; Mitchell *et al.,* 2008). Conversely, previous studies suggest the proteinaceous tests of *Hyalosphenia* taxa are most resistant to decomposition (Ruzicka, 1982; Mitchell *et al.,* 2008). Therefore, the monospecific presence of *Hyalosphenia subflava* observed in *core SI-2* could be the result of idiosomic and xenosomic taxa that would typically comprise assemblages associated with the modern zone of *Hyalopshenia subflava* not being preserved, whereas the proteinaceous test of *Hyalosphenia subflava* has resisted degradation. This interpretation is supported by the investigation of Roe *et al.* (2002) which observed sharp downcore decreases in fossil test abundances in salt-marsh sediments with idiosomic tests being the least preserved. Poor preservation of idiosomic taxa is also indicated by examining the assemblages of all previous studies of fossil testate amoebae in salt-marsh sediments which show no record of idiosomic taxa beyond only the shallowest (ca. upper 5 cm depth) deposits despite relatively high abundances in the modern assemblages (Roe *et al.*, 2002; Charman *et al.,* 2010; Barnett *et al.,* 2015). The obvious implication of differential preservation of salt-marsh

testate amoebae is that degradation of parts of the fossil assemblages will cause poor analogue situations. The xenosomic taxa which are found in the modern zone of *Hyalosphenia subflava* assemblages were largely absent in the fossil assemblages where *Hyalosphenia subflava* was present. Xenosomic taxa are generally considered more robust to degradation (e.g. Mitchell *et al.*, 2008). The absence of xenosomic taxa where *Hyalosphenia subflava* dominate in the Swan Inlet core suggest that degradation of some of these taxa may have occurred. This inference is supported by the observations of Swindles and Roe (2007) who demonstrated differential dissolution of xenosomic taxa even within genera (e.g. *Difflugia*). Further research on the taphonomy of salt-marsh testate amoebae is necessary to better understand the preservation of xenosomic taxa and the potential impacts of differential preservation of testate amoebae for sea-level studies.

7.3.2 Summary and implications for future studies

All three microorganism groups were shown to be valuable sea-level indicators because they occupy distinct vertical niches in the contemporary salt-marsh at Swan Inlet. The presence or absence of a particular group or combination of groups permits a simple and robust indicative meaning to be applied for segments of the intertidal zone. Foraminifera alone were not a suitable proxy, however, surveyed sample elevations were closely matched by elevations predicted by Weighted-Average Partial-Least Squares (WA-PLS) regressions for diatom, testate amoebae and combined models. In terms of precision, diatom-based models performed best being capable of predicting sea level to within ± 0.07 m, whereas testate amoebae and combined models demonstrated predictive abilities to within ± 0.08 m and ± 0.09 m respectively. However, a lack of modern analogue for a number of fossil samples in both the testate amoebae and diatom datasets can potentially cause inaccuracies in

the reconstructions. Combining the foraminiferal data with the testate amoebae and diatom data into a multiproxy transfer function did not improve analogue quality.

Ideally future sea-level studies should pursue a multiproxy approach in order to achieve the most robust reconstructions. The practical problem with a multiproxy approach is that analysis is time-consuming. Foraminiferal analysis is simple and relatively time-efficient so is recommended. In order to achieve an accurate reconstruction for the most feasible investment in time, a pragmatic approach to deciding on which additional proxies to include could prove most feasible, as follows. Conduct initial 'reconnaissance' analysis on fossil sediments to identify which microorganism groups are preserved, particularly which are preserved in greatest diversity. Detailed analyses could then be targeted only for the microfossil group that is best preserved. Recent studies have developed robust regional-scale sea-level transfer functions for diatoms (Wilson and Lamb, 2012) and testate amoebae (Barnett *et al.,* 2017). The virtue of regional transfer functions is that they do not require local modern training sets to be developed in order to produce a reconstruction. Moreover, the longer environmental gradient and greater range of sub-environments sampled means regional-scale transfer functions are likely to provide better analogues than local training sets (e.g. Gehrels *et al.,* 2001). However, because of intra-site variability the most accurate diatom transfer functions are achieved by local transfer functions (or regional transfer functions underpinned by local training sets) (Woodwroffe and Long, 2010; Wilson and Lamb, 2012). Little intra-site variability is observed between testate amoebae assemblages across the North Atlantic region (Charman *et al.,* (2010); Barnett *et al.,*2017); this observation is extended to the South Atlantic with comparable modern distributions also observed from the Falkland Islands (this study). Therefore, in other Atlantic sites it may be possible to accurately reconstruct sea-level

by only gathering new fossil testate amoebae data. This would reduce the amount of analytical time required in future studies as modern training sets do not need to be collected.

7.4 Sea-level changes in the Falkland Islands

The central focus of this PhD project has been to improve the understanding of Holocene and recent sea-level changes in the Southern Hemisphere by establishing a new sea-level record from the Falkland Islands (**Aim 1**). With reference to previously published sea-level records, this section discusses the significance and wider implications of the Holocene and Common Era sea-level reconstructions presented in **Chapter 6** and the evidence to support or reject the research hypothesis of this thesis that 20th sea-level change has had a significant contribution from melting of Northern Hemisphere land-based ice.

7.4.1 Holocene sea-level changes

In **Chapter 6** the reconstructed Holocene sea-level history spanning the last ca. 8.5 ka BP for the Falkland Islands was presented based on 9 new sea-level index points (**Figure 6.4**). Based on this sea-level reconstruction and underpinning sedimentological and microfossil analyses, it is possible to interpret the Holocene development of the Swan Inlet marsh as a direct response to sea-level changes. Under rising sea levels a salt marsh developed which was suddenly drowned around 8.4 ka BP. At this time the salt marshes were transformed in to tidal flats across the entire estuary. Following the drowning, RSL kept rising until ca. 7 ka BP when it reached a position between +0.13 m and -0.25 m present sea level (**Figure 6.4**; **Table 6.4**). After this highstand, between ca. 7 ka BP and ca. 5.4 ka BP there was a RSL fall in the Falkland Islands. After ca. 5.4 ka BP RSL gradually rose up to present level.

Holocene sea-level data in the nearby South Atlantic region are relatively sparse and generally of poor quality (cf. Milne *et al.,* 2005). On the coastline of Tierra Del Fuego, Schellmann and Radtke (2010) present evidence of early Holocene rise with RSL reaching a position close to present ca. 8.6ka BP and a middle Holocene highstand between 2-3 m above present sea level at around ca. 7.4 ka BP. There was no evidence to suggest a middle Holocene highstand of such magnitude in the Falkland Islands although the timing of the highstand is consistent. It is, however, quite possible that due to oceanographic and tectonic differences between the Falkland Islands and continental Patagonia significant RSL differences between these locations would occur (cf. Milne *et al.,* 2005). Furthermore, there is no evidence in the results of this study to support a RSL highstand several metres above present in the Falkland Islands as suggested by Roberts (1984). Because the Falkland Islands are in an intermediate- to far-field location, the highstand (and subsequent fall in RSL to present) is likely owing to one, or a combination, of the following processes: (i) hydro-isostatic loading of the continental shelf (continental levering) (Clark *et al.,* 1978; Nakada and Lambeck,1989); (ii) a global fall in the ocean surface due to both hydro- and glacio-isostatic loading of the Earth's surface (ocean siphoning)(Mitrovica and Milne, 2002), and (iii) the mass redistribution associated with ocean siphoning resulting in perturbations in Earth's rotational processes (Milne and Mitrovica, 2008). Indeed, in northern South America, small sea-level highstands (<1.0 m above present) have been recorded in Suriname and Guyana (Roeleveld and van Loon, 1979). These highstands have been inferred to have been caused by hydro-isostatic loading of the continental shelf, causing uplift of the continent to produce a highstand in the mid- to late Holocene (Milne *et al.,* 2005).

When compared with GIA modelled predictions of RSL for the Falkland Islands no unique model solution was able to reconcile the RSL recorded by the sea-level data presented in this study (**Figure 6.4**). Similar discrepancies between GIA model predictions and proxy-derived sea-level observations in the South Atlantic were present in previous studies in the region (Rostami *et al.,* 2000; Milne *et al.*, 2005). It was previously concluded that these discrepancies were likely a result of (assumed) poor-quality proxy RSL data (Milne *et al.,* 2005). The fact that the data of this study, with no evidence to suggest these data are of poor-quality, is not well-resolved by the GIA models, challenges this assumption. Holocene RSL changes in the Falkland Islands are controlled by ice-ocean mass flux and GIA so sea-level data are not affected by tectonics, local ice-loading effects and large tidal ranges like in mainland southern South America (Rostami *et al*., 2000; Bentley and McCulloch, 2005; Milne *et al*., 2005). The coastline of the Falkland Islands is in fact one of the few coastal locations in the world where the mid-Holocene RSL was within a few metres of the eustatic value and where predicted RSL is relatively insensitive to Earth model parameters (Milne and Mitrovica, 2008). The Holocene RSL history of the Falkland Islands can therefore be an important constraint on the net global ice-ocean mass flux and, hence, global climate change (Clark and Mix, 2002). Better understanding the causes of this discrepancy presents new challenges for both the sea-level modelling and data communities. At present there is a lack of knowledge of the melt history of the Antarctic Ice Sheet, the sensitivity to changes in the Patagonian Ice Sheet, and the water-loading effects of the wide Patagonian continental shelf. More high-quality Holocene sea-level data from the South Atlantic region is therefore required to provide valuable constraints for GIA models i.e. ice-ocean parameters and to improve the knowledge on the Antarctic and Patagonian ice-ocean mass fluxes.

7.4.2 Evidence for rapid sea-level rise prior to the 8.2 ka BP cold event?

The drowning of the tidal flat sediments at ca. 8.4 ka BP is potentially significant because it is synchronous with a sea-level jump known from Northern Hemisphere locations (Hijma and Cohen, 2010; Kendall *et al*., 2008; Lawrence *et al*., 2016). This jump is assumed to be caused by the sudden drainage of the glacial lakes Agassiz and Ojibway into the North Atlantic (Barber *et al*., 1999). This drainage event is associated with a severe weakening of the Atlantic Meridional Overturning Circulation (AMOC) believed to have caused the 8.2 ka BP abrupt climate cooling event (Alley *et al.,* 1997; de Vernal *et al.,* 1997; Daley *et al.,* 2011). It is possible to place an estimate for this jump of 0.89 ± 0.22 m in magnitude based on stratigraphic evidence from Swan Inlet, as follows. The sea-level position (-3.46 m SID) before the drowning is recorded by the contact between the reworked peat and tidal flat sands in core *SI-6* where this contact lies on bedrock (**Figure 6.2**). The post-drowning sea-level position (-2.575 m SID) is inferred from the tidal flat deposits where they attain their highest position in the 2005 bank section and are overlain by salt-marsh sediments (**Figure 6.3**). Both contacts in *core SI-6* and the 2005 bank section are the stratigraphic equivalents of the transition between salt marsh and tidal flat in the modern environment. The magnitude of the sea-level jump therefore simply represents the height difference between the two contacts. The dates in the 2005 bank section (~7 ka BP) indicate that the tidal flat environment persisted for about another millennium subsequent to the initial drowning. As there was likely to be additional RSL rise during this time then this value should be regarded as a maximum estimate. The error (±0.22 m) reflects uncertainties in relating elevations to Swan Inlet Datum (SID) (Appendix C).

Understanding the magnitude of the sea-level jump associated with the 8.2 ka BP event is critically important as these observations can be used to assess the accuracy

of climate and ice-sheet model simulations of abrupt change during the early Holocene and for predicting future changes in the AMOC (e.g. Morrill *et al.,* 2013). The jump estimate from the Falkland Islands represents the first attempt to use sea-level data from a far-field, Southern Hemisphere site to constrain this sea-level jump. Owing to the far-field location of the Falkland Islands the value derived from here can be regarded as being close to the 'true' eustatic magnitude of the event (Kendall *et al.*, 2008). This estimate from the Falkland Islands is much lower than Northern Hemisphere eustatic-corrected sea-level estimates of 1.5 ± 0.7 m, 3.0 ± 1.3 m and 2.7 ± 0.3 m from RSL studies in the Mississippi Delta, The Netherlands, and Scotland, respectively (Hijma and Cohen, 2010; Li *et al*., 2012; Lawrence *et al*., 2016), but is in agreement with glaciological and model-based estimates (e.g. De Vernal *et al*., 1997; Barber *et al*., 1999; Wiersma *et al*., 2006; Lambeck *et al.,* 2017). At present, it is not clear whether the meltwater release responsible for the 8.2 ka BP event occurred as a single event or as multiple events (multiple sea-level jumps). It has been suggested that two jumps are being recorded in the estimate from the Netherlands (Törnqvist and Hijma, 2012), while the estimate from Scotland (Lawrence *et al.,* 2016) records three phases of abrupt sea-level rise. There is no evidence in the Swan Inlet stratigraphy to suggest multiple jumps. However, the lower estimate from the Falkland Islands compared to Northern Hemisphere estimates could suggest multiple jumps in the Northern Hemisphere record additional melt-signals from the Southern Hemisphere. Sea-level theory predicts Southern Hemisphere meltwater sources (e.g. from Antarctica) are not detected in the Falkland Islands but are detected in the Northern Hemisphere sites (Mitrovica *et al.,* 2011). Therefore, if there was a Southern Hemisphere source at ca. 8.4 ka BP in addition to the Northern Hemisphere source (Barber *et al*., 1999) the differences between the estimates could be a result of a sea-level jump caused by a Southern Hemisphere melt-source not being recorded in the

Falkland Islands. It could, however, be that the differences between the sea-level jump estimates reflect variable preservation of the jumps and/or underestimates of the vertical uncertainties between studies. More detailed stratigraphic and micropalaeontological analyses of the Swan Inlet sediments are required to elucidate a lack (or presence) of multiple stages of sea-level rise and to make a more precise estimate.

7.4.3 Sea-level changes in the Common Era

Aim 1 of this thesis was focused on developing a precise and accurate sea-level reconstruction for the Falkland Islands in order to improve the understanding of recent sea-level changes in the relatively un-studied Southern Hemisphere and to test the hypothesis that 20th century sea-level rise has had significant contribution from Northern Hemisphere melt sources. The sea-level reconstruction presented in **Figure 6.20** has the potential to fulfil this aim as it represents the first precise (decimetre-scale vertical resolution) high-resolution (subcentennial temporal resolution) for the South Atlantic region and the longest continuous Common Era sea-level record in the Southern Hemisphere. The sea-level reconstruction was derived from the upper 90 cm of core *SI-2*. The stratigraphy of the upper 90 cm of *Core SI-2* indicated an overall regressive sequence (**Section 6.2.4**; **6.2.5**) which transitioned from middle to upper salt-marsh environments. The sea-level reconstruction was, however, characterised by an overall transgression which documented an early rising sea-level trend, a 'flat' sea level in the middle, and a recent inflexion towards the present (**Figure 6.16**). The regressive nature of the sequence despite an observed transgressive sea-level reconstruction indicates that the Swan Inlet marsh maintained surface elevation through vertical accretion which kept pace with the rate of sea-level rise (cf. Stevenson *et al.,* 1986; Morris *et al.,* 2002; Beckett *et al.,* 2016).

In order to confidently interpret trends in the reconstruction, reliable accuracy of the record must be demonstrated. The suite of statistical measures presented and discussed in **Section 6.3.4** used to assess for issues and omit potentially inaccurate data goes some way to achieving confidence in the final reconstruction. After removal of problematic data, the fact that both the testate amoebae and diatom reconstructions show the same broad trends provides more confidence that the reconstruction is reliable and suggests the independent approaches used to develop each reconstruction are valid. Indeed, the probability of two independent reconstructions being inaccurate but demonstrating comparable trends is likely very small. Additional justification to support the interpretation that the reconstruction is accurate is provided by the significance tests (**Figure 6.17**) which showed 100% more variance is explained by the reconstruction than by reconstructions derived from randomly-trained data. A direct test of reconstruction accuracy can be achieved by comparing the sea-level reconstruction with independent, instrumentally measured tide gauge observations from the Falkland Islands. Instrumental sea-level data for the Falkland Islands were obtained from the nearby tide-gauges installed at Stanley (Holgate *et al*., 2013; PSMSL, 2016). Near-continuous tide-gauge data which overlap with the sea-level reconstruction is only available for the periods 1965-1969 and 1993-2013 (PSMSL, 2016). This was supplemented with mean sea level measurements (tide gauge) from 1842, 1981-1982 and 1984 reconciled with the Stanley tide-gauge data by Woodworth *et al.* (2010). When the full vertical and age uncertainties are considered, the reconstructed sea-level record is in good agreement with the available tide gauge data for the period 1842-2013 (**Figure 7.2**). In fact, with the exception of the 1842 data, the instrumental data plot close to the mean reconstructed values. The 1842 data are derived from only three months of measurements collected in the winter of 1842 (Woodworth *et al.,* 2010). Thus, the greater difference between the 1842 and

reconstructed mean data could be due to seasonal variability not captured in the 1842 measurements. Based on the validation in **Figure 7.2** the most recent (last ca. 170 years) sea-level reconstruction can therefore be deemed accurate.

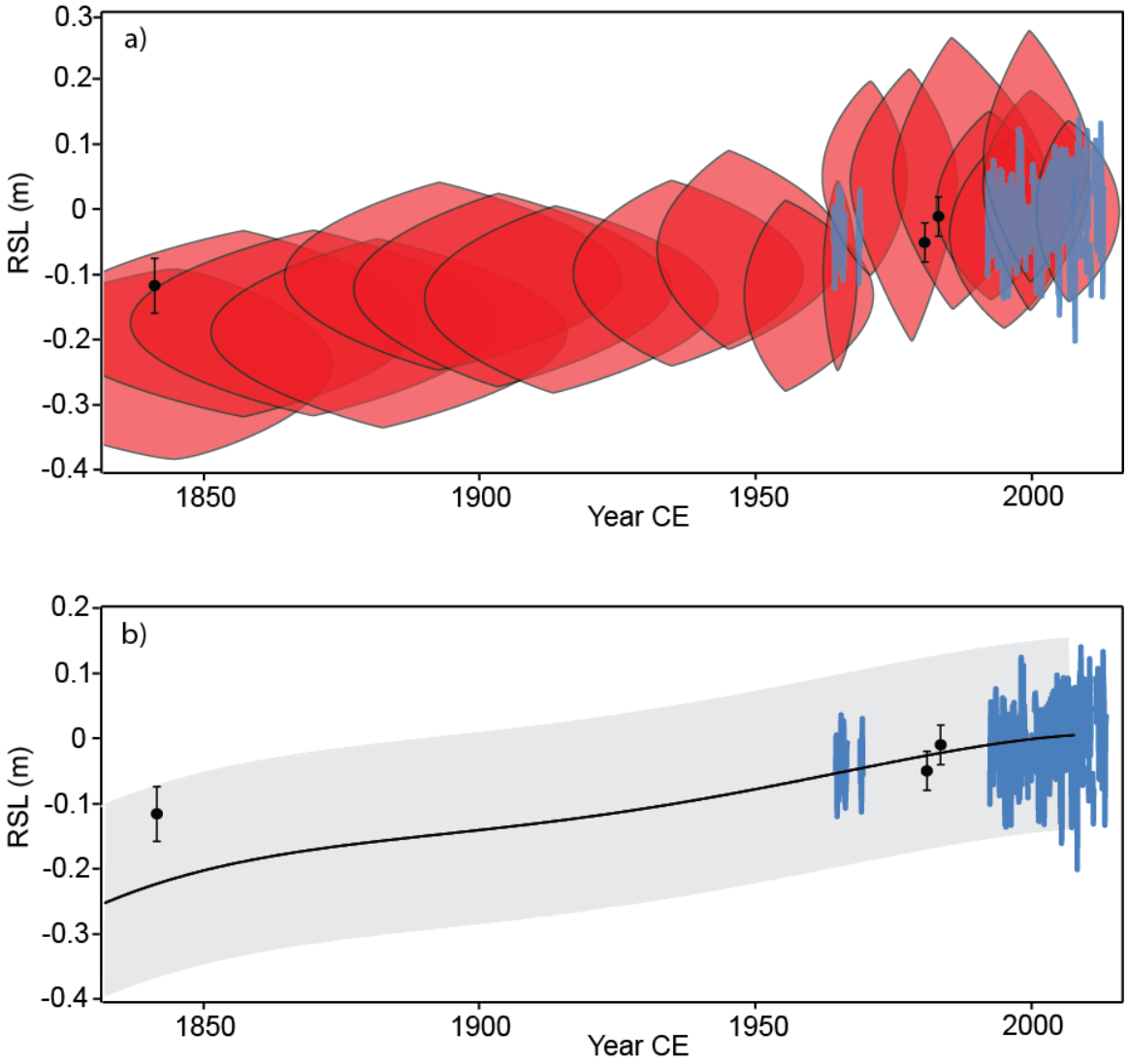

***Figure 7.2**: Instrumental sea-level observations from the Falkland Islands compared with a) the sea-level reconstruction from Swan Inlet for the period 1842-2013 (**Figure 6.19**). Instrumental observations: Stanley (blue lines), 1842, 1981-1982 and 1984 (black dots) – data plotted relative to 1993-2013 mean. b) Swan Inlet sea-level reconstruction summarised by a 4th order polynomial regression of the mean reconstructed RSL values (black line) plus full error limits (grey band) - data presented in **Table 6.9**.*

On the basis of the validation with tide-gauge data it could be assumed that the earlier part of the reconstruction (ca. 700-1842 CE) exhibits a comparable degree of accuracy

to the most recent part of the reconstruction. However, post-depositional lowering of SLIPs caused by compaction potentially invalidates this assumption. The compaction assessment in **Chapter 6** (**Figure 6.18**) indicated that compaction has likely occurred, but overall compaction was small indicated by a difference of less than 0.01 mm/yr between the observed rates of change for reliable and susceptible sea-level data. This interpretation is consistent with the modelling results of Brain *et al.* (2012), which conclude that salt-marsh sequences with comparable stratigraphy to that from which the Common Era SLIPs were obtained (<1 m long, uniform regressive stratigraphy) experience little compaction. Further support for this interpretation is provided by the bulk density data (**Figure 6.5**), which reveal a relatively constant bulk density indicating a lack of compaction (*sensu* Gehrels *et al.,* 2006). A first-order decompaction exercise, based on the differences between average linear rates of RSL change calculated for reliable and susceptible SLIPs, was conducted to investigate the degree to which this small-scale compaction influences the reconstructed sea-level trends (**Figure 6.18**). Because compaction is a non-linear process this linear method of decompaction should be regarded as illustrative (rather than diagnostic) of the potential influence of post-depositional lowering on the reconstructed RSL trend. The compacted and decompacted RSL reconstructions presented in **Figure 6.20** indicate that compaction may alter the observed timing of changes in the long-term rate of RSL change. The 'true' RSL magnitude is assumed likely to be greater than the decompacted trend toward the middle of the reconstruction and likely to be smaller than the most recent decompacted trend. Testing this assumption would require complex geotechnical modelling which is beyond the scope of this study (e.g. Brain *et al.,* 2015). Whilst it is possible that compaction may be greater than that inferred from the compaction assessment, it is assumed unlikely that compaction has a significant influence on the magnitude of sea-level change for the most recent part of the sea-

level reconstruction. This assumption is supported by the instrumental observations, which cannot be influenced by compaction, being in good agreement with the most recent reconstruction. Moreover, owing to the time-dependant nature of compaction processes (Brain *et al.,* 2015) the influence on the reconstructed curve would produce a gradual inflexion rather than the sharp inflexion observed in the Falklands Islands curve (**Figure 6.2**).

In addition to recognising the influence of compaction, important considerations should be made when interpreting the sea-level reconstruction (**Figure 6.20**). One should avoid over-interpretation by fully appreciating the joint age and RSL uncertainty. Indeed, it is possible to construct many possible sea-level histories through the ranges of RSL uncertainties for all SLIPs (e.g. oscillations). Thus, it is assumed the reconstruction reflects long-term (multi-decadal) trends which summarise the complex and dynamic interactions contributing to sea-level change. Relatedly, caution should be applied when interpreting average linear rates of RSL change (**Figure 6.20**). It is important to recognise that a linear model assumes the age and RSL variables are fixed and therefore does not account for the uncertainty in the reconstruction (only mean values are considered). Thus, the calculated rates of RSL change (with 95% uncertainty interval) are likely overly precise estimates. Recent studies have overcome this problem by applying 'error-in-variables' regression models which take account of all the available uncertainties to produce probabilistic estimates of RSL rates (e.g. Cahill *et al.,* 2015; Parnell and Gehrels, 2015). Unfortunately, it was not possible to apply such a model to the Falklands Islands reconstruction as the resolution of radiocarbon calibrations in the current iterations of these models (Cahill *et al.* 2015; Parnell, 2016) is unable to resolve the post-bomb radiocarbon chronology (**Section 6.2.6**). It is anticipated that this issue will be resolved in the next iterations of the error-

in-variables models (Andrew Parnell, personal communication, March 2016). However, because there is a relatively large number of SLIPs and RSL uncertainty is relatively small for the Falkland Islands reconstruction, the rates calculated by linear methods may well be close to the rates calculated by an error-in-variables model (cf. Parnell and Gehrels, 2015).

When the Falklands Islands sea-level reconstruction is compared with the interpretations of Woodworth *et al.'s* (2010) analysis of tide gauge data from the Falkland Islands (**Figure 2.2**) the linear rates calculated in **Section 6.2.8** are generally in good agreement. The compacted and decompacted Falkland Islands reconstructions (**Figure 6.20**) indicate a near-stable RSL trend between the 16th and 20th century with an average rate between -0.05 and +0.1 mm/yr. The reconstruction indicates that RSL departed from this stable trend by the 20th century (**Figure 6.20**). This is consistent with observations of a 20th century acceleration evident in proxy and tide gauge records (Church and White, 2006, 2011; Gehrels and Woodworth, 2013). Although the timing of this departure differs between the decompacted (1932-1972 CE, **Figure 6.20a**) and non-corrected (1813-1920 CE, **Figure 6.20b**) reconstructions, it is unlikely that compaction affected the reconstruction during this period (for the reasons discussed previously). It can therefore be assumed that that accelerated rates of sea-level change began ca. 1813-1920 CE (**Figure 6.20b**). The Woodworth *et al.* (2010) analyses indicate that 20th century sea-level had departed (accelerated) from the long-term rate by the end of the century. In Woodworth *et al.'s* (2010) analysis a lack of data between 1842 and 1981-1982 prevent the timing of this departure from being discerned, but the available data support the 20th Century trends of the reconstruction. Woodworth *et al.,* (2010) removed the contribution of GIA based on Peltier *et al.*'s (2004) model predictions of vertical land motion in the Falkland Islands of -0.69 mm/yr

since the mid-19th century (corrected value from Woodworth *et al*.'s (2011) erratum). Due to the issues highlighted in **Section 7.4.1** with GIA predictions poorly reconciling sea-level data for the Falkland Islands and elsewhere in southern South America (Milne *et al.,* 2005), these values may well be inaccurate. However, for the purpose of comparison the same rates are adopted to correct the recent rates of RSL change for the Falkland Islands reconstruction (**Figure 6.20b**). Woodworth *et al.,* (2011) calculate an accelerated rate of 2.60 ± 0.58 mm/yr since 1992. This compares to a rate of 2.99 ± 0.62 mm/yr between 1932-1972 and present for the Falkland Islands reconstruction. Within the associated ranges of uncertainty, both rates are in good agreement with a rate of 2.6 mm/yr recorded by satellite altimetry since 1992 CE.

7.4.4 Accelerated sea-level rise in the 20th century: a significant Northern Hemisphere melt source?

The recent acceleration observed in the Falkland Islands sea-level reconstruction supports the conclusions of global analyses that 20th century sea-levels have accelerated (Gehrels and Woodworth, 2013; Kopp *et al.,* 2016). To date, the reconstruction from the Falkland Islands is only the third Southern Hemisphere record of sufficient length for the timing of a recent acceleration to be detectable, and the first from the South Atlantic. The magnitude of the recent acceleration observed in records from Tasmania (Gehrels *et al.,* 2012) and New Zealand (Gehrels *et al.,* 2008, 2012) was greater than that observed in Northern Hemisphere records (Gehrels and Woodworth, 2013; **Table 1.1**). The cause of the 20th century acceleration has widely been attributed to global temperature increases (Kemp *et al.* 2011; Church *et al.,* 2013; Kopp *et al.,* 2016) but the contributions to the sudden inflexion around the start of the 20th century are poorly understood (Church and White, 2011; Church *et al.,*2013). The greater magnitude of the 20th century acceleration in Tasmania and New Zealand

records compared with Northern Hemisphere records lead Gehrels and Woodworth (2013) to hypothesise that the melting of Northern Hemisphere ice masses could be an important contributor. This hypothesis is based on the observations of distinct, non-uniform spatial patterns of sea-level change caused by melting ice sheets and glaciers (Mitrovica *et al.,* 2001; Tamisiea *et al.,* 2003a) termed 'sea-level fingerprints'. The pattern of such a sea-level fingerprint depends on the location of the melt source and associated redistribution of the gravitational perturbation exerted by the ice mass (Mitrovica *et al.,* 2001), but is broadly characterised by the greatest magnitude of sea-level rise occurring in far-field locations (Tamisiea *et al.,* 2003, 2011; Kopp *et al.* 2010). Thus, the greater magnitude of the sea-level acceleration observed in the Southern Hemisphere is consistent with a Northern Hemisphere melt source. Furthermore, the modelling study of Kopp *et al.* (2010) suggests that the greatest sea-level change caused by Greenland ice loss occur in the South Atlantic (**Figure 1.3**). No direct observations of early 20th century Northern Hemisphere ice sheet melt exist, but the Falklands Islands reconstruction therefore offers a means to test the hypothesis using the sea-level fingerprinting methodology.

In order to test the hypothesis, the timing and magnitude of accelerated sea-level rise in the Falkland Islands must be reliably established. This is achieved following the method of Gehrels and Woodworth (2013). This method uses visual inspection to determine the start of accelerated rates by comparing the recent reconstructed RSL record (last 300 years) with the late-Holocene background rate of RSL change for the Falkland Islands. Importantly, this method does not require corrections for vertical land movements caused by GIA as subtracting the late-Holocene background rate from the modern rate effectively eliminates this influence (Gehrels and Woodworth, 2013). The late Holocene background rate is assumed from the linear rate consistent with the

Holocene SLIPs for the Falkland Islands presented in **Section 6.2.3**. For this calculation only the three most recent SLIPs (ca. 5.5ka to 0.5 ka BP) presented in **Section 6.23** were used as the earlier SLIPs (prior to 7 Ka BP) capture early Holocene sea-level rise as a result of rapid temperature rise following the last glaciation (Smith *et al.* 2011). The two basal slips (from 88 cm *core SI-2*) of the Common Era reconstruction were also used (**Section 6.2.8**). Based on these data a late Holocene background rate of 0.1 mm/yr is adopted (**Figure 7.3**). It is noted that this rate calculation is limited by the small number of data points but is consistent with the predicted rate using Bradley *et al.*'s (2016) GIA model which provided the best fit for these data (**Figure 6.4**). Similar limitations were also associated with late Holocene rates calculated for Tasmania and New Zealand (Gehrels and Woodworth, 2013). The non-compaction corrected RSL reconstruction is used for this comparison because, as discussed above, it is assumed unlikely that this recent data is affected by compaction.

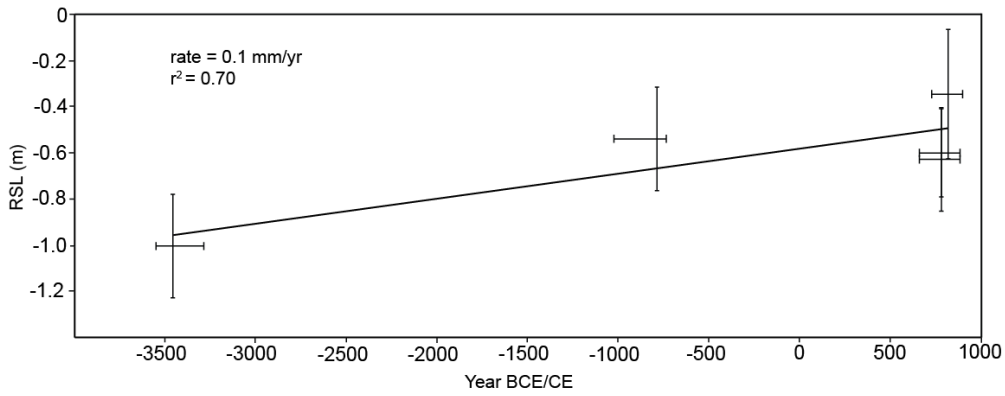

Figure 7.3: *Late Holocene rate of sea-level rise for the Falkland Islands as determined by linear regression (straight line) through the sea level index points (crosses).*

The comparison between the late Holocene background rate of sea-level rise and recent RSL reconstruction for the Falkland Islands (**Figure 7.4**) suggests that modern

sea-level rise departed from the background trend around the start of the 20th century. This is indicated by the post 1900 CE SLIPs plotting consistently above the late Holocene trend and, within the range of uncertainties, all SLIPs prior to this plotting closer to, or above, the late Holocene trend (**Figure 7.4**). The timing of the sea-level acceleration indicated by this observation (visual inspection) is consistent with that interpreted by the change-point analysis in **Section 6.2.8**. Moreover, the timing is consistent with that observed in all available proxy and tide-gauge records of sufficient length to detect the onset of the acceleration (**Figure 7.4**; Gehrels and Woodworth, 2013).

Through visual inspection of the reconstructions, the magnitude of the acceleration in the Falkland Islands does not appear obviously greater than the magnitudes of the accelerations observed in Tasmania and New Zealand. Gehrels and Woodworth (2013 table 3) compare the late Holocene background rates with post-acceleration (post-1930) rates calculated from tide gauge data. Based on this comparison the magnitude of the New Zealand acceleration can be inferred from the difference between the late Holocene background rate (-0.1 mm/yr) and post-acceleration rate (2.4 mm/yr) as 2.3 mm/yr. This comparison is not possible for the Falkland Islands or Tasmania because no nearby tide-gauge data are available for the post-acceleration period. However, less certain post-acceleration rates can be inferred by comparing the difference between the late Holocene background rate and the post-acceleration rates of the reconstructions. The magnitude of the acceleration based on this comparison is 3.3 mm/yr for Tasmania (**Table 1.1,** Gehrels *et al.,* 2012). For the Falklands Islands reconstruction the mean average linear rate for the period 1932-1972 CE to present of 2.3 mm/yr (**Figure 6.20**) is adopted for the post-acceleration rate which gives a magnitude of 2.2 mm/yr for the acceleration in the Falkland Islands.

These inferred magnitudes suggest that the 20th century acceleration in the Falkland Islands is similar to, but not greater than, the magnitude in either New Zealand or Tasmania, which supports the interpretation based on visual inspection (**Figure 7.20**). However, the 2.2 mm/yr magnitude inferred for the acceleration in the Falkland Islands is greater than the magnitudes observed for Northern Hemisphere sites (Gehrels and Woodworth, 2013; Table 1).

The greater magnitude of the recent sea-level acceleration interpreted from the Falkland Islands reconstruction is consistent with the spatial pattern expected by a significant contribution from a Northern Hemisphere melt source to global sea-level rise observed in the early 20th century (Mitrovica *et al.,* 2001). However, because the magnitude of the acceleration is not greater in the Falkland Islands than in Tasmania and New Zealand it is not possible to confidently suggest that a Northern Hemisphere melt source produced the greater magnitudes observed in the Southern Hemisphere. It should be noted that the greater magnitude predicted for the Falkland Islands by Kopp *et al.* (2010) is based on modelled ice loss from Greenland. It could therefore be possible that the sea-level fingerprints produced by contributions from other Northern Hemisphere melt sources (e.g. mountain glaciers in Alaska, western North America and Arctic Canada), for which no model predictions are available, produce a larger sea-level rise in the South Pacific than the South Atlantic (c.f. Tamisiea *et al.* (2003b). Additionally, other unknown causes for the differences observed between Northern Hemisphere and Southern Hemisphere records cannot be ruled out. For example, it could be that the greater magnitude of the sea-level acceleration in the Southern Hemisphere reconstructions reflects different oceanographic, atmospheric and/or steric sea-level contributions between hemispheres (c.f. Wake *et al.*, 2006; Yin *et al.* 2009, 2010, 2011; Zuo *et al.* 2010; Purkey *et al.* 2010, 2013).

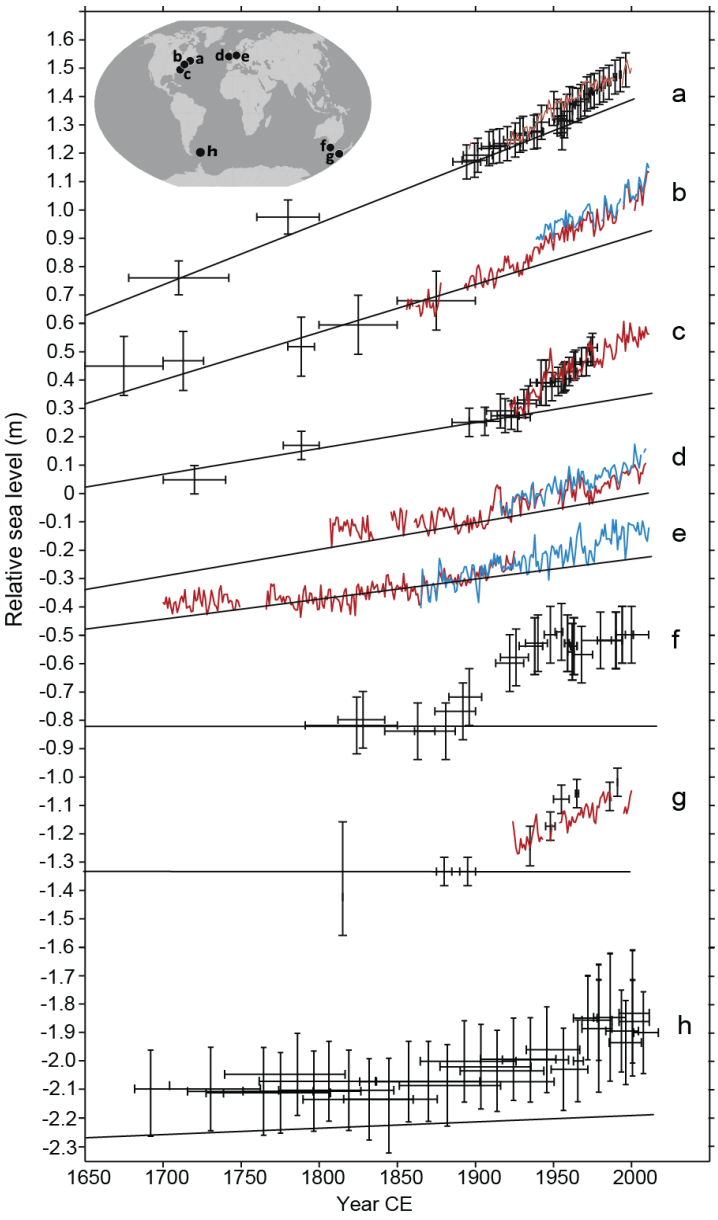

***Figure 7.4**: Recent sea-level changes (last 200–350 years) compared with late Holocene background trend of sea-level change. Red and blue lines are tide-gauge records. Sea-level index points from proxy data are shown as crosses reflecting age and altitudinal uncertainties. a. Chezzetcook, Nova Scotia (Gehrels et al., 2005), with tide-gauge record from Halifax. b. Barn Island, Connecticut, USA (Donnelly et al., 2004), with tide-gauge records from New York City (red line) and New London (blue line). c. Sand Point, North Carolina, USA (Kemp et al., 2009, 2011), with tide-gauge record from Charleston, South Carolina. d. Tide-gauge records from Brest (red line) and Newlyn (blue line) compared with late Holocene trend of relative sea-level change at Thurlestone, Devon, United Kingdom (Gehrels et al., 2011). e. Instrumental sea-level record from Amsterdam (red line) and tide-gauge record from Den Helder (blue line), compared with late Holocene trend of relative sea-level change at Schokland, the Netherlands (van de Plassche et al.,2005). f. Little Swanport, Tasmania, Australia (Gehrels et al., 2012). g. Pounawea southeastern New Zealand (Gehrels et al., 2008), with tide-gauge record from Lyttelton. h. Swan Inlet, Falkland Islands (this study).*

Chapter 8 – Conclusions

8.1 Project summary

This project has sought to provide a better understanding of the character of a 20th century acceleration in the rate of sea-level rise observed in global and regional records. Specifically, the focus of this project was on improving the understanding of factors contributing to the 20th century acceleration by investigating the apparent geographical differences evident in these observations. Sea-level data in the Southern Hemisphere are limited but, based on two recent records from Tasmania and New Zealand (Gehrels *et al.,* 2008, 2012), indicate the sea-level acceleration is of greater magnitude than in the Northern Hemisphere. Sea-level theory indicates this spatial pattern could result from the melting of Northern Hemisphere land-based ice. Therefore, the purpose of **Aim 1** of this thesis was to test the hypothesis that early 20th century sea-level rise had a significant contribution from Northern Hemisphere ice loss. Models suggest that the greatest magnitudes of sea-level rise caused by Northern Hemisphere ice loss occur in the South Atlantic, in the seas surrounding the Falkland Islands. Thus, **Aim 1** was to produce a proxy-derived sea-level reconstruction for the Falkland Islands of sufficient length and resolution to investigate the pattern of early 20th century sea-level change in the Falkland Islands.

Aim 2 of this project focused on better understanding and improving the use of salt-marsh testate amoebae in sea-level studies. Testate amoebae are becoming increasingly used as proxy-indicators to reconstruct past sea-level changes. However, the factors governing the modern distributions and their preservation in salt marshes are poorly understood and analytical practices have not been standardised. This study

therefore intended to improve the understanding of seasonal influences on salt-marsh testate amoebae in order to better inform sampling strategies.

The investigations undertaken toward fulfilment of the two central aims of this project also enabled additional, complimentary research questions of wider-relevance to sea-level studies to be investigated. First, it was necessary to produce a Holocene sea-level reconstruction for the Falkland Islands in order to provide a context for considering the Common Era reconstruction. The Holocene sea-level reconstruction provided an opportunity to investigate Holocene relative sea-level changes and their implications for our understanding of ice-ocean mass fluxes. Secondly, the multiproxy nature of the investigations in the Falkland Islands provided an opportunity to investigate the relative utility, and evaluate the feasibility, of individual proxy-groups to sea-level studies.

8.2 Holocene sea-level changes in the Falkland Islands

Through sedimentological and chronological analyses of the salt-marsh lithostratigraphy at Swan Inlet, Falkland Islands, Holocene sea-level changes were reconstructed. The Holocene sea-level reconstruction showed a rising early Holocene rise from ca. 8.5 ka BP which reached a mid-Holocene sea-level peak height between +0.13 m and -0.25 m present sea level ca. 7 ka BP. The highstand in the Falkland Islands is significantly lower than that observed in other Southern Hemisphere records. Following this highstand, sea-level fell until ca. 5.5 ka BP reaching a position around -1.0 m and has since gently risen to present level. No single GIA model was able to reconcile all of the reconstructed data, but observations were in best agreement with the ICE5G_VM2 model (Peltier, 2004) for the early Holocene, and with the continental mantle model (Lambeck *et al*, 2017) and the Bradley *et al.* (2016) model for the late Holocene. Reconciling the Holocene data with model predictions presents a challenge

for GIA models as there are no obvious causes for the mismatch. More high-quality Holocene sea-level data from the South Atlantic region is therefore required to provide valuable constraints for GIA models i.e. ice-ocean parameters and could potentially improve the knowledge on the Antarctic and Patagonian ice-ocean mass fluxes.

The Holocene RSL record for the Falkland Islands demonstrated that sea-level rise during the early Holocene was punctuated by a sea-level jump broadly synchronous with the meltwater release from the Laurentide Ice Sheet around 8.4 ka BP, which has been suggested to be the cause of the 8.2 ka BP cold event. A magnitude of 0.89 ± 0.22 m was calculated for this jump but, until the end of the drowning is better dated, this should be regarded as a maximum constraint. This jump estimate from the Falkland Islands represented the first attempt to use sea-level data from a far-field, Southern Hemisphere site to constrain this sea-level jump. It was suggested by the comparisons with Northern Hemisphere estimates and sea-level fingerprinting theory that a Southern Hemisphere melt source synchronous with the widely-attributed Laurentide melt source may have contributed to the jump. Future studies from other Southern Hemisphere sites are required to provide better constraints on the jump estimate and test the possibility of a Northern Hemisphere contribution.

8.3 Common Era sea-level changes in the Falkland Islands

Through a combination of chronostratigraphic and biostratigraphic analyses conducted on a 0.9 m core sampled from Swan Inlet, Falkland Islands, Common Era sea-level changes spanning the last ca. 2000 years were established. These Common Era sea-level changes were based on testate amoebae and diatom reconstructions of relative sea level change. The reconstruction indicated an overall sea-level transgression in the Falkland Islands during the Common Era. This transgression

indicated a gently rising rate no greater than 0.55 ± 0.08 mm/yr between the 8th and 16th centuries CE which stabilised between the 15th and 20th centuries (-0.05 ± 0.21 mm/yr) at which point the rate accelerated up to ~2.3 mm/yr until present. Statistical assessments and comparisons with independent instrumental sea-level data for the Falkland Islands suggested the reconstruction was reliable.

Change-point analysis and comparisons with the late Holocene background rate of sea-level change indicated that sea-level accelerated in the Falkland Islands around the start of the 20th century which is consistent with the timing of accelerated sea-level rise observed in regional and global analyses of proxy and instrumental records. The consistent timing between the Falkland Islands and other sites across the globe indicate a glacio-eustatic origin for the acceleration. The magnitude of the 20th century acceleration in the Falkland Islands appeared to be greater than in Northern Hemisphere sites and similar to other Southern Hemisphere sites (Tasmania and New Zealand). This pattern of change supports the hypothesis that the early 20th century sea-level change had a significant contribution from a Northern Hemisphere land-based ice melt source. The magnitude of the 20th century acceleration not being greater than other Southern Hemisphere sites is not consistent with the pattern expected if for a Greenland melt source. This could indicate other and/or additional Northern Hemisphere melt sources contributed, but other oceanographic and/or steric contributions cannot be ruled out as factors responsible for differences observed in the spatial pattern of the acceleration.

8.4 The use of testate amoebae in sea-level studies

In this project, modern distributions of salt-marsh testate amoebae were studied over one annual cycle, at the Fal-Ruan salt marsh in Cornwall (UK), to investigate the influence of seasonal factors on their distributions. Seasonal variations in both the living and dead assemblages of salt-marsh testate amoebae were observed. Variations in the live assemblages did not occur simultaneously for all species which suggested that this variance may not be related to environmental factors that are correlated with the seasonal cycle. Variations in the live assemblages were consistent with variations observed in the death assemblages which indicated the death assemblage is not sufficiently-time averaged to negate short-term compositional changes in the modern distributions. It is therefore recommended that for transfer function development both living and dead tests should be counted as these better represent the assemblages that become incorporated into the fossil record. Future investigations which measure a range of environmental variables and their relative effects on live testate amoebae over seasonal cycles are required in order to better understand the factors influencing assemblage variance. Transfer functions were generated which simulated all possible seasonal sampling strategies to investigate the influence on reconstructive performance. Greater accuracies were demonstrated by transfer functions generated from training sets that were collected through repeat sampling encompassing multiple seasons. It is therefore recommended that future studies construct modern training sets of both live and dead testate amoebae data obtained from a repeat sampling strategy.

Modern and fossil testate amoebae assemblages were investigated at Swan Inlet (Falkland Islands) in order to reconstruct sea level. In the modern environment testate amoebae demonstrated a quantifiable vertical distribution along the marsh elevation

gradient, suggesting they are suitable sea-level indicators. The modern distributions in the Falkland Islands were similar to the distributions of salt-marsh testate amoebae observed in North Atlantic salt-marshes suggesting global-scale transfer functions may be possible. Future investigations of salt-marsh distributions in marshes outside of the Atlantic region are needed to test this possibility. Preservation issues were indicated by a lack of idiosomic taxa in the Falkland Islands core samples at depths below 5 cm. This resulted in a lack of modern analogues. Other salt-marsh studies of fossil testate amoebae observed a similar lack of idiosomic tests. Because idiosomic tests often comprise a large proportion of the contemporary upper marsh assemblages, where the most precise sea-level data can be obtained, this observation presents a major limitation of testate amoebae to sea-level studies.

REFERENCES

Adie , R. J. (1953) 'New Evidence of Sea-level Changes in the Falkland Islands'. *Falkland Islands Dependencies Survey Scientific Reports*, No. 9 pp 1-10.

Adl, S. M., Simpson, A. G., Farmer, M. A., Andersen, R. A., Anderson, O. R., Barta, J. R., Bowser, S. S., Brugerolle, G., Fensome, R. A. and Fredericq, S. (2005) 'The new higher level classification of eukaryotes with emphasis on the taxonomy of protists'. *Journal of Eukaryotic Microbiology*, 52 (5). pp 399-451.

Adl, S. M., Leander, B. S., Simpson, A. G., Archibald, J. M., Anderson, O. R., Bass, D., Bowser, S. S., Brugerolle, G., Farmer, M. A. and Karpov, S. (2007) 'Diversity, nomenclature, and taxonomy of protists'. *Systematic Biology*, 56 (4). pp 684-689.

Adl, S. M., Simpson, A. G., Lane, C. E., Lukeš, J., Bass, D., Bowser, S. S., Brown, M. W., Burki, F., Dunthorn, M. and Hampl, V. (2012) 'The revised classification of eukaryotes'. *Journal of Eukaryotic Microbiology*, 59 (5). pp 429-514.

Aldiss, D. and Edwards, E. (1999) 'The geology of the Falkland Islands'. *British Geological Survey Technical Report* WC/99110.

Allen, J. R. L. (1990) 'Constraints on measurement of sea-level movements from salt-marsh accretion rates'. *Journal of the Geological Society*, 147 (1). pp 5-7.

Allen, J. R. L. P., K. (1992) *Saltmarshes: Morphodynamics, conservation and engineering significance.* Cambridge: Cambridge Univserity Press.

Allen, J. R. L. (2000) 'Morphodynamics of Holocene salt marshes: a review sketch from the Atlantic and Southern North Sea coasts of Europe'. *Quaternary Science Reviews*, 19 (12). pp 1155-1231.

Alley, R. B., Mayewski, P. A., Sowers, T., Stuiver, M., Taylor, K. C. and Clark, P. U. (1997) 'Holocene climatic instability: A prominent, widespread event 8200 yr ago'. *Geology*, 25 (6). pp 483-486.

Appleby, P. (2001) 'Chronostratigraphic techniques in recent sediments'. *Tracking environmental change using lake sediments.* Springer, pp 171-203.

Appleby, P. and Oldfield, F. (1992) 'Applications of lead-210 to sedimentation studies'. In: Ivanovich, M and Harmon, R.S. (1992) *Uranium-series disequilibrium: applications to earth, marine, and environmental sciences,* 2nd ed, Clarendon Press, Wotton-under-Edge, UK.

Ball, D. (1964) 'Loss-on-ignition as an estimate of organic matter and organic carbon in non-calcareous soils'. *Journal of Soil Science*, 15 (1). pp 84-92.

Barber, D. C., Dyke, A., Hillaire-Marcel, C., Jennings, A. E., Andrews, J. T., Kerwin, M. W., Bilodeau, G., McNeely, R., Southon, J., Morehead, M. D. and Gagnon, J. M. (1999) 'Forcing of the cold event of 8,200 years ago by catastrophic drainage of Laurentide lakes'. *Nature*, 400 (6742). pp 344-348.

Barbieri, R., (2001) 'Taphonomic implications of foraminiferal composition and abundance in intertidal mud flats, Colorado River delta (Mexico)'. *Micropaleontology,* 47(1), pp.73-86.

Barlow, N. L. M., Shennan, I. and Long, A. J. (2012) 'Relative sea-level response to Little Ice Age ice mass change in south central Alaska: Reconciling model predictions and geological evidence'. *Earth and Planetary Science Letters*, 315–316 pp 62-75.

Barlow, N. L. M., Shennan, I., Long, A. I., Gehrels, W. R., Saher, M. H., Woodroffe, S. A. and Hillier, C. (2013) 'Salt marshes as late Holocene tide gauges'. *Global and Planetary Change*, 106 pp 90-110.

Barlow, N. L. M., Long, A. J., Saher, M. H., Gehrels, W. R., Garnett, M. H. and Scaife, R. G. (2014) 'Salt-marsh reconstructions of relative sea-level change in the North Atlantic during the last 2000 years'. *Quaternary Science Reviews*, 99 pp 1-16.

Barnett, R. L., Charman, D. J., Gehrels, W. R., Saher, M. H. and Marshall, W. A. (2013) 'Testate Amoebae as Sea-level Indicators in Northwestern Norway: Developments in Sample Preparation and Analysis'. *Acta Protozoologica*, 52 (3). pp 115-128.

Barnett, R. L., Gehrels, W. R., Charman, D. J., Saher, M. H. and Marshall, W. A. (2015) 'Late Holocene sea-level change in Arctic Norway'. *Quaternary Science Reviews*, 107 pp 214-230.

Barnett, R. L., Garneau, M. and Bernatchez, P. (2016) 'Salt-marsh sea-level indicators and transfer function development for the Magdalen Islands in the Gulf of St. Lawrence, Canada'. *Marine Micropaleontology*, 122 pp 13-26.

Barnett, R. L., Newton, T. L., Charman, D. J. and Gehrels, W.R (2017) 'Salt-marsh testate amoebae as precise and widespread indicators of sea-level change'. *Earth-Science Reviews*, 164 pp 193-207.

Baskaran, M. (2011) 'Po-210 and Pb-210 as atmospheric tracers and global atmospheric Pb-210 fallout: a review'. *Journal of Environmental Radioactivity*, 102 (5). pp 500-513.

Batterbee, R., Anderson, N. and Appleby, P. (1988) 'Lake acidification in the United Kingdom 1800-1986: evidence from analysis of lake sediments'. Enis, London pp.68.

Batterbee, R., Jones, V., Flower, R., Cameron, N., Bennion, H., Carvalho, L. and Juggins, S. (2001) 'Diatoms'. *Tracking environmental change using lake sediments*, 3 pp 155-202.

Beckett, L. H., Baldwin, A. H. and Kearney, M. S. (2016) 'Tidal Marshes across a Chesapeake Bay Subestuary Are Not Keeping up with Sea-Level Rise'. *PLoS ONE*, 11 (7). pp e0159753.

Bengtsson, L. and Enell, M. (1986) 'Chemical analysis'. *Handbook of Holocene palaeoecology and palaeohydrology*, pp 423-451.

Bennett, K. (1994) 'Confidence intervals for age estimates and deposition times in late-Quaternary sediment sequences'. *The Holocene*, 4 (4). pp 337-348.

Bentley, M. J. and McCulloch, R. D. (2005) 'Impact of neotectonics on the record of glacier and sea level fluctuations, Strait of Magellan, Southern Chile'. *Geografiska Annaler: Series A, Physical Geography*, 87 (2). pp 393-402.

Berkeley, A., Perry, C. T., Smithers, S. G. and Horton, B. P. (2008) 'The spatial and vertical distribution of living (stained) benthic foraminifera from a tropical, intertidal environment, north Queensland, Australia'. *Marine Micropaleontology*, 69 (2). pp 240-261.

Bernhard, J. M., Ostermann, D. R., Williams, D. S. and Blanks, J. K. (2006) 'Comparison of two methods to identify live benthic foraminifera: A test between Rose Bengal and CellTracker Green with implications for stable isotope paleoreconstructions'. *Paleoceanography*, 21 (4).

Beyens, L. and Meisterfeld, R. (2002) 'Protozoa: testate amoebae'. *Tracking environmental change using lake sediments.* Springer, pp 121-153.

Bindoff, N. L., Willebrand, J., Artale, V., Cazenave, A., Gregory, J., Guley, S., Hanawa, K., Le Quéré, C., Levitus, S., Nojiri, Y., Shum, C. K., Talley, L. D. and Unnikrishnan, A. (2007) 'Observations: Oceanic climate change and sea level'. in Solomon, S., Qin, D., Manning, M., Chen, Z., Marquis, M., Averyt, K.B., Tignor, M. and Miller, H.L. (eds.) *Climate Change 2007: The Physical Science Basis.* Cambridge, UK: Cambridge University Press, 5 5 pp pp. 385-432.

Binford, M. W., Kahl, J. S. and Norton, S. A. (1993) 'Interpretation of210Pb profiles and verification of the CRS dating model in PIRLA project lake sediment cores'. *Journal of Paleolimnology*, 9 (3). pp 275-296.

Birks, H. J. B. (1995) 'Quantitative palaeoenvironmental reconstructions'. in Maddy, D. and Brew, J.S. (eds.) *Statistical Modelling of Quaternary Science Data: Technical Guide 5.* Cambridge: Quaternary Research Association, 6 6 pp 161-254.

Birks, H. (1998) 'DG Frey and ES Deevey Review 1: Numerical tools in palaeolimnology–Progress, potentialities, and problems'. *Journal of Paleolimnology*, 20 (4). pp 307-332.

Birks, H. H. and Birks, H. J. B. (2006) 'Multi-proxy studies in palaeolimnology'. *Vegetation history and Archaeobotany*, 15 (4). pp 235-251.

Bittermann, K., Rahmstorf, S., Perrette, M. and Vermeer, M. (2013) 'Predictability of 20th century sea-level rise from past data'. *Environmental Research Letters*, 8 (1) 1-7.

Blaauw, M and Christen, A.J. (2011) 'Flexible paleoclimate age-depth models using an autoregressive gamma process.' *Bayesian Analysis*. 6 (3) 457-474.

Blaauw, M. and Heegaard, E. (2012) 'Estimation of age-depth relationships'. *Tracking environmental change using lake sediments.* Springer, pp 379-413.

Blanco, S., Alvarez, I. and Cejudo, C. (2008) 'A test on different aspects of diatom processing techniques'. *Journal of Applied Phycology*, 20 (4). pp 445-450.

Blytt, A. (1876) ‘Essay on the immigration of the Norwegian flora during alternating rainy and dry periods’ Christiania : A. Cammermeyer.

Booth, R., Lamentowicz, M. and Charman, D. (2010) 'Preparation and analysis of testate amoebae in peatland paleoenvironmental studies'. *Mires and Peat*, 7 (02). pp 1-7.

Booth, R. and Sullivan, M. (2007) 'Key of testate amoebae inhabiting Sphagnum-dominated peatlands with an emphasis on taxa preserved in Holocene sediments'. Technical guide. Lehigh University, Bethlehem, Pennysylvania, USA.

Bradley, S. L., Milne, G. A., Shennan, I. and Edwards, R. (2011) 'An improved glacial isostatic adjustment model for the British Isles'. *Journal of Quaternary Science*, 26 (5). pp 541-552.

Bradley, S. L., Milne, G. A., Horton, B. P. and Zong, Y. (2016) 'Modelling sea level data from China and Malay-Thailand to estimate Holocene ice-volume equivalent sea level change'. *Quaternary Science Reviews*, 137 pp 54-68.

Brain, M. J. (2006) *Autocompaction of mineralogenic intertidal sediments.* PhD thesis, University of Durham, UK.

Brain, M. J. (2015) 'Compaction'. *Handbook of Sea-Level Research*, pp 452-469.

Brain, M. J., Long, A. J., Petley, D. N., Horton, B. P. and Allison, R. J. (2011) 'Compression behaviour of minerogenic low energy intertidal sediments'. *Sedimentary Geology*, 233 (1-4). pp 28-41.

Brain, M. J., Long, A. J., Woodroffe, S. A., Petley, D. N., Milledge, D. G. and Parnell, A. C. (2012) 'Modelling the effects of sediment compaction on salt marsh reconstructions of recent sea-level rise'. *Earth and Planetary Science Letters*, 345 pp 180-193.

Brain, M. J., Kemp, A. C., Horton, B. P., Culver, S. J., Parnell, A. C. and Cahill, N. (2015) 'Quantifying the contribution of sediment compaction to late Holocene salt-marsh sea-level reconstructions, North Carolina, USA'. *Quaternary Research*, 83 (1). pp 41-51.

Bronk-Ramsey, C. (2009) 'Bayesian analysis of radiocarbon dates'. *Radiocarbon*, 51 (1). pp 337-360.

Buzas, M. A., Hayek, L.-A. C., Reed, S. A. and Jett, J. A. (2002) 'FORAMINIFERAL DENSITIES OVER FIVE YEARS IN THE INDIAN RIVER LAGOON, FLORIDA: A MODEL OF PULSATING PATCHES'. *The Journal of Foraminiferal Research*, 32 (1). pp 68-92.

Cahill, N., Kemp, A. C., Horton, B. P. and Parnell, A. C. (2015) 'Modeling sea-level change using errors-in-variables integrated Gaussian processes'. *The Annals of Applied Statistics*, 9 (2). pp 547-571.

Callard, S. L., Gehrels, W. R., Morrison, B. V. and Grenfell, H. R. (2011) 'Suitability of salt-marsh foraminifera as proxy indicators of sea level in Tasmania'. *Marine Micropaleontology*, 79 (3-4). pp 121-131.

Camacho, S., Connor, S., Asioli, A., Boski, T. and Scott, D. (2015) 'Testate amoebae and tintinnids as spatial and seasonal indicators in the intertidal margins of Guadiana Estuary (southeastern Portugal)'. *Ecological Indicators*, 58 pp 426-444.

Cambray, R. S., Cawse, P., Garland, J., Gibson, J. A. B., Johnson, P., Lewis, G., Newton, D., Salmon, L. and Wade, B. (1987) 'Observations on radioactivity from the Chernobyl accident'. *Nuclear energy*, 26 (2). pp 77-101.

Carlin, B.P., Gelfand, A.E. and Smith, A.F., (1992) 'Hierarchical Bayesian analysis of changepoint problems'*. Applied statistics*, pp.389-405.

Cavalier-Smith, T. (2002) 'The phagotrophic origin of eukaryotes and phylogenetic classification of Protozoa'. *International journal of systematic and evolutionary microbiology*, 52 (2). pp 297-354.

Cavalier-Smith, T. (2010) 'Origin of the cell nucleus, mitosis and sex: roles of intracellular coevolution'. *Biology direct*, 5 (1). pp 1.

Charman, D.J. (1999) Biodiversity and fossil testate amoebae. Journal of Biogeography, 26,89-96.

Charman, D.J. (2015) 'Testate amoebae'. *Handbook of Sea-Level Research*, pp 281-294.

Charman, D.J. and Warner, B.G. (1992) 'Relationship between testate amoebae (Protozoa: Rhizopoda) and microenvironmental parameters on a forested peatland in northeastern Ontario'. *Canadian Journal of Zoology*, 70 (12). pp 2474-2482.

Charman, D. J. and Warner, B. G. (1997) 'The ecology of testate amoebae (Protozoa: Rhizopoda) in oceanic peatlands in Newfoundland, Canada: modelling hydrological relationships for palaeoenvironmental reconstruction'. *Ecoscience*, 4 (4). pp 555-562.

Charman, D. J., Roe, H. M. and Gehrels, W. R. (1998) 'The use of testate amoebae in studies of sea-level change: a case study from the Taf Estuary, south Wales, UK'. *Holocene*, 8 (2). pp 209-218.

Charman, D. J., Hendon, D. and Woodland, W. A. (2000) *The Identification of Testate Amoebae (Protozoa: Rhizopoda) in Peats.* Issue 9 of Technical Guide. Quaternary Research Association.

Charman, D. J., Roe, H. M. and Gehrels, W. R. (2002) 'Modern distribution of saltmarsh testate amoebae: regional variability of zonation and response to environmental variables'. *Journal of Quaternary Science*, 17 (5-6). pp 387-409.

Charman, D. J., Gehrels, W. R., Manning, C. and Sharma, C. (2010) 'Reconstruction of recent sea-level change using testate amoebae'. *Quaternary Research*, 73 (2). pp 208-219.

Christen, J. A. (1994) 'Summarizing a set of radiocarbon determinations: a robust approach'. *Applied Statistics*, pp 489-503.

Christen, J. A. and P´erez, S. (2009). 'A new robust statistical model for radiocarbon data'. *Radiocarbon*, 51(3): 1047–1059.

Church, J., A., Clark, P. U., Cazenave, A., Gregory, J. M., Jevrejeva, S., Levermann, A., Merrifield, M. A., Milne , G. A., Nerem, S. R., Nunn, P., Payne, A. J., Pfeffer, T. W., Stammer, D. and Unnikrishnan, A. S. (2013) 'Sea Level Change'. in Ipcc (ed.) *Climate Change 2013 The Physical Science Basis.* Cambridge, United Kingdom: Cambridge University Press.

Church, J. A., Gregory, J. M., Huybrechts, P., Kuhn, M., Lambeck, K., Nhuan, M. T., Qin, D. and Woodworth, P. L. (2001) 'Changes in sea level'. *Climate change 2001: The scientific basis. Contribution of Working Group I to the Third Assessment Report of the Intergovernmental Panel on Climate Change*, pp 639-693.

Church, J. A. and White, N. J. (2006) 'A 20th century acceleration in global sea-level rise'. *Geophysical Research Letters*, 33 pp L01602.

Clark, J.A., Farrell, W.E. and Peltier, W.R., (1978) 'Global changes in postglacial sea level: a numerical calculation'. *Quaternary research*, 9(3): 265-287.

Clark, P. U. and Mix, A. C. (2002) 'Ice sheets and sea level of the Last Glacial Maximum'. *Quaternary Science Reviews*, 21 (1–3). pp 1-7.

Corbett, D. R. and Walsh, J. (2015) '210lead and 137cesium'. *Handbook of Sea-Level Research*, pp 361-372.

Craft, C., Clough, J., Ehman, J., Joye, S., Park, R., Pennings, S., Guo, H. and Machmuller, M. (2009) 'Forecasting the effects of accelerated sea-level rise on tidal marsh ecosystem services'. *Frontiers in Ecology and the Environment*, 7 (2). pp 73-78.

Culver, S. J. and Horton, B. P. (2005) 'Infaunal marsh foraminifera from the outer banks, North Carolina, USA'. *Journal of Foraminiferal Research*, 35 (2). pp 148-170.

Culver, S. J. and Lipps, J. H. (2003) 'Predation on and by Foraminifera'. *Predator—Prey Interactions in the Fossil Record.* Springer, pp 7-32.

Daley, T. J., Thomas, E. R., Holmes, J. A., Street-Perrott, F. A., Chapman, M. R., Tindall, J. C., Valdes, P. J., Loader, N. J., Marshall, J. D., Wolff, E. W., Hopley, P. J., Atkinson, T., Barber, K. E., Fisher, E. H., Robertson, I., Hughes, P. D. M. and Roberts, C. N. (2011) 'The 8200 yr BP cold event in stable isotope records from the North Atlantic region'. *Global and Planetary Change*, 79 (3–4). pp 288-302.

de Rijk, S. (1995) 'Salinity control on the distribution of salt marsh foraminifera (Great Marshes, Massachusetts)'. *The Journal of Foraminiferal Research*, 25 (2). pp 156-166.

De Vernal, A., Rochon, A., Turon, J.-L. and Matthiessen, J. (1997) 'Organic-walled dinoflagellate cysts: palynological tracers of sea-surface conditions in middle to high latitude marine environments'. *Geobios*, 30 (7). pp 905-920.

Dean Jr, W. E. (1974) 'Determination of carbonate and organic matter in calcareous sediments and sedimentary rocks by loss on ignition: comparison with other methods'. *Journal of Sedimentary Research*, 44 (1).

Donnelly, J. P. and Bertness, M. D. (2001) 'Rapid shoreward encroachment of salt marsh cordgrass in response to accelerated sea-level rise'. *Proceedings of the National Academy of Sciences*, 98 (25). pp 14218-14223.

Donnelly, J. P., Cleary, P., Newby, P. and Ettinger, R. (2004) 'Coupling instrumental and geological records of sea-level change: Evidence from southern New England of an increase in the rate of sea-level rise in the late 19th century'. *Geophysical Research Letters*, 31 (5).

Douglas, B. C. (2001) 'Sea level change in the era of the recording tide gauge'. *Sea Level Rise, History and Consequences, International Geophysics Series*, 75 pp 37-64.

du Châtelet, E. A., Guillot, F., Recourt, P., Ventalon, S. and Tribovillard, N. (2010) 'Influence of sediment grain size and mineralogy on testate amoebae test construction'. *Comptes Rendus Geoscience*, 342 (9). pp 710–717.

Dutton, A., Carlson, A. E., Long, A. J., Milne, G. A., Clark, P. U., DeConto, R., Horton, B. P., Rahmstorf, S. and Raymo, M. E. (2015) 'Sea-level rise due to polar ice-sheet mass loss during past warm periods'. *Science*, 349 (6244).

Edwards, R.J. and Wright, A. (2015) 'Foraminifera'. *Handbook of Sea-Level Research.* John Wiley and Sons, Ltd, pp 191-217.

Edwards, R. J. (2006) 'Mid-to late-Holocene relative sea-level change in southwest Britain and the influence of sediment compaction'. *The Holocene*, 16 (4). pp 575-587.

Edwards, R. J. and Horton, B. P. (2000) 'Reconstructing relative sea-level change using UK salt-marsh foraminifera'. *Marine Geology*, 169 (1-2). pp 41-56.

Edwards, R. J. and Horton, B. P. (2006) 'Developing detailed records of relative sea-level change using a foraminiferal transfer function: an example from North Norfolk, UK'. *Philosophical Transactions of the Royal Society a-Mathematical Physical and Engineering Sciences*, 364 (1841). pp 973-991.

Edwards, R. J., van de Plassche, O., Gehrels, W. R. and Wright, A. J. (2004) 'Assessing sea-level data from Connecticut, USA, using a foraminiferal transfer function for tide level'. *Marine Micropaleontology*, 51 (3-4). pp 239-255.

Elliott, E. (2015) *Holocene sea-level change at the Steart Peninsula, Somerset: Development and application of a multi-proxy sea-level transfer function for the Severn Estuary region.* PhD, University of the West of England. Available from: http://eprints.uwe.ac.uk/26508

Emery, K. and Hülsemann, J. (1964) 'Shortening of Sediment Cores Collected in Open Barrel Gravity CORERS1'. *Sedimentology*, 3 (2). pp 144-154.

Engelhart, S. E., Horton, B. P., Douglas, B. C., Peltier, W. R. and Toernqvist, T. E. (2009) 'Spatial variability of late Holocene and 20(th) century sea-level rise along the Atlantic coast of the United States'. *Geology*, 37 (12). pp 1115-1118.

Fadil, A., Denys, P., Tenzer, R., Grenfell, H. R. and Willis, P. (2013) 'New Zealand 20th century sea level rise: Resolving the vertical land motion using space geodetic

and geological data'. *Journal of Geophysical Research: Oceans,* 118 (11). pp 6076-6091.

Farrell, W. E. and Clark, J. A. (1976) 'On postglacial sea level'. Geophysical Journal of the Royal Astronomical Society, 46 (3). pp 647-667.

Fatela, F. and Taborda, R. (2002) 'Confidence limits of species proportions in microfossil assemblages'. *Marine Micropaleontology*, 45 (2). pp 169-174.

Figueira, B. O., Grenfell, H. R., Hayward, B. W. and Alfaro, A. C. (2012) 'Comparison of Rose Bengal and CellTracker Green staining for identification of live salt-marsh foraminifera'. *The Journal of Foraminiferal Research*, 42 (3). pp 206-215.

Flower, R. (1993) 'Diatom preservation: experiments and observations on dissolution and breakage in modern and fossil material'. *Hydrobiologia*, 269-270 (1). pp 473-484.

French, J. (2006) 'Tidal marsh sedimentation and resilience to environmental change: Exploratory modelling of tidal, sea-level and sediment supply forcing in predominantly allochthonous systems'. *Marine Geology*, 235 (1–4). pp 119-136.

Gale, S., Haworth, R. and Pisanu, P. (1995) 'The 210 Pb chronology of late Holocene deposition in an eastern Australian lake basin'. *Quaternary Science Reviews*, 14 (4). pp 395-408.

Gehrels, W. R. (1994) 'Determining relative sea-level change from salt-marsh foraminifera and plant zones on the coast of Maine, USA'. *Journal of Coastal Research*, pp 990-1009.

Gehrels, W. R. (1999) 'Middle and late holocene sea-level changes in Eastern Maine reconstructed from foraminiferal saltmarsh stratigraphy and AMS C-14 dates on basal peat'. *Quaternary Research*, 52 (3). pp 350-359.

Gehrels, W. R. (2000) 'Using foraminiferal transfer functions to produce high-resolution sea-level records from salt-marsh deposits, Maine, USA'. *Holocene*, 10 (3). pp 367-376.

Gehrels, W. R. (2010) 'Late Holocene land- and sea-level changes in the British Isles: implications for future sea-level predictions'. *Quaternary Science Reviews*, 29 (13-14). pp 1648-1660.

Gehrels, W. R. and Woodworth, P. L. (2013) 'When did modern rates of sea-level rise start?'. *Global and Planetary Change*, 100 pp 263-277.

Gehrels, W. R. and Anderson, W. P., Jr. (2014) 'Reconstructing Holocene sea-level change from coastal freshwater peat: A combined empirical and model-based approach'. *Marine Geology*, 353 pp 140-152.

Gehrels, W. R., Belknap, D. F. and Kelley, J. T. (1996) 'Integrated high-precision analyses of Holocene relative sea-level changes: Lessons from the coast of Maine'. *Geological Society of America Bulletin*, 108 (9). pp 1073-1088.

Gehrels, W. R., Roe, H. M. and Charman, D. J. (2001) 'Foraminifera, testate amoebae and diatoms as sea-level indicators in UK saltmarshes: a quantitative multiproxy approach'. *Journal of Quaternary Science*, 16 (3). pp 201-220.

Gehrels, W. R., Roe, H. M. and Charman, D. J. (2002) 'Foraminifera, testate amoebae and diatoms as sea-level indicators in UK saltmarshes: a quantitative multiproxy approach (vol 16, pg 201, 2001)'. *Journal of Quaternary Science*, 17 (3). pp 285-285.

Gehrels, W. R., Milne, G. A., Kirby, J. R., Patterson, R. T. and Belknap, D. F. (2004) 'Late Holocene sea-level changes and isostatic crustal movements in Atlantic Canada'. *Quaternary International*, 120 pp 79-89.

Gehrels, W. R., Kirby, J. R., Prokoph, A., Newnham, R. M., Achterberg, E. P., Evans, H., Black, S. and Scott, D. B. (2005) 'Onset of recent rapid sea-level rise in the western Atlantic Ocean'. *Quaternary Science Reviews*, 24 (18-19). pp 2083-2100.

Gehrels, W.R. Larsen, G., Kirby, J. R., Eiriksson, J., Heinemeier, J. and Shimmield, T. (2006a) 'Rapid sea-level rise in the North Atlantic Ocean since the first half of the nineteenth century'. *Holocene*, 16 (7). pp 949-965.

Gehrels, W. R., Hendon, D. and Charman, D. J. (2006b) 'Distribution of testate amoebae in salt marshes along the North American East Coast'. *Journal of Foraminiferal Research*, 36 (3). pp 201-214.

Gehrels, W. R., Hayward, B., Newnham, R. M. and Southall, K. E. (2008) 'A 20th century acceleration of sea-level rise in New Zealand'. *Geophysical Research Letters*, 35 (2).

Gehrels, W. R., Dawson, D. A., Shaw, J. and Marshall, W. A. (2011) 'Using Holocene relative sea-level data to inform future sea-level predictions: An example from southwest England'. *Global and Planetary Change*, 78 (3-4). pp 116-126.

Gehrels, W. R., Callard, S. L., Moss, P. T., Marshall, W. A., Blaauw, M., Hunter, J., Milton, J. A. and Garnett, M. H. (2012) 'Nineteenth and twentieth century sea-level changes in Tasmania and New Zealand'. *Earth and Planetary Science Letters*, 315 pp 94-102.

Gilbert, D., Mitchell, E. A., Bourdier, G. and Francez, A.-J. (2003) 'Population dynamics and food preferences of the testate amoeba Nebela tincta major-bohemica-collaris complex (Protozoa) in a Sphagnum peatland'. *Acta Protozoologica*, 42 (2). pp 99-104.

Goodwin, I. D. and Harvey, N. (2008). 'Subtropical sea-level history from coral microatolls in the Southern Cook Islands, since 300 AD'. *Marine Geology*, 253, 14–25.

Goodsite, M. E. R., W.,Heinemeier, J.,Lange, T.,Ooi, S. ,Appleby, P.G.,Shotyk, W.,van der Knaap, W.O.,Lohse, C.Hansen, T.S. (2001) 'High-resolution AMS C-14 dating of post-bomb peat archives of atmospheric pollutants'. *Radiocarbon*, 43 pp 495-515.

Grimm, E. C. (1987) 'CONISS - A Fortran program for stratigraphcially coinstrained cluster-analysis bu the method of incremental sun of squares'. *Computers and Geosciences*, 13 (1). pp 13-35.

Grimm, E. C. (1990) 'Tilia and Tilia Graph: PC Spreadsheet and Graphics Software for Pollen Data'. *INQUA Working Group on Data-Handling Methods*, Newsletter 4.

Grinsted A., Moore J.C. and Jevrejeva S. (2009) ‘Reconstructing sea level from paleo and projected temperatures 200 to 2100 AD’. *Climate Dynnamics,* 34:461–472.

Guilbault, J.-P., Clague, J. J. and Lapointe, M. (1995) 'Amount of subsidence during a late Holocene earthquake—Evidence from fossil tidal marsh foraminifera at Vancouver Island, west coast of Canada'. Palaeogeography, Palaeoclimatology, Palaeoecology, 118 (1). pp 49-71.

Guilbault, J.-P. and Patterson, R. (2000) 'Correlation between marsh foraminiferal distribution and elevation in coastal British Columbia, Canada', *Proceedings of the Fifth International Workshop on Agglutinated Foraminifera. Grzybowski Foundation Special Publication*. pp. 117-125.

Harvey, M., Hansom, J. and MacKenzie, A. (2007) 'Constraints on the use of anthropogenic radionuclide-derived chronologies for saltmarsh sediments'. *Journal of Environmental Radioactivity*, 95 (2). pp 126-148.

Hatté, C. and Jull, A. (2007) 'Radiocarbon Dating| Plant Macrofossils'. In Elias, S. A. eds *Encyclopedia of Quaternary Science*. pp2958-2965.

Hawkes, A. D., Horton, B., Nelson, A. and Hill, D. (2010) 'The application of intertidal foraminifera to reconstruct coastal subsidence during the giant Cascadia earthquake of AD 1700 in Oregon, USA'. *Quaternary International*, 221 (1). pp 116-140.

Haynes, S. (2011) ‘Salt-marsh testate amoebae as sea-level indicators: Vidarholmi marsh, western Iceland’. MSc thesis, Plymouth University, UK.

Heal, O. (1962) 'The abundance and micro-distribution of testate amoebae (Rhizopoda: Testacea) in Sphagnum'. *Oikos*, pp 35-47.

Heiri, O., Lotter, A.F. and Lemcke, G., (2001) ‘Loss on ignition as a method for estimating organic and carbonate content in sediments: reproducibility and comparability of results’. *Journal of paleolimnology*, 25(1), pp.101-110.

Hendon, D. and Charman, D. J. (1997) 'The preparation of testate amoebae (Protozoa: Rhizopoda) samples from peat'. *The Holocene*, 7 (2). pp 199-205.

Hijma, M. P. and Cohen, K. M. (2010) 'Timing and magnitude of the sea-level jump preluding the 8200 yr event'. *Geology*, 38 (3). pp 275-278.

Hill, M. O. (1973) 'Diversity and evenness: a unifying notation and its consequences'. *Ecology*, 54 (2). pp 427-432.

Hill, T. C. B., Woodland, W. A., Spencer, C. D. and Marriott, S. B. (2007) 'Holocene sea-level change in the Severn Estuary, southwest England: a diatom-based sea-level transfer function for macrotidal settings'. *Holocene*, 17 (5). pp 639-648.

Hippensteel, S. P., Martin, R. E., Nikitina, D. and Pizzuto, J. E. (2000) 'The formation of Holocene marsh foraminiferal assemblages, middle Atlantic coast, USA: implications for Holocene sea-level change'. *The Journal of Foraminiferal Research*, 30 (4). pp 272-293.

Hippensteel, S. P., Martin, R. E., Nikitina, D. and Pizzuto, J. E. (2002) 'Interannual variation of marsh foraminiferal assemblages (Bombay Hook National Wildlife

Refuge, Smyrna, DE): Do foraminiferal assemblages have a memory?'. *The Journal of Foraminiferal Research*, 32 (2). pp 97-109.

Hogg, A. G., Hua, Q., Blackwell, P. G., Niu, M., Buck, C. E., Guilderson, T. P., Heaton, T. J., Palmer, J. G., Reimer, P. J., Reimer, R. W., Turney, C. S. M. and Zimmerman, S. R. H. (2013) 'SHCal13 Sotuhern Hemisphere Calibration, 0-50,000 years cal. BP'. *Radiocarbon*, 55 (4). pp 1889-1903.

Holgate, S. J., Matthews, A., Woodworth, P. L., Rickards, L. J., Tamisiea, M. E., Bradshaw, E., Foden, P. R., Gordon, K. M., Jevrejeva, S. and Pugh, J. (2013) 'New data systems and products at the permanent service for mean sea level'. *Journal of Coastal Research*, 29 (3). pp 493-504.

Höök, M. and Tang, X. (2013) 'Depletion of fossil fuels and anthropogenic climate change—A review'. *Energy Policy*, 52 pp 797-809.

Horton, B. P. and Edwards, R.J. (2003) 'Seasonal Distributions of Foraminifera and Their Implications for Sea-Level Studies, Cowpen Marsh, UK'. *Society for Sedimentary Geology Special Publications*.

Horton, B. P. and Edwards, R. J. (2005) 'The application of local and regional transfer functions to the reconstruction of Holocene sea levels, north Norfolk, England'. *Holocene*, 15 (2). pp 216-228.

Horton, B. P. and Murray, J. W. (2006) 'Patterns in cumulative increase in live and dead species from foraminiferal time series of Cowpen Marsh, Tees Estuary, UK: Implications for sea-level studies'. *Marine Micropaleontology*, 58 (4). pp 287-315.

Horton, B. P. and Shennan, I. (2009) 'Compaction of Holocene strata and the implications for relative sea-level change on the east coast of England'. *Geology*, 37 (12). pp 1083-1086.

Horton, B. P., Edwards, R. J. and Lloyd, J. M. (1999) 'A foraminiferal-based transfer function: Implications for sea-level studies'. *Journal of Foraminiferal Research*, 29 (2). pp 117-129.

Horton, B. P., Innes, J. B., Shennan, I., Lloyd, J. M. and McArthur, J. J. (2004) 'Holocene coastal change in East Norfolk, UK: palaeoenvironmental data from Somerton and Winterton Holmes, near Horsey'. *Proceedings of the Geologists Association*, 115 pp 209-220.

Horton, B., Sawai, Y., Smol, J. and Stoermer, E. (2010) 'Diatoms as indicators of former sea levels, earthquakes, tsunamis, and hurricanes'. *The diatoms: applications for the Environmental and Earth Sciences*, (Ed. 2). pp 357-372.

Hua, Q. (2009) 'Radiocarbon: a chronological tool for the recent past'. *Quaternary Geochronology*, 4 (5). pp 378-390.

Hua, Q. and Barbetti, M. (2004) 'Review of tropospheric bomb C-14 data for carbon cycle modeling and age calibration purposes'. *Radiocarbon*, 46 (3). pp 1273-1298.

Hua, Q., Barbetti, M. and Rakowski, A. Z. (2013) 'Atmospheric radiocarbon for the period 1950–2010'. *Radiocarbon*, 55 (4). pp 2059-2072.

Imbrie, J. K. and Kipp, N.G. (1971) 'A new micropaleontological method for paleoclimatology: Application to a Late Pleistocene Caribbean core'. in Foster-Flint, R.T., K.K. (ed.) *The Late Cenozoic Glacial Ages.* New Haven: Yale Univeristy Press.

Jackson, S. T. and Williams, J. W. (2004) 'Modern analogs in Quaternary paleoecology: Here today, gone yesterday, gone tomorrow?'. *Annual Review of Earth and Planetary Sciences*, 32 pp 495-537.

Jassey, V. E., Shimano, S., Dupuy, C., Toussaint, M.-L. and Gilbert, D. (2012) 'Characterizing the feeding habits of the testate amoebae Hyalosphenia papilio and Nebela tincta along a narrow “fen-bog” gradient using digestive vacuole content and 13 C and 15 N isotopic analyses'. *Protist*, 163 (3). pp 451-464.

Jevrejeva, S., Moore, J. C., Grinsted, A. and Woodworth, P. L. (2008) 'Recent global sea level acceleration started over 200 years ago?'. *Geophysical Research Letters*, 35 (8). pp L08715.

Jonasson, K. E. and Patterson, R. T. (1992) 'Preservation potential of salt marsh foraminifera from the Fraser River delta, British Columbia'. *Micropaleontology*, pp 289-301.

Jones, V. J. and Juggins, S. (1995) 'The construction of a diatom-based chlorophyll a transfer function and its application at three lakes on Signy Island (maritime Antarctic) subject to differing degrees of nutrient enrichment'. *Freshwater Biology*, 34 (3). pp 433-445.

Jongman, R. H., ter Braak, C. J. and van Tongeren, O. F. (1995) *Data analysis in community and landscape ecology.* vol. 2. Cambridge university press Cambridge.

Juggins, S. (2003) *C2 User Guide.* Software for Ecological and Palaeoecological Data Analysis and Visualisation. Newcastle-upon-Tyne, UK: University of Newcastle.

Juggins, S. (2015) 'rioja: Analysis of Quaternary Science Data, R package version (0.9-5)'.

Juggins, S. and Birks, H. J. (2012) 'Quantitative Environmental Reconstructions from Biological Data'. in Birks, H.J.B., Lotter, A.F., Juggins, S. and Smol, J.P. (eds.) *Tracking environmental change using lake sediments.* Springer Netherlands, 14 14 pp 431-494.

Jull, A. (2007) 'RADIOCARBON DATING| AMS Method'. In Elias, S. A. eds *Encyclopedia of Quaternary Science*. pp2958-2965.

Kaye, C. A. and Barghoorn, E. S. (1964) 'Late Quaternary sea-level change and crustal rise at Boston, Massachusetts, with notes on the autocompaction of peat'. *Geological Society of America Bulletin*, 75 (2). pp 63-80.

Kemp, A. C. and Telford, R. J. (2015) 'Transfer functions'. *Handbook of Sea-Level Research: John Wiley and Sons, Chichester*, pp 470-499.

Kemp, A. C., Horton, B. P., Culver, S. J., Corbett, D. R., van de Plassche, O., Gehrels, W. R., Douglas, B. C. and Parnell, A. C. (2009a) 'Timing and magnitude of recent accelerated sea-level rise (North Carolina, United States)'. *Geology*, 37 (11). pp 1035-1038.

Kemp, A. C., Horton, B. R., Corbett, D. R., Culver, S. J., Edwards, R. J. and van de Plassche, O. (2009b) 'The relative utility of foraminifera and diatoms for reconstructing late Holocene sea-level change in North Carolina, USA'. *Quaternary Research*, 71 (1). pp 9-21.

Kemp, A. C., Horton, B. P., Donnelly, J. P., Mann, M. E., Vermeer, M. and Rahmstorf, S. (2011) 'Climate related sea-level variations over the past two millennia'. *Proceedings of the National Academy of Sciences of the United States of America*, 108 (27). pp 11017-11022.

Kemp, A. C., Horton, B. P., Vane, C. H., Bernhardt, C. E., Corbett, D. R., Engelhart, S. E., Anisfeld, S. C., Parnell, A. C. and Cahill, N. (2013) 'Sea-level change during the last 2500 years in New Jersey, USA'. Quaternary Science Reviews, 81 pp 90-104.

Kemp, A. C., Bernhardt, C. E., Horton, B. P., Kopp, R. E., Vane, C. H., Peltier, W. R., Hawkes, A. D., Donnelly, J. P., Parnell, A. C. and Cahill, N. (2014) 'Late Holocene sea- and land-level change on the US southeastern Atlantic coast'. *Marine Geology*, 357 pp 90-100.

Kendall, R. A., Mitrovica, J. X., Milne, G. A., Törnqvist, T. E. and Li, Y. (2008) 'The sea-level fingerprint of the 8.2 ka climate event'. *Geology*, 36 (5). pp 423-426.

Kidson, C. and Heyworth, A. (1976) 'The Quaternary deposits of the Somerset Levels'. *Quarterly Journal of Engineering Geology and Hydrogeology*, 9 (3). pp 217-235.

Kim, S.-H., Kelly, P. B. and Clifford, A. J. (2009) 'Accelerator mass spectrometry targets of submilligram carbonaceous samples using the high-throughput Zn reduction method'. *Analytical chemistry*, 81 (14). pp 5949-5954.

Kirwan, M. L., Guntenspergen, G. R., D'Alpaos, A., Morris, J. T., Mudd, S. M. and Temmerman, S. (2010) 'Limits on the adaptability of coastal marshes to rising sea level'. *Geophysical Research Letters*, 37 (23).

Kirwan, M. L. and Megonigal, J. P. (2013) 'Tidal wetland stability in the face of human impacts and sea-level rise'. *Nature*, 504 (7478). pp 53-60.

Knott, J. F., Nuttle, W. K. and Hemond, H. F. (1987) 'Hydrologic parameters of salt marsh peat'. *Hydrological Processes*, 1 (2). pp 211-220.

Kopp, R. E., Mitrovica, J. X., Griffies, S. M., Yin, J. J., Hay, C. C. and Stouffer, R. J. (2010) 'The impact of Greenland melt on local sea levels: a partially coupled analysis of dynamic and static equilibrium effects in idealized water-hosing experiments'. *Climatic Change*, 103 (3). pp 619-625.

Kopp, R. E., Kemp, A. C., Bittermann, K., Horton, B. P., Donnelly, J. P., Gehrels, W. R., Hay, C. C., Mitrovica, J. X., Morrow, E. D. and Rahmstorf, S. (2016) 'Temperature-driven global sea-level variability in the Common Era'. *Proceedings of the National Academy of Sciences*, 113 (11). pp E1434-E1441.

Kosakyan, A., Gomaa, F., Mitchell, E. A., Heger, T. J. and Lara, E. (2013) 'Using DNA-barcoding for sorting out protist species complexes: a case study of the Nebela

tincta–collaris–bohemica group (Amoebozoa; Arcellinida, Hyalospheniidae)'. *European journal of protistology*, 49 (2). pp 222-237.

Krammer, K. and Lange-Bertalot, H. (1991a) 'Bacillariophyceae 4.Teil, Achnantaceae. Kritische Erganzungen zu Navicula (Lineolatae) vmd Gomphonema. '. in Ettl, H., Gartner, G., Gerloff, J., Heynig, H. and Mollenhauer, D. (eds.) *Susswasserflora von Mitteleuropa. Band 2/4. .* Stuttgart: Gustav Fischer Verlag.

Krammer, K. and Lange-Bertalot, H. (1991b) 'Bacillariophyceae ,3.Teil Centrales, Fragilariaceae, Eunotiaceae'. in Ettl, J., Gerloff, H., Heynig, H. and Mollenhauer, D. (eds.) *Siisswasserflora von Mitteleuropa. Band 2/3.* Stuttgart: Gustav Fischer Verlag.

Krammer, K. and Lange-Bertalot, H. (1997a) 'Bacillariophyceae, 1 .Teil, Naviculaceae'. in Ettl, H., Gerloff, H.J., Heynig, H. and Mollenhauer, D. (eds.) *Susswasserflora von Mitteleuropa, Band 2/1. .* Jena: Gustav Fischer.

Krammer, K. and Lange-Bertalot, H. (1997b) 'Bacillariophyceae, 2.Teil Bacillariaceae, Epithemiaceae, Surirellaceae'. in Ettl, H., Gerloff, H.J., Heynig, H. and Mollenhauer, D. (eds.) *Susswasserflora von Mitteleuropa, Band 2/2. .* Jena: Gustav Fischer.

Lagerheim, G. (1902) 'Untersuchungen über fossile Algen, I, II'. GFF, 24 (7). pp 475-500.

Lambeck, K., (1989) 'The Earth's Variable Rotation: Some Geophysical Causes'. In *Reference Frames*. pp. 241-284. Springer Netherlands.

Lambeck, K., Smither, C. and Ekman, M. (1998) 'Tests of glacial rebound models for Fennoscandinavia based on instrumented sea- and lake-level records'. *Geophysical Journal International*, 135 (2). pp 375-387.

Lambeck, K., Rouby, H., Purcell, A., Sun, Y. and Sambridge, M. (2014) 'Sea level and global ice volumes from the Last Glacial Maximum to the Holocene'. *Proceedings of the National Academy of Sciences*, 111 (43). pp 15296-15303.

Lambeck, K. P., A., Zhao, S. (2017) 'Inferences about the North American Late Wisconsin ice sheet and mantle viscosity from glacial rebound analyses.'. *Quaternary Science Reviews*,

Lamentowicz, M. and Mitchell, E. A. (2007) 'Testate amoebae as ecological and palaeohydrological indicators in peatlands—the Polish experience'. Wetlands: Monitoring, Modelling and Management. Taylor and Francis, New York, pp 85-90.

Lawrence, T. and Long, A.J. and Gehrels, W.R. and Jackson, L. and Smith, D.E. (2016) 'Relative sea-level data from southwest Scotland constrain meltwater-driven sea-level jumps prior to the 8.2 kyr BP event.', *Quaternary science reviews.*

Laybourn, G. and Whymant, L., (1980) 'The effect of diet and temperature on reproductive rate in Arcella vulgaris Ehrenberg (Sarcodina: Testacida)'. *Oecologia*, 45(2),282-284.

Legendre, P. and Fortin, M. J. (1989) 'Spatial pattern and ecological analysis'. Vegetatio, 80 (2). pp 107-138.

Legendre, P. and Birks, H. J. B. (2012) 'From classical to canonical ordination'. *Tracking environmental change using lake sediments.* Springer, pp 201-248.

Leorri, E., Cearreta, A. and Horton, B. P. (2008) 'A foraminifera-based transfer function as a tool for sea-level reconstructions in the southern Bay of Biscay'. *Geobios*, 41 (6). pp 787-797.

Lepš, J. and Šmilauer, P. (2003) 'Multivariate analysis of ecological data using CANOCO'. Cambridge university press, Cambridge, UK.

Li, Y.-X., Törnqvist, T. E., Nevitt, J. M. and Kohl, B. (2012) 'Synchronizing a sea-level jump, final Lake Agassiz drainage, and abrupt cooling 8200 years ago'. *Earth and Planetary Science Letters*, 315–316 pp 41-50.

Lipps, J. H. (1988) 'Predation on foraminifera by coral reef fish: taphonomic and evolutionary implications'. *Palaios*, pp 315-326.

Long, A. J., Woodroffe, S. A., Milne, G. A., Bryant, C. L. and Wake, L. M. (2010) 'Relative sea level change in west Greenland during the last millennium'. *Quaternary Science Reviews*, 29 (3–4). pp 367-383.

Long, A. J., Roberts, D. H. and Rasch, M. (2003) 'New observations on the relative sea level and deglacial history of Greenland from Innaarsuit, Disko Bugt'. *Quaternary Research*, 60 (2). pp 162-171.

Long, A. J., Woodroffe, S. A., Milne, G. A., Bryant, C. L., Simpson, M. J. R. and Wake, L. M. (2012) 'Relative sea-level change in Greenland during the last 700 yrs and ice sheet response to the Little Ice Age'. *Earth and Planetary Science Letters*, 315–316 pp 76-85.

Long, A. J., Barlow, N. L. M., Gehrels, W. R., Saher, M. H., Woodworth, P. L., Scaife, R. G., Brain, M. J. and Cahill, N. (2014) 'Contrasting records of sea-level change in the eastern and western North Atlantic during the last 300 years'. *Earth and Planetary Science Letters*, 388 pp 110-122.

Longmore, M. (1982) 'The caesium-137 dating technique and associated applications in Australia-a review'. *Archaeometry: an australasion perspective.* pp 310-321.

Lousier, J. D. and Parkinson, D. (1981) 'The disappearance of the empty tests of litter-and soil-testate amoebae (Testacea, Rhizopoda, Protozoa)'. *Archiv für Protistenkunde*, 124 (3). pp 312-336.

Magurran, A. E. (2013) *Measuring biological diversity.* John Wiley and Sons, UK.

Maher, L. J., Heiri, O. and Lotter, A. F. (2012) 'Assessment of uncertainties associated with palaeolimnological laboratory methods and microfossil analysis'. *Tracking environmental change using lake sediments.* Springer, pp 143-166.

Mariotti, G. and Fagherazzi, S. (2010) 'A numerical model for the coupled long-term evolution of salt marshes and tidal flats'. *Journal of Geophysical Research: Earth Surface*, 115 (F1).

Marshall, W. A., Gehrels, W. R., Garnett, M. H., Freeman, S. P. H. T., Maden, C. and Xu, S. (2007) 'The use of 'bomb spike' calibration and high-precision AMS C-14 analyses to date salt-marsh sediments deposited during the past three centuries'. *Quaternary Research*, 68 (3). pp 325-337.

Marshall, W. A., Clough, R. and Gehrels, W. R. (2009) 'The isotopic record of atmospheric lead fall-out on an Icelandic salt marsh since AD 50'. *Science of the Total Environment*, 407 (8). pp 2734-2748.

Massey, A. C., Gehrels, W. R., Charman, D. J. and White, S. V. (2006) 'An intertidal foraminifera-based transfer function for reconstructing Holocene sea-level change in southwest England'. *Journal of Foraminiferal Research*, 36 (3). pp 215-232.

McCune, B. (1997) 'Influence of noisy environmental data on canonical correspondence analysis'. *Ecology*, 78 (8). pp 2617-2623.

McGranahan, G., Balk, D. and Anderson, B. (2007) 'The rising tide: assessing the risks of climate change and human settlements in low elevation coastal zones'. *Environment and Urbanization*, 19 (1). pp 17-37.

Medioli, F., Scott, D. B., Collins, E., Asioli, S. and Reinhardt, E. (1999) 'The thecamoebian bibliography'. *Palaeontologia electronica*, 2 (1).

Melillo, J. M., Richmond T.C. and Yohe, G.W. (2014) ‘Climate Change Impacts in the United States: The Third National Climate Assessment.’ *U.S. Global Change Research Program*, 841 pp.

Mengel, M., Levermann, A., Frieler, K., Robinson, A., Marzeion, B. and Winkelmann, R. (2016) 'Future sea level rise constrained by observations and long-term commitment'. *Proceedings of the National Academy of Sciences*, 113 (10). pp 2597-2602.

Merrifield, M. A. and Maltrud, M. E. (2011) 'Regional sea level trends due to a Pacific trade wind intensification'. *Geophysical Research Letters*, 38 pp L21605.

Met Office (2014) 'Recent Storms and Flood in the UK'. *Met Office report http://www.metoffice.gov.uk/media/pdf/n/i/Recent_Storms_Briefing_Final_07023.pdf*

Milne, G. A. and Mitrovica, J. X. (1998) 'Postglacial sea-level change on a rotating Earth'. *Geophysical Journal International*, 133 (1). pp 1-19.

Milne, G. A. and Mitrovica, J. X. (2008) 'Searching for eustasy in deglacial sea-level histories'. *Quaternary Science Reviews*, 27 (25-26). pp 2292-2302.

Milne, G. A., Long, A. J. and Bassett, S. E. (2005) 'Modelling Holocene relative sea-level observations from the Caribbean and South America'. *Quaternary Science Reviews*, 24 (10-11). pp 1183-1202.

Mitchell, E. A. D. (2013) 'Potential implications of differential preservation of testate amoeba shells for paleoenvironmental reconstruction in peatlands'. *Journal of Paleolimnology*, 40 (2). pp 603-618.

Mitchell, E. A., Payne, R. J., van der Knaap, W. O., Lamentowicz, Ł., Gąbka, M. and Lamentowicz, M. (2013) 'The performance of single-and multi-proxy transfer

functions (testate amoebae, bryophytes, vascular plants) for reconstructing mire surface wetness and pH'. *Quaternary Research*, 79 (1). pp 6-13.

Mitchell, E. A. D., Payne, R. J. and Lamentowicz, M. (2008) 'Potential implications of differential preservation of testate amoeba shells for paleoenvironmental reconstruction in peatlands'. *Journal of Paleolimnology*, 40 (2). pp 603-618.

Mitrovica, J. X., Tamisiea, M. E., Davis, J. L. and Milne, G. A. (2001) 'Recent mass balance of polar ice sheets inferred from patterns of global sea-level change'. *Nature*, 409 (6823). pp 1026-1029.

Mitrovica, J. X., Gomez, N., Morrow, E., Hay, C., Latychev, K. and Tamisiea, M. E. (2011) 'On the robustness of predictions of sea-level fingerprints'. *Geophysical Journal International*, 187 (2). pp 729-742.

Molinari, J. and xfa (1996) 'A Critique of Bulla's Paper on Diversity Indices'. *Oikos*, 76 (3). pp 577-582.

Moore, D.M., (1968) The vascular flora of the Falkland Islands (Vol. 60). British Antarctic Survey.

Morrill, C., LeGrande, A. N., Renssen, H., Bakker, P. and Otto-Bliesner, B. (2013) 'Model sensitivity to North Atlantic freshwater forcing at 8.2 ka'. *Climate of the Past*, 9 (2). pp 955-968.

Morris, K., Butterworth, J. and Livens, F. (2000) 'Evidence for the remobilization of Sellafield waste radionuclides in an intertidal salt marsh, West Cumbria, UK'. *Estuarine, Coastal and Shelf Science*, 51 (5). pp 613-625.

Morris, J. T., Sundareshwar, P., Nietch, C. T., Kjerfve, B. and Cahoon, D. R. (2002) 'Responses of coastal wetlands to rising sea level'. *Ecology*, 83 (10). pp 2869-2877.

Morton, R. A. and White, W. A. (1997).'Characteristics of and Corrections for Core Shortening in Unconsolidated Sediments'. *Journal of Coastal Research*, 13(3), 761-769.

Morvan, J., Debenay, J.-P., Jorissen, F., Redois, F., Bénéteau, E., Delplancke, M. and Amato, A.-S. (2006) 'Patchiness and life cycle of intertidal foraminifera: Implication for environmental and paleoenvironmental interpretation'. *Marine Micropaleontology*, 61 (1–3). pp 131-154.

Murray, J. (1976) 'Comparative studies of living and dead benthic foraminiferal distributions'. *Foraminifera*, 2 pp 45-109.

Murray, J. W. (1982) 'Benthic foraminifera: The validity of living, dead or total assemblages for the interpretation of palaeoecology'. *Journal of Micropalaeontology*, 1 (1). pp 137-140.

Murray, J. W. (1991) 'Ecology and distribution of benthic foraminifera'. *Biology of Foraminifera. Academic Press, London*, pp 221-253.

Murray, J. W. (2000) 'Revised taxonomy, An Atlas of British Recent Foraminiferids'. *Journal of Micropalaeontology*, 19 pp 44-44.

Murray, J. W. and Alve, E. (1999) 'Natural dissolution of modern shallow water benthic foraminifera: taphonomic effects on the palaeoecological record'. *Palaeogeography, Palaeoclimatology, Palaeoecology*, 146 (1). pp 195-209.

Murray, J. W. and Alve, E. (2000) 'Major aspects of foraminiferal variability (standing crop and biomass) on a monthly scale in an intertidal zone'. *The Journal of Foraminiferal Research*, 30 (3). pp 177-191.

Murray, J. W. and Bowser, S. S. (2000) 'Mortality, protoplasm decay rate, and reliability of staining techniques to recognize 'living'foraminifera: a review'. *The Journal of Foraminiferal Research*, 30 (1). pp 66-70.

Nakada, M. and Lambeck, K. (1987) 'Glacial rebound and relative sea-level variations - a new appraisal'. *Geophysical Journal of the Royal Astronomical Society*, 90 (1). pp 171-224.

Nakada, M. and Lambeck, K., (1989) 'Late Pleistocene and Holocene sea-level change in the Australian region and mantle rheology'. *Geophysical Journal International*, 96(3): 497-517.

Neville, L. A., Christie, D. G., McCarthy, F. M. and MacKinnon, M. D. (2010) 'Biogeographic variation in Thecamoebian (Testate amoeba) assemblages in lakes within various vegetation zones of Alberta, Canada'. *International Journal of Biodiversity and Conservation*, 2 (8). pp 215-224.

Ooms, M., Beyens, L. and Temmerman, S. (2011) 'Testate amoebae as estuarine water-level indicators: modern distribution and the development of a transfer function from a freshwater tidal marsh (Scheldt estuary, Belgium)'. *Journal of Quaternary Science*, 26 (8). pp 819-828.

Ooms, M., Beyens, L. and Temmerman, S. (2012) 'Testate Amoebae as Proxy for Water Level Changes in a Brackish Tidal Marsh'. *Acta Protozoologica*, 51 (3). pp 271-289.

Oppenheim, D. R. (1991) 'Seasonal Changes in Epipelic Diatoms Along an Intertidal Shore, Berrow Flats, Somerset'. *Journal of the Marine Biological Association of the United Kingdom*, 71 (03). pp 579-596.

Orson, R., Warren, R. and Niering, W. (1998) 'Interpreting sea level rise and rates of vertical marsh accretion in a southern New England tidal salt marsh'. *Estuarine, Coastal and Shelf Science*, 47 (4). pp 419-429.

Overpeck, J. T., Webb, R. S. and Webb, T. (1992) 'Mapping eastern North American vegetation change of the past 18 ka: No-analogs and the future'. *Geology*, 20 (12). pp 1071-1074.

Palmer, A., J.M. and Abbott, W., H. (1986) 'Diatoms as sea-level indicators'. in van de Plassche, O. (ed.) *Sealevel research: A manual for the collection and evaluation of data.* Norwich: Geo Books, pp 435–456.

Palmer, T., Nicholls, R. J., Wells, N. C., Saulter, A. and Mason, T. (2014) 'Identification of 'energetic' swell waves in a tidal strait'. *Continental Shelf Research*, 88 pp 203-215.

Parnell, A. C. (2005) 'The statistical analysis of former sea level'. PhD Thesis, University of Sheffield, UK.

Parnell, A. C. and Gehrels, W. R. (2015) 'Using chronological models in late Holocene sea level reconstructions from salt marsh sediments'. *Handbook of Sea-Level Research*, pp 500.

Parnell, A. C., Haslett, J., Allen, J. R. M., Buck, C. E. and Huntley, B. (2008) 'A flexible approach to assessing synchroneity of past events using Bayesian reconstructions of sedimentation history'. *Quaternary Science Reviews*, 27 (19–20). pp 1872-1885.

Parnell, A. C., Buck, C. E. and Doan, T. K. (2011) 'A review of statistical chronology models for high-resolution, proxy-based Holocene palaeoenvironmental reconstruction'. Quaternary Science Reviews, 30 (21–22). pp 2948-2960.

Patterson, R. T. and Fishbein, E. (1989) 'Re-examination of the statistical methods used to determine the number of point counts needed for micropalaentological quantitative research'. *Journal of Paleontology*, 63 (2). pp 245-248.

Patterson, R. T., Gehrels, W. R., Belknap, D. F. and Dalby, A. P. (2004) 'The distribution of salt marsh foraminifera at Little Dipper Harbour New Brunswick, Canada: applicable transfer functions in sea-level research'. *Quaternary International*, 120 pp 185-194.

Pawlowski, J. and Burki, F. (2009) 'Untangling the phylogeny of amoeboid protists'. *Journal of Eukaryotic Microbiology*, 56 (1). pp 16-25.

Payne, R. J. and Mitchell, E. A. (2009) 'How many is enough? Determining optimal count totals for ecological and palaeoecological studies of testate amoebae'. *Journal of Paleolimnology*, 42 (4). pp 483-495.

Payne, R. J., Telford, R. J., Blackford, J. J., Blundell, A., Booth, R. K., Charman, D. J., Lamentowicz, L., Lamentowicz, M., Mitchell, E. A. D., Potts, G., Swindles, G. T., Warner, B. G. and Woodland, W. (2012) 'Testing peatland testate amoeba transfer functions: Appropriate methods for clustered training-sets'. *Holocene*, 22 (7). pp 819-825.

Peltier, W. R. (2004) 'Global glacial isostasy and the surface of the ice-age earth: The ice-5G (VM2) model and grace'. *Annual Review of Earth and Planetary Sciences*, 32 pp 111-149.

Pennisi, E. (2003) 'Modernizing the tree of life'. *Science*, 300 (5626). pp 1692-1697.

Permanent Service for Mean Sea Level (PSMSL), 2011, "Tide Gauge Data", Retrieved from http://www.psmsl.org/data/obtaining/.

Pielou, E. C. (1966) 'Species-diversity and pattern-diversity in the study of ecological succession'. *Journal of Theoretical Biology*, 10 (2). pp 370-383.

Piotrowska, N., Blaauw, M., Mauquoy, D. and Chambers, F.M., 2011. Constructing deposition chronologies for peat deposits using radiocarbon dating. Mires and Peat, 7(10), pp.1-14.

Pizzuto, J. E. and Schwendt, A. E. (1997) 'Mathematical modeling of autocompaction of a Holocene transgressive valley-fill deposit, Wolfe Glade, Delaware'. *Geology*, 25 (1). pp 57-60.

Plastino, W., Kaihola, L., Bartolomei, P. and Bella, F. (2001) 'Cosmic background reduction in the radiocarbon measurements by liquid scintillation spectrometry at the underground laboratory of Gran Sasso'. *Radiocarbon*, 43 (2; PART A). pp 157-162.

Plater, A. J., Kirby, J. R., Boyle, J. F., Shaw, T. and Mills, H. (2015) 'Loss on ignition and organic content'. *Handbook of Sea-Level Research*, pp 312-330.

Preiss, N., Mélières, M. A. and Pourchet, M. (1996) 'A compilation of data on lead 210 concentration in surface air and fluxes at the air-surface and water-sediment interfaces'. *Journal of Geophysical Research: Atmospheres*, 101 (D22). pp 28847-28862.

Prell, W. L. (1985) *Stability of low-latitude sea-surface temperatures: an evaluation of the CLIMAP reconstruction with emphasis on the positive SST anomalies. Final report.* Brown Univ., Providence, RI (USA). Dept. of Geological Sciences. Available.

Purkey, S. G. and Johnson, G. C. (2010) 'Warming of global abyssal and deep southern ocean waters between the 1990s and 2000s: contributions to global heat and sea level rise budgets'. *Journal of Climate*, 23 (23). pp 6336-6351.

Purkey, S. G. and Johnson, G. C. (2013) 'Antarctic Bottom Water Warming and Freshening: Contributions to Sea Level Rise, Ocean Freshwater Budgets, and Global Heat Gain'. *Journal of Climate*, 26 (16). pp 6105-6122.

Rahmstorf, S. (2007) 'A semi-empirical approach to projecting future sea-level rise'. *Science*, 315 (5810). pp 368-370.

Rahmstorf, S., Perrette, M. and Vermeer, M. (2012) 'Testing the robustness of semi-empirical sea level projections'. *Climate Dynamics*, 39 (3-4). pp 861-875.

Redfield, A. C. (1972) 'Development of a New England Salt Marsh'. *Ecological Monographs*, 42 (2). pp 201-237.

Reed, D. J. (1995) 'The response of coastal marshes to sea-level rise: Survival or submergence?'. *Earth Surface Processes and Landforms*, 20 (1). pp 39-48.

Reimer, P. and Reimer, R. (2007) 'Radiocarbon Dating| Calibration'. In Elias, S. A. eds *Encyclopedia of Quaternary Science*. pp.2941-2950

Reimer, P.J., Baillie, M.G., Bard, E., Bayliss, A., Beck, J.W., Bertrand, C.J., Blackwell, P.G., Buck, C.E., Burr, G.S., Cutler, K.B. and Damon, P.E., (2004) 'IntCal04 terrestrial radiocarbon age calibration, 0–26 cal kyr BP'. *Radiocarbon*, *46*(03), pp.1029-1058.

Reimer, P. J., Brown, T. A. and Reimer, R. W. (2004) 'Discussion: reporting and calibration of post-bomb 14C data'. *Radiocarbon*, 46 (3). pp 1299-1304.

Rignot, E., Velicogna, I., van den Broeke, M. R., Monaghan, A. and Lenaerts, J. (2011) 'Acceleration of the contribution of the Greenland and Antarctic ice sheets to sea level rise'. *Geophysical Research Letters*, 38 pp L05503.

Roberts, D. E. (1984) *Quaternary history of the Falklands*. PhD Thesis,University of Aberdeen, UK.

Roe, H. M., Charman, D. J. and Gehrels, W. R. (2002) 'Fossil testate amoebae in coastal deposits in the UK: implications for studies of sea-level change'. *Journal of Quaternary Science*, 17 (5-6). pp 411-429.

Roe, H. M., Doherty, C. T., Patterson, R. T. and Swindles, G. T. (2009) 'Contemporary distributions of saltmarsh diatoms in the Seymour-Belize Inlet Complex, British Columbia, Canada: Implications for studies of sea-level change'. *Marine Micropaleontology*, 70 (3-4). pp 134-150.

Roeleveld, W. and van Loon, A. J. (1979) 'The Holocene development of the young coastal plain of Suriname'. *Geologie en Mijnbouw*, 58 (4). pp 21-28.

Ross, J. C. (1847) *A Voyage of Discovery and Research in the Southern and Antarctic Regions, during the Years 1839-43.* vol. 2. Murray, London, UK.

Rossi, V., Horton, B. P., Corbett, D. R., Leorri, E., Perez-Belmonte, L. and Douglas, B. C. (2011) 'The application of foraminifera to reconstruct the rate of 20th century sea level rise, Morbihan Golfe, Brittany, France'. *Quaternary Research*, 75 (1). pp 24-35.

Rostami, K., Peltier, W. R. and Mangini, A. (2000) 'Quaternary marine terraces, sea-level changes and uplift history of Patagonia, Argentina: comparisons with predictions of the ICE-4G (VM2) model of the global process of glacial isostatic adjustment'. *Quaternary Science Reviews*, 19 (14-15). pp 1495-1525.

Ruzicka, E. (1982) 'Die subfossile Testaceen des Krottensees (Salzburg, Oesterreich)'. *Limnology* 1pp 49-88.

Sachs, H. M., Webb III, T. and Clark, D. (1977) 'Paleoecological transfer functions'. *Annual Review of Earth and Planetary Sciences*, 5 pp 159.

Sawai, Y., Horton, B. P. and Nagumo, T. (2004) 'The development of a diatom-based transfer function along the Pacific coast of eastern Hokkaido, northern Japan - An aid in paleoseismic studies of the Kuril subduction zone'. *Quaternary Science Reviews*, 23 (23-24). pp 2467-2483.

Schaeffer, M., Hare, W., Rahmstorf, S. and Vermeer, M. (2012) 'Long-term sea-level rise implied by 1.5°C and 2°C warming levels'. *Nature Climate Change*, 2 pp 867-870.

Schellmann, G. and Radtke, U. (2010) 'Timing and magnitude of Holocene sea-level changes along the middle and south Patagonian Atlantic coast derived from beach ridge systems, littoral terraces and valley-mouth terraces'. *Earth-Science Reviews*, 103 (1). pp 1-30.

Schröter, D. (2001) *'*Structure and Function of the Decomposer Food Webs of Forests along a European North-South-transect with Special Focus on Testate

Amobeae (Protozoa)'. PhD Thesis, Department of Animal Ecology, Universität Giessen, Germany.

Scott, D. S. and Medioli, F. S. (1978) 'Vertical zonations of marsh foraminifera as accurate indicators of former sea-levels.'. *Nature*, 272 (5653). pp 528-531.

Scott, D. B. and Medioli, F. S. (1980a) 'Living vs. total foraminiferal populations: their relative usefulness in paleoecology'. *Journal of Paleontology*, pp 814-831.

Scott, D. B. and Medioli, F. S. (1980b) 'Quantitative studies of marsh foraminiferal distributions in Nova Scotia; implications for sea level studies'. *Special Publications-Cushman Foundation for Foraminiferal Research*.

Scott, D. and Medioli, F. (1986) 'Foraminifera as sea-level indicators'. *Sea-level Research.* Springer, pp 435-456.

Scott, D. B., Medioli, F. S. and Schafer, C. T. (1977) 'Temporal changes in foraminiferal distributions in Miramichi River estuary, New Brunswick'. Canadian Journal of Earth Sciences, 14 (7). pp 1566-1587.

Scott, D. B., Medioli, F. S. and Duffett, T. E. (1984) 'Holocene rise of relative sea-level at Sable Island, Nova Scotia, Canada'. *Geology*, 12 (3). pp 173-176.

Scott, D.B., Suter, J.R. and Kosters, E.C., (1991) 'Marsh foraminifera and arcellaceans of the lower Mississippi Delta: controls on spatial distributions'. *Micropaleontology*, pp.373-392.

Scott, D.B., Medioli, F.S. and Schafer, C.T., (2001). Monitoring in coastal environments using foraminifera and thecamoebian indicators. Cambridge University Press, Cambridge, UK.

Sernander, R. (1908) 'On the evidences of postglacial changes of climate furnished by the peat-mosses of Northern Europe'. GFF, 30 (7). pp 465-473.

Shannon, C.E. (1948) 'A mathematical theory of communication'. *Bell System Technical Journal*, 27, 379–423.

Shennan, I. (1986) 'Flandrian sea-level changes in the Fenland. II: Tendencies of sea-level movement, altitudinal changes, and local and regional factors'. *Journal of Quaternary Science*, 1 (2). pp 155-179.

Shennan, I. and Horton, B. (2002) 'Holocene land- and sea-level changes in Great Britain'. *Journal of Quaternary Science*, 17 (5-6). pp 511-526.

Shennan, I., Long, A. J. and Horton, B. P. (2015) *Hanbook of Sea-Level Research.* Sussex, UK: John Wiley and Sons.

Sibley, A., Cox, D. and Titley, H. (2015) 'Coastal flooding in England and Wales from Atlantic and North Sea storms during the 2013/2014 winter'. *Weather*, 70 (2). pp 62-70.

Simpson, E.H. (1949) 'Measurement of diversity'. *Nature* 163:688.

Sleigh, M. A. (1973) *The biology of protozoa.* Edward Arnold, London.

Sleigh, M.A.(2003). Protozoa and other protists. 3rd Edition. Cambridge University Press, Cambridge, London.

Smith, J. N. (2001) 'Why should we believe 210Pb sediment geochronologies?'. *Journal of Environmental Radioactivity*, 55 (2). pp 121-123.

Smith, D. H., R.G.,Cox, E.J. (1996) 'Predation of epipelic diatoms by the amphipod Corophium volutator and the polychaete Nereis diversicolor'. *Marine Ecology Progress Series*, 145 pp 8.

Smith, D.E., Harrison, S., Firth, C.R. and Jordan, J.T., (2011) 'The early Holocene sea level rise'. *Quaternary Science Reviews*, 30(15), pp.1846-1860.

Smithers, S. G. and Woodroffe, C. D. (2001) 'Coral microatolls and 20th century sea level in the eastern Indian Ocean'. *Earth and Planetary Science Letters*, 191 (1). pp 173-184.

Smol, J. P. and Stoermer, E. F. (2010) *The diatoms: applications for the environmental and earth sciences.* Cambridge University Press.

Southall, K. E., Gehrels, W. R. and Hayward, B. W. (2006) 'Foraminifera in a New Zealand salt marsh and their suitability as sea-level indicators'. *Marine Micropaleontology*, 60 (2). pp 167-179.

Stevenson, J., Ward, L. and Kearney, M. (1986) 'Vertical accretion in marshes with varying rates of sea level rise'. In Wolfe, D.A. (1986) *Esturarine Variability,*Academic Press, New York, pp.241-249.

Stockmarr, J. (1971) 'Tablets with spores used in absolute pollen analysis'. *Pollen et Spores*, 13, pp 615–621.

Stuiver, M. and Polach, H. A. (1977) 'Reporting of C-14 data-Discussion'. *Radiocarbon*, 19 (3). pp 355-363.

Stuiver, M. and Reimer, P. J. (1986) 'A computer program for radiocarbon age calibration'. *Radiocarbon*, 28 (2B). pp 1022-1030.

Sullivan, M. E. and Booth, R. K. (2011) 'The potential influence of short-term environmental variability on the composition of testate amoeba communities in Sphagnum peatlands'. *Microbial Ecology*, 62 (1). pp 80-93.

Swindles, G. T. and Roe, H. M. (2007) 'Examining the dissolution characteristics of testate amoebae (Protozoa: Rhizopoda) in low pH conditions: Implications for peatland palaeoclimate studies'. *Palaeogeography, Palaeoclimatology, Palaeoecology*, 252 (3–4). pp 486-496.

Switzer, A. D. and Pile, J. (2015) 'Grain size analysis'. *Handbook of Sea-Level Research*, pp 331.

Szkornik, K., Gehrels, W. R. and Kirby, J. R. (2006) 'Salt-marsh diatom distributions in Ho Bugt (western Denmark) and the development of a transfer function for reconstructing Holocene sea-level changes'. *Marine Geology*, 235 (1-4). pp 137-150.

Tamisiea, M., Mitrovica, J., Davis, J. and Milne, G. (2003) 'Long wavelength sea level and solid surface perturbations driven by polar ice mass variations:

fingerprinting Greenland and Antarctic ice sheet flux'. *Earth Gravity Field from Space—From Sensors to Earth Sciences.* Springer, pp 81-93.

Tamisiea, M. E. and Mitrovica, J. X. (2011) 'The Moving Boundaries of Sea Level Change Understanding the Origins of Geographic Variability'. *Oceanography*, 24 (2). pp 24-39.

Tamisiea, M. E., Mitrovica, J. X. and Davis, J. L. (2003) 'A method for detecting rapid mass flux of small glaciers using local sea level variations'. *Earth and Planetary Science Letters*, 213 (3). pp 477-485.

Telford, R., Andersson, C., Birks, H. and Juggins, S. (2004) 'Biases in the estimation of transfer function prediction errors'. *Paleoceanography*, 19 (4).

Telford, R. and Birks, H. (2005) 'The secret assumption of transfer functions: problems with spatial autocorrelation in evaluating model performance'. *Quaternary Science Reviews*, 24 (20). pp 2173-2179.

Telford, R. and Birks, H. (2009) 'Evaluation of transfer functions in spatially structured environments'. *Quaternary Science Reviews*, 28 (13). pp 1309-1316.

Telford, R. and Birks, H. (2011a) 'A novel method for assessing the statistical significance of quantitative reconstructions inferred from biotic assemblages'. *Quaternary Science Reviews*, 30 (9). pp 1272-1278.

Telford, R. J. and Birks, H. J. B. (2011b) 'Effect of uneven sampling along an environmental gradient on transfer-function performance'. *Journal of Paleolimnology*, 46 (1). pp 99-106.

ter Braak, C. J. F. (1986) 'Canonical Correspondence Analysis: A New Eigenvector Technique for Multivariate Direct Gradient Analysis'. *Ecology*, 67 (5). pp 1167-1179.

ter Braak, C. J. F.(1987) 'The analysis of vegetation-environment relationships by canonical correspondence analysis'. *Theory and models in vegetation science.* Springer, pp 69-77.

ter Braak, C. J. F. (1995) 'Non-linear methods for multivariate statistical calibration and their use in palaeoecology: a comparison of inverse (k-nearest neighbours, partial least squares and weighted averaging partial least squares) and classical approaches'. *Chemometrics and Intelligent Laboratory Systems*, 28 (1). pp 165-180.

ter Braak, C.J. F. and Looman, C. N. (1986) 'Weighted averaging, logistic regression and the Gaussian response model'. *Vegetatio*, 65 (1). pp 3-11.

ter Braak, C. J.F. and Prentice, I. C. (1988) 'A theory of gradient analysis'. *Advances in ecological research*, 18 pp 271-317.

ter Braak, C. J. F. and van Dame, H. (1989) 'Inferring pH from diatoms: a comparison of old and new calibration methods'. *Hydrobiologia*, 178 (3). pp 209-223.

ter Braak, C. J. F. and Juggins, S. (1993) 'Weighted averaging partial least squares regression (WA-PLS): an improved method for reconstructing environmental variables from species assemblages'. *Hydrobiologia*, 269 (1). pp 485-502.

ter Braak, C. J. F. and Smilauer, P. (2002) 'CANOCO reference manual and CanoDraw for Windows user's guide: software for canonical community ordination (version 4.5)'.

Thompson, P. R., Hamlington, B. D., Landerer, F. W. and Adhikari, S. (2016) 'Are long tide gauge records in the wrong place to measure global mean sea level rise?'. *Geophysical Research Letters*, 43 (19). pp 10,403-410,411.

Tolonen, K. (1966) 'Stratigraphic and rhizopod analyses on an old raised bog, Varrassuo, in Hollola, South Finland', *Annales Botanici Fennici*. JSTOR, pp. 147-166.

Tolonen, K. (1986) 'Rhizopod analysis'. *Handbook of Holocene palaeoecology and palaeohydrology*, pp 645-666.

Tooley, M. J. (1978) 'Interpretation of Holocene sea-level changes'. *GFF*, 100 (2). pp 203-212.

Törnqvist, T. E., van Ree, M. H., van't Veer, R. and van Geel, B. (1998) 'Improving methodology for high-resolution reconstruction of sea-level rise and neotectonics by paleoecological analysis and AMS 14 C dating of basal peats'. *Quaternary Research*, 49 (1). pp 72-85.

Törnqvist, T. E., Wallace, D. J., Storms, J. E., Wallinga, J., Van Dam, R. L., Blaauw, M., Derksen, M. S., Klerks, C. J., Meijneken, C. and Snijders, E. M. (2008) 'Mississippi Delta subsidence primarily caused by compaction of Holocene strata'. Nature Geoscience, 1 (3). pp 173-176.

Törnqvist, T. E. and Hijma, M. P. (2012) 'Links between early Holocene ice-sheet decay, sea-level rise and abrupt climate change'. *Nature Geoscience*, 5 (9). pp 601-606.

Troels-Smith, J. (1955) 'Karakterisering af lose jordarter. Characterization of unconsolidated sediments'.

Tuomisto, H. (2010) 'A diversity of beta diversities: straightening up a concept gone awry. Part 2. Quantifying beta diversity and related phenomena'. *Ecography*, 33 (1). pp 23-45.

Turetsky, M. R., Manning, S. W. and Wieder, R. K. (2004) 'Dating recent peat deposits'. *Wetlands*, 24 (2). pp 324-356.

Uehara, K., Scourse, J. D., Horsburgh, K. J., Lambeck, K. and Purcell, A. P. (2006) 'Tidal evolution of the northwest European shelf seas from the Last Glacial Maximum to the present'. *Journal of Geophysical Research: Oceans*, 111 (C9).

UNSCEAR (2000) 'effects of Ionizing Radiation'. *United Nations, New York*, pp 453-487.

van Asselen, S., Stouthamer, E. and Van Asch, T. W. (2009) 'Effects of peat compaction on delta evolution: a review on processes, responses, measuring and modeling'. *Earth-Science Reviews*, 92 (1). pp 35-51.

van de Plassche, O. (1986) *Sea-level research: a manual for the collection and evaluation of data.* Netherlands: Springer Netherlands.

van de Plassche, O. (1991) 'Late Holocene Sea-Level Fluctuations on the Shore of Connecticut Inferred from Transgressive and Regressive Overlap Boundaries in Salt-Marsh Deposits'. *Journal of Coastal Research*, pp 159-179.

van de Plassche, O., van der Schrier, G., Weber, S. L., Gehrels, W. R. and Wright, A. J. (2003) 'Sea-level variability in the northwest Atlantic during the past 1500 years: A delayed response to solar forcing?'. *Geophysical Research Letters*, 30 (18).

van de Plassche, O., Bohncke, S. J. P., Makaske, B. and van der Plicht, J. (2005) 'Water-level changes in the Flevo area, central Netherlands (5300–1500 BC): implications for relative mean sea-level rise in the Western Netherlands'. *Quaternary International*, 133–134 pp 77-93.

Vermeer, M. and Rahmstorf, S. (2009) 'Global sea level linked to global temperature'. *Proceedings of the National Academy of Science*, 106 pp 21527-21532.

Vos, P. C. and de Wolf, H. (1993) 'Diatoms as a tool for reconstructing sedimentary environments in coastal wetlands; methodological aspects', *Twelfth International Diatom Symposium*. Springer, pp. 285-296.

Wake, L., Milne, G. and Leuliette, E. (2006) '20th Century sea-level change along the eastern US: unravelling the contributions from steric changes, Greenland ice sheet mass balance and Late Pleistocene glacial loading'. *Earth and Planetary Science Letters*, 250 (3). pp 572-580.

Wall, A., Gilbert, D., Magny, M. and Mitchell, E.A.D. (2009) 'Testate amoeba analysis of lake sediments: impact of filter size and total count on estimates of density, diversity and community structure'. *Journal of Paleolimnology*, 43, 689– 704.

Wallach, D. and Goffinet, B. (1987) 'Mean squared error of prediction in models for studying ecological and agronomic systems'. Biometrics, pp 561-573.

Waller, M., Long, A. and Schofield, J. (2006) 'Interpretation of radiocarbon dates from the upper surface of late-Holocene peat layers in coastal lowlands'. *The Holocene*, 16 (1). pp 51-61.

Walton, W. (1952), Techniques for recognition of living foraminifera, Contrib. Cushman Found. Foraminiferal Res., 3, pp56 – 60.

Warner, B. G., Asada, T. and Quinn, N. P. (2007) 'Seasonal influences on the ecology of testate amoebae (Protozoa) in a small Sphagnum peatland in Southern Ontario, Canada'. *Microbial Ecology*, 54 (1). pp 91-100.

Watcham,E., Shennan, I. and Barlow, N.L.M.(2013) 'Scale considerations in using diatoms as indicators ofsea-level change: lessons from Alaska '. *Journal of Quaternary Science*, 28 (2). pp 165-179.

Watson, C., Burgette, R., Tregoning, P., White, N., Hunter, J., Coleman, R., Handsworth, R. and Brolsma, H. (2010) 'Twentieth century constraints on sea level change and earthquake deformation at Macquarie Island'. *Geophysical Journal International*, 182 pp 781-796.

Weber, C. A. (1900) 'Über die Moore mit besonderer Berücksichtigung der zwischen Unterweser und Unterelbe liegenden'. Jahrbuch der Männer vom Morgenstern, 3 pp 3-23.

Whittaker, R. H. (1969) 'New concepts of kingdoms of organisms'. *Science*, 163 (3863). pp 150-160.

Wiersma, A. and Renssen, H. (2006) 'Model–data comparison for the 8.2 kaBP event: confirmation of a forcing mechanism by catastrophic drainage of Laurentide Lakes'. *Quaternary Science Reviews*, 25 (1). pp 63-88.

Wilson, G. P. and Lamb, A. L. (2012) 'An assessment of the utility of regional diatom-based tidal-level transfer functions'. *Journal of Quaternary Science*, 27 (4). pp 360-370.

Woodland, W. A., Charman, D. J. and Sims, P. C. (1998) 'Quantitative estimates of water tables and soil moisture in Holocene peatlands from testate amoebae'. *The Holocene*, 8 (3). pp 261-273.

Woodroffe, C. D., McGregor, H. V., Lambeck, K., Smithers, S. G. and Fink, D. (2012) 'Mid-Pacific microatolls record sea-level stability over the past 5000 yr'. *Geology*, 40 (10). pp 951-954.

Woodroffe, S. A. (2006) ‘Holocene relative sea-level changes in Cleveland Bay, north Queensland, Australia’. PhD Thesis, Durham University, UK.

Woodroffe, S. A. and Horton, B. P. (2005) 'Holocene sea-level changes in the Indo-Pacific'. *Journal of Asian Earth Sciences*, 25 (1). pp 29-43.

Woodroffe, S. A. and Long, A. J. (2010) 'Reconstructing recent relative sea-level changes in West Greenland: local diatom-based transfer functions are superior to regional models'. *Quaternary International*, 221 (1). pp 91-103.

Woodworth, P. L., White, N. J., Jevrejeva, S., Holgate, S. J., Church, J. A. and Gehrels, W. R. (2009) 'Evidence for the accelerations of sea level on multi-decade and century timescales'. *International Journal of Climatology*, 29 (6). pp 777-789.

Woodworth, P. L., Pugh, D. T. and Bingley, R. M. (2010) 'Long-term and recent changes in sea level in the Falkland Islands'. *Journal of Geophysical Research: Oceans*, 115 (C9).

Woodworth, P., Pugh, D. and Bingley, R. (2011) 'Correction to “Long-term and recent changes in sea level in the Falkland Islands”'. *Journal of Geophysical Research: Oceans*, 116 (C11).

Woodworth, P. L., Menendez, M. and Gehrels, W. R. (2011) 'Evidence for Century-Timescale Acceleration in Mean Sea Levels and for Recent Changes in Extreme Sea Levels'. *Surveys in Geophysics*, 32 (4-5). pp 603-618.

Wright, A. J., Edwards, R. J. and van de Plassche, O. (2011) 'Reassessing transfer-function performance in sea-level reconstruction based on benthic salt-marsh foraminifera from the Atlantic coast of NE North America'. *Marine Micropaleontology*, 81 (1-2). pp 43-62.

Yin, J., Griffies, S. M. and Stouffer, R. J. (2010) 'Spatial variability of sea level rise in twenty-first century projections'. *Journal of Climate*, 23 (17). pp 4585-4607.

Yin, J., Schlesinger, M. E. and Stouffer, R. J. (2009) 'Model projections of rapid sea-level rise on the northeast coast of the United States'. *Nature Geoscience*, 2 (4). pp 262-266.

Yin, J. J., Overpeck, J. T., Griffies, S. M., Hu, A. X., Russell, J. L. and Stouffer, R. J. (2011) 'Different magnitudes of projected subsurface ocean warming around Greenland and Antarctica'. *Nature Geoscience*, 4 (8). pp 524-528.

Zong, Y. (1997) 'Implications of Paralia sulcata abundance in Scottish isolation basins'. *Diatom Research*, 12 (1). pp 125-150.

Zong, Y. and Horton, B. P. (1998) 'Diatom zones across intertidal flats and coastal saltmarshes in Britain'. *Diatom Research*, 13 (2). pp 375-394.

Zong, Y. and Sawai, Y. (2015) 'Diatoms'. *Handbook of Sea-Level Research*, pp 233-248.

Zuo, J., Du, L., Zhang, J. and Chen, M. (2010) 'Global distribution of thermosteric contribution to sea level rising trend'. *Journal of Ocean University of China*, 9 (3). pp 199-209.

APPENDIX A – Photographs of the Swan Inlet, Falklands field site

Figure A1: Overview of Swan Inlet marsh looking South towards the open coast.

Figure A2: Upper-marsh and middle-marsh surface transecst (T1 and T3)

Figure A3 : Low-marsh surface transect (T2) and vegetation zonations.

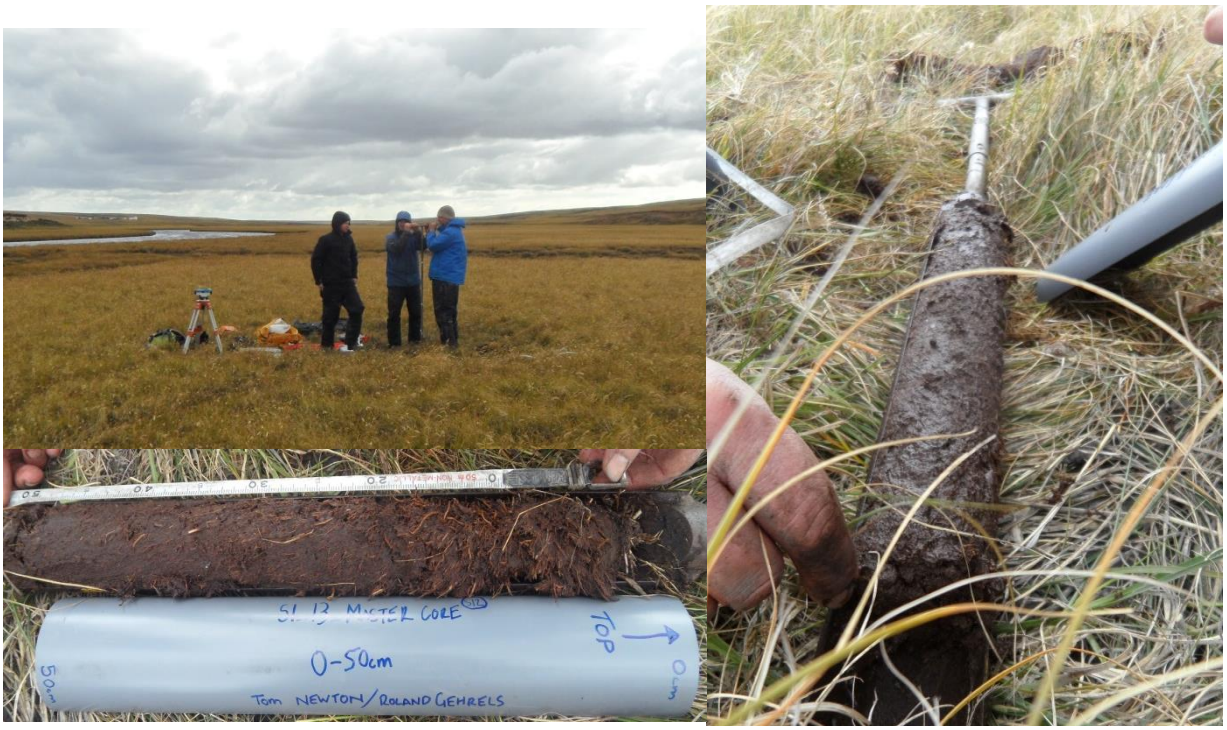

Figure A4 : Swan Inlet master core (SI-2).

Figure A5 : Bank section (2013)

APPENDIX B – Photographs of the Fal-Ruan, UK field site

Figure B1: High-marsh environments at Fal-Ruan looking North. Note the bridge in the background which crosses the River Fal ca. 50m downstream of the mean tidal limit.

Figure B2: Woodland-saltmarsh-mudflat transition at Fal-Ruan.

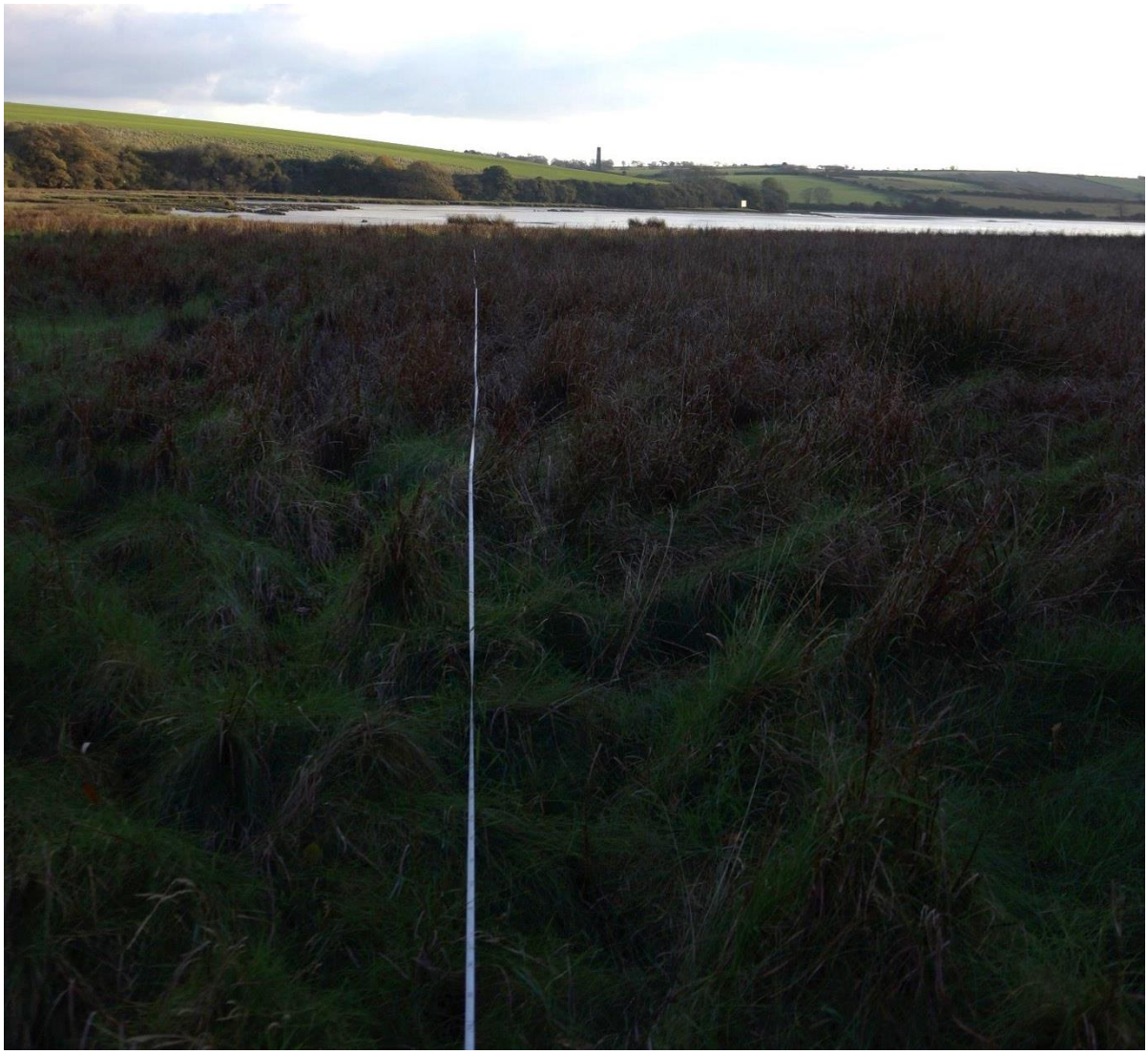

Figure B3: Surface sampling transect at Fal Ruan.

APPENDIX C - Swan Inlet Datum 2013 calculations

Relating the 2005 bank section to Swan Inlet Datum 2013 (SID)

The bank section sampled at Swan Inlet in 2005 was not surveyed to a permanent datum, but it was surveyed relative to the highest tide level of the tide that preceded the sampling of this bank section on 17th Janurary 2005. Based on pressure transducer measurements taken at Swan Inlet in 2013 (Figure C1) it is assumed the amplitudes of the highest tides at Swan Inlet and Stanley are comparable. The surface of the 2005 bank section was 0.245 m above the 17/01/2005 high tide. Based on Stanley tidal data obtained from Phil Woodworth (National Oceaanography Centre, Liverpool) the 17/01/2005 high tide was 0.181 m above MHHW Stanley. The level of MHHW at Swan Inlet was calculated from the 2013 tidal data (Figure C1) as -1.51 m SID. The surface height of the 2005 bank section was therefore related to SID by using the level of mean highest high water (MHHW) at Swan Inlet and Stanley as the common datum, as follows:

$$(-1.51 + 0.18) + 0.245$$

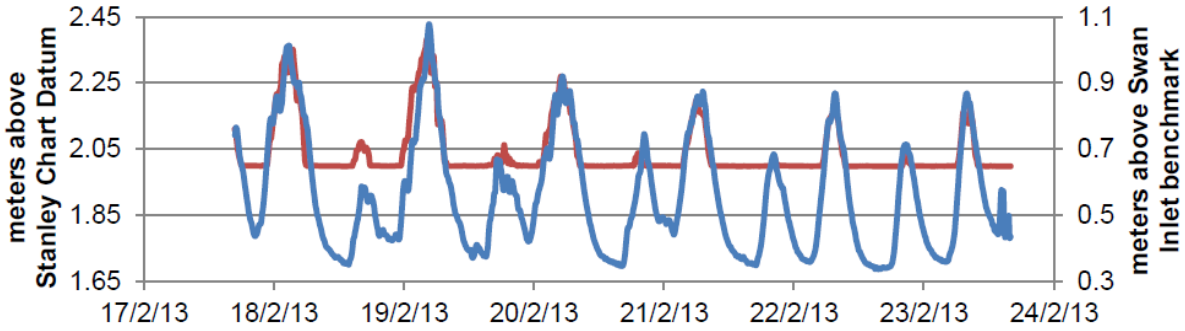

Figure C3: Pressure transducer measurements at Swan Inlet (in blue) compared with the half-tide measurements by the Stanley B-gauge (in red; courtesy of Phil Woodworth, National Oceanography Centre Liverpool). The good match between the higher high waters allows us to relate elevations in Swan Inlet to chart Datum (and mean sea level) at Stanley.

APPENDIX D – Testate amoebae data from Fal-Ruan seasonal investigations

Table S1a: November 2013 absolute count data (death assemblages)

November 2013 Death assemblages

Station #	Elevation (m OD)	Arcella catinus	Arcella discoides type	Pseudodifflugia fulva type	Centropyxis cassis type	Centropyxis delicatula type	Centropyxis platystoma type	Centropyxiella sp.	Centropyxis ecornis	Difflugia pristis type	Difflugia lucida type	Cyphoderia ampulla	Tracheleuglypha dentata	Psuedohyalosphenia type	Euglypha tuberculata type	Euglypha rotunda	Trinema lineare	Assulina muscorum	Valkanovia elegans	Difflugia oblonga-lacustris type	Quadrulella symmetrica	Heleopera petricola	Cyclopyxis arcelloides	Hyalosphenia subflava	Corythion dubium	Nebela collaris	Campuscus type
1	2.03	0	0	9	15	2	0	91	1	5	1	14	1	0	0	0	0	0	0	0	0	0	0	0	0	0	0
2	2.1	0	0	9	46	13	0	57	0	0	0	22	6	6	0	0	0	0	0	2	0	0	0	1	0	1	2
3	2.19	0	2	15	49	10	4	14	2	6	0	14	7	8	0	0	0	0	0	0	0	0	0	0	0	0	0
4	2.26	1	4	8	82	37	6	23	0	6	4	21	13	5	0	0	0	0	0	0	0	0	0	0	0	0	0
5	2.3	0	0	9	103	25	4	2	0	10	10	13	3	0	0	0	0	0	0	0	0	0	0	0	0	0	3
6	2.35	0	0	2	40	25	3	0	0	0	0	5	47	0	0	0	0	0	0	0	0	0	0	0	0	0	0
7	2.42	0	0	24	27	25	0	4	0	6	0	6	38	0	0	0	0	0	0	3	1	0	4	0	0	0	0
8	2.48	2	0	14	21	18	2	0	0	5	12	20	28	0	0	0	0	0	0	2	0	0	0	0	0	0	0
9	2.55	0	3	16	13	20	3	1	0	1	4	10	69	0	2	0	1	0	0	0	2	0	0	0	0	0	0
10	2.63	3	1	24	16	21	6	1	0	2	2	6	52	0	4	0	0	0	0	0	5	0	0	0	1	0	1

Table S1b: November 2013 absolute count data (live assemblages)

November 2013 Live assemblages

Station #	Elevation (m OD)	Arcella catinus	Arcella discoides type	Pseudodifflugia fulva type	Centropyxis cassis type	Centropyxis delicatula type	Centropyxis platystoma type	Centropyxiella sp.	Centropyxis ecornis	Difflugia pristis type	Difflugia lucida type	Cyphoderia ampulla	Tracheleuglypha dentata	Psuedohyalosphenia type	Euglypha tuberculata type	Euglypha rotunda	Trinema lineare	Assulina muscorum	Valkanovia elegans	Difflugia oblonga-lacustris type	Quadrulella symmetrica	Heleopera petricola	Cyclopyxis arcelloides	Hyalosphenia subflava	Corythion dubium	Nebela collaris	Campuscus type
1	2.03	0	0	2	0	0	0	0	0	0	0	0	0	0	0	0	0	0	0	0	0	0	0	0	0	0	0
2	2.1	0	0	0	2	0	0	3	0	0	0	3	0	0	0	0	0	0	0	0	0	0	0	0	0	0	1
3	2.19	0	0	0	0	0	0	0	0	0	0	2	2	3	0	0	0	0	0	0	0	0	0	0	0	0	0
4	2.26	0	0	5	8	0	0	1	0	0	0	0	0	1	0	0	0	0	0	0	0	0	0	0	0	0	0
5	2.3	0	0	0	2	0	0	0	0	0	0	2	0	0	0	0	0	0	0	0	0	0	0	0	0	0	0
6	2.35	0	0	8	0	0	0	0	0	0	0	2	3	0	0	0	0	0	0	0	0	0	0	0	0	0	0
7	2.42	0	1	0	0	0	0	0	0	0	6	0	2	0	0	0	0	0	0	0	0	0	0	0	0	0	0
8	2.48	0	0	0	0	0	0	0	0	0	6	2	0	0	0	0	0	0	0	0	0	0	0	0	0	0	0
9	2.55	2	2	0	0	0	0	0	0	2	4	0	0	0	0	0	0	0	0	0	0	0	0	0	0	0	0
10	2.63	0	0	0	0	0	0	0	0	0	4	0	0	0	0	0	0	0	0	0	0	0	0	0	0	0	0

Table S2a: December 2013 absolute count data (death assemblages)

December 2013 death assemblages																									
Station #	Elevation (m OD)	Arcella catinus	Arcella discoides type	Assulina muscorum	Campuscus type	Centropyxiella sp.	Centropyxis cassis type	Centropyxis delicatula type	Centropyxis ecornis	Centropyxis platystoma type	Corythion dubium	Cyclopyxis arcelloides	Cyphoderia ampulla	Difflugia lucida type	Difflugia oblonga-lacustris type	Difflugia pristis type	Euglypha rotunda	Euglypha tuberculata type	Heleopera petricola	Hyalosphenia subflava	Nebela collaris	Pseudodifflugia fulva type	Psuedohyalosphenia type	Quadrullela symmetrica	Tracheleuglypha dentata	Trinema lineare	Valkanovia elegans
1	2.03	0	0	0	0	57	30	2	0	8	0	0	16	15	0	4	0	0	0	0	0	12	7	0	0	0	0
2	2.1	0	0	0	1	33	32	12	0	0	1	0	18	6	2	0	0	0	0	0	0	12	5	0	0	0	0
3	2.19	0	2	0	0	14	64	18	4	7	0	0	22	4	0	11	0	0	0	0	0	7	0	0	13	0	0
4	2.26	1	0	0	1	0	54	28	1	0	0	0	15	2	1	2	0	0	0	0	0	9	0	0	29	0	0
5	2.3	0	0	0	5	1	59	28	5	0	0	0	2	8	4	1	0	0	0	0	0	8	3	0	16	0	0
6	2.35	2	0	0	3	0	83	28	0	1	0	6	0	0	5	1	0	0	1	0	1	1	0	0	30	1	0
7	2.42	0	0	0	2	6	30	16	0	0	1	5	3	6	4	0	2	3	2	1	3	30	1	1	34	1	0
8	2.48	1	4	0	1	3	52	28	0	8	0	3	4	10	0	6	1	4	2	0	0	12	0	0	42	2	0
9	2.55	6	2	3	0	0	28	7	0	4	0	0	18	6	0	3	1	5	0	0	0	9	0	2	35	2	0
10	2.63	7	6	1	0	2	24	10	11	22	1	0	8	0	0	27	3	7	0	0	0	25	0	4	21	0	2

Table S2b: December 2013 absolute count data (live assemblages)

December 2013 live assemblages																									
Station #	Elevation (m OD)	Arcella catinus	Arcella discoides type	Assulina muscorum	Campuscus type	Centropyxiella sp.	Centropyxis cassis type	Centropyxis delicatula type	Centropyxis ecornis	Centropyxis platystoma type	Corythion dubium	Cyclopyxis arcelloides	Cyphoderia ampulla	Difflugia lucida type	Difflugia oblonga-lacustris type	Difflugia pristis type	Euglypha rotunda	Euglypha tuberculata type	Heleopera petricola	Hyalosphenia subflava	Nebela collaris	Pseudodifflugia fulva type	Psuedohyalosphenia type	Quadrullela symmetrica	Tracheleuglypha dentata	Trinema lineare	Valkanovia elegans
1	2.03	0	0	0	1	0	0	0	0	0	0	0	0	0	0	0	0	0	0	0	0	1	3	0	0	0	0
2	2.1	0	0	0	0	0	3	0	0	0	0	0	0	0	0	0	0	0	0	0	0	15	1	0	0	0	0
3	2.19	0	0	0	0	0	0	0	0	0	0	0	0	0	0	0	0	0	0	0	0	1	0	0	1	0	0
4	2.26	0	0	0	1	0	1	2	0	0	0	0	0	0	0	0	0	0	0	0	0	0	1	0	8	0	0
5	2.3	0	0	0	0	0	1	0	0	0	0	0	0	0	0	0	0	0	0	0	0	0	0	0	4	0	0
6	2.35	0	0	0	0	0	8	0	0	0	0	0	0	0	0	0	0	0	0	0	0	2	0	0	12	0	0
7	2.42	0	0	0	0	0	2	0	0	0	0	0	0	1	1	0	0	0	0	0	0	0	0	0	22	0	0
8	2.48	0	0	0	0	0	0	0	0	0	0	0	0	0	0	0	0	0	0	0	0	0	0	0	5	0	0
9	2.55	0	0	0	0	0	2	0	0	0	0	0	2	0	0	0	0	0	0	0	0	2	0	0	9	0	0
10	2.63	0	0	0	0	0	0	0	0	0	0	0	0	0	2	0	0	1	0	0	0	0	0	0	3	0	0

Table S3a: January 2014 absolute count data (death assemblages)

January 2014 death assemblages																										
Station #	Elevation (m OD)	Arcella catinus	Arcella discoides type	Assulina muscorum	Campuscus type	Centropyxiella sp.	Centropyxis cassis type	Centropyxis delicatula type	Centropyxis ecornis	Centropyxis platystoma type	Corythion dubium	Cyclopyxis arcelloides	Cyphoderia ampulla	Difflugia lucida type	Difflugia oblonga-lacustris type	Difflugia pristis type	Euglypha rotunda	Euglypha tuberculata type	Heleopera petricola	Hyalosphenia subflava	Nebela collaris	Pseudodifflugia fulva type	Psuedohyalosphenia type	Quadrullela symmetrica	Tracheleuglypha dentata	Trinema lineare	Valkanovia elegans
1	2.03	0	0	0	0	30	60	6	6	3	0	0	15	6	1	0	0	0	0	0	0	3	1	0	0	0	0
2	2.1	3	3	0	0	51	33	6	21	0	0	0	39	0	0	6	0	0	0	0	0	6	0	0	3	0	0
3	2.19	0	0	0	1	21	42	12	6	6	0	0	0	0	0	3	0	0	0	0	0	6	6	0	21	0	0
4	2.26	0	0	0	3	0	69	60	3	0	0	1	9	6	0	3	0	0	0	0	0	8	5	0	15	0	0
5	2.3	4	0	0	0	1	50	25	1	5	0	0	12	2	0	6	0	0	0	0	0	4	0	0	12	0	0
6	2.35	0	0	0	0	0	45	30	0	3	0	3	7	0	2	0	0	1	0	0	0	9	0	0	38	0	0
7	2.42	0	1	0	1	6	33	23	0	0	0	5	9	9	1	2	1	2	2	1	1	11	0	1	27	3	0
8	2.48	3	1	1	0	0	30	27	0	3	3	2	18	21	0	5	1	4	0	0	0	6	0	4	14	2	0
9	2.55	1	1	2	1	2	26	24	0	3	2	1	8	8	0	5	1	3	0	1	0	2	1	1	70	1	1
10	2.63	4	1	1	0	6	16	21	1	5	0	0	6	4	0	14	4	6	0	1	0	18	0	3	50	2	1

Table S3b: January 2014 absolute count data (live assemblages)

January 2014 live assemblages																										
Station #	Elevation (m OD)	Arcella catinus	Arcella discoides type	Assulina muscorum	Campuscus type	Centropyxiella sp.	Centropyxis cassis type	Centropyxis delicatula type	Centropyxis ecornis	Centropyxis platystoma type	Corythion dubium	Cyclopyxis arcelloides	Cyphoderia ampulla	Difflugia lucida type	Difflugia oblonga-lacustris type	Difflugia pristis type	Euglypha rotunda	Euglypha tuberculata type	Heleopera petricola	Hyalosphenia subflava	Nebela collaris	Pseudodifflugia fulva type	Psuedohyalosphenia type	Quadrullela symmetrica	Tracheleuglypha dentata	Trinema lineare	Valkanovia elegans
10	2.63	0	0	0	0	0	0	0	0	0	0	0	0	0	0	0	0	2	0	0	0	5	0	1	4	0	0
9	2.55	0	0	0	0	0	0	0	0	0	0	0	2	0	0	0	0	0	0	0	0	6	0	0	0	0	0
8	2.48	0	0	0	0	0	3	0	0	0	0	0	9	6	0	4	0	0	0	0	0	12	0	0	9	0	0
7	2.42	0	0	0	0	0	6	3	0	0	0	1	0	0	0	0	0	0	0	0	0	10	0	0	33	0	0
6	2.35	0	0	0	0	0	3	0	0	0	0	0	3	0	0	0	0	0	0	0	0	3	0	0	21	0	0
5	2.3	0	0	0	0	0	6	0	0	0	0	1	0	2	0	0	0	0	0	0	0	0	0	0	0	0	0
4	2.26	0	0	0	0	0	0	0	0	0	0	0	0	0	0	0	0	0	0	0	0	0	0	0	3	0	0
3	2.19	0	0	0	1	0	3	0	0	0	0	0	3	0	0	0	0	0	0	0	0	0	4	0	3	0	0
2	2.1	0	0	0	0	0	0	0	0	0	0	0	0	0	0	0	0	0	0	0	0	0	0	0	0	0	0
1	2.03	0	0	0	0	0	0	0	0	0	0	0	0	0	0	0	0	0	0	0	0	0	2	0	0	0	0

Table S4a: February 2014 absolute count data (death assemblages)

January 2014 death assemblages																												
Station #	Elevation (m OD)	Arcella catinus	Arcella discoides type	Assulina muscorum	Campuscus type	Centropyxiella sp.	Centropyxis cassis type	Centropyxis delicatula type	Centropyxis ecornis	Centropyxis platystoma type	Corythion dubium	Cryptodifflugia oviformis	Cyclopyxis arcelloides	Cyphoderia ampulla	Difflugia lucida type	Difflugia oblonga-lacustris type	Difflugia pristis type	Euglypha rotunda	Euglypha tuberculata type	Heleopera petricola	Hyalosphenia ovalis	Hyalosphenia subflava	Nebela collaris	Nebela langeniformis	Pseudodifflugia fulva type	Psuedohyalosphenia type	Quadrullela symmetrica	Tracheleuglypha dentata	Trigonopyxis minuta	Trinema lineare	Valkanovia elegans
10	2.63	0	2	1	0	0	13	1	8	13	2	0	0	2	4	0	22	1	3	0	0	0	0	0	38	0	3	8	0	1	2
9	2.55	2	11	0	0	4	12	2	0	0	1	0	0	6	5	0	16	2	1	1	0	1	0	0	36	0	4	15	0	1	3
8	2.48	9	5	0	0	0	6	6	0	0	0	1	0	0	2	1	2	0	1	0	0	0	1	0	56	0	0	8	1	4	3
7	2.42	2	4	1	0	2	11	12	2	4	0	0	4	0	2	0	5	1	1	1	0	0	2	0	47	0	2	12	1	0	0
6	2.35	6	0	0	0	3	45	6	0	3	0	0	0	12	0	0	3	0	0	0	0	0	0	0	27	0	0	21	0	0	0
5	2.3	9	0	0	0	6	69	12	0	0	0	0	1	11	12	0	6	0	0	0	0	0	0	0	15	0	0	12	0	0	0
4	2.26	1	0	0	0	8	30	16	2	4	0	0	0	4	0	0	8	0	0	0	0	0	0	0	29	0	0	24	0	0	0
3	2.19	2	0	0	1	17	0	24	0	0	0	0	0	57	0	1	9	0	0	0	0	0	0	0	17	2	0	21	0	0	0
2	2.1	0	1	0	3	51	42	18	0	0	0	0	0	22	0	0	6	0	0	0	0	0	0	0	15	3	0	12	0	0	0
1	2.03	0	0	0	1	73	20	0	0	0	0	1	1	12	0	1	0	0	0	1	0	0	0	0	21	5	0	14	0	0	0

Table S4b: February 2014 absolute count data (live assemblages)

January 2014 live assemblages																														
Station #	Elevation (m OD)	Arcella catinus	Arcella discoides type	Assulina muscorum	Campuscus type	Centropyxiella sp.	Centropyxis cassis type	Centropyxis delicatula type	Centropyxis ecornis	Centropyxis platystoma type	Corythion dubium	Cryptodifflugia oviformis	Cyclopyxis arcelloides	Cyphoderia ampulla	Difflugia lucida type	Difflugia oblonga-lacustris type	Difflugia pristis type	Euglypha rotunda	Euglypha tuberculata type	Heleopera petricola	Hyalosphenia ovalis	Hyalosphenia subflava	Nebela collaris	Nebela langeniformis	Pseudodifflgia fulva type	Psuedohyalosphenia type	Quadrullela symmetrica	Tracheleuglypha dentata	Trigonopyxis minuta	Trinema lineare	Valkanovia elegans
10	2.63	0	0	0	0	0	0	0	0	0	0	0	0	0	0	0	0	0	1	0	0	0	0	0	6	0	1	0	0	0	0
9	2.55	0	1	0	0	0	0	0	0	0	0	0	0	0	1	0	0	0	0	0	0	0	0	0	6	0	0	1	0	0	0
8	2.48	0	4	0	0	0	12	0	0	0	0	0	0	0	0	0	4	0	0	0	0	0	0	0	64	0	0	6	0	2	0
7	2.42	0	0	0	1	0	6	2	0	0	0	0	0	0	0	0	1	0	0	1	0	0	0	0	42	0	0	0	0	0	0
6	2.35	0	0	0	0	0	0	0	0	0	0	0	0	0	0	0	0	0	0	0	0	0	0	0	17	0	0	0	0	0	0
5	2.3	0	0	0	0	0	6	0	0	0	0	0	0	0	0	0	3	0	0	0	0	0	0	0	15	0	0	3	0	0	0
4	2.26	0	0	0	0	2	0	0	0	0	0	0	0	0	0	0	2	0	0	0	0	0	0	0	6	0	0	2	0	0	0
3	2.19	0	0	0	0	0	1	0	0	0	0	0	0	0	0	0	0	0	0	0	0	0	0	0	1	3	0	0	0	0	0
2	2.1	0	0	0	1	0	0	0	0	0	0	0	0	2	0	0	0	0	0	0	0	0	0	0	0	0	0	3	0	0	0
1	2.03	0	0	0	0	0	0	0	0	0	0	0	0	2	0	0	0	0	0	0	0	0	0	0	0	2	0	0	0	0	0

Table S5a: March 2014 absolute count data (death assemblages)

March 2014 death assemblages																														
Station #	Elevation (m OD)	Arcella catinus	Arcella discoides type	Assulina muscorum	Campuscus type	Centropyxiella sp.	Centropyxis cassis type	Centropyxis delicatula type	Centropyxis ecornis	Centropyxis platystoma type	Corythion dubium	Cryptodifflugia oviformis	Cyclopyxis arcelloides	Cyphoderia ampulla	Difflugia lucida type	Difflugia oblonga-lacustris type	Difflugia pristis type	Euglypha rotunda	Euglypha tuberculata type	Heleopera petricola	Hyalosphenia ovalis	Hyalosphenia subflava	Nebela collaris	Nebela langeniformis	Pseudodifflgia fulva type	Psuedohyalosphenia type	Quadrullela symmetrica	Tracheleuglypha dentata	Trigonopyxis minuta	Trinema lineare	Valkanovia elegans
10	2.63	6	15	2	0	0	3	12	0	6	1	0	0	0	3	0	12	1	3	0	0	0	0	0	81	0	5	33	0	2	1
9	2.55	0	0	0	0	3	27	15	0	6	0	0	0	9	15	1	15	1	2	0	0	0	0	0	30	0	4	48	0	1	0
8	2.48	2	4	0	0	2	22	10	0	2	0	0	0	4	19	0	15	1	0	0	0	0	0	0	47	0	1	28	0	0	0
7	2.42	4	8	1	1	6	9	4	0	0	0	1	4	0	2	3	12	0	1	0	0	2	1	0	60	0	0	44	0	1	0
6	2.35	2	2	0	0	0	12	10	0	0	0	0	2	2	4	2	0	0	0	0	1	1	0	0	62	0	1	2	0	0	0
5	2.3	3	0	0	0	0	29	9	0	1	0	0	2	21	2	1	27	0	0	1	0	0	0	0	21	1	0	39	2	0	0
4	2.26	3	0	0	3	12	24	15	0	0	0	0	0	0	8	0	0	0	0	1	1	1	0	0	37	0	1	9	1	0	0
3	2.19	0	0	0	2	16	52	24	4	0	0	0	0	4	0	0	8	0	0	0	0	0	0	0	12	3	0	12	0	0	0
2	2.1	0	0	0	1	45	45	9	9	3	0	0	0	6	0	0	0	0	0	0	0	0	1	0	18	4	0	9	0	0	0
1	2.03	0	3	0	3	51	6	6	15	0	0	0	0	30	0	1	0	0	0	0	0	0	0	0	30	2	0	1	0	0	0

Table S5b: March 2014 absolute count data (live assemblages)

March 2014 live assemblages																														
Station #	Elevation (m OD)	Arcella catinus	Arcella discoides type	Assulina muscorum	Campuscus type	Centropyxiella sp.	Centropyxis cassis type	Centropyxis delicatula type	Centropyxis ecornis	Centropyxis platystoma type	Corythion dubium	Cryptodifflugia oviformis	Cydopyxis arcelloides	Cyphoderia ampulla	Difflugia lucida type	Difflugia oblonga-lacustris type	Difflugia pristis type	Euglypha rotunda	Euglypha tuberculata type	Heleopera petricola	Hyalosphenia ovalis	Hyalosphenia subflava	Nebela collaris	Nebela langeniformis	Pseudodifflgia fulva type	Psuedohyalosphenia type	Quadrullela symmetrica	Tracheleuglypha dentata	Trigonopyxis minuta	Trinema lineare	Valkanovia elegans
10	2.63	0	0	0	0	0	0	0	0	0	0	0	0	0	0	0	6	0	0	0	0	0	0	0	9	0	0	0	0	0	0
9	2.55	0	0	0	0	0	0	0	0	0	0	0	0	0	0	0	0	0	0	0	0	0	0	0	0	0	0	0	0	0	0
8	2.48	0	0	0	0	0	8	0	0	0	0	0	0	0	1	0	1	0	0	0	0	0	0	0	3	0	0	4	0	0	0
7	2.42	4	0	0	0	0	1	0	0	0	0	0	0	0	0	0	0	0	0	0	0	0	0	0	8	0	0	6	0	0	0
6	2.35	0	0	0	0	0	6	0	0	0	0	0	0	0	4	0	0	0	0	0	0	0	0	0	28	0	0	4	0	0	0
5	2.3	0	0	0	0	0	3	0	0	0	0	0	0	0	0	0	0	0	0	0	0	0	0	0	6	0	0	0	0	0	0
4	2.26	0	0	0	0	0	30	9	0	0	0	0	0	0	1	0	0	0	0	0	0	0	0	0	50	0	0	3	0	0	0
3	2.19	0	0	0	0	0	8	0	0	0	0	0	0	0	0	0	0	0	0	0	0	0	0	0	0	0	0	0	0	0	0
2	2.1	0	0	0	1	0	0	0	0	0	0	0	0	0	0	0	0	0	0	0	0	0	0	0	0	0	0	0	0	0	0
1	2.03	0	0	0	0	0	0	0	0	0	0	0	0	0	0	0	0	0	0	0	0	0	0	0	0	1	0	0	0	0	0

Table S6a: April 2014 absolute count data (death assemblages)

April 2014 death assemblages

Station #	Elevation (m OD)	Arcella catinus	Arcella discoides type	Assulina muscorum	Campuscus type	Centropyxiella sp.	Centropyxis cassis type	Centropyxis delicatula type	Centropyxis ecornis	Centropyxis platystoma type	Corythion dubium	Cryptodifflugia oviformis	Cyclopyxis arcelloides	Cyphoderia ampulla	Difflugia lucida type	Difflugia oblonga-lacustris type	Difflugia pristis type	Euglypha rotunda	Euglypha tuberculata type	Heleopera petricola	Hyalosphenia ovalis	Hyalosphenia subflava	Nebela collaris	Nebela langeniformis	Pseudodifflgia fulva type	Psuedohyalosphenia type	Quadrullela symmetrica	Tracheleuglypha dentata	Trigonopyxis minuta	Trinema lineare	Valkanovia elegans
10	2.63	1	6	2	0	2	8	10	0	0	0	0	0	0	10	1	14	2	3	1	0	0	0	0	60	0	3	12	0	1	1
9	2.55	4	0	0	0	0	8	0	1	0	0	0	0	0	8	1	6	1	1	0	0	1	0	0	78	0	2	19	0	2	1
8	2.48	1	2	0	0	1	24	8	0	0	0	0	0	1	6	0	5	2	2	0	0	0	0	0	70	0	4	28	0	3	1
7	2.42	10	6	0	0	0	22	8	0	0	2	0	1	0	4	0	1	1	1	0	0	0	0	0	26	0	0	40	0	1	0
6	2.35	3	1	0	1	0	20	3	0	0	0	0	2	0	5	0	11	0	0	0	0	0	0	1	71	0	0	12	0	1	0
5	2.3	3	0	0	3	8	51	12	0	0	0	0	3	14	11	1	0	0	0	1	0	0	1	0	47	0	0	1	0	0	0
4	2.26	6	0	0	2	8	22	8	0	0	0	0	0	4	2	0	6	0	0	1	0	1	0	0	38	1	0	26	0	0	0
3	2.19	9	0	0	0	33	45	15	0	0	0	0	0	6	3	0	6	0	0	0	0	0	0	0	18	0	0	6	0	0	0
2	2.1	4	0	0	2	30	26	2	6	0	0	1	0	28	0	0	2	0	0	0	0	0	0	0	28	3	0	4	0	0	0
1	2.03	0	0	0	3	93	6	0	0	0	0	0	0	45	0	1	12	0	0	0	0	0	0	0	12	4	0	0	0	0	0

Table S6b: April 2014 absolute count data (live assemblages)

April 2014 live assemblages

Station #	Elevation (m OD)	Arcella catinus	Arcella discoides type	Assulina muscorum	Campuscus type	Centropyxiella sp.	Centropyxis cassis type	Centropyxis delicatula type	Centropyxis ecornis	Centropyxis platystoma type	Corythion dubium	Cryptodifflugia oviformis	Cyclopyxis arcelloides	Cyphoderia ampulla	Difflugia lucida type	Difflugia oblonga-lacustris type	Difflugia pristis type	Euglypha rotunda	Euglypha tuberculata type	Heleopera petricola	Hyalosphenia ovalis	Hyalosphenia subflava	Nebela collaris	Nebela langeniformis	Pseudodifflgia fulva type	Psuedohyalosphenia type	Quadrullela symmetrica	Tracheleuglypha dentata	Trigonopyxis minuta	Trinema lineare	Valkanovia elegans
10	2.63	0	0	0	0	0	0	0	0	0	0	0	0	0	0	0	0	0	1	0	0	0	0	0	4	0	0	0	0	0	0
9	2.55	0	0	0	0	0	0	0	0	0	0	0	0	0	6	0	0	0	1	0	0	0	0	0	6	0	0	9	0	1	0
8	2.48	0	0	0	0	0	0	0	0	0	0	0	0	0	0	0	1	0	1	0	0	0	0	0	4	0	2	0	0	0	0
7	2.42	0	0	0	0	0	22	2	0	0	0	0	1	0	2	0	0	0	0	0	0	0	0	0	10	0	0	2	0	0	0
6	2.35	0	0	0	0	0	5	0	0	0	0	0	0	0	0	0	1	0	0	0	0	0	0	0	6	0	0	0	0	0	0
5	2.3	0	0	0	2	0	3	2	0	0	0	0	1	0	0	0	2	0	0	0	0	0	0	0	2	0	0	2	0	0	0
4	2.26	0	0	0	1	0	8	0	0	0	0	0	0	0	0	0	2	0	0	0	0	0	0	0	12	0	0	2	0	0	0
3	2.19	0	0	0	0	0	0	0	0	0	0	0	0	0	0	0	0	0	0	0	0	0	0	0	0	0	0	0	0	0	0
2	2.1	0	0	0	1	6	0	0	0	0	0	0	0	0	0	0	0	0	0	0	0	0	0	0	0	0	0	0	0	0	0
1	2.03	0	0	0	1	0	0	0	0	0	0	0	0	0	0	0	0	0	0	0	0	0	0	0	0	2	0	0	0	0	0

Table S7a: May 2014 absolute count data (death assemblages)

May 2014 Death assemblages

Station #	Elevation (m OD)	Arcella catinus	Arcella discoides type	Assulina muscorum	Campuscus type	Centropyxiella sp.	Centropyxis cassis type	Centropyxis delicatula type	Centropyxis ecornis	Centropyxis platystoma type	Corythion dubium	Cryptodifflugia oviformis	Cyclopyxis arcelloides	Cyphoderia ampulla	Difflugia lucida type	Difflugia oblonga-lacustris type	Difflugia pristis type	Euglypha rotunda	Euglypha tuberculata type	Heleopera petricola	Hyalosphenia ovalis	Hyalosphenia subflava	Nebela collaris	Nebela langeniformis	Pseudodifflgia fulva type	Psuedohyalosphenia type	Quadrullela symmetrica	Tracheleuglypha dentata	Trigonopyxis minuta	Trinema lineare	Valkanovia elegans
10	2.63	6	11	0	0	1	20	17	4	6	0	0	0	12	51	0	14	1	3	0	0	0	0	0	12	0	1	14	0	0	1
9	2.55	2	12	1	0	0	8	8	0	2	2	0	0	18	18	0	16	3	5	0	0	0	0	0	20	0	3	32	0	0	1
8	2.48	20	14	2	1	0	23	13	4	4	0	0	0	10	20	0	2	0	3	0	0	2	0	0	32	0	0	48	0	1	0
7	2.42	8	0	0	1	4	20	21	0	0	0	0	0	10	12	0	6	0	0	2	0	1	1	0	90	0	0	21	0	1	0
6	2.35	2	0	0	0	0	44	14	4	2	0	1	0	2	13	1	0	0	0	1	0	0	0	0	40	0	0	10	0	0	0
5	2.3	0	0	0	2	4	66	8	10	0	0	0	3	8	8	0	0	0	0	0	0	0	0	0	12	0	0	4	0	0	0
4	2.26	0	0	0	2	0	53	17	6	0	0	1	1	1	15	0	0	0	0	1	0	0	1	0	18	0	0	16	0	1	0
3	2.19	0	0	0	1	15	84	36	9	6	0	2	2	12	0	0	3	0	0	0	1	0	0	0	6	1	0	0	1	0	0
2	2.1	3	3	0	1	39	36	30	39	3	0	0	0	12	0	2	0	0	0	1	0	0	0	1	30	4	0	3	2	0	0
1	2.03	0	3	0	2	72	12	0	9	6	0	1	1	18	0	1	0	0	0	0	1	1	0	0	18	5	0	9	0	0	0

Table S7b: May 2014 absolute count data (live assemblages)

Station #	Elevation (m OD)	Arcella catinus	Arcella discoides type	Assulina muscorum	Campuscus type	Centropyxiella sp.	Centropyxis cassis type	Centropyxis delicatula type	Centropyxis ecornis	Centropyxis platystoma type	Corythion dubium	Cryptodifflugia oviformis	Cyclopyxis arcelloides	Cyphoderia ampulla	Difflugia lucida type	Difflugia oblonga-lacustris type	Difflugia pristis type	Euglypha rotunda	Euglypha tuberculata type	Heleopera petricola	Hyalosphenia ovalis	Hyalosphenia subflava	Nebela collaris	Nebela langeniformis	Pseudodifflgia fulva type	Psuedohyalosphenia type	Quadrullela symmetrica	Tracheleuglypha dentata	Trignopyxis minuta	Trinema lineare	Valkanovia elegans
10	2.63	0	0	0	0	0	0	0	0	0	0	0	0	0	0	0	0	0	0	0	0	0	0	0	0	0	0	0	0	0	0
9	2.55	0	0	0	0	0	0	0	0	0	0	0	0	3	0	0	0	0	1	0	0	0	0	0	0	0	1	2	0	0	0
8	2.48	0	0	0	0	0	10	0	0	0	0	0	0	0	2	0	0	0	0	0	0	0	0	0	0	0	0	2	0	0	0
7	2.42	0	0	0	0	0	0	0	0	0	0	0	0	0	0	0	2	0	0	0	0	0	0	0	0	0	0	0	0	0	0
6	2.35	0	0	0	0	0	0	0	0	0	0	0	0	0	0	0	0	0	0	0	0	0	0	0	0	0	0	0	0	0	0
5	2.3	0	0	0	0	0	2	0	6	0	0	0	1	0	2	0	0	0	0	0	0	0	0	0	0	0	0	0	0	0	0
4	2.26	0	0	0	0	0	6	0	0	0	0	0	0	0	0	0	0	0	0	0	0	0	0	0	2	0	0	2	0	0	0
3	2.19	0	0	0	0	0	0	0	0	0	0	0	0	0	0	0	0	0	0	0	0	0	0	0	0	0	0	0	0	0	0
2	2.1	0	0	0	0	0	0	0	0	0	0	0	0	0	0	0	0	0	0	0	0	0	0	0	0	2	0	0	0	0	0
1	2.03	0	0	0	1	0	0	0	0	0	0	0	0	0	0	0	0	0	0	0	0	0	0	0	1	0	0	0	0	0	0

Table S8a: June 2014 absolute count data (death assemblages)

June 2014 Death assemblages

Station #	Elevation (m OD)	Arcella catinus	Arcella discoides type	Assulina muscorum	Campuscus type	Centropyxiella sp.	Centropyxis cassis type	Centropyxis delicatula type	Centropyxis ecornis	Centropyxis platystoma type	Corythion dubium	Cryptodifflugia oviformis	Cyclopyxis arcelloides	Cyphoderia ampulla	Difflugia lucida type	Difflugia oblonga-lacustris type	Difflugia pristis type	Euglypha rotunda	Euglypha tuberculata type	Heleopera petricola	Hyalosphenia ovalis	Hyalosphenia subflava	Nebela collaris	Nebela langeniformis	Pseudodifflgia fulva type	Psuedohyalosphenia type	Quadrullela symmetrica	Tracheleuglypha dentata	Trignopyxis minuta	Trinema lineare	Valkanovia elegans
10	2.63	9	12	1	0	0	15	3	6	9	1	0	0	15	18	0	27	2	3	0	0	1	0	0	54	0	4	21	0	1	2
9	2.55	0	15	1	0	0	9	24	3	0	2	0	1	6	12	1	7	1	2	0	0	1	0	0	30	0	3	30	0	0	1
8	2.48	9	15	0	0	0	12	12	0	0	1	0	0	12	21	0	18	3	1	0	0	0	0	0	42	0	1	6	0	1	0
7	2.42	15	0	0	1	0	42	12	0	0	0	0	0	15	3	0	3	1	1	1	0	0	1	0	24	0	1	30	0	1	1
6	2.35	3	6	0	2	0	75	33	3	0	0	0	1	6	3	1	6	0	0	1	1	0	0	0	6	0	0	18	0	2	0
5	2.3	3	0	0	4	6	66	27	24	0	0	0	0	15	3	0	0	0	0	0	0	0	0	0	9	0	0	12	0	0	0
4	2.26	0	0	0	2	0	69	30	0	0	0	1	2	6	6	1	6	0	0	0	0	1	0	0	12	1	0	66	1	1	0
3	2.19	0	0	0	1	31	29	25	10	1	0	2	1	30	0	1	0	0	0	0	0	1	1	0	15	1	0	35	0	0	0
2	2.1	0	9	0	1	29	54	6	66	0	0	1	0	14	3	0	0	0	0	0	0	0	0	0	6	4	0	9	0	0	0
1	2.03	0	3	0	3	102	9	0	57	3	0	1	0	6	0	1	0	0	0	1	1	1	0	1	6	5	0	0	1	0	0

Table S8b: June 2014 absolute count data (live assemblages)

June 2014 Live assemblages

Station #	Elevation (m OD)	Arcella catinus	Arcella discoides type	Assulina muscorum	Campuscus type	Centropyxiella sp.	Centropyxis cassis type	Centropyxis delicatula type	Centropyxis ecornis	Centropyxis platystoma type	Corythion dubium	Cryptodifflugia oviformis	Cyclopyxis arcelloides	Cyphoderia ampulla	Difflugia lucida type	Difflugia oblonga-lacustris type	Difflugia pristis type	Euglypha rotunda	Euglypha tuberculata type	Heleopera petricola	Hyalosphenia ovalis	Hyalosphenia subflava	Nebela collaris	Nebela langeniformis	Pseudodifflgia fulva type	Psuedohyalosphenia type	Quadrullela symmetrica	Tracheleuglypha dentata	Trignopyxis minuta	Trinema lineare	Valkanovia elegans
10	2.63	0	0	0	0	0	0	0	3	0	0	0	0	0	0	0	0	0	0	0	0	0	0	3	0	1	0	0	0	0
9	2.55	0	0	0	0	0	21	0	0	0	0	0	0	0	0	0	5	0	0	0	0	0	0	3	0	1	15	0	0	0
8	2.48	0	0	0	0	0	12	0	0	0	0	0	0	0	0	0	0	0	1	0	0	0	0	0	0	0	3	0	0	0
7	2.42	0	0	0	0	0	3	0	0	0	0	0	1	0	0	0	0	0	0	0	0	0	0	0	0	0	3	0	0	0
6	2.35	0	0	0	1	0	42	3	0	0	0	0	0	0	0	0	0	0	0	0	0	0	0	0	0	0	9	0	0	0
5	2.3	0	0	0	1	0	6	0	3	0	0	0	0	3	0	0	0	0	0	0	0	0	0	0	0	0	0	0	0	0
4	2.26	0	0	0	0	0	6	0	0	0	0	0	0	0	0	0	0	0	0	0	0	0	0	0	0	0	6	0	0	0
3	2.19	0	0	0	0	0	0	0	0	0	0	0	0	0	0	0	0	0	0	0	0	0	0	0	0	0	0	0	0	0
2	2.1	0	0	0	2	0	0	0	3	0	0	0	0	3	0	0	0	0	0	0	0	0	0	0	0	0	0	0	0	0
1	2.03	0	0	0	1	0	0	0	0	0	0	0	0	0	0	0	0	0	0	0	0	0	0	0	1	0	0	0	0	0

Table S9a: July 2014 absolute count data (death assemblages)

July 2014 Death assemblages																															
Station #	Elevation (m OD)	Arcella catinus	Arcella discoides type	Assulina muscorum	Campuscus type	Centropyxiella sp.	Centropyxis cassis type	Centropyxis delicatula type	Centropyxis ecornis	Centropyxis platystoma type	Corythion dubium	Cryptodifflugia oviformis	Cyclopyxis arcelloides	Cyphoderia ampulla	Difflugia lucida type	Difflugia oblonga-lacustris type	Difflugia pristis type	Euglypha rotunda	Euglypha tuberculata type	Heleopera petricola	Hyalosphenia ovalis	Hyalosphenia subflava	Nebela collaris	Nebela langeniformis	Pseudodifflugia fulva type	Psuedohyalosphenia type	Quadrulella symmetrica	Tracheleuglypha dentata	Trignopyxis minuta	Trinema lineare	Valkanovia elegans
10	2.63	3	8	0	0	0	30	23	3	5	0	0	0	5	11	0	15	3	4	0	0	0	0	0	29	0	1	14	0	0	0
9	2.55	0	6	1	0	0	21	18	1	3	1	0	1	6	9	0	15	2	5	0	0	0	0	0	15	0	2	50	0	2	1
8	2.48	0	8	2	1	0	24	12	0	3	1	0	0	11	12	1	6	3	2	0	0	0	1	0	39	0	1	42	0	1	0
7	2.42	4	3	0	3	3	23	12	1	1	0	0	0	9	6	0	4	0	1	1	0	0	0	0	48	0	0	33	0	0	0
6	2.35	2	3	0	3	1	56	15	6	1	0	0	4	10	5	1	1	0	0	1	0	0	0	0	27	0	0	24	0	1	0
5	2.3	3	0	0	2	2	58	17	14	1	0	0	0	12	5	0	6	0	0	0	0	0	0	0	21	0	0	13	0	0	0
4	2.26	0	0	0	0	6	50	21	21	0	0	0	0	14	5	0	3	0	0	0	0	0	0	0	12	0	0	12	0	0	0
3	2.19	0	3	0	0	26	36	16	36	3	0	0	0	17	1	0	4	0	0	0	0	0	0	0	6	3	0	5	0	0	0
2	2.1	0	3	0	0	40	28	10	29	0	0	0	0	23	0	0	0	0	0	0	0	0	0	0	9	1	0	3	0	0	0
1	2.03	0	5	0	0	71	12	3	23	0	0	2	1	30	3	0	1	0	0	0	0	0	0	0	5	5	0	0	1	0	0

Table S9b: July 2014 absolute count data (live assemblages)

July 2014 Live assemblages																															
Station #	Elevation (m OD)	Arcella catinus	Arcella discoides type	Pseudodifflugia fulva type	Centropyxis cassis type	Centropyxis delicatula type	Centropyxis platystoma type	Centropyxiella sp.	Centropyxis ecornis	Difflugia pristis type	Difflugia lucida type	Cyphoderia ampulla	Tracheleuglypha dentata	Psuedohyalosphenia type	Euglypha tuberculata type	Euglypha rotunda	Trinema lineare	Assulina muscorum	Valkanovia elegans	Difflugia oblonga-lacustris type	Quadrulella symmetrica	Heleopera petricola	Cyclopyxis arcelloides	Hyalosphenia subflava	Corythion dubium	Nebela collaris	Campuscus type	Trignopyxis minuta	Hyalosphenia ovalis	Nebela langeniformis	Cryptodifflugia oviformis
10	2.63	0	0	0	5	1	1	0	0	5	2	1	4	0	1	0	0	0	0	0	0	0	0	0	0	0	0	0	0	0	0
9	2.55	0	0	0	6	0	0	0	0	4	1	0	15	0	2	0	0	0	0	0	0	0	0	0	0	0	0	0	0	0	0
8	2.48	0	0	0	4	0	0	0	0	1	2	1	11	0	0	0	0	0	0	0	0	0	0	0	0	0	0	0	0	0	0
7	2.42	0	0	0	8	0	0	0	1	1	1	0	9	0	0	0	0	0	0	0	0	0	0	0	0	0	0	0	0	0	0
6	2.35	0	0	0	17	0	0	0	1	0	0	1	6	0	0	0	0	0	0	0	0	0	0	0	0	0	1	0	0	0	0
5	2.3	0	0	0	22	1	0	0	3	0	1	0	1	0	0	0	0	0	0	0	0	0	0	0	0	0	0	0	0	0	0
4	2.26	0	0	0	13	0	0	0	5	0	0	1	3	0	0	0	0	0	0	0	0	0	0	0	0	0	0	0	0	0	0
3	2.19	0	0	0	7	1	0	2	6	0	0	2	1	0	0	0	0	0	0	0	0	0	0	0	0	0	1	0	0	0	0
2	2.1	0	0	0	4	0	0	4	5	0	0	3	0	0	0	0	0	0	0	0	0	0	0	0	0	0	1	0	0	0	0
1	2.03	0	0	0	2	0	0	9	4	0	0	2	0	1	0	0	0	0	0	0	0	0	0	0	0	0	0	0	0	0	0

Table S10a: August 2014 absolute count data (death assemblages)

August 2014 Death assemblages																															
Station #	Elevation (m OD)	Arcella catinus	Arcella discoides type	Assulina muscorum	Campuscus type	Centropyxiella sp.	Centropyxis cassis type	Centropyxis delicatula type	Centropyxis ecornis	Centropyxis platystoma type	Corythion dubium	Cryptodifflugia oviformis	Cyclopyxis arcelloides	Cyphoderia ampulla	Difflugia lucida type	Difflugia oblonga-lacustris type	Difflugia pristis type	Euglypha rotunda	Euglypha tuberculata type	Heleopera petricola	Hyalosphenia ovalis	Hyalosphenia subflava	Nebela collaris	Nebela langeniformis	Pseudodifflugia fulva type	Psuedohyalosphenia type	Quadrulella symmetrica	Tracheleuglypha dentata	Trignopyxis minuta	Trinema lineare	Valkanovia elegans
10	2.63	3	6	1	0	0	23	13	0	4	0	0	0	4	13	0	15	2	1	0	0	1	0	0	44	0	3	18	0	3	1
9	2.55	0	5	1	0	0	18	15	0	3	0	0	0	5	8	1	13	1	2	1	0	0	0	0	35	0	1	35	0	1	0
8	2.48	0	6	0	0	0	20	10	0	3	0	0	1	9	10	0	5	1	3	0	0	0	0	0	33	0	0	41	0	0	0
7	2.42	4	3	0	1	3	19	10	8	0	0	0	2	19	5	0	3	0	0	0	0	0	0	0	40	0	0	27	0	2	0
6	2.35	8	2	0	0	0	46	13	5	1	0	0	0	25	4	0	1	0	0	0	0	0	0	0	23	0	0	20	0	0	0
5	2.3	4	0	0	4	1	49	14	11	1	0	0	0	14	0	0	5	0	0	0	0	0	0	0	18	1	0	11	0	0	0
4	2.26	1	0	0	0	5	42	18	18	0	0	0	0	25	0	0	3	0	0	0	0	0	0	0	10	3	0	16	0	0	0
3	2.19	0	3	0	0	21	30	14	25	0	0	0	0	14	1	0	4	0	0	0	0	0	0	0	5	0	0	4	0	0	0
2	2.1	0	2	0	0	33	23	8	24	1	0	0	0	19	0	0	1	0	0	0	0	0	0	0	8	0	0	3	0	0	0
1	2.03	0	4	0	0	65	8	2	21	0	0	0	0	25	0	0	1	0	0	0	0	0	0	0	4	5	0	0	0	0	0

Table S10b: August 2014 absolute count data (live assemblages)

August 2014 Death assemblages

Station #	Elevation (m OD)	Arcella catinus	Arcella discoides type	Assulina muscorum	Campuscus type	Centropyxiella sp.	Centropyxis cassis type	Centropyxis delicatula type	Centropyxis ecornis	Centropyxis platystoma type	Corythion dubium	Cryptodifflugia oviformis	Cyclopyxis arcelloides	Cyphoderia ampulla	Difflugia lucida type	Difflugia oblonga-lacustris type	Difflugia pristis type	Euglypha rotunda	Euglypha tuberculata type	Heleopera petricola	Hyalosphenia ovalis	Hyalosphenia subflava	Nebela collaris	Nebela langeniformis	Pseudodifflugia fulva type	Psuedohyalosphenia type	Quadrulella symmetrica	Tracheleuglypha dentata	Trignopyxis minuta	Trinema lineare	Valkanovia elegans
10	2.63	0	0	0	0	0	5	2	0	1	0	0	0	0	2	0	4	0	1	0	0	0	0	0	3	0	1	4	0	0	0
9	2.55	0	0	0	0	0	3	4	0	0	0	0	0	0	4	0	3	0	0	0	0	0	0	0	1	0	0	11	0	0	0
8	2.48	0	0	0	0	0	2	1	0	0	0	0	0	0	0	0	1	0	0	0	0	0	0	0	1	0	2	13	0	0	0
7	2.42	0	0	0	0	0	1	2	0	0	0	0	0	0	1	0	0	0	0	0	0	0	0	0	0	0	0	4	0	0	0
6	2.35	0	0	0	1	0	9	1	3	0	0	0	0	0	0	0	0	0	0	0	0	0	0	0	1	0	0	3	0	0	0
5	2.3	0	0	0	0	0	12	0	5	0	0	0	0	0	0	0	0	0	0	0	0	0	0	0	1	0	0	1	0	0	0
4	2.26	0	0	0	1	0	15	1	6	0	0	0	0	0	0	0	1	0	0	0	0	0	0	0	0	0	0	2	0	0	0
3	2.19	0	0	0	1	4	7	2	5	0	0	0	0	0	0	0	0	0	0	0	0	0	0	0	0	1	0	1	0	0	0
2	2.1	0	0	0	0	6	2	0	7	0	0	0	0	0	0	0	0	0	0	0	0	0	0	0	0	2	0	0	0	0	0
1	2.03	0	0	0	0	5	0	0	4	0	0	0	0	0	0	0	0	0	0	0	0	0	0	0	0	1	0	0	0	0	0

Table S11a: September 2014 absolute count data (death assemblages)

September 2014 Death assemblages

Station #	Elevation (m OD)	Arcella catinus	Arcella discoides type	Assulina muscorum	Campuscus type	Centropyxiella sp.	Centropyxis cassis type	Centropyxis delicatula type	Centropyxis ecornis	Centropyxis platystoma type	Corythion dubium	Cryptodifflugia oviformis	Cyclopyxis arcelloides	Cyphoderia ampulla	Difflugia lucida type	Difflugia oblonga-lacustris type	Difflugia pristis type	Euglypha rotunda	Euglypha tuberculata type	Heleopera petricola	Hyalosphenia ovalis	Hyalosphenia subflava	Nebela collaris	Nebela langeniformis	Pseudodifflugia fulva type	Psuedohyalosphenia type	Quadrulella symmetrica	Tracheleuglypha dentata	Trignopyxis minuta	Trinema lineare	Valkanovia elegans
10	2.63	3	18	1	0	1	18	6	3	6	0	0	0	3	15	0	30	0	1	0	0	0	0	0	63	0	2	15	0	0	0
9	2.55	2	1	0	0	3	27	15	1	6	2	0	0	9	12	0	9	1	3	1	0	0	0	0	27	0	3	39	0	1	1
8	2.48	0	6	0	0	0	9	12	1	0	0	0	0	21	3	0	9	0	0	1	0	0	0	0	60	0	0	36	0	0	0
7	2.42	0	9	0	2	6	27	12	1	0	0	0	1	33	15	0	1	0	0	0	0	0	0	0	54	0	0	15	0	0	0
6	2.35	0	3	0	2	3	85	30	0	0	0	0	0	30	12	0	1	0	0	0	0	0	0	0	12	0	0	21	0	0	0
5	2.3	0	0	0	0	24	51	6	6	3	0	0	0	57	3	0	6	0	0	0	0	0	0	0	3	0	0	6	0	0	0
4	2.26	0	6	0	1	28	27	12	12	0	0	0	2	21	6	0	3	0	0	0	0	0	0	0	9	0	0	42	0	0	0
3	2.19	0	1	0	1	12	21	9	65	1	0	1	0	33	2	0	1	0	0	0	0	0	0	0	3	2	0	9	0	0	0
2	2.1	0	3	0	0	54	3	1	13	1	0	0	0	57	2	0	0	0	0	1	0	0	0	0	6	3	0	0	0	0	0
1	2.03	0	0	0	1	90	0	0	21	0	0	1	0	33	0	0	1	0	0	0	2	0	0	0	0	6	0	0	0	0	0

Table S11b: September 2014 absolute count data (live assemblages)

September 2014 Live assemblages

Station #	Elevation (m OD)	Arcella catinus	Arcella discoides type	Assulina muscorum	Campuscus type	Centropyxiella sp.	Centropyxis cassis type	Centropyxis delicatula type	Centropyxis ecornis	Centropyxis platystoma type	Corythion dubium	Cryptodifflugia oviformis	Cyclopyxis arcelloides	Cyphoderia ampulla	Difflugia lucida type	Difflugia oblonga-lacustris type	Difflugia pristis type	Euglypha rotunda	Euglypha tuberculata type	Heleopera petricola	Hyalosphenia ovalis	Hyalosphenia subflava	Nebela collaris	Nebela langeniformis	Pseudodifflugia fulva type	Psuedohyalosphenia type	Quadrulella symmetrica	Tracheleuglypha dentata	Trignopyxis minuta	Trinema lineare	Valkanovia elegans
10	2.63	0	0	0	0	0	0	0	0	0	0	0	0	0	3	0	3	0	0	0	0	0	0	0	3	0	0	3	0	0	0
9	2.55	0	0	0	0	0	0	0	0	0	0	0	0	0	3	0	6	0	0	0	0	0	0	0	3	0	0	9	0	0	0
8	2.48	0	0	0	1	0	0	0	0	0	0	0	0	3	3	0	0	0	0	0	0	0	0	0	1	0	0	3	0	0	0
7	2.42	0	0	0	0	0	6	0	0	0	0	0	0	0	0	0	0	0	0	0	0	0	0	0	1	0	0	1	0	0	0
6	2.35	0	0	0	0	0	8	0	0	0	0	0	0	9	3	0	0	0	0	0	0	0	0	0	6	0	0	0	0	0	0
5	2.3	0	0	0	1	6	0	0	0	0	0	0	0	3	0	0	0	0	0	0	0	0	0	0	0	0	0	0	0	0	0
4	2.26	0	0	0	0	2	3	0	0	0	0	0	0	15	3	0	0	0	0	0	0	0	0	0	0	0	0	0	0	0	0
3	2.19	0	0	0	0	1	3	0	4	0	0	0	0	15	0	0	0	0	0	0	0	0	0	0	0	1	0	0	0	0	0
2	2.1	0	0	0	0	1	0	0	2	0	0	0	0	3	3	0	0	0	0	0	0	0	0	0	0	0	0	0	0	0	0
1	2.03	0	0	0	0	1	0	0	0	0	0	0	0	0	0	0	0	0	0	0	0	0	0	0	0	1	0	15	0	0	0

Table S12a: October 2014 absolute count data (death assemblages)

October 2014 Death assemblages

Station #	Elevation (m OD)	Arcella catinus	Arcella discoides type	Assulina muscorum	Campuscus type	Centropyxiella sp.	Centropyxis cassis type	Centropyxis delicatula type	Centropyxis ecornis	Centropyxis platystoma type	Corythion dubium	Cryptodifflugia oviformis	Cyclopyxis arcelloides	Cyphoderia ampulla	Difflugia lucida type	Difflugia oblonga-lacustris type	Difflugia pristis type	Euglypha rotunda	Euglypha tuberculata type	Heleopera petricola	Hyalosphenia ovalis	Hyalosphenia subflava	Nebela collaris	Nebela langeniformis	Pseudodifflugia fulva type	Psuedohyalosphenia type	Quadrulella symmetrica	Tracheleuglypha dentata	Trignopyxis minuta	Trinema lineare	Valkanovia elegans
10	2.63	2	8	0	0	1	37	3	2	16	1	0	0	4	10	0	20	1	2	0	0	0	0	0	18	0	3	12	0	0	0
9	2.55	1	3	0	0	2	29	3	0	0	0	0	0	15	1	0	2	2	3	0	0	0	0	0	15	0	4	85	0	1	1
8	2.48	5	19	0	1	6	9	15	0	3	0	0	0	39	15	0	1	0	1	0	0	0	0	0	10	0	0	42	0	0	0
7	2.42	6	9	0	2	0	21	3	9	0	1	0	3	34	0	1	0	0	1	1	0	0	0	0	35	0	1	44	0	2	0
6	2.35	1	15	0	4	0	42	15	1	0	0	0	0	27	3	0	2	0	0	0	0	0	0	0	3	0	0	33	0	0	0
5	2.3	6	2	0	0	6	42	21	6	0	0	0	0	37	1	0	0	0	0	0	0	0	0	0	9	0	0	3	0	0	0
4	2.26	1	0	0	0	9	93	9	27	0	0	0	0	15	0	0	3	0	0	0	0	0	0	0	0	1	0	3	0	0	0
3	2.19	0	3	0	1	41	0	2	97	0	0	2	0	21	0	0	0	0	0	0	0	0	1	1	9	4	0	6	0	1	0
2	2.1	2	1	0	0	54	7	9	34	0	0	0	0	63	0	1	0	0	0	0	0	0	0	0	6	3	0	0	1	0	0
1	2.03	1	1	0	1	60	0	7	36	0	0	0	0	31	0	0	0	0	0	0	0	0	0	0	11	2	0	2	0	1	0

Table S12b: October 2014 absolute count data (live assemblages)

October 2014 Live assemblages

Station #	Elevation (m OD)	Arcella catinus	Arcella discoides type	Assulina muscorum	Campuscus type	Centropyxiella sp.	Centropyxis cassis type	Centropyxis delicatula type	Centropyxis ecornis	Centropyxis platystoma type	Corythion dubium	Cryptodifflugia oviformis	Cyclopyxis arcelloides	Cyphoderia ampulla	Difflugia lucida type	Difflugia oblonga-lacustris type	Difflugia pristis type	Euglypha rotunda	Euglypha tuberculata type	Heleopera petricola	Hyalosphenia ovalis	Hyalosphenia subflava	Nebela collaris	Nebela langeniformis	Pseudodifflugia fulva type	Psuedohyalosphenia type	Quadrulella symmetrica	Tracheleuglypha dentata	Trignopyxis minuta	Trinema lineare	Valkanovia elegans
10	2.63	0	0	0	0	0	3	0	0	2	0	0	0	0	0	0	0	0	1	1	0	0	0	0	4	0	0	0	0	0	0
9	2.55	0	0	0	0	0	4	0	0	0	0	0	0	6	0	0	0	0	0	0	0	0	0	0	0	0	0	8	0	0	0
8	2.48	0	0	0	0	0	0	0	0	0	0	0	0	9	3	0	0	0	1	0	0	0	0	0	1	0	0	0	0	0	0
7	2.42	0	0	0	0	0	0	0	0	0	0	0	0	2	0	0	0	0	0	0	0	0	0	0	0	0	0	1	0	0	0
6	2.35	0	0	0	2	0	9	0	0	0	0	0	0	3	0	0	0	0	0	0	0	0	0	0	0	0	0	0	0	0	0
5	2.3	0	0	0	1	0	0	0	0	0	0	0	0	0	0	0	0	0	0	0	0	0	0	0	0	0	0	0	0	0	0
4	2.26	0	0	0	0	0	6	0	0	0	0	0	0	0	0	0	0	0	0	0	0	0	0	0	0	0	0	0	0	0	0
3	2.19	0	0	0	0	0	0	0	3	0	0	0	0	0	0	0	0	0	0	0	0	0	0	0	0	0	0	0	0	0	0
2	2.1	0	0	0	0	6	0	0	0	0	0	0	0	6	0	0	0	0	0	0	0	0	0	0	0	1	0	0	0	0	0
1	2.03	0	0	0	0	9	0	0	3	0	0	0	0	2	0	0	1	0	0	0	0	0	0	0	0	0	0	0	0	0	0

Table S13a: November 2014 absolute count data (death assemblages)

November 2014 Death assemblages

Station #	Elevation (m OD)	Arcella catinus	Arcella discoides type	Assulina muscorum	Campuscus type	Centropyxiella sp.	Centropyxis cassis type	Centropyxis delicatula type	Centropyxis ecornis	Centropyxis platystoma type	Corythion dubium	Cryptodifflugia oviformis	Cyclopyxis arcelloides	Cyphoderia ampulla	Difflugia lucida type	Difflugia oblonga-lacustris type	Difflugia pristis type	Euglypha rotunda	Euglypha tuberculata type	Heleopera petricola	Hyalosphenia ovalis	Hyalosphenia subflava	Nebela collaris	Nebela langeniformis	Pseudodifflugia fulva type	Psuedohyalosphenia type	Quadrulella symmetrica	Tracheleuglypha dentata	Trignopyxis minuta	Trinema lineare	Valkanovia elegans
10	2.63	3	5	0	0	0	28	6	0	19	0	0	0	2	11	0	21	0	0	0	0	0	0	0	25	0	0	30	0	0	0
9	2.55	2	5	0	0	3	18	9	0	0	0	0	0	18	0	0	8	0	1	0	0	0	0	0	14	0	2	75	0	1	0
8	2.48	5	15	0	0	0	14	19	1	2	1	0	0	29	15	0	10	0	0	0	0	0	0	0	11	0	0	29	0	0	0
7	2.42	7	9	0	2	3	24	3	9	2	0	0	0	31	0	0	0	0	0	1	0	0	0	0	25	0	1	38	0	0	0
6	2.35	0	6	0	1	0	41	19	0	0	0	0	1	22	1	0	0	0	0	0	0	0	0	0	15	0	0	47	0	0	0
5	2.3	4	0	0	1	4	65	25	4	0	0	0	0	22	2	1	6	0	0	0	0	0	0	0	12	0	0	6	0	0	0
4	2.26	1	0	0	0	13	93	13	13	0	0	0	0	12	0	0	2	0	0	0	0	0	0	0	0	1	0	3	0	0	0
3	2.19	0	2	0	1	39	47	0	35	0	0	2	0	14	0	0	0	0	0	0	0	0	0	0	9	3	0	5	0	0	0
2	2.1	0	3	0	0	59	17	8	29	0	0	0	0	28	0	0	1	0	0	0	0	0	0	0	5	2	0	3	1	0	0
1	2.03	1	0	0	0	87	0	4	25	0	0	1	1	26	0	1	0	0	0	0	0	0	0	0	4	3	0	5	0	0	0

Table S13b: November 2014 absolute count data (live assemblages)

November 2014 Death assemblages

Station #	Elevation (m OD)	Arcella catinus	Arcella discoides type	Assulina muscorum	Campuscus type	Centropyxiella sp.	Centropyxis cassis type	Centropyxis delicatula type	Centropyxis ecornis	Centropyxis platystoma type	Corythion dubium	Cryptodifflugia oviformis	Cydopyxis arcelloides	Cyphoderia ampulla	Difflugia lucida type	Difflugia oblonga-lacustris type	Difflugia pristis type	Euglypha rotunda	Euglypha tuberculata type	Heleopera petricola	Hyalosphenia ovalis	Hyalosphenia subflava	Nebela collaris	Nebela langeniformis	Pseudodifflugia fulva type	Psuedohyalosphenia type	Quadrulella symmetrica	Tracheleuglypha dentata	Trignopyxis minuta	Trinema lineare	Valkanovia elegans
10	2.63	0	0	0	0	0	0	0	0	1	0	0	0	0	1	0	0	0	0	0	0	0	0	0	2	0	0	2	0	0	0
9	2.55	0	0	0	0	0	0	0	0	0	0	0	0	0	0	0	0	0	0	0	0	0	0	0	0	0	0	1	0	0	0
8	2.48	0	1	0	1	0	0	2	0	0	0	0	0	0	2	0	0	0	0	0	0	0	0	0	1	0	0	3	0	0	0
7	2.42	1	1	0	0	0	1	1	0	0	0	0	0	0	0	0	0	0	0	0	0	0	0	0	2	0	0	2	0	0	0
6	2.35	0	0	0	0	0	4	0	0	0	0	0	0	0	0	0	0	0	0	0	0	0	0	0	0	0	0	4	0	0	0
5	2.3	0	0	0	0	0	3	3	0	0	0	0	0	0	0	0	0	0	0	0	0	0	0	0	0	0	0	0	0	0	0
4	2.26	0	0	0	0	3	5	4	2	0	0	0	0	0	0	0	0	0	0	0	0	0	0	0	0	0	0	0	0	0	0
3	2.19	0	0	0	0	3	1	0	8	0	0	0	0	0	0	0	0	0	0	0	0	0	0	0	0	0	0	0	0	0	0
2	2.1	0	0	0	0	6	0	0	6	0	0	0	0	0	0	0	0	0	0	0	0	0	0	0	0	0	0	0	0	0	0
1	2.03	0	0	0	0	10	0	0	1	0	0	0	0	0	0	0	0	0	0	0	0	0	0	0	0	1	0	0	0	0	0

APPENDIX E – Swan Inlet, Falkland Islands species data

Table S14a: Absolute modern (surface) diatom count data from Swan Inlet for core SI-2

Elevation (m SID)	-0.95	-0.99	-1	-1.06	-1.09	-1.11	-1.12	-1.14	-1.16	-1.18	-1.2	-1.22	-1.25	-1.31	-1.34	-1.36	-1.39	-1.4	-1.42	-1.43	-1.445	-1.48	-1.488	-1.49	-1.5	-1.51	-1.54	-1.57	-1.59	-1.62	-1.66	-1.69	-1.73	-1.76	-1.8	-1.9	-1.92	-1.93	-1.94
Achnanthes brevipes																																								
Achnanthes kuelbsii	1	2				3		4	26	15	20	63	54	1	24	1	53	7	28	34	36	28	56	41	65	90	30	54	34	39	66	56	86	90	114	108	134	200	190
Achnanthes lancoleata											4	24	4	6	10	37	52	2		3	1			3	2	10														
Achnanthes lutherii																3				1	1																			
Amphora ovails																						64	10					3			1	1	1						3
Caloneis bacillum	3	2		2	10	16	20	18	7	1		3	24	39	45	18	8	7	24	24	44	10	14	6	23	12	18	6	8	9	11	18	12	8	10	6	21	30	18
Cocconeis placentula				1					12	1					10		12	5	2	11	10	1	14	8	3	14	12	1	20	6	2	3	8	12	1	2	8	2	7	1
Cocconeis scutellum	6								1									4																						
Cosmioneis hawaiiensis												24	6			1	1																							
Ctenophora pulchella	5			6	12	10	6	10		9	12		15	5	33	36	32	56	35	14	28	19	13		6	32	34	26	50		26	74	24	46	28	100	21	8	19	2
Cymbella lacustris											48	13	5	6																									
Cymbella turgidula																						1						2	2						3	2			
Diatoma monoliliformis				1																		1				4		3				1				3			
Diatomella balfouriana																							1															1		
Diploneis elliptica	3	1	1															1																						
Diploneis oblengella																		1																						
Diploneis oblongella	1	1				36	30	24	36	13	10	5	9	3	2	1				8		16	54	38	5	108	33	28	4	14	18	33	39	53	44	22	6	21	30	6	2
Distrionella incognita	1	1		1		26		2	2		5	11	9	3	6	2	1	5	1	13	6	4	18	12	4	2	9	4	2	8	4	2	1	1	1	2	1	2	6	2
Epithema adnanta																																							
Eunotia intermedia																																							
Eunotia minor	1	4		4	4	2	2	4	1	9	12	6	6	3	2	2	7	5	1	10	1	2	8	5	1	3	9	20	8	24	3	6	4	3	6	6	6	13	6
Eunotia silvahercynia	2	1																																					
Fallacia pygmaea																																							1
Fragilaria brevistrata var. trianga														1																									
Fragilaria construens	3	2		4	18		8	6	13	2	6	45	54	9	21	14	28	7	6	22	30	18	54	38	1	75	16	16	34	11	16	78	17	72	65	16	26	21	30	99
Fragilaria fasiculata		7		16		4				3	4	9	8	2	8	8	1	18	10	13	12	4	12	3	17	9	11	12	8	4	14	11	8	17	14	6	8	18	30	2
Fragilaria capucina												4																												
Frustulia rhomboides		1											1	30	28	56	24	56	68	50	48	36	6	9	6	24	4	14	2	1	17	6	24	20	1	1	1	1	1	1
Gomphonema parvulum														4	56	8	14	24	3	48	1	36	2	6	3	4	6	20	1	14	12	1	1	2	16	14	15	3	1	1	14
Gyrosigma wansbeckii	1													9	3	2	24	2	3	1	1	2	3	3	1	6	4	1	3	1	1	2	1	4	2	1	1	1	1	1	1
Hannaea arcus																																							
Haslea crucigera																																							
Mastalogia elliptica																																							
Melosira monoliliformis	1	30	3	4	132	150	28	36	41	12	33	12	27	42	114	24	81	121	110	40	38	22	49	8	33	75	36	21	11	56	48	116	47	51	44	28	6	30	3	1
Navicula elegans	81	100			6	36	28	20	41	12	18	16	3	24	4	8	4	15	20	36	24	20	16	8	2	24	21	11	3	48	0	2	4	6	2	10	8	21	14	30	1
Navicula halophila					6	10	6	4	18	6	16	3	6	9	8	4	16	7	2	6	6	4	3	2	1	2	4	3	6	4	2	3	1	2	1	1	1	10	14	6	14	1	14	1
Nedium iridis																																							
Nitzschia brevissima												36																												
Nitzschia capitellata	4	2			4	8	4	4	2	63	32		9	7	24	56	20	8	20	24	18	18	11	4	2	9	1	6	26	4	2	1	2	1	1	1	4	2	1	1
Nitzschia flexa																		20	8																					
Nitzschia gracillis										2					1	2																									
Nitzschia lancoleata	2			1	4				43	1			2	6	3																									
Nitzschia sigma							2		17					2							8		4	3																	
Nitzschia sigmoidea												1								8			4	3																
Nitzschia thermaloides																																							
Opephora pacifica		1		10	6	8	6	8	6	24	22	3	35	3	6	12	14	11	5	6	16	4	28	33	14	9	7	22	5	3	27	12	16	15	7	4	12	8	12	18
Opephora pacifica		1		4	6	2	18	7	12	15	1	2	3	6	12	1	7	1	5	1	4	6	1	4	1	2	8	4	1	3	2	1	1	1	2	1	1	1	1		
Paralia sulcata				6	4	20	18	6	12	14	2	1	3	9	7	8	13	6	5	2	1	15	1	6	1	14	12	6	3	2	1	1	1	9	2	1	1	1	1		
Pinnularia borealis	62	18		10	32	40	120	8	20	12	5	12	15	3	17	25	3	19	10	30	10	9	1	4	46	108	2	8	4	46	1	8	10	2	38	1	6	4	1		
Pinnularia microstauron	36	27	1	8	38	58	5		49	35	48	3	9	12	47	6	33	2	4	14	12	32	1	2	8	51	20	4	1	39	1	42	1	6	1	2	1	1		
Pinnularia virdis	194	165		27	58	40	120	6	20	12	15	50	75	1	25	4	32	4	19	10	2	4	28	49	4	108	30	20	1	4	40	4	4	4	53	3	44	1	6		
Planothidium delicatulum				2	2	4	8	4	10	6	1	20	44	1	16	1	4	12	8	1	4	1	4	49	14	1	2	1	1	1	4	4	4	4	1	2	1	1	1		
Podosira stelliger																																							
Rhabdomena arcuatum				6	14	10	4	2	10	8	1	5	60	1	4	2	12	8	3	18	1	14	4	14	1	6	8	1	1	1	4	12	6	1	1	1	1	1	1		
Rhabdomena minutum																																							
Rhopalodia acuminata	3	3		1	6	14	10	5	2	3	4	2	8	1	2	3	1	3	2	4	4	18	2	13	1	14	6	3	2	3	1	6	2	6	1	1	1	1	1		
Rhopalodia brebissonii	1	3		6	4	4	8	6	15	9	1	12	5	1	6	2	28	6	2	8	14	12	32	2	58	1	1	5	1	1	1	1	1	1	1	1	1	1	1		
Rossithidium nodosum	3	3		6	14	10	6	4	10	30	11	36	9	15	33	16	22	10	6	3	8	2	8	23	1	6	4	1	5	4	8	6	12	16	28	6	1	8	6		
Stauroforma exiguiformis	9	7		8	14	10	6	6	10	30	11	36	9	15	33	16	22	10	6	3	8	2	8	25	1	6	4	1	5	4	8	6	12	16	12	6	1	1	4		
Stauroneis phoenicenteron																																							
Suriella brebosonii					6	4	10	5	1	4	1	5	1	1	1	1	1	1	1	4	2	1	1	1	1	1	1	1	1	1	1	1	1	1	1	1	1	1	1		
Trachyneis aspera																																							
Unknown	3	7		4	5	5	6	2	5	3	1	1	3	5	4	2	6	3	1	4	2	7	3	6	3	4	3	4	1	3	3	8	4	2	3	4	6	4	1		

Table S14b: Absolute fossil (core) diatom count data from Swan Inlet for core SI-2

Core depth (cm)	Achnanthes brevipes	Achnanthes kuelbsii	Achnanthes lanceolata	Achnanthes undulatum	Actinocyclus normanii	Actinocyclus undulatus	Amphora ovalis	Caloneis bacillum	Cocconeis placentula	Cocconeis scutellum	Cosmioneis hawaiiensis	Ctenophora pulchella	Cymbella spp.	Diploneis elliptica	Diploneis oblongella	Epithemia adnata	Eunotia minor	Eunotia subarcuatoides	Fragilaria construens	Fragilaria fasciculata	Frustulia cupidata	Frustulia rhomboides	Gomphonema parvulum	Gyrosigma wansbeckii	Hasleа crucigera	Luticola sp.	Melosira moniliformis	Navicula elegans	Navicula gracilis	Navicula halophila	Neidium iridis	Nitzschia capitellata	Nitzschia gracilis	Nitzschia hyercynium	Nitzschia linearis	Nitzschia sigma	Nitzschia sigmoidea	Opephora pacifica	Parallia sulcata	Pinnularia viridis	Pinnularia microstauron	Pinnularia borealis	Planothidium delicatulum	Podosira stelliger	Rhopalodia acuminata	Rhopalodia brebissonii	Rossithidium nodosum	Staurosirella phoenicentron	Staurosira atomus	Stauroforma sp.	Surirella brebissonii	Tetracyclus sp.	Trachyneis aspera	Tryblionella gracilis	Unknown
1	0	3	0	1	0	0	0	5	0	0	0	2	0	1	1	1	13	0	1	6	0	0	0	0	0	0	0	119	0	0	0	1	1	0	0	0	0	5	1	39	41	31	15	0	1	1	0	0	5	0	2	0	0	0	7
2	1	9	0	0	0	0	0	5	0	0	0	2	2	0	1	3	8	0	13	6	0	0	1	0	0	0	0	90	0	0	0	1	0	0	0	0	0	19	0	14	63	26	9	0	0	0	0	0	21	0	0	0	0	0	6
3	0	0	0	0	0	0	1	6	3	4	0	11	1	0	1	2	9	0	5	3	0	0	0	2	0	2	0	123	1	1	2	2	0	0	0	0	0	12	5	9	47	21	14	1	1	2	0	0	5	0	0	1	0	0	5
4	0	6	0	0	0	0	0	0	9	0	3	0	0	0	0	0	4	0	1	12	0	0	0	0	0	3	0	135	4	0	9	0	0	0	0	0	0	21	0	63	111	9	3	0	0	0	5	0	18	0	0	0	0	0	3
5	0	30	0	0	0	0	0	13	0	4	0	11	0	0	2	0	20	0	14	16	0	0	0	0	0	0	0	188	0	0	0	0	0	0	0	0	0	18	10	62	64	53	7	0	0	0	0	0	33	0	0	0	0	0	8
6	1	10	0	0	0	0	0	13	2	2	0	13	0	1	0	0	3	0	10	11	0	0	0	0	1	0	0	64	0	3	0	0	0	1	0	0	0	19	0	33	89	8	8	0	0	0	4	0	15	0	0	0	0	0	3
7	0	0	0	0	0	0	1	0	0	4	0	0	0	0	0	3	4	0	4	7	0	0	0	0	0	0	0	167	0	0	0	3	0	0	0	0	0	4	0	56	32	4	4	0	0	0	0	0	5	0	0	0	0	0	5
8	2	0	0	0	0	0	0	0	0	3	0	0	0	0	0	0	0	0	3	9	0	0	0	3	0	1	0	207	6	0	8	2	0	0	0	0	0	3	0	69	39	3	3	0	0	0	0	0	6	0	0	0	0	0	7
9	0	0	0	0	0	0	0	0	0	0	0	3	0	0	0	0	1	0	0	9	0	0	0	0	0	0	0	78	0	0	6	0	0	0	0	0	0	0	0	243	27	1	1	0	0	0	0	0	4	0	0	0	0	0	1
10	0	0	0	1	0	0	0	6	0	0	0	1	0	0	0	0	0	0	0	0	0	0	0	2	0	0	0	99	0	0	3	0	0	0	0	0	0	0	3	180	12	3	0	0	0	0	0	0	3	0	3	0	0	0	1
11	0	0	0	0	0	0	0	0	0	0	0	0	0	3	0	0	12	0	0	6	0	0	0	0	0	0	0	126	2	0	0	0	0	0	0	0	0	0	3	225	30	3	3	0	0	0	0	0	15	0	3	0	0	0	0
12	1	0	0	0	0	0	0	0	0	1	0	5	0	2	3	1	0	0	4	3	0	0	0	0	0	0	0	103	2	2	5	1	0	0	0	0	0	0	0	168	26	3	2	0	0	0	2	0	3	0	0	0	0	0	3
13	0	0	0	0	0	0	0	1	0	0	0	3	0	2	1	3	2	0	0	0	0	0	0	0	0	0	0	111	0	0	3	0	0	0	0	0	0	2	0	252	27	1	0	0	0	0	0	0	1	0	0	0	0	0	0
14	0	0	0	0	0	0	0	0	3	1	1	24	0	0	0	0	12	0	0	5	1	0	0	0	0	1	0	128	0	0	6	0	0	0	0	0	0	0	0	222	96	4	8	0	0	6	0	0	6	0	0	0	0	0	0
15	0	1	0	0	0	0	0	9	0	1	0	6	1	3	0	0	0	0	3	6	0	2	0	0	1	0	0	219	0	0	9	0	0	0	0	0	0	12	0	75	63	9	2	0	0	0	1	0	3	0	1	0	0	0	0
16	0	2	2	0	0	0	0	3	3	2	0	0	0	1	4	0	1	0	0	6	1	0	0	1	0	0	1	150	0	5	1	0	1	0	1	1	0	5	0	120	29	4	0	0	0	0	1	0	6	0	0	0	1	0	0
17	0	0	0	0	0	0	0	0	0	0	0	9	2	0	0	0	1	0	0	0	0	0	1	0	0	0	0	138	0	0	0	0	0	0	0	0	0	12	0	162	60	3	6	1	0	0	0	0	12	0	0	0	0	0	3
18	14	0	0	0	0	0	1	1	0	0	0	0	0	4	0	0	2	0	2	5	0	0	0	0	0	0	0	206	0	1	0	0	0	0	0	0	0	0	3	62	42	2	2	0	0	0	0	0	4	8	0	0	0	0	5
19	2	1	0	0	0	0	0	0	0	0	0	0	0	3	0	0	6	0	0	3	0	1	0	0	0	0	0	204	0	0	0	1	0	0	0	1	0	3	0	105	81	6	4	1	0	0	0	0	18	0	1	0	0	0	0
20	0	1	0	0	0	0	0	7	0	0	0	3	0	1	3	0	4	0	1	7	0	0	0	0	0	0	0	150	0	0	0	1	0	0	0	0	0	7	0	67	37	7	2	0	0	0	1	0	10	0	1	0	0	0	4
21	0	0	0	1	0	0	0	6	0	0	0	0	1	9	0	0	3	0	0	9	0	0	0	0	0	0	0	99	0	0	3	3	0	0	0	0	0	18	30	120	45	3	9	0	0	0	0	0	15	0	0	0	0	0	3
22	0	1	0	0	0	0	0	0	0	0	1	6	0	3	3	0	1	0	2	6	0	1	1	0	0	0	0	165	0	3	0	0	0	0	0	0	0	3	7	138	21	1	9	0	0	0	6	0	2	0	0	0	0	0	2
23	0	0	1	0	0	0	0	3	0	3	0	3	0	3	0	3	2	0	6	6	0	1	0	0	0	0	0	66	0	0	0	0	0	0	0	0	0	9	6	159	21	0	12	0	0	0	2	0	6	0	0	0	0	0	0
24	0	0	0	0	0	0	0	1	3	0	0	6	0	6	0	0	3	0	2	8	0	0	0	0	0	0	0	138	0	6	0	3	1	0	0	0	0	5	9	60	48	15	1	0	0	0	3	0	21	0	0	0	0	0	0
25	0	0	1	0	0	0	0	0	0	0	6	3	0	3	1	0	3	0	0	2	0	0	0	0	0	0	0	46	0	0	0	0	0	0	0	0	0	0	3	209	24	5	0	0	0	0	0	0	0	0	0	0	0	0	3
28	0	0	1	0	0	0	1	6	4	0	0	10	0	5	3	0	10	0	1	1	0	1	1	0	0	0	0	36	0	1	0	2	0	0	0	0	0	6	10	144	33	4	0	0	2	3	0	0	10	0	0	0	0	0	7
32	0	0	0	0	0	0	0	36	0	1	1	10	1	12	24	0	5	0	0	6	0	0	0	0	0	0	0	20	0	0	0	4	0	0	0	0	0	4	12	138	24	0	0	0	0	0	0	0	0	0	0	0	0	0	3
36	0	8	0	0	0	0	0	30	6	12	1	30	0	10	20	0	10	0	6	26	0	3	0	0	0	0	0	32	0	20	0	0	0	0	0	0	0	20	20	82	72	10	4	0	0	0	1	0	22	0	0	0	0	0	1
40	0	14	0	0	0	0	0	48	0	1	0	12	0	6	14	0	1	0	12	4	0	6	0	0	0	0	0	16	0	20	0	0	0	0	0	0	0	26	6	32	32	4	26	0	0	0	6	0	30	0	0	0	0	0	0
44	1	10	0	1	0	0	0	44	1	10	4	14	0	8	32	0	4	0	12	14	0	20	0	1	0	0	0	14	0	36	0	0	0	0	0	0	0	20	10	40	54	1	24	0	0	0	8	0	72	0	0	0	0	0	0
48	0	3	0	0	0	0	0	45	2	7	0	8	0	23	37	0	2	0	0	8	0	26	0	0	2	0	0	6	0	7	0	0	0	0	0	1	0	16	11	57	17	1	4	0	0	0	1	3	9	0	0	0	0	1	4
52	0	7	0	1	0	0	1	40	4	6	0	10	0	7	16	0	2	0	16	6	0	9	0	0	0	0	0	14	0	13	0	1	0	0	0	0	0	25	4	17	34	4	19	0	0	0	7	0	42	0	0	0	0	0	0
54	0	20	0	1	0	0	0	48	2	8	6	18	0	20	16	0	4	0	18	12	0	14	0	0	0	0	1	36	0	32	0	0	2	0	0	0	0	24	0	38	46	4	24	0	0	0	8	1	46	0	1	0	0	0	0
56	0	14	0	0	0	0	1	40	10	16	4	16	0	12	18	0	4	0	30	10	0	14	0	0	1	0	0	34	0	26	0	8	4	0	0	4	0	20	14	36	38	1	28	4	0	4	8	1	62	0	0	2	0	4	0
58	0	6	0	0	0	0	0	36	2	16	2	20	0	16	22	0	0	0	48	6	0	24	0	0	0	0	0	10	0	1	0	12	6	0	0	0	0	32	18	16	14	0	26	1	1	1	12	0	120	0	0	1	1	0	0
62	0	20	0	0	0	0	1	20	1	6	8	12	0	8	8	0	6	0	80	12	0	20	0	0	0	0	1	4	4	4	0	16	1	0	0	0	0	90	10	20	14	0	42	0	0	1	12	0	134	0	4	6	0	0	0
66	0	6	0	0	0	0	0	48	1	4	8	20	0	18	18	0	16	0	40	16	0	50	0	0	0	0	0	10	2	6	0	9	0	0	0	0	0	70	14	10	2	0	40	0	4	8	6	1	40	0	8	0	0	0	1
70	0	41	0	0	0	0	0	23	11	3	0	11	0	3	6	0	0	0	42	1	0	8	0	0	0	0	0	0	0	0	0	23	5	0	1	0	0	71	3	5	9	0	87	0	0	3	33	0	45	0	0	0	0	0	0
74	0	45	0	0	1	0	1	11	11	10	11	26	0	5	0	0	7	0	35	8	0	5	6	0	1	0	6	5	0	0	0	26	1	0	3	0	0	70	6	6	5	1	79	0	0	6	18	0	40	0	0	1	0	0	0
78	0	25	0	2	0	0	0	17	4	3	11	21	1	2	3	0	1	0	36	6	0	6	4	2	0	0	10	2	5	1	0	12	0	0	3	0	0	40	8	6	0	1	48	0	2	6	9	0	52	0	0	0	0	0	6
80	0	9	0	3	0	0	0	8	0	0	0	8	0	2	0	0	0	0	26	2	0	18	3	2	0	0	7	2	0	0	1	6	0	0	2	0	0	60	0	18	0	0	31	0	0	0	4	3	174	0	0	0	0	0	0
84	0	20	0	0	0	0	0	12	10	6	0	10	0	8	4	0	6	0	50	6	0	6	8	0	0	0	20	6	0	0	0	8	4	0	4	0	0	150	10	6	6	1	58	0	6	1	22	0	92	0	0	0	0	0	0
86	0	24	0	0	0	0	0	12	1	4	0	6	0	10	0	0	0	0	76	10	0	10	4	1	0	0	0	1	0	0	0	24	0	0	0	4	0	100	4	8	6	0	36	0	1	0	36	0	130	0	0	1	0	0	0
90	6	26	0	0	0	0	0	6	6	10	1	8	0	12	0	0	1	0	46	8	0	12	0	0	0	0	1	1	0	1	0	12	0	0	0	0	0	70	6	1	14	1	50	0	0	1	16	0	168	0	0	0	4	0	0
60	3	9	0	0	0	0	0	81	0	6	0	12	0	8	3	0	5	1	20	18	0	45	0	4	0	0	0	3	0	12	0	9	0	0	0	0	0	103	6	7	15	0	30	3	2	1	9	0	246	0	0	0	0	6	11
64	0	6	0	0	0	2	0	51	0	2	2	23	0	14	6	0	0	0	13	33	0	33	6	3	0	0	6	6	0	0	0	12	0	0	0	0	0	124	18	5	12	1	39	0	1	0	3	0	180	0	0	0	0	0	9
68	0	27	0	0	0	1	1	30	0	21	3	51	2	26	10	0	11	0	24	23	0	45	7	0	0	0	9	6	0	0	4	12	0	0	0	1	0	41	24	9	18	3	12	0	0	0	6	0	66	0	0	0	0	1	13
72	0	60	0	0	0	3	0	18	0	0	9	78	0	3	21	0	5	0	9	15	0	3	6	2	0	0	0	7	0	18	0	11	0	0	0	0	0	114	9	15	18	0	90	0	7	1	27	0	87	1	0	0	0	0	11
76	0	45	0	0	0	0	0	51	0	6	0	15	2	2	1	0	3	0	15	0	0	0	2	1	0	0	24	3	0	6	0	9	0	0	0	0	0	201	0	6	9	0	31	0	5	0	0	0	84	0	0	1	0	0	6
84	0	57	0	0	0	0	0	6	27	6	0	48	1	2	3	0	0	0	16	15	0	9	21	0	1	0	51	0	0	14	0	6	0	0	0	1	1	474	6	3	0	0	63	0	2	16	24	0	96	0	0	0	0	0	24
88	1	33	0	0	0	0	0	12	21	12	1	15	0	6	0	0	6	0	18	12	0	12	0	1	0	0	15	2	0	39	0	9	0	0	0	0	0	561	12	5	5	0	66	6	0	30	18	1	101	0	6	0	0	0	18

Table S15a: Absolute modern (surface) testate amoebae count data for core SI-2

Sample ID	Elevation (m SID)	Arcella discoides	Assulina muscorum	Hylosphenia subflava	Centropyxis cassis type	Centropyxis platystoma type	Centropyxiella sp.	Certesella martiali	Corythion dubium	Cyclopyxis arcelloides type	Cyphoderia ampulla	Difflugia bryophila	Difflugia pristis type	Difflugia pulex type	Euglypha compressa	Euglypha rotunda type	Euglypha tuberculata type	Heleopera petricola	Nebela griseola type	Nebela lageniformis	Tracheleuglypha dentata type	Trinema linere	Trinema complantanatum	Valkanovia elegans	Psuedohyalosphenia sp.
T1_17.6	-1.39	3	0	8	2	1	1	0	0	2	39	2	26	10	0	0	1	1	0		1	0	0	0	4
T1_21	-1.36	0	0	0	4	1	0	0	0	2	16	2	64	24	0	0	0	0	0	0	2	3	0	0	0
T1_24	-1.34	2	0	2	2	0	4	0	0	1	0	5	60	18	0	0	0	0	0	0	4	3	0	0	7
T1_25.6	-1.31	1	0	0	0	0	0	0	0	0	1	1	105	2	0	0	0	0	0	0	13	3	0	0	12
T1_26	-1.25	1	0	1	7	0	16	0	0	0	0	6	0	66	0	0	0	0	0	0	26	14	0	0	0
T1_26.3	-1.22	0	0	1	3	0	21	0	0	0	6	0	0	76	1	0	1	0	0	0	13	13	0	0	0
T1_34.5	-1.20	0	0	3	2	1	39	0	0	0	5	10	1	59	0	5	0	0	0	0	14	0	0	0	0
T1_37.75	-1.18	0	0	0	1	1	5	0	0	0	1	4	1	24	0	27	3	5	0	3	36	6	0	0	0
T1_42	-1.16	0	0	2	2	0	21	0	0	0	2	6	0	30	0	0	0	0	0	0	22	19	0	0	0
T1_43.85	-1.14	0	1	0	5	1	3	0	1	0	0	0	2	52	0	0	17	2	0	8	16	1	0	0	0
T1_45	-1.12	0	0	0	2	0	20	1	0	2	1	6	1	56	0	5	1	1	0	1	22	6	0	0	0
T1_45.5	-1.11	0	0	0	5	1	2	0	1	0	0	0	0	22	0	3	4	1	0	0	74	3	0	0	0
T1_47	-1.09	0	0	0	2	0	14	0	1	1	0	0	0	48	0	3	11	1	0	0	35	6	0	0	0
T1_50	-1.06	0	0	1	5	1	0	0	0	1	0	0	0	32	1	7	3	6	0	1	47	4	0	0	0
T1_73	-1.00	0	2	35	3	0	0	0	1	7	0	0	1	9	0	13	38	23	2	1	55	2	6	0	0
T1_97	-0.99	0	5	9	0	1	0	2	4	4	0	0	3	7	4	2	40	12	5	0	18	2	11	12	0
T1_123	-0.97	0	1	26	3	0	3	0	6	4	0	0	0	35	2	2	18	0	2	3	9	2	0	5	0
T1_130	-0.95	0	4	5	0	0	0	10	2	21	0	0	2	1	11	1	19	5	2	1	10	3	7	19	0
T1_127.5	-0.93	0	4	10	0	0	0	7	7	0	0	0	2	10	5	6	24	13	2	0	27	0	3	0	0
T1_124.5	-0.91	0	1	7	0	0	0	0	2	0	0	0	0	6	10	0	31	7	11	0	14	1	7	16	0
T3_2	-0.89	0	3	42	11	2	9	0	2	34	0	3	1	85	1	1	21	1	3	0	22	14	2	8	0
T3_4	-0.85	0	18	0	2	0	0	14	18	15	0	0	0	0	14	2	14	6	0	0	1	6	2	34	0
T3_6	-0.81	1	19	1	0	1	0	7	18	0	0	0	0	0	0	4	26	8	1	3	5	1	3	28	0
T3_29	-0.78	0	3	0	4	2	4	12	4	9	0	0	0	0	17	1	12	10	0	0	5	2	11	14	0
T3_32	-0.75	0	1	22	1	2	0	2	0	15	0	0	0	22	3	0	13	1	0	0	11	0	0	9	0
T3_37	-0.71	1	5	19	0	0	7	0	2	17	0	0	0	20	1	4	10	1	6	0	19	12	0	0	0
T3_37.9	-0.67	0	19	0	0	1	1	5	14	0	0	0	0	0	10	4	20	9	1	0	1	1	9	13	0
T3_38.5	-0.64	0	0	3	1	0	37	0	1	8	0	4	0	61	0	1	9	0	0	0	13	5	0	3	0

Table s15b: Absolute fossil (core) testate amoebae count data for core SI-2

Depth (cm)	Assulina muscorum	Centropyxiella sp.	Centropyxis cassis type	Centropyxis platystoma	Certesella martiali	Corythian dubium	Cyclopyxis arcelloides type	Difflugia bryophila	Difflugia pristis type	Difflugia pulex type	Euglypha tuberculata type	Eyglypha compressor	Heleopera petricola	Hylosphenia subflava	Nebela griseola type	Nebela langeniformis	Psuedohyalosphenia sp.	Tracheleuglypha dentata type	Trinema lineare	Valkanovia elegans
0	0	0	5	0	1	1	2	0	5	12	14	0	3	19	0	0	0	40	1	0
1	2	0	0	0	2	0	16	0	0	55	5	2	3	5	5	0	0	5	1	0
2	1	0	0	0	3	0	11	1	1	25	0	0	5	17	33	0	0	3	0	1
3	1	0	0	0	0	1	11	0	0	51	7	0	6	22	20	0	0	3	0	2
4	1	0	0	0	0	0	36	0	0	16	0	0	0	106	12	0	0	2	0	0
5	2	0	0	0	2	0	6	0	0	11	0	0	4	67	7	2	0	2	0	0
8	0	0	0	0	0	0	0	0	0	0	0	0	0	100	0	0	0	1	0	0
12	0	0	0	0	0	0	0	0	0	2	0	0	0	152	0	0	0	0	0	0
16	0	0	0	0	0	0	0	0	0	0	0	0	0	53	0	0	0	0	0	0
20	0	1	0	0	0	0	2	0	0	2	0	0	0	81	0	0	0	0	0	0
24	0	0	0	0	0	0	0	1	0	0	0	0	0	40	0	0	0	0	0	0
28	0	0	0	0	0	0	0	0	1	0	0	0	0	120	0	0	0	0	0	0
32	0	0	0	0	0	0	0	0	0	0	0	0	0	100	0	0	0	0	0	0
36	0	0	0	0	0	0	0	0	0	0	0	0	0	100	0	0	0	0	0	0
40	0	0	0	0	0	0	0	1	0	3	0	0	0	97	0	0	0	0	0	0
52	0	0	0	0	0	0	1	1	0	0	0	0	0	100	0	0	0	0	0	0
56	0	3	0	0	0	0	3	0	0	0	0	0	0	100	0	0	0	0	0	0
58	0	4	1	0	0	0	0	1	0	6	0	0	0	94	1	0	0	0	1	0
60	0	36	0	0	0	0	0	46	30	38	0	0	0	10	0	0	0	0	0	0
62	0	49	4	0	0	0	1	28	5	28	0	0	0	1	0	0	0	0	0	0
64	0	26	0	0	0	0	0	18	14	65	0	0	0	4	0	0	0	0	0	0
66	0	25	2	0	1	0	0	17	20	40	0	0	0	1	0	0	0	0	0	0
68	0	20	3	0	0	0	0	22	18	43	0	0	0	0	0	0	0	0	0	0
70	0	0	10	0	0	0	1	41	54	64	0	0	0	0	0	0	0	0	0	0
72	0	20	0	4	0	0	3	23	12	49	0	0	0	0	0	0	0	0	0	0
74	0	27	0	0	0	0	0	50	5	25	0	0	0	0	0	0	3	0	0	0
76	0	21	2	6	0	0	0	18	6	60	0	0	0	0	0	0	2	0	0	0
78	0	54	12	0	0	0	0	42	36	3	0	0	0	10	0	0	0	0	0	0
80	0	12	7	0	0	0	4	26	20	38	0	0	0	0	0	0	0	0	0	0
82	0	30	2	0	0	0	0	41	9	22	0	0	0	0	0	0	0	0	0	0
84	0	1	5	1	0	0	3	17	30	41	0	0	0	2	0	0	0	0	0	0
86	0	25	0	0	0	0	0	20	29	26	0	0	0	0	0	0	0	0	0	0
88	0	2	6	0	0	0	3	2	80	15	0	0	0	0	0	0	0	0	0	0
90	0	2	6	0	0	0	0	6	60	4	0	0	0	0	0	0	0	0	0	0

Table s16a: Absolute modern (surface) foraminifera count data for core SI-2

Elevation (m SID)	Trochamminita salsa	Miliammina fusca	Trochammina inflata	Jadammina macrescens
-1.09	3	0	0	0
-1.11	5	0	0	0
-1.13	19	0	0	0
-1.14	23	0	0	0
-1.16	14	0	0	0
-1.18	25	0	0	0
-1.2	100	0	0	0
-1.22	66	0	0	1
-1.25	150	0	0	0
-1.31	170	0	0	0
-1.36	204	1	0	0
-1.39	250	1	0	0
-1.4	307	0	0	0
-1.42	172	0	0	1
-1.43	100	0	0	0
-1.45	349	0	0	0
-1.48	110	0	0	0
-1.48	100	0	0	0
-1.49	336	2	0	0
-1.5	100	0	0	0
-1.51	132	0	0	0
-1.54	140	0	3	2
-1.57	90	5	5	0
-1.59	13	1	1	0
-1.62	92	12	2	0
-1.66	72	19	0	0
-1.69	96	20	0	0
-1.73	161	25	0	0
-1.76	181	47	0	1
-1.8	121	26	0	0
-1.9	81	20	0	1
-1.92	196	123	0	0
-1.93	111	38	0	0
-1.94	169	65	0	0
-1.96	59	89	0	0

Table s16b: Absolute fossil (core) foraminifera count data for core SI-2

Depth (cm)	Trochamminita salsa	Miliammina fusca
40	64	0
41	130	0
42	140	0
43	146	0
44	56	0
45	157	0
46	53	0
47	130	0
48	100	0
49	89	0
50	137	0
72	10	0
76	10	0
80	109	0
84	166	0
88	510	14
92	221	0